LINEARLY MODULATED OPTICALLY STIMULATED LUMINESCENCE OF SEDIMENTARY QUARTZ: PHYSICAL MECHANISMS AND IMPLICATIONS FOR DATING

JOY SARGITA SINGARAYER

Linacre College

Thesis submitted for the degree
of

Doctor of Philosophy
at the

University of Oxford

Trinity Term 2002

ABSTRACT

The optically stimulated luminescence (OSL) signal from sedimentary quartz has previously been found to be the sum of several physically distinct signal components. In this thesis the technique of linearly modulated OSL (LM OSL), in which the stimulation intensity is linearly increased during measurement, was employed to further investigate the OSL signal components. The method of LM OSL and subsequent fitting procedures used to separate the contributions of the components were rigorously tested using specifically developed numerical and analytical models.

In a survey of a number of sedimentary samples five common OSL components were observed; the 'fast' and 'medium' components as identified in earlier studies and three slow components 'S1', 'S2' and 'S3'. The fast, medium, S1 and S2 components displayed first-order characteristics while S3 did not (e.g. dose dependent bleaching rate).

The behaviour of the components, relevant to optical dating, was empirically examined and observed to be markedly different. The fast, medium and S1 components were demonstrated to be thermally stable, having lifetimes, $\tau > 10^7$ years. Component S2 was found to be thermally unstable and associated with the TL region at ~280°C. The calculated lifetime of S2 at ambient temperatures was calculated to be ~19ka at 20°C, estimated by isothermal decay analysis as for the fast, medium and S1 components.

A single-aliquot regenerative-dose protocol was developed for obtaining component-resolved equivalent dose estimates. Examination of the dose response of the components demonstrated the potential of component S3 for extending the upper age limit of quartz optical dating ($D_0 > 400$Gy). Component S2 was observed to saturate at relatively low doses ($D_0 \sim 30$Gy) and the fast, medium and S1 components all showed similar dose response characteristics ($D_0 \sim 200$Gy).

Photoionization cross-section spectra were obtained for the fast and medium components. It was found that the difference in the response of the OSL components to photon energy could be exploited in several ways; firstly, to separate the components by selection of appropriate photon energies/temperatures to successively bleach one component with negligible reduction in the next, thereby avoiding the need for complicated, lengthy fitting procedures, and secondly, the change of signal form following incomplete resetting, allows identification of partial bleaching of sediments.

ACKNOWLEDGEMENTS

TABLE OF CONTENTS

LIST OF FIGURES

LIST OF TABLES

LIST OF PARAMETERS

D_e	Equivalent (total absorbed) dose (Gy)
D_0	The dose at which the slope of the dose response curve is 1/e of the initial slope (Gy)
β	Absorbed laboratory dose (Gy)
D_R	Annual dose rate (Gyka^{-1})
X	Integrated OSL following natural/regeneration dose (counts)
S	Integrated OSL following a test dose (counts)
L	Integrated, sensitivity-corrected OSL (counts)
L_{max}	Integrated OSL intensity at dose saturation (counts)
w_i	Weight of single D_e estimate according to its error
$\overline{D}_e$	Weighted mean Equivalent dose (Gy)
$\hat{\sigma}_{\overline{De}}$	Weighted standard error (Gy)
$I(t)$, $I_{CW}(t)$, $I_{LM}(t)$	Instantaneous luminescence emission intensity; CW – continuous wave/constant intensity, LM – linearly modulated optical stimulation intensity (counts s^{-1})
I_0	Initial luminescence emission intensity (counts s^{-1})
t_{peak}	Illumination time at which LM OSL of a single component peaks (s)
I_{peak}	Intensity of LM OSL of a single component at t_{peak} (counts)
n	Concentration of trapped electrons (cm^{-3})
n_0	Initial concentration of trapped electrons, at $t = 0$ (cm^{-3})
N	Concentration of electron traps (cm^{-3})
f	Decay constant ($f=1/\tau$) (s^{-1})
m	Concentration of trapped holes (cm^{-3})
n_C	Concentration of mobile electrons (in the conduction band) (cm^{-3})
t	Time (s)
n_D	Concentration of electrons in thermally disconnected traps (cm^{-3})
A_n	Conduction band to electron trap probability (s^{-1})
A_m	Conduction band to hole centre probability (s^{-1})
$P(t)$	Stimulation photon flux at sample (cm^{-2}s^{-1})
P_0	Maximum stimulation photon flux at sample (cm^{-2}s^{-1})
σ	Photoionization cross-section of electron trapping state (cm^2)
λ	Stimulation wavelength (nm)
t_{max}	Total measurement time (s)
b	Kinetic order
α	Tikhonov regularization parameter
τ	Retention lifetime of trapped charge; length of time an electron is expected to remain trapped (s)
s	Frequency factor (s^{-1})
E	Trap (thermal) Depth (eV)
k_B	Boltzmann's Constant $\approx 8.615 \times 10^{-5}$ (eV $°K^{-1}$)
B	Heating rate ($°Ks^{-1}$)
T	Temperature ($°K$)
I_∞	OSL intensity at T=∞ (counts)
E^*	Thermal assistance energy: $E^*=\phi(E_0-h\nu)$ where ϕ is a constant, E_0 is the optical depth, and $h\nu$ is the stimulating photon energy (eV)
η	Thermal quenching scaling factor

K	Thermal quenching frequency factor (s^{-1})
W	Activation energy (eV)
χ	Sensitivity of the 110°C TL peak to a small test dose
ζ	Photo-transfer efficiency (OSL traps to 110°C TL trap)
$h\nu$	Stimulating photon energy; (eV)
E_{i0}	Optical ionization energy (eV)
$\hbar\omega$	Phonon energy (eV)
E_F	Fermi energy level (eV)
$\rho(E)$	Density of states
d_{FC}	Franck-Condon effect parameter
S_C	Coupling coefficient
ψ	Impurity wavefunction
$\phi_{n,k}$	Band wavefunction
E_g	Band gap width (eV)
E_i	Equilibrium binding energy (eV)
E_p	Optical gap (eV)

Chapter | 1

1 | INTRODUCTION

1.1 Background to optical dating of sediments

The following generalised background to optical dating is taken from a number of standard texts including Aitken (1985), McKeever (1985), Aitken (1998) and Lowe and Walker (1997).

'Optically stimulated luminescence' describes the emission of light when light is shone on an insulator or semiconductor, following previous absorption of energy from radiation. When luminescent minerals, such as quartz or feldspar, are exposed to ionising radiation (mainly α, β, or γ-radiation) they acquire a luminescence signal, due to the redistribution of electronic charge in the crystal lattice. During irradiation electrons in the outer shells of atoms are excited into the conduction band. Most recombine immediately but a small proportion becomes trapped in local 'meta-stable' levels, or traps, located within the forbidden gap (usually connected with impurity atoms or other types of lattice defects). Similarly, a proportion of the holes, created as the electrons are ionised, is trapped in localised states. The net charge redistribution continues for the duration of exposure to radiation. With sufficient optical (or thermal) stimulation the trapped electrons can be 'freed' from the trap and recombination can then occur with a trapped charge carrier of the opposite sign. The excess energy from the recombination process is emitted as light and/or heat that can be recorded.

The use of optically stimulated luminescence (OSL) for dating of sediments was first introduced by Huntley *et al.* (1985). In the natural environment mineral grains are exposed to ionising radiation provided largely by potassium, thorium and uranium, and to a smaller extent, cosmic rays. Grains subsequently separated from their parent rock/sediment by erosional processes, are transported (through air or water, for example) enabling the exposure to natural sunlight necessary to zero the considerable latent signal that may have accumulated during previous burial. It is the last zeroing event to take place that is dated using optically stimulated luminescence (OSL) techniques. Following deposition the stored luminescence signal once again accumulates as sediment is exposed to ionising radiation.

Measurement of the naturally accumulated OSL and calibration of this signal using the OSL signal following known laboratory radiation doses allows an estimate of the total absorbed radiation dose in the natural environment to be made. The total absorbed dose is referred to as the paleodose and the estimate of this, based on luminescence measurements is called the

"Equivalent Dose" or D_e. This represents the dose required to produce the luminescence signal observed in the natural sample. The OSL signal is directly related to the burial period. In principle, once the environmental dose rate is calculated, the age (burial period) of the sample can be found using the following equation:

$$\text{Age (ka)} \quad = \quad \frac{\text{Equivalent Dose (Gy)}}{\text{Dose-Rate (Gy.ka}^{-1})} \qquad (1.1)$$

assuming the dose rate is constant through time. For successful optical dating several fundamental requirements must be fulfilled. The signal must be relatively stable, i.e. the trap(s) where electrons are held must have adequate retention lifetimes for dating. The dose response of the signal must be well defined to obtain accurate estimates of equivalent dose. It must be possible to reset the signal, which for sedimentary samples is achieved through exposure to light during transport. Finally, the environmental dose rate must be well defined. In practice, dose rates are estimated typically using several methods, such as on-site gamma spectrometry, which measures directly the gamma activity of the sediment (from which total dose rate can be calculated), or using neutron activation analysis (NAA) to determine the concentrations of the radioelements in the sediment.

Luminescence dating (by OSL or TL) is an example of an absolute dating technique. The term 'absolute', as it applies in this context, pertains to techniques whose dates are independent of other chronologies or dating methods. Other examples include potassium-argon and uranium series dating. Absolute dating techniques are vital for palaeo-environmental reconstruction from very often spatially disparate and fragmentary deposits.

The reconstruction of Quaternary environments is important for many reasons. The Quaternary (approximately the last two million years) has been a time of immense global environmental and evolutionary changes. Such dramatic changes have had a profound impact on the landscape both geologically and environmentally. It has also been suggested that environmental change during this time played an important role in the evolution of humans, both physically and culturally. The use of dating techniques provides crucial evidence for the reconstruction of these significant past events and processes. Luminescence dating is the only absolute method that directly dates sediment deposition placing it in a unique position among Quaternary dating techniques.

The variety of dating techniques that can be applied to Quaternary deposits have inherent properties that limit their application to certain geological materials (depending on the physical / chemical basis of the technique), and to a particular age range. Fig. 1.1 provides a summary of the age range and applicability of the main Quaternary dating techniques. The datable range of optical dating depends on a variety of factors including the mineral being dated. For quartz, the mineral used in the present study, the lower limit can be of the order of 10s of years, depending on the sensitivity of the sample and the environmental dose rate. The upper limit can be several 100ka, depending on the dose saturation level, again the dose rate, and thermal stability of the signal. Quartz is often the chosen mineral for optical dating for a number of reasons. It is highly abundant in sediments, in part due to its resistance to weathering. Also, it is relatively easy to separate from bulk sediment samples. Additionally, there is no evidence of signal instability in quartz.

1.2 The OSL components of quartz

Huntley *et al.* (1985) observed that the decrease in the OSL emission of quartz upon illumination (stimulated with a constant intensity) did not follow a simple exponential as one would expect from a single trap system with first order kinetics. The same emission was found by Smith and Rhodes (1994) to be well approximated by the sum of three exponential signal components that they called the fast, medium and slow (or long-term) components after their relative optical depletion rates. Bailey *et al.* (1997) demonstrated that the most probable explanation is that the OSL signal originates from three physically distinct traps with different rates of charge loss. The slow component of quartz appeared to have an exceptionally a high dose saturation level in several samples and high thermal stability, indicating its potential for extending the upper datable limit of optical dating using quartz (Bailey, 2000a).

In the studies described above the luminescence emission was stimulated using a constant intensity (continuous-wave or CW OSL). A novel method for measuring OSL was proposed by Bulur (1996) which involved linearly ramping the intensity of the stimulation source during measurement of the luminescence. This produces peak-shaped OSL instead of a monotonically decaying CW OSL signal. Parallels can be drawn with the more familiar phenomenon of measuring thermoluminescence (TL) peaks by ramping the temperature during measurement.

(a)

(b)
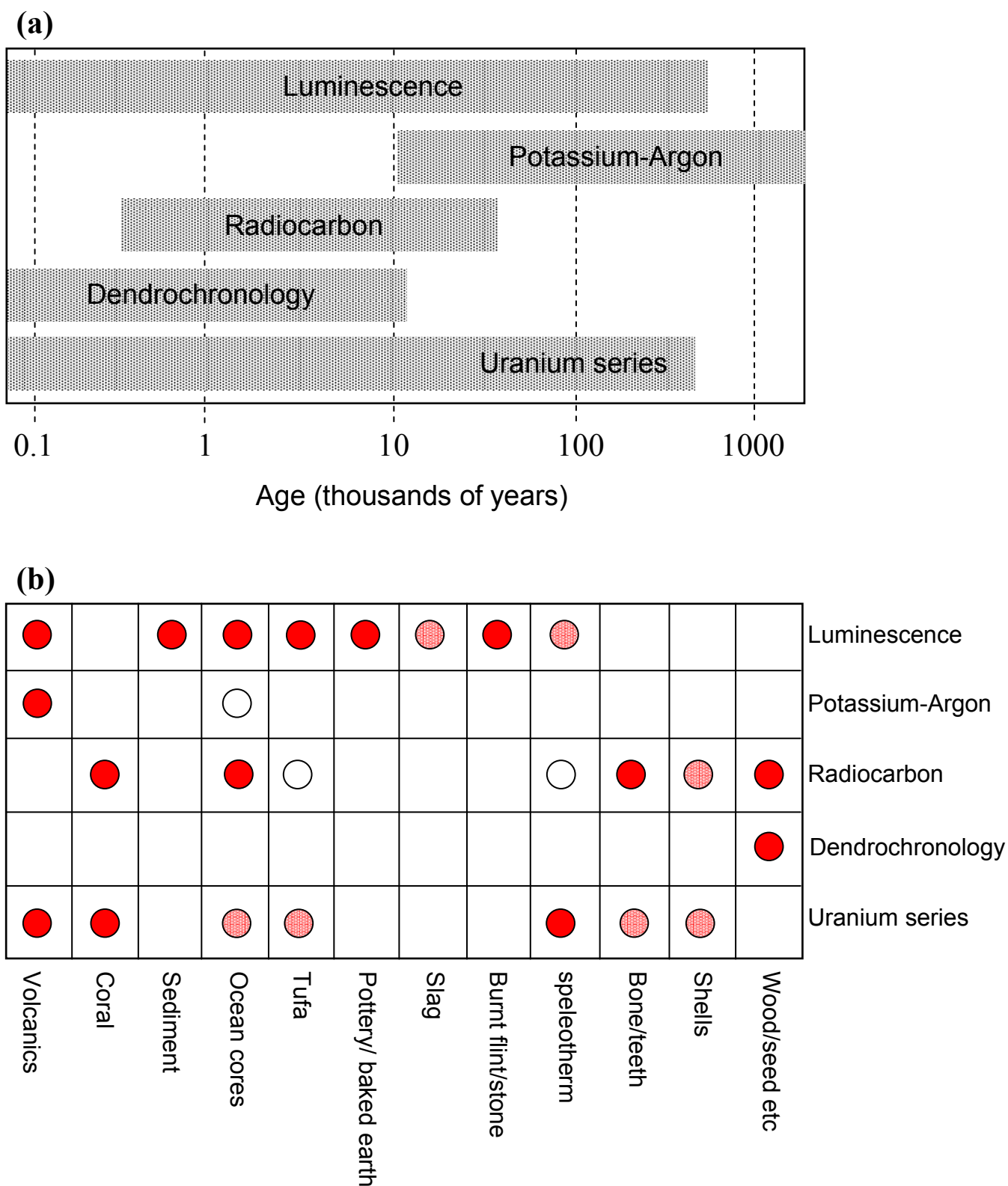
Fig. 1.1 (a) Datable age ranges of various Quaternary dating methods. Absolute limits vary slightly depending on individual circumstances. (b) Types of deposit/remains to which various dating techniques are applicable. The extent of applicability is indicated by: Red circle for high probability of a reliable date, pale red circle for when qualifications need to be made, open circle for low probability of reliable dating.
Modified from Aitken (1998).

Using the LM OSL technique the structure of the signal, in terms of number of components and kinetics, is recorded with greater clarity. The technique of LM OSL applied to a heated quartz sample by Bulur *et al.* (2000) enabled the identification of four first-order components.

Considering the discrepancy between the studies a reanalysis of the behaviour is necessary to reconcile the CW and LM OSL findings, including re-evaluation of the potential applications for long-range dating using the slow component.

1.3 Thesis scope and format

This thesis is aimed at investigating the behaviour of the OSL components of quartz relevant to optical dating, following the work of Bailey *et al.* (1997) and Bulur *et al.* (2000). The linearly modulated OSL system of measurement has been employed for the majority of the measurements reported. The principal areas of investigation are described below.

- Comprehensive assessment of linearly-modulated OSL and the deconvolution of LM OSL curves [Chapter 3]

- Response of the OSL components to heating. In particular, examination of the thermal stability of each component [Chapter 4]

- Response of OSL components to optical stimulation. A new strategy for separating the OSL components is proposed based on their responses to different photon energies [Chapter 5]

- Development of methods for component-resolved equivalent dose determination and applications of component-resolved measurements to various aspects of optical dating [Chapter 6 and 7]

The main conclusions of the study are summarised in Chapter 8.

Chapter | 2

2 | TECHNICAL INFORMATION

2.1 Introduction

Presented in this chapter are the basic procedures that were employed for collection and preparation of samples and descriptions of apparatus used to provide a variety of treatments on prepared grains, including measurement of OSL.

Samples from a variety of environmental and chronological (from <100a, to ~1Ma) contexts have been collected specifically. This required the use of various sampling strategies, described in the next sections. A range of apparatus was used to provide measurements for different elements of the luminescence dating process, and for empirical investigation of the luminescence properties of quartz. The equipment employed is outlined in this section. A brief discussion of the relevant aspects of error analysis in luminescence dating methods is also undertaken.

2.2 Sample collection

A large number of the samples collected were marine deposits. Although this is perhaps not the ideal environment for sampling, these samples were taken where independent dating techniques had been applied previously. The chronological control thus provided (see chapter 7) was used for testing the optical dating techniques to be developed during the study (see chapter 7). The stratigraphically older marine sediments had incurred considerable cementation. This occurs when minerals, dissolved in water, precipitate out onto the sedimentary grain surfaces as the water flows through the sediment. The mineral precipitates, mostly carbonates, effectively glue the grains together into a solid rock. Extraction of these hard, cemented sands, whilst maintaining sample integrity was achieved by removing a large block (usually at least 20cm^3) of material using a hammer and chisel. It was important that a block of sufficient size could be obtained, so that the outer (light exposed) layer could be removed to leave sufficient volume of material for dating, and that the sediment did not have an open structure, as light penetration may be significant. Several seconds of exposure to daylight is sufficient to reduce the OSL dating signal of quartz significantly (see Aitken, 1998, for a summary of reported observations). Having released a block of material, with

minimum exposure to light, it was immediately transferred to opaque black bags (the kind used in hospitals to protect x-ray film were used) for transportation to the laboratory. In suitably dim lighting in the laboratory (see section 2.3) the surface layer (2-5mm) was removed. To ensure that the entire outer surface was removed blocks were sprayed with black paint prior to scraping. Removal of the whole outer (painted) layer was then more reliably achieved.

For more precise sampling of cemented sediments a diamond corer was employed (by Dr E. J. Rhodes, for the Moroccan samples; see chapter 7). The same approach to the removal of the outer layer of the material described above was used for these samples.

Other softer sediment samples were collected by hammering light-tight steel or PVC cylinders into vertical sections. The cylinders used were immediately capped at both ends and sealed in opaque black bags to minimize light exposure. In the laboratory the outer (light-exposed) 3 - 4 centimetres from each end were discarded. The discarded material was subsequently used for measurements of environmental dose rate and moisture content (see section 2.4.2).

Estimation of the environmental dose rate can be obtained by several methods. For a summary of available methods see Aitken (1998). Owing to limits of time and sample mass only the techniques of field gamma spectrometry and neutron activation analysis (NAA) were used for the samples collected. For neutron activation analysis (NAA) the amount of material required is of the order of tens of grams. The sediment from the discarded outer layer of the collected material was sufficient for this purpose. Additionally, measurements of current environmental gamma dose rates have, for the majority of the samples collected, been obtained in the field using a portable gamma spectrometer. This method required no extra sample collection. The details of each method and their relative merits are discussed in section 2.4.2.

2.3 Preparation of samples for OSL measurement

The standard procedures for refining the sand-sized quartz fraction from a mixed sedimentary sample have been used (following Stokes, 1992). Sample preparation was performed under 'safe' laboratory lighting conditions, i.e. lighting of a sufficiently low photon energy, and low power that there is negligible bleaching of the quartz luminescence over the order of hours/days, but adequate light levels to allow procedures to be carried out safely and easily. This was achieved using Na vapour lamps, which emit most of their energy in the sodium D doublet at 589.0 and 589.6nm (Spooner *et al.*, 2000). Yellow/amber lighting provides a good

compromise between sufficiently low photon energy (i.e. low bleaching efficiency) and comfort for the human eye (photopic vision peak response is approximately 555nm, diminishing to 10% at 650nm, (Spooner *et al.*, 2000)). The lamp intensities used for sample preparation were < 1μW cm^{-2} (measured using a Molectron radiometer).

However, slow optical depletion rates can occur even at such low photon energies (Bailey, 1998a; Singarayer and Bailey, 2002) so care still has to be taken in preparation not to expose samples to lengthy periods of illumination. Special attention is required with the use of drying ovens (Bailey, 1998a), as at elevated temperatures the optical eviction of quartz luminescence will proceed at a faster rate due to thermally assisted detrapping.

A flowchart of the generalised procedure for separating the coarse grain quartz fraction from sedimentary samples is presented in Fig. 2.1. The preparation of each sample began with a treatment of dilute hydrochloric acid (~ 12%) to remove carbonates. In the case of cemented samples, the HCl treatment reduced the sediment sample into its constituent grains. Samples were then washed several times in distilled H_2O to remove products of the acid treatment. Once dried, in an oven (at 50°C), the sediment was sieved to separate grain size fractions at approximately 50μm resolution. The modal grain size was retained for further preparation. This was typically 90-125μm or 125-180μm diameter. In cases where the largest volumes were >180μm the 180-250μm grain size was chosen.

In general, coarse grain fractions (i.e. >90μm) were chosen for ease of preparation, dose rate calculations and inter-sample comparisons. For samples deficient in coarse grains, preparation of the fine grain fraction (4-11μm) can be undertaken. A detailed description of the procedure for fine grain preparation is described in Rees-Jones (1995), and is also outlined for completeness in Fig. 2.1. However, this was not necessary for any of the samples collected in the course of this study.

The grain size fraction chosen was subsequently treated with 48% hydrofluoric acid (HF) for approximately 50-60 minutes (Rendell and Wood, 1994). The purpose of this is twofold. Firstly, it removes the majority of feldspar grains that may be present in the fraction. Secondly, the procedure etches away the outer layers of the quartz grains (~ 20-30μm). During burial around 80% of the total alpha dose is deposited within the top 30μm (typical ranges 10-50μm; Aitken, 1985). Therefore, the alpha contribution can be almost totally eliminated from the determination of equivalent dose and dose rate. Following the HF treatment the sample was washed with 10% HCl and then distilled H_2O to remove fluoride precipitates. The sample was then dried at 50°C.

Quartz was separated from the remaining sample by density separation, using a 2.68 g cm^{-3} solution of sodium polytungstate. Grains were immersed in sodium polytungstate and centrifuged for 10 minutes. Grains of density <2.68 g cm^{-3} (almost entirely quartz, $\rho \cong 2.65$ g cm^{-3}) were subsequently poured off from higher density minerals (e.g. zircon) after freezing the bottom of the container using liquid nitrogen.

The refined quartz fraction was given a final wash with distilled H_2O to remove the polytungstate solution. Once dried overnight at 50°C the sample was re-sieved to the original grain size resolution.

Sub-samples (aliquots) of the prepared quartz grains were mounted on 1cm diameter aluminium or stainless steel discs using viscous silicone oil (Dow Corning 200/60000cS). A monolayer of quartz grains (~5mg) was deposited per disc. The disc and oil were known to produce preheat and irradiation independent, non-decaying background signals (Rhodes, 1990).

Testing sample purity

A simple test of sample purity, with respect to feldspar as the primary source of contamination, was undertaken on each of the aliquots used throughout the study. It is known that luminescence can be stimulated from feldspars using low-energy, infrared photons (E ~ 1.4eV) at ambient temperatures, ~20°C (Hütt *et al.*, 1988). In contrast, negligible amounts of luminescence are observed from pure quartz when stimulated under the same conditions (Spooner and Questiaux, 1989). For that reason all aliquots were subjected to 30-40s of infrared stimulation at up to 0.25 Wcm^{-2} (see section 2.4.1 for details of infrared source). The presence of rapid OSL decay above background levels was taken as an indication of feldspar contamination.

Samples with many aliquots displaying significant IRSL decays were treated with HF again and underwent subsequent density-separation, in an attempt to completely remove any feldspar contamination (i.e. until negligible OSL decay upon IR illumination was observed). This had to be done on only two samples (TQA and TQQ) after observing considerable IRSL decays in aliquots of both samples. Following one additional cycle of HF and sodium polytungstate treatments both samples displayed no measurable IRSL decay.
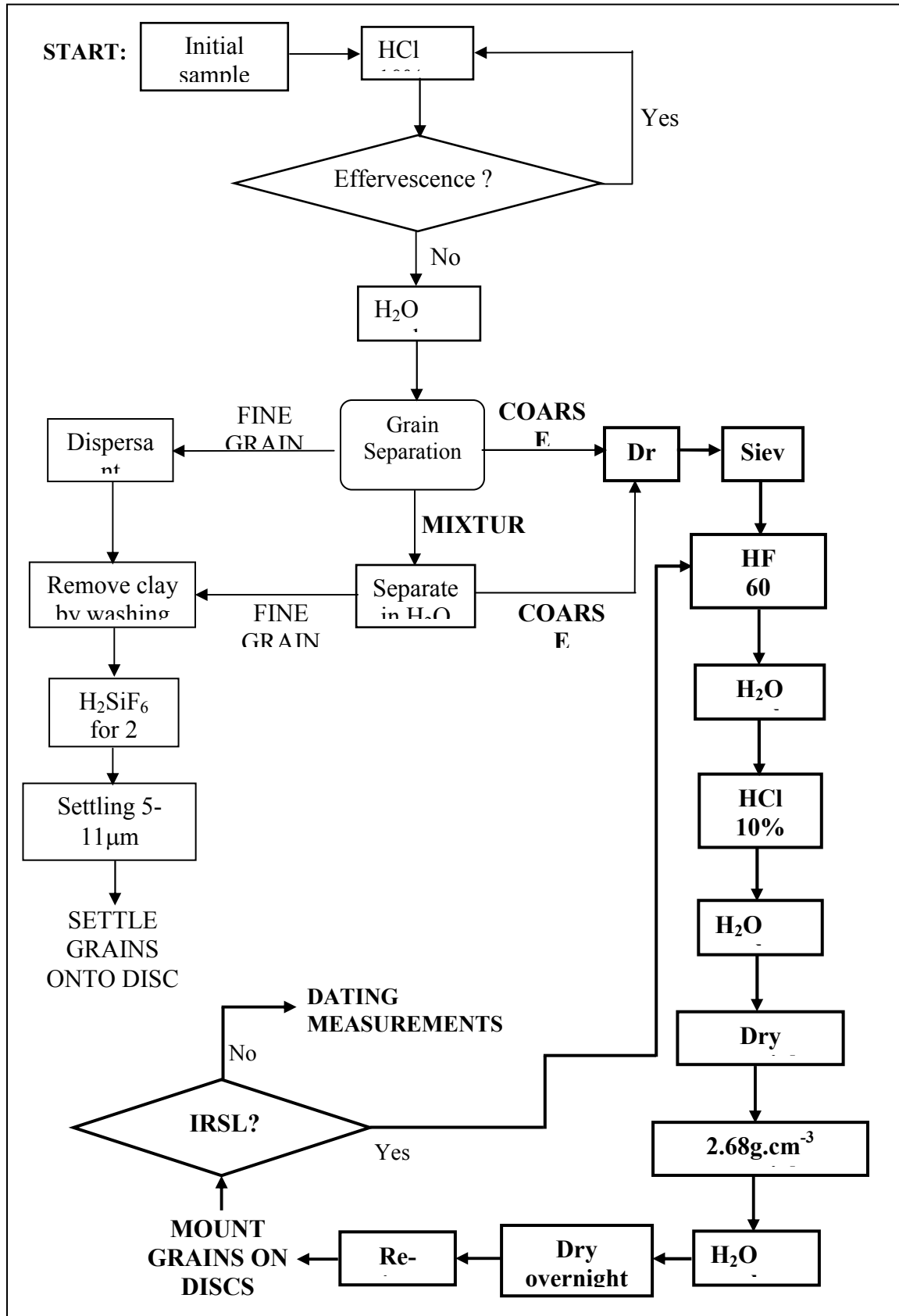
Fig. 2.1 Standard sample preparation used for refining the quartz fraction from sedimentary samples (Modified from Bailey and Rhodes, 2001)

2.4 Measurement apparatus

2.4.1 Measurement of luminescence

Luminescence measurements (OSL and TL) were made using automated Risø luminescence readers. Several generations of readers were utilized throughout the course of the study. A major difference between the readers was in the optical excitation source. In one model (TL-DA-12) optical stimulation was provided by a 75W filtered halogen lamp. Using a 3mm HA3 heat-absorbing filter, 9mm Schott GG420 filters and a broadband interference filter a stimulation band of 420 – 560nm at $\sim 12 \mathrm{Wcm^{-2}}$ was obtained (Bøtter-Jensen and Duller, 1992). Infrared stimulation in this reader model was provided by an array of 32 IR emitting diodes (880 Δ 80 nm, $\sim$ 40 $\mathrm{Wcm^{-2}}$). This reader shall be referred to as R3.

Two other readers were equipped with GG420 filtered blue light-emitting diodes (LEDs). The TL-DA-15 excitation unit contained 6 clusters of 7 NICHIA 470 Δ 20nm LEDs arranged in a ring, as illustrated in Fig. 2.2, individually focussed on the sample position (Bøtter-Jensen *et al.*, 2000). The total maximum intensity at the aliquot was $\sim 20 \mathrm{Wcm^{-2}}$. A 1W solid state IR laser diode (830 Δ 10nm, $\sim$ 400 $\mathrm{mWcm^{-2}}$ stimulation intensity) was also incorporated into the Tl-DA-15 reader. All direct hardware control was performed by a 'mini-sys' computer (Markey *et al.*, 1997). The Mini-sys Windows programme, as developed by Markey *et al* (1997), was used for editing and executing measurement sequences. This reader model will be hereafter referred to as R4a. Note that the excitation unit on R4a was substituted with a more powerful one during the course of this study. The same number of LED clusters was incorporated; however, each LED produced a slightly higher maximum light intensity. The maximum stimulation intensity at the sample chamber with the new excitation unit was $\sim 36 \mathrm{mWcm^{-2}}$ and will be referred to as reader R4b in further sections.

Reader TL-DA-10 contained an array of 5 equivalent blue LED clusters. This was to allow an input for external stimulation sources via a liquid light guide at the 6th cluster position equivalent in TL-DA-15. As a result the maximum source intensity was 17% lower ($\sim 16 \mathrm{Wcm^{-2}}$). IR stimulation was identical to that for TL-DA-15 (i.e. IR laser diode, 830 Δ 10nm, $\sim$ 400 $\mathrm{Wcm^{-2}}$). This reader will be referred to as R2 (the apparently arbitrary numbering of the Risø reader models results from the order that the readers were originally purchased by the laboratory).

There was an additional Risø reader, R1, available for administering beta dosing and measuring TL. This reader had no light source for OSL. This system was used only for annealing a number of samples before measurement in the other readers.
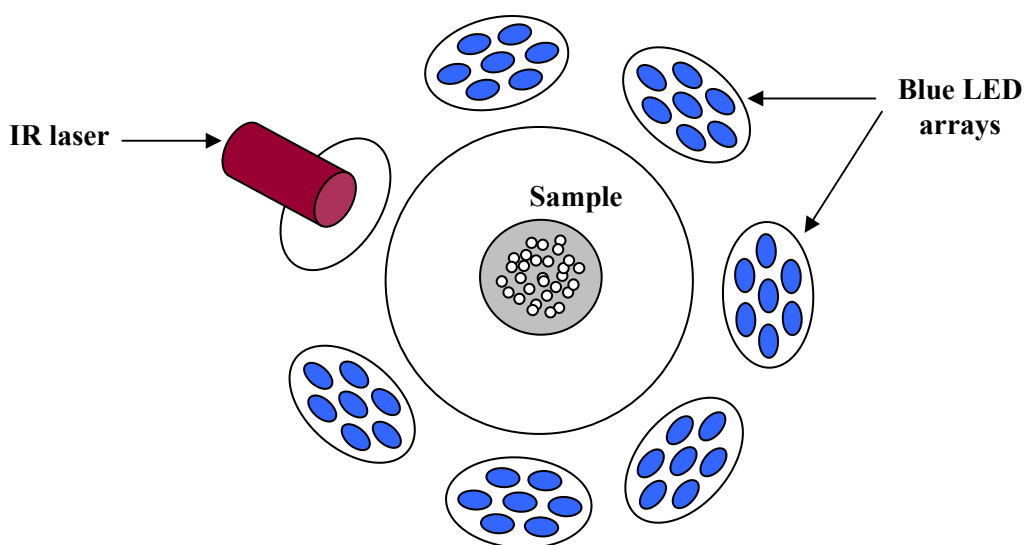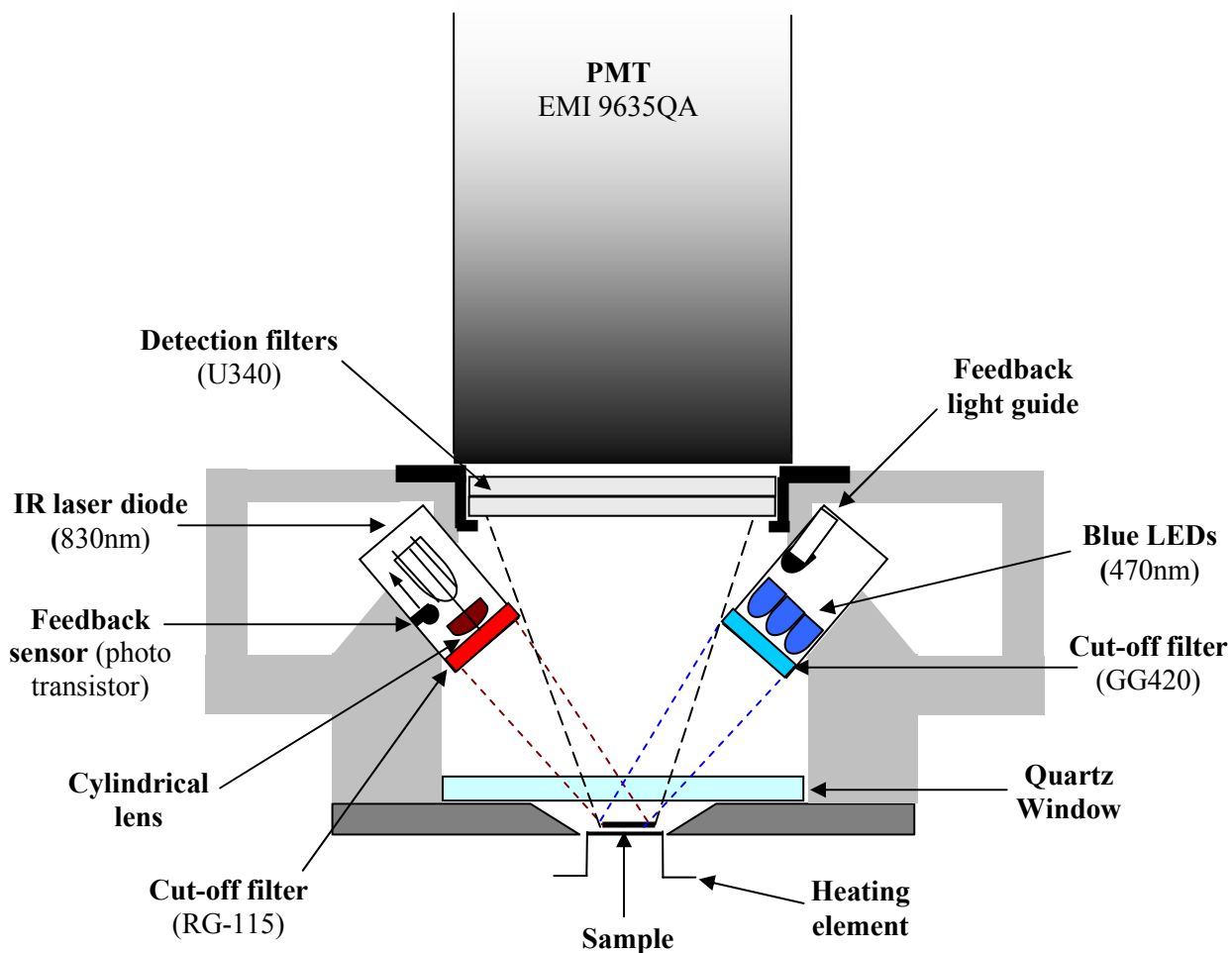
Fig. 2.2 Schematic diagram of the blue LED and IR laser diode OSL unit (TL-DA-15 and TL-DA-10 readers). Modified from Bøtter-Jensen *et al.* (2000).

For the majority of OSL measurements blue LED stimulation (provided by TL-DA-10, TL-DA-15) was favoured over the filtered Halogen lamp source due to the higher intensities available and smaller spread in stimulation wavelength. Variation of stimulation intensity during OSL readout (described in Chapter 3) could be performed on TL-DA-15 only (R4a and b). In all automated readers the luminescence emissions were typically filtered using 6mm U340 filters to detect the UV region using EMI 9635Q photomultiplier tubes. Graphs of the Risø reader's respective excitation and emission bands are presented in Fig. 2.3.

All readers were equipped with sealed ^{90}Sr/^{90}Y β-irradiation sources of various strengths. An additional α-irradiation source attachment was incorporated into TL-DA-12 (R3). Table 2.1 contains details of all the Risø readers, including irradiator source strengths.

Additionally, Risø reader R4b incorporated single grain measurement equipment described by Duller *et al.* (1999). The single grain system composed a 10mW Nd:YVO4 diode pumped laser to optically stimulate luminescence at 532nm from 100 grains mounted on each specially manufactured sample disc (Bøtter-Jensen *et al.*, 2000).

	TL-DA-12 (R3)	**TL-DA-10 (R2)**	**TL-DA-15 (R4a/b)**
OSL source	Filtered halogen lamp 460-520 nm ~12 mW cm^{-2}	36 blue LEDs 470Δ20 nm ~16 mW cm^{-2}	42 blue LEDs 470Δ20 nm ~20/36 mW cm^{-2}
IR source	880Δ80 nm, LEDs ~40 mW cm^{-2}	830Δ10nm laser diode ~400 mW cm^{-2}	830Δ10nm laser diode ~400 mW cm^{-2}
β - source	^{90}Sr 1.2Gy/minute	^{90}Sr 1.28Gy/minute	^{90}Sr 3.1Gy/minute
α - source	*^{241}Am 0.3Gy/s (fine grain on Al)*	NO	NO

Table 2.1 Information concerning the optical and irradiation sources incorporated in each of the automated Risø reader models.
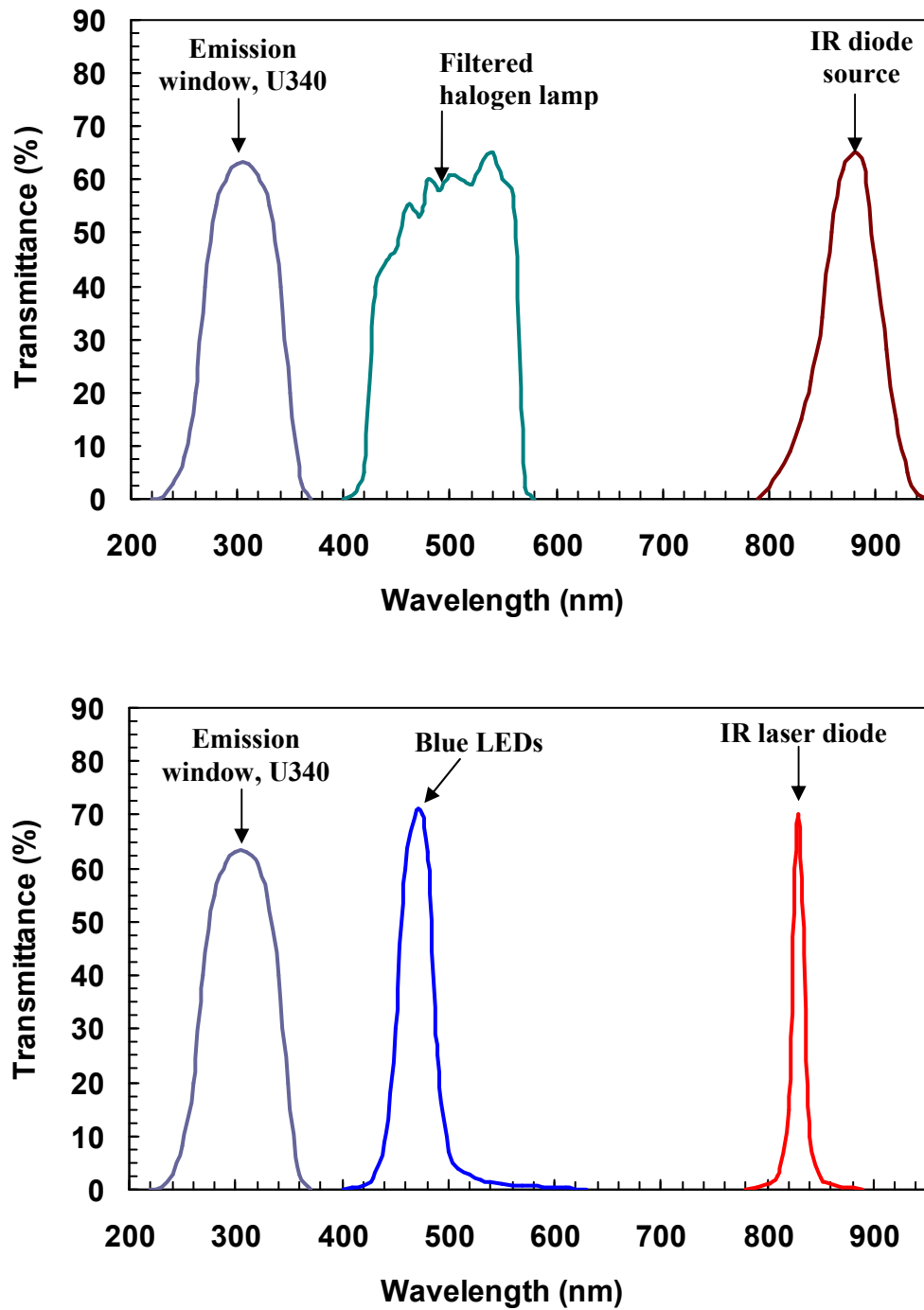
Fig. 2.3 The excitation and emission windows of the Risø TL-DA-12 (upper) reader and TL-DA-10, TL-DA-15 readers (lower). Excitation is provided by the various stimulation sources described in section 2.4.1.
Redrawn from Bailey (1998), Aitken (1998) and Bøtter-Jensen et al. (1999).

Peripheral equipment

Other apparatus employed on occasions included an Oriel 300W filtered xenon lamp solar simulator. Section 5.3.2 contains a discussion of relevant aspects of the solar simulator and the emission spectrum.

An external bleaching unit was built with interchangeable LED clusters of a variety of wavelengths. The clusters used produced light at 375, 430, 470, 500, 525, 590 and 640nm. The details are given in section 5.2.1.3. The unit was mounted on a heater plate to enable bleaching using any of the above wavelength sources at raised temperatures.

An Elsec β-irradiator was used occasionally for dosing large numbers of aliquots sequentially.

2.4.2 Dose rate determination

There are numerous methods to evaluate the environmental dose rate, either on-site or in the laboratory including, thick source alpha counting, field gamma spectrometry, flame photometry, neutron activation analysis (NAA) and inductively coupled plasma mass spectrometry (ICP-MS). Constraints of time and collected sediment volume dictated that for most of the samples the dose rate was determined by field gamma spectrometry measurements and, if possible, NAA. The methods utilized are outlined below.

Portable (field) gamma spectrometry

A micronomad gamma spectrometer was used with NaI scintillation crystal. A probe, housing the scintillator was inserted into the cavity left from sample extraction. Measurements of the gamma activity took typically a minimum of one hour (longer for sites with low radioactivity). Subsequently a total gamma dose rate of the surrounding environment could be estimated via summing all counts over a threshold (for high statistical precision), or, by selecting relevant energy windows, the contributions from U, K and Th and cosmic rays could be obtained. Comparison to known concentration standards then allows estimates of U, K and Th concentrations to be made. The total (alpha, beta and gamma) dose could be subsequently estimated. This is a convenient and efficient way of determining present day dose rates. It has the advantage of producing rapid, low cost in-field results with no involved laboratory procedures required. Additionally, measurements are made at field moisture conditions and include cosmic ray influence. Errors are derived mostly from counting statistics and systematic errors in calibration (concentrations of radioisotopes in the calibration blocks). However, the temperature in the field can affect the measured spectrum

positions due to scintillation and probe temperature dependencies. This can result in changes in window count rates in preset counting windows with temperature but can be stabilized with an internal reference radioisotope source (Stokes, 1994). For further details concerning portable gamma spectrometry and its application to optical dating see e.g. Stokes (1994) and Gilmore and Hemingway (1995).

Neutron Activation Analysis (NAA)

Direct estimates of radioisotope concentrations can be made via neutron activation analysis. Samples of raw sediment (10-20g, usually taken from the stripped outer layer of the bulk material collected for D_e determination; see section 2.2.2. Note that only material that was not painted prior to stripping was used to obtain reliable results) were sent for commercial analysis to Becquerel Laboratories, Australia. For this technique, samples are subjected to neutron irradiation, leaving them in a highly unstable state (Parry, 1991). The subsequent radioactive decay is then measured using high-resolution gamma-spectrometry to give concentrations of U, K and Th (e.g. Parry, 1991). This method provides high precision results, however, the small sample sizes analysed using NAA may lead to concern about how representative the data are. Additionally, only the top of the radioactive decay chains are measured. These factors may in some instances mean the dose rate estimates calculated from NAA analysis do not match bulk sediment activity.

Cosmic ray dose rate

The cosmic ray dose rate was calculated as a function of global position, total overburden, altitude using equations given in Prescott and Hutton (1994), and where possible recorded as part of the energy specific field gamma spectrometry measurements. Unfortunately, due to sedimentation/erosion processes, these methods are not expected to represent the average cosmic ray dose-rate. However, the cosmic dose rate is usually a small fraction of the total dose rate, except in low radioactivity sites.

2.5 Noise and background signal components

The presence of noise in any measurement is a fundamental and unavoidable problem. It is inherent in instrumentation due to the underlying physics. During the measurement of OSL noise is recorded as random fluctuations in signal level and cannot be completely removed. Also present in OSL measurements is an unwanted background component. This can originate from several sources, such as PMT dark count (mainly due to thermionic emission

of electrons), filter breakthrough or proximity to the beta source (see Aitken, 1998, for fuller explanations). Background levels therefore depend on temperature (of the measurement chamber, and the wider surroundings) and optical excitation power/wavelength. Correct measurement and subsequent subtraction of background levels are required, taking these factors into consideration.

Typically background is assumed to be equivalent to the signal from a 'dead' disc recorded under the same conditions as the OSL measurement. The term 'dead' disc refers to an aliquot with grains that have been either heated (to ~700°C) or bleached to empty all the luminescence traps. The background is sensitive to the disc material (either aluminium or stainless steel) so this was kept consistent between OSL and background measurement.

Several background determinations were also performed using a blank disc. Although this would appear not to be as relevant as using a 'dead' disc, in addition to convenience, this was on occasion the only way to ensure that no decay (from OSL components resistant to bleaching/heating) was observed.

A comparison of the backgrounds measured from a dead disc and a blank disc measured on reader R4b is illustrated in Fig. 2.4. No signal decay was observed from the dead disc but the average background level is higher than for the blank disc.

2.6 Error analysis

Error is always present in OSL measurement, a result partly of the inbuilt noise. Therefore, in processing OSL data, either for D_e estimation or experimental investigations, the error on each integrated OSL measurement is given by 'counting statistics' errors assuming Poisson statistics. For example, if X_i is the integrated OSL from the initial part of the decay curve then the range for X_i is given by $X_i \pm \sqrt{X_i}$. For further calculations involving a number of data points the errors on each value are propagated in the standard way to give an uncertainty on the final calculated result:

For a calculated value y, where $y = f(x_1, x_2, x_3 ... x_n)$, and the range of x_i, from its associated uncertainty, is $x_i \pm \sigma_{xi}$, the overall error in y can be calculated through the addition of the partial derivatives of y with respect to each term. This is given by

$$\sigma_y = \sqrt{\sum_i \left(\frac{\partial y}{\partial x} \cdot \sigma_{xi} \right)^2} . \tag{2.1}$$

The range of y is $y \pm \sigma_y$.
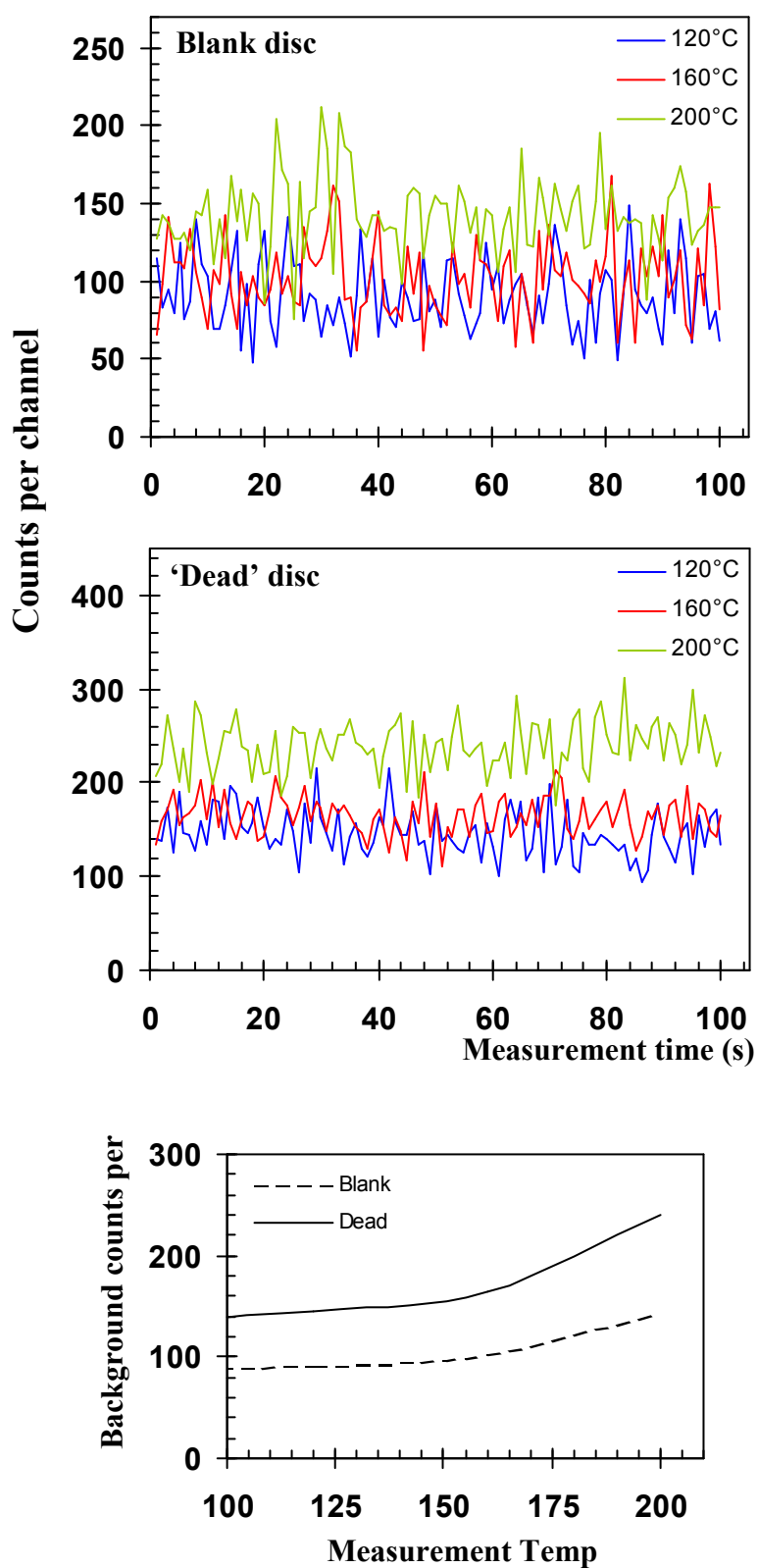
Fig. 2.4 Measurement of background from a blank Al disc (top), and 'dead' disc (middle), from constant power stimulation at various measurement temperatures. The lower plot shows the change in average counts per second with measurement temperature for both blank and 'dead' discs. See section 2.5 for further details.

Error Analysis relevant to dating

Calculated OSL dates depend on the estimate of total absorbed dose (D_e) and the annual dose rate (D_R). Errors are incurred on both of these estimates. This section contains details of how the errors are calculated and combined to give an overall estimate of uncertainty on the estimate of age.

The method of obtaining estimates of D_e using the SAR technique (Murray and Wintle, 2000) is given in section 6.2. The D_e is obtained by interpolating between the points of the dose response curve. Uncertainties are calculated for each of the points included in the dose response, and also on the interpolation.

Each of the points on the growth curve is defined as

$$L(\beta)_i = \frac{X_i - k \cdot x_i}{S_i - k \cdot s_i} \tag{2.2}$$

where X_i is the integrated OSL from the regeneration dose, x_i is the background, S_i is the integrated OSL from the test dose (see section 6.2), s_i is the background and k is a scaling factor. The error on each term is given by counting statistics, and these are propagated, as above, to give the uncertainty on $L(\beta)_i$.

If the dose response can be approximated to a straight line, a weighted least squares linear fit is used for interpolation. In this case the errors are calculated analytically using the standard formula from Green and Margerison (1983). If the dose response is significantly non-linear then, typically, a single saturating exponential function is used. The uncertainty in this case is calculated using a Monte Carlo method (where the dose response data is 'randomised' using normally distributed probabilities and used to obtain a D_e value. The spread in values (the standard deviation) is then used to calculate the error on the mean D_e for each aliquot). For each aliquot (i) measured the range in D_e is given by $D_{ei} \pm \sigma_{Dei}$.

Typically, for a single sample, D_e estimates are obtained for several aliquots (12 aliquots being a common number). The estimates are grouped to give an overall D_e, using a weighted average. Each aliquot D_e is weighted according to the equation,

$$w_i = \frac{1}{\sigma_{Dei}^2} \bigg/ \sum_i \frac{1}{\sigma_{Dei}^2} \tag{2.3}$$

The weighted mean is then given by

$$\overline{D}_e = \sum_i D_{ei} \cdot w_i \tag{2.4}$$

The weighted standard error is defined as

$$\widehat{\sigma}_{\overline{De}} = \sqrt{\frac{\sum_i w_i (D_{ei} - \overline{D}_e)}{1 - \frac{1}{n}}} \Big/ \sqrt{n}$$

(2.5)

where n is the number of aliquots.

The sample age is then estimated by dividing the weighted mean D_e by the dose rate. The error on the final age calculation is found through standard error propagation from the weighted standard error of the D_e (as above) and the dose rate error (uncertainty obtained through combining the errors in U, K and Th concentrations and water content etc.).

Chapter | 3

3 | LINEARLY MODULATED OSL AND DECONVOLUTION

3.1 Introduction

As discussed in Chapter 1, the OSL from quartz is the sum of several components (Bailey *et al.*, 1997; Bulur *et al.*, 2000). This study is primarily concerned with separating and observing the behaviour of the quartz OSL components. For much of the experimental work in this area a technique called linearly modulated OSL, referred to as LM OSL (developed by Bulur, 1996), has been used to record the OSL, rather than standard continuous wave stimulation. The linearly modulated method of optical stimulation produces peak shaped luminescence, as opposed to a monotonically decaying signal, and thus allows greater visual clarification of the components. The concept and theory behind the technique is explained in detail in this chapter.

Deconvolution techniques have been used in conjunction with the LM OSL technique to identify the components. The methods of deconvolution undertaken are also described in this chapter. Their reliability and limits have been investigated. The results of these investigations are summarized.

3.2 LM-OSL: concepts and theory

3.2.1 Comparison of CW and LM measurement techniques

Continuous wave (CW) OSL, as introduced by Huntley *et al.* (1985) is measured using constant power, constant temperature and constant stimulation wavelength. Attempts to categorize the CW OSL signal of quartz in terms of kinetic order and number of components has been undertaken by several authors (e.g. Huntley *et al.*, 1996; Smith and Rhodes, 1994). Bailey *et al.*, (1997) successfully fitted quartz CW OSL decays, measured at raised temperature, to the sum of three first order exponential components. These they called the fast, medium and slow components, according to their relative decay rates.

Fig. 3.1 shows an example of a CW OSL decay from quartz sample TQN. When CW OSL is measured at raised temperature (160°C in this case) there is a rapid initial decay, which according to Bailey *et al.* (1997) is composed of the fast and medium components, followed by a small, very slowly decaying portion (the 'slow' component). Quartz experimental decay

curves can often be well approximated by the sum of several exponential curves, suggesting that several first order components are superimposed. However, retrapping and other non-first order interactions can produce similar non-exponential decay forms, and the lack of structure in the monotonically decaying signal may lead to ambiguity in interpretation. Although Bailey *et al.*, (1997) produced substantial experimental evidence to support their hypothesis there was initially some opposition to their findings.

The method of LM-OSL involves linearly increasing the power (photon flux) of the stimulation source during the measurement, resulting in OSL in the form of peaks (see quartz example Fig. 3.1). Similar to CW OSL, the shape of the OSL (peak) depends on the order of kinetics. Only multiple trap contributions result in multiple peaks present in the LM OSL (retrapping will have the effect of modifying the peak shape rather than inducing extra LM OSL peaks), thereby allowing the determination of the number of constituent signals more easily than using conventional CW OSL. Bulur *et al.* (2000) observed that the LM OSL from quartz stimulated at 470nm produced multiple, overlapping peaks. Using this technique, the fast and slow component peaks were clearly identifiable, verifying the multi-trap hypothesis of Bailey *et al.* (1997). Using curve-fitting routines, an additional fourth OSL component was also identified for the sample investigated. Fig. 3.1 shows a comparison between recorded CW and LM OSL for sample TQN. The LM-OSL recorded has multiple peaks and shows more clearly than CW OSL that there are multiple trapping states represented. In the case of simple first-order kinetics, the position of the peak is dependent on the photo-ionisation cross-section of the trap. Trapping states that have peak positions at shorter times have larger photo-ionisation cross-sections (i.e. detrapping probability) and are easier to bleach than those with peak positions at longer times (see section 3.2.2 for the equations describing LM-OSL peak position, t_{max}). One may then immediately get a sense of the relative detrapping rates of the different components using the linear modulation technique. The use of LM OSL under a variety of measurement conditions and pre-treatments has allowed greater understanding of the OSL components from deconvolution and visual analysis of the data. This is explored further in subsequent chapters.
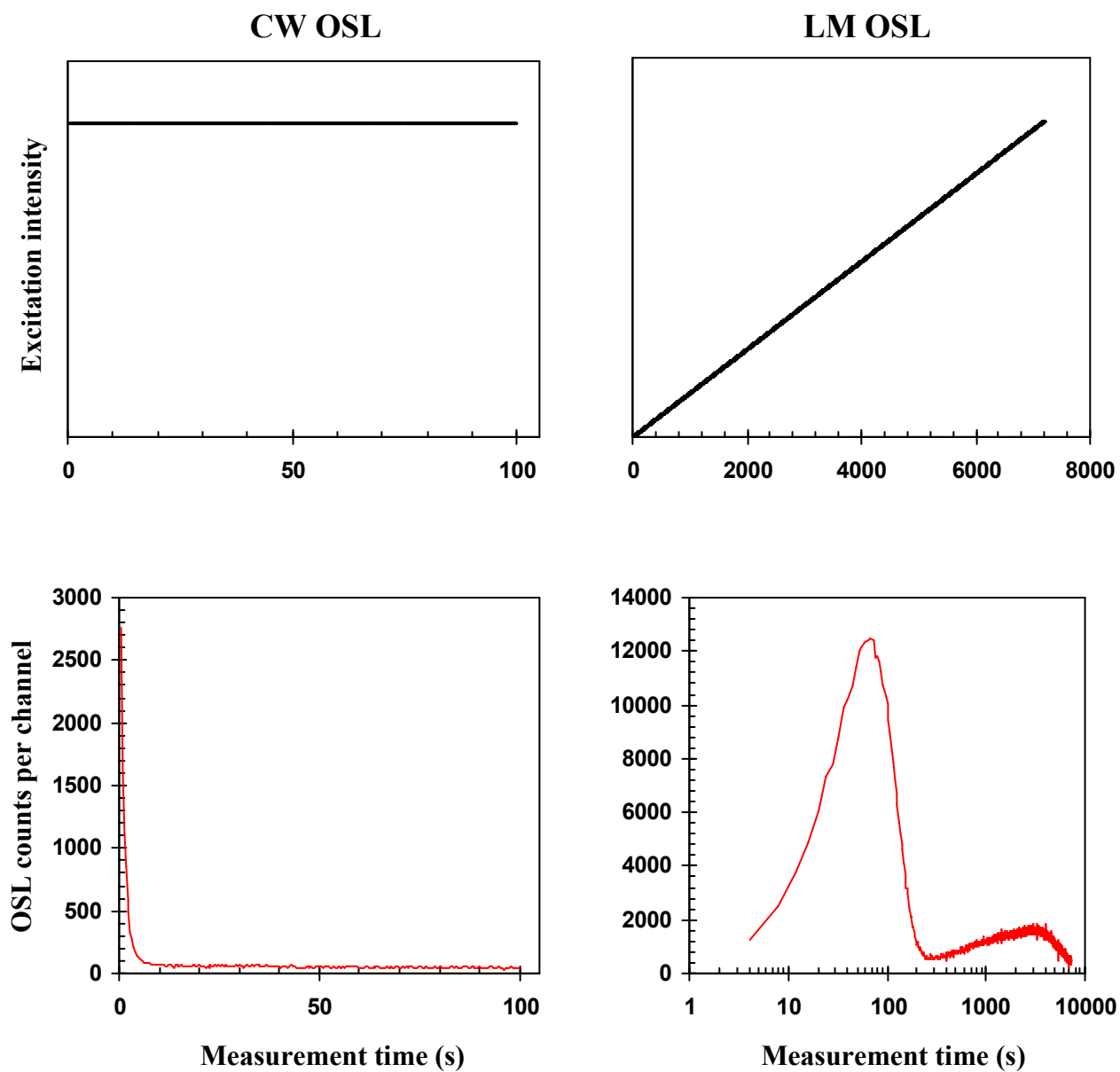
CW OSL

LM OSL

Fig 3.1 Example quartz CW and LM OSL curves, from sample TQN given a 20Gy beta dose, preheat to 260°C and OSL stimulation at 470nm, 160°C.

3.2.2 Analytical solutions: CW and LM-OSL

The analytical solutions for CW OSL and LM OSL can be derived using simplifying assumptions, which depend on the assumed order of kinetics.

First order kinetics

For the first order model, it is assumed that once an electron is freed from its trap the probability of it returning (retrapping) to the trap is much less than the probability of it recombining at *m* (see Figure 3.2a) (Randall and Wilkins, 1945). Thus, instantaneous luminescence emission, *I(t)*, is proportional to the rate of release of electrons:

$$I(t) = -\frac{dn}{dt} = fn \qquad (3.1)$$

where n is the concentration of trapped electrons. The rate of change of n is fn, where f is the decay constant of the trap. It is assumed that the number of electrons in the conduction band is always negligible compared with those trapped, i.e. time spent in the conduction band is short, and $\frac{dn}{dt}, \frac{dm}{dt} >> \frac{dn_C}{dt}$, i.e. quasi-equilibrium.

By rearranging Equation 3.1, and integrating both sides (Equation 3.2), an expression for $n(t)$, the concentration of trapped charge through time (Equation 3.4) can be found, given a constant stimulation photon flux (as for CW-OSL):

$$\int_{n_0}^{n} \frac{dn}{n} = \int_{0}^{t} -fdt \qquad (3.2)$$

$$n(t) = n_0 \exp(-ft) \qquad (3.3)$$

By again using the Equation 3.1, the analytical solution for $I_{CW}(t)$ is:

$$I_{CW}(t) = fn = fn_0 \exp(-ft) \qquad (3.4)$$

where n_0 is the concentration of trapped charge at $t = 0$.

To find an expression for first order LM OSL intensity, $I_{LM}(t)$, the assumption that intensity is proportional to the rate of release of electrons again applies (Equation 3.1). For the duration of a CW-OSL measurement the photon flux remains at a constant level, however during LM-OSL it is linearly increased from zero to a maximum preset value. Consequently, the decay constant will vary during LM OSL measurement, as it has a dependence on the stimulation photon flux.
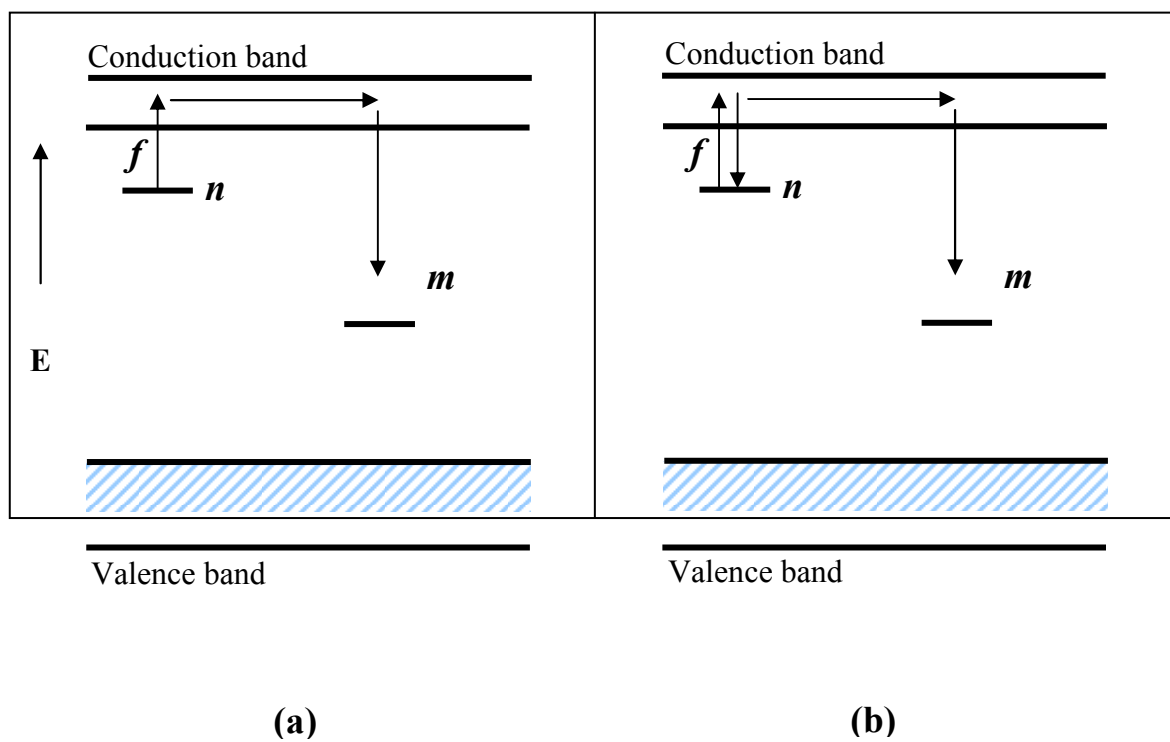
Fig 3.2 Energy transitions involved in the production of (a) first order OSL (b) second/general order OSL.

The form of the dependence is given in equation 3.5.

$$f(P) = \sigma P(t) \tag{3.5}$$

Here $P(t)$ is the photon flux of the stimulating source, and σ is the photo-ionisation cross-section of the trap.

A linear ramp $P(t)$ can be described by,

$$P(t) = \frac{dP}{dt} t = \frac{P_0}{t_{max}} t \tag{3.6}$$

Here, P_0 is the maximum stimulation intensity and t_{max} is the total measurement time (see Fig. 3.3a). By substituting equations 3.5 and 3.6 into 3.1 one obtains

$$\frac{dn}{dt} = \frac{-\sigma P_0 t}{t_{max}} n \tag{3.7}$$

Using the same derivation procedure described by equations 3.2 to 3.4 an analytical solution for $I_{LM}(t)$ from a single trapping state can be found from 3.7.

$$I_{LM}(t) = n_0 \frac{\sigma P_0 t}{t_{max}} \exp\left(-\frac{\sigma P_0 t^2}{2t_{max}}\right) \tag{3.8}$$

Fig. 3.3b illustrates the form of the LM OSL from first (and also second and third) order kinetics using computer simulations. The rate of release of electrons increases as the light-source intensity increases, resulting in an increase of the amount of luminescence produced. After reaching a maximum intensity, the luminescence decreases as the concentration of trapped electrons is reduced. The equations derived here all assume there is a single photon dependence on detrapping, as found for quartz by e.g. Spooner (1994).

For a single first order peak, taking the time derivative and setting this to zero results in the following equation for t_{peak}, peak position, and subsequently I_{peak}, peak maximum.

$$t_{peak} = \sqrt{\frac{t_{max}}{\sigma P_0}} \tag{3.9}$$

$$I_{peak} = \frac{n_0}{t_{peak}} \exp\left(-\frac{1}{2}\right) \tag{3.10}$$

Equations 3.9 and 3.10 could theoretically be used to determine the trap parameters, n_0 and σ, without the need for integration or curve fitting, provided one could be sure that the measured OSL derives from a single or well-separated trap of definite known order. This, however, may prove to be very difficult in real terms for most luminescent minerals.
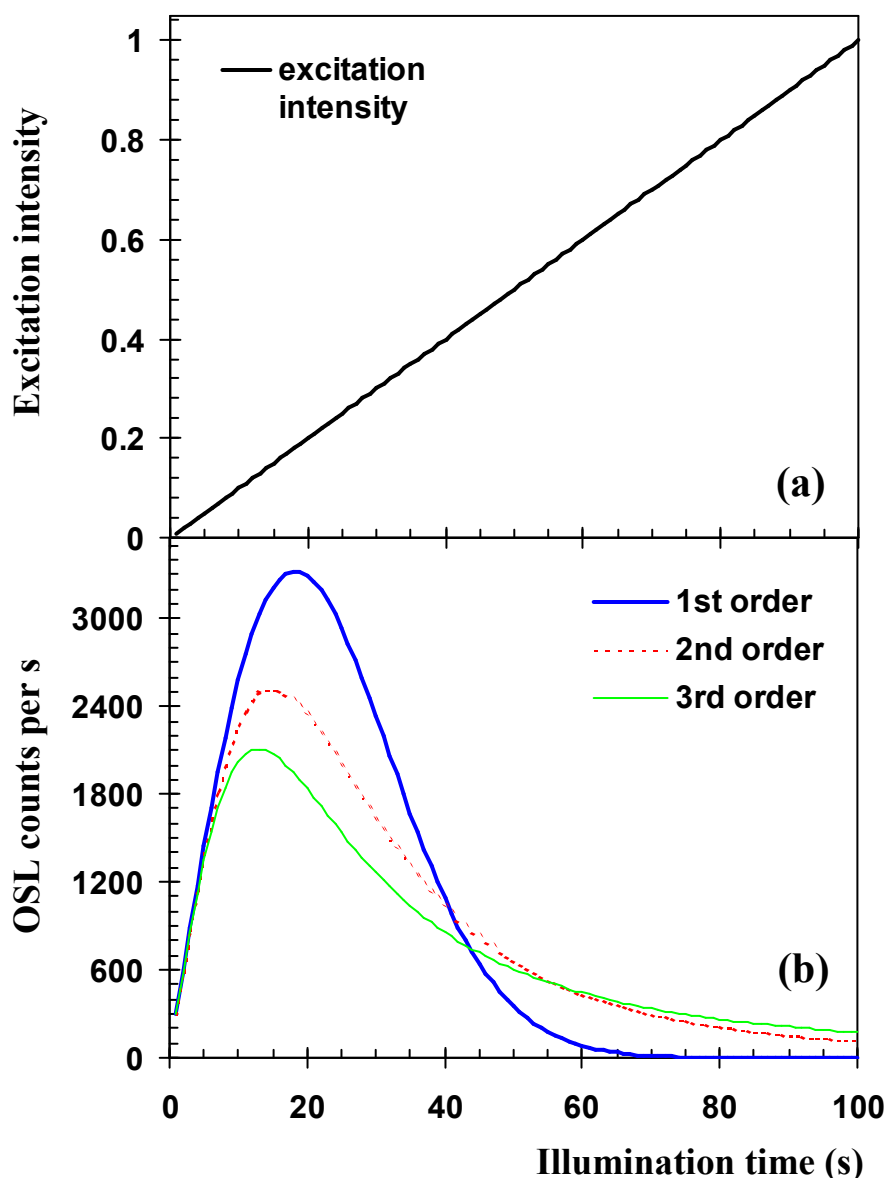
Fig. 3.3 (a) Simulated excitation intensity ramp used for (b) computer simulations of LM OSL peaks of different kinetic orders. See section 3.2.2 text for further details.

For the case of multiple components contributing to LM OSL, if all are first order, the contributions of all contributing states, i, can be summed in the following way:

$$I_{LM}(t) = \sum_i n_{0i} \frac{\sigma_i P_0}{t_{max}} t \exp\left(-\frac{\sigma_i P_0 t^2}{2t_{max}}\right) \tag{3.11}$$

These equations are used in the deconvolution techniques outlined in further sections to separate overlapping LM OSL components.

General order

For the general order model the probability of charge retrapping before recombination is taken into account. The general order model was first introduced by May and Partridge (1964) to describe TL glow curves that did not conform to either first or second order shapes. The equation 3.1, used to derive the first order solutions, is not applicable in this case. The change in trapped electrons for the general order model, as given in Bulur (1996), is given by

$$\frac{dn}{dt} = -\frac{f}{n_0^{b-1}} n^b \tag{3.12}$$

where b, the kinetic order, is a dimensionless positive real number, $b > 1$, and $f = \sigma P_0$.

Using the same method of derivation as for first order kinetics the solution for general order OSL decay can be described by:

$$I_{CW}(t) = n_0 \sigma P_0 [(b-1)\sigma P_0 t + 1]^{b/(1-b)} \tag{3.13}$$

For LM OSL, assuming the same linear ramp as for the first order model, equations 3.5 and 3.6 are used in conjunction with equation 3.12 to find the following expression.

$$\frac{dn}{dt} = \frac{\sigma P_0 t}{t_{max} n_0^{b-1}} n^b \tag{3.14}$$

Again using $I_{LM}(t) = -dn/dt$ one can derive a solution for $I_{LM}(t)$:

$$I_{LM}(t) = n_0 \frac{\sigma P_0 t}{t_{max}} \left[(b-1)\frac{\sigma P_0 t^2}{2t_{max}} + 1\right]^{b/(1-b)} \tag{3.15}$$

Equations describing peak position, t_{peak}, and peak maximum, I_{peak}, for the general order case can be found in Table 3.1.

Second order

Second order kinetics is a subset of the general order case where the probability of retrapping is equal to the probability of recombination. Solutions can be found by allowing b to equal 2 in equations 3.13 (CW OSL) and 3.15 (LM OSL) giving:

$$I_{CW}(t) = \frac{n_0 \sigma P_0}{(1 + \sigma P_0 t)^2} \tag{3.16}$$

$$I_{LM}(t) = \frac{n_0 \dfrac{\sigma P_0 t}{t_{max}}}{(1 + \dfrac{\sigma P_0 t^2}{2t_{max}})^2} \tag{3.17}$$

The LM OSL parameters, t_{peak} and I_{peak} for this second order model can be found in Table 3.1 also.

[Note: As discussed in Bailey *et al.* (1997) even if retrapping does occur this does not necessarily result in $b > 1$. If the pathways available to released charge remain constant then first order OSL may be expected. For further details see section 4.2.]

As noted by Bulur and Göksu (1999), the equations describing CW and LM OSL given above taken from Bulur (1996) were derived for the specific condition of a saturated trap, i.e. $n_0 = N$. As a result there is not the dependence on the peak position, t_{peak}, on trapped charge concentration that is expected. Therefore modified equations have been derived for the more generalised situation. This does not affect the first order case since there is no dependence on the form of the OSL on trapped charge concentration. For the general order case the starting point, as empirically derived by Rasheedy (1993), is:

$$\frac{dn}{dt} = \frac{f}{RN^{b-1}} n^b \tag{3.18}$$

where $f (= \sigma P)$, n and b have the same meaning as before. N is the concentration of traps and $R (= A_n/A_m)$ is the ratio of trapping probabilities of the trap (A_n) and the luminescence centre (A_m). Using the same methods as before and assuming constant stimulation intensity (CW OSL) an equation for trapped charge concentration can be obtained:

$$n = n_0 \left[\frac{(b-1)\sigma P_0 t n_0^{b-1}}{RN^{b-1}} + 1 \right]^{\frac{1}{1-b}} \tag{3.19}$$

Combining equations 3.18 and 3.19 gives the solution for CW OSL

$$I_{CW}(t) = \frac{\sigma P_0}{RN^{b-1}} n_0^b \left[\frac{(b-1)\sigma P_0 t n_0^{b-1}}{RN^{b-1}} + 1 \right]^{\frac{b}{1-b}} \tag{3.20}$$

	First order	General order	Second order
$I_{CW}(t)$	$I_{CW}(t) = n_0\sigma P_0 \exp(-\sigma P_0 t)$	$I_{CW}(t) = n_0\sigma P_0 \left[(b-1)\sigma P_0 t + 1\right]^{b/(1-b)}$	$I_{CW}(t) = \dfrac{n_0\sigma P_0}{(1+\sigma P_0 t)^2}$
$I_{LM}(t)$	$I_{LM}(t) = n_0 \dfrac{\sigma P_0 t}{t_{max}} \exp\left(-\dfrac{\sigma P_0 t^2}{2t_{max}}\right)$	$I_{LM}(t) = n_0 \dfrac{\sigma P_0 t}{t_{max}} \left[(b-1)\dfrac{\sigma P_0 t^2}{2t_{max}}+1\right]^{b/(1-b)}$	$I_{LM}(t) = \dfrac{n_0 \dfrac{\sigma P_0 t}{t_{max}}}{(1+\dfrac{\sigma P_0 t^2}{2t_{max}})^2}$
t_{peak}	$t_{peak} = \sqrt{\dfrac{t_{max}}{\sigma P_0}}$	$t_{peak} = \sqrt{\dfrac{2t_{max}}{\sigma P_0(b+1)}}$	$t_{peak} = \sqrt{\dfrac{2t_{max}}{3\sigma P_0}}$
I_{peak}	$I_{peak} = \dfrac{n_0}{t_{peak}} \exp\left(-\dfrac{1}{2}\right)$	$I_{peak} = \dfrac{2n_0}{(b+1)t_{peak}}\left(\dfrac{2b}{b+1}\right)^{b/(1-b)}$	$I_{peak} = \dfrac{3}{8}\dfrac{n_0}{t_{peak}}$

Table 3.1 Analytical solutions describing CW and LM OSL for various kinetic orders, as derived by Bulur (1996). Solutions to the LM OSL peak position, t_{peak}, and peak maximum, I_{peak}, are shown also.

If non-constant excitation intensity is used (i.e. LM OSL) then the following starting equation applies:

$$\frac{dn}{dt} = \frac{\sigma P_0 t}{t_{max} R N^{b-1}} n^b \tag{3.21}$$

where all parameters have the same meanings as noted previously. Working through in a similar fashion gives the following equation for linearly modulated OSL intensity:

$$I_{LM}(t) = \frac{\sigma P_0 t}{t_{max} R N^{b-1}} n_0^b \left[\frac{(b-1)\sigma P_0 t^2 n_0^{b-1}}{2 t_{max} R N^{b-1}} + 1 \right]^{b/1-b} \tag{3.22}$$

From this the peak position, t_{peak}, and peak maximum, I_{peak} are, as given in Bulur and Göksu (1999):

$$t_{peak} = \sqrt{\frac{2 t_{max} R N^{b-1}}{(b+1)\sigma P_0 n_0^{b-1}}} \tag{3.23}$$

$$I_{peak} = \frac{2 n_0}{(b+1)} \frac{1}{t_{peak}} \left[\frac{2b}{b+1} \right]^{b/1-b} \tag{3.24}$$

These equations for $I_{CW}(t)$ and $I_{LM}(t)$ have the same form as the equations derived by Bulur (1996), but importantly there is a dependence of the peak position on the initial charge concentration in the modified equations that is expected from a non-first order system. See section 4.2, Figs 4.1 and 4.2, for graphical illustrations and further discussion of this.

3.2.3 Factors affecting photoionization cross-section

The photoionization cross-section, σ, of a trapping state has a dependence on the incident photon energy/wavelength (e.g. Spooner, 1994). While this may be less important for OSL from a single trapping state, in the case where multiple traps are contributing the wavelength dependence (i.e. photoionization spectra) of each trap type may be different. Therefore the choice of wavelength will determine the form of the overall OSL signal. OSL data obtained at one particular wavelength may be more easily interpreted than at others due to the relative difference in photoionization cross-section producing better-resolved component peaks (Whitley, 2000). This can be a useful, or even critical, factor to consider in order to correctly interpret data (in terms of e.g. number of constituent traps). In this case, LM OSL will also certainly be easier to interpret than will equivalent CW OSL measurements made at the same wavelengths. Optical cross-section spectra have been calculated for quartz LM OSL (Singarayer and Bailey, 2002). A full discussion of the theory and empirical results are presented in section 5.3.1.

Optical transitions between bound states of defects in quartz (and in most solids) may involve absorption and emission of phonons (Stoneham, 1979), the quantised vibrational energy associated with heat. In this case the electron-phonon coupling results in the modification of the photoionization spectra, especially for deep defects (Stoneham, 1979). In addition, because of electron-phonon coupling the optical eviction of charge from OSL traps can be achieved at lower photon energies than expected, i.e. coupling has the effect of broadening the photo-ionisation spectra. This broadening effect is also discussed for quartz OSL in section 5.3.1. The theory has been well studied for semiconductors (e.g. Noras, 1980; Stoneham, 1979). An increase in measurement temperature of LM OSL results in an increase in the rate of optical eviction of charge, i.e. LM OSL peak position at increasingly shorter times. This is the well-studied mechanism of 'thermal assistance'. Spooner (1994) observed that thermal assistance of the quartz OSL signal could be described by an Arrhenius equation, with activation energy that depended on stimulation wavelength.

3.2.4 Other forms of modulation

As outlined in the sub-section above the choice of stimulating wavelength could assist with separating the different components. Another possibly useful variant is the ramping function used. It is theoretically viable to use ramping functions other than linear to obtain peak-shaped OSL although not possible using the current experimental set-up (see chapter 2 for details of apparatus). For example, a quadratic or exponential function could be used. In the case of quartz, this would not have the effect of allowing greater separation of overlapping components, as would be achieved via stimulating at different wavelengths (section 3.2.3) since all components have been found to have a similar linear dependences of intensity on power (see section 5.3.3). However, it could, depending on the relative photo-ionisation cross-sections of the contributing components, allow better resolution of the components over the data collection channels.

As long as the form of the ramp can be described mathematically, analytical solutions for the OSL produced can be derived by simply replacing equation 3.6 with an appropriate equation to describe the relation between P and t, and substituting this into the relevant equations.

Fig. 3.4 shows computer simulated OSL produced using various ramping functions. The OSL comprised four first order components, of similar cross-sections and magnitude as fitted to experimental quartz LM OSL. The standard linear ramp is shown, and compared to quadratic and saturating exponential ramps, all up to the same maximum stimulation intensity (Fig. 3.5a), and constant power is shown. For the relative cross-sections of the OSL components,

the exponential ramp allows the measurement of more of the slowest component than the other ramping functions (as the total incident power is greater). The quadratic ramp allows better distribution of the peak positions in time to get good resolution in all the components. However, none of these alternatives was available at the time. Therefore, most measurements have been performed using a linear ramp or at constant power (see section 3.4 for details).
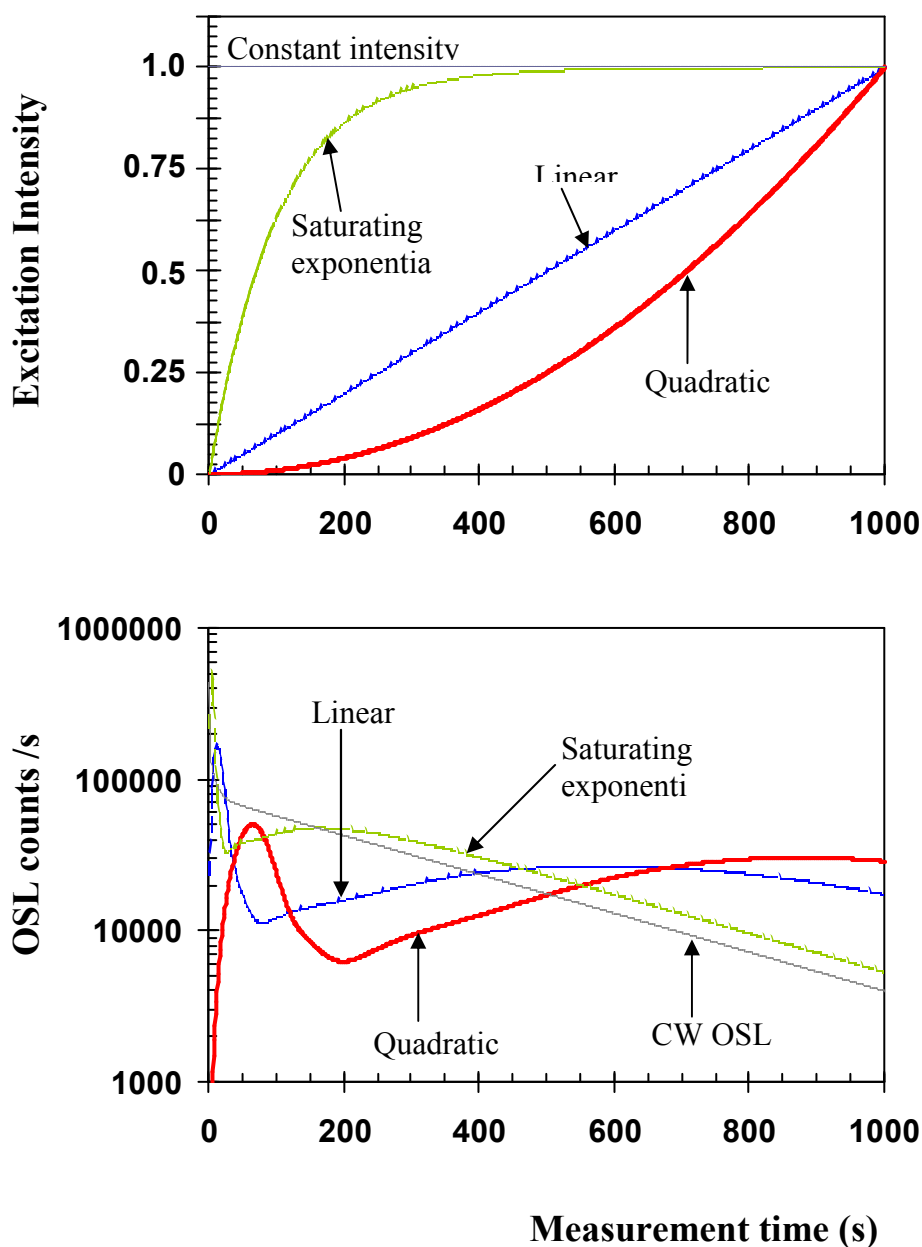
Fig. 3.4 (a) Various simulated stimulation ramping functions (constant power, linear, quadratic, saturating exponential) were used to calculate simulated ramped OSL (b) from four contributing trapping states.
[Relative cross-sections − 1:0.2:0.15:0.00037, Magnitudes − 2750000:850000:700000:26000000]

3.3 Review of previous studies using LM OSL

Bulur (1996) first introduced the technique of linearly modulated OSL as a potential method for obtaining OSL trap parameters without the need for complex data analysis. He derived the equations governing LM-OSL for first, second and general order kinetics using a single trap model (as described in section 3.2.2) and obtained preliminary experimental results for potassium feldspar grains using linearly modulated infrared stimulation (LM-IRSL).

Since then, LM-OSL from various minerals has been observed (e.g. see Bulur and Göksu, 1997) for ZnS and SrS LM-IRSL, Bulur and Göksu (1999) for K and Na feldspars LM-IRSL). However, in view of the fact that quartz is one of the most widely used materials for luminescence dating and dosimetry, most recent LM studies have typically used thermally annealed quartz samples under blue light stimulation.

Bøtter-Jensen *et al*. (1999) reported that the LM-OSL signal from quartz consisted of an initial sharp peak followed by an increasing tail. Bulur *et al*. (2000) performed a more detailed study using higher stimulation powers (20mWcm^{-2}) and longer measurement times. This allowed them to see a second broad peak in the LM-OSL of slowly depleting component(s). Through a series of thermal stability and dose response experiments, in conjunction with curve fitting studies, they showed that the LM-OSL curve from quartz at raised temperature could be approximated to the sum of four first-order components with photo-ionisation cross-sections ranging over several orders of magnitude. From measurements at various temperatures, they also determined an intermediate OSL component, and identified it as originating from the 110°C TL peak. In contradiction to work done by Bailey (2000a) on a very thermally stable slow component, all the OSL components were found to be completely eroded by heating to >480°C. The dose response of each component was determined for a single heated sample. The results, in agreement with experiments done using CW-OSL (Bailey, 2000a; Singarayer *et al*., 2000), showed that the slower components had higher dose responses than the first, indicating the potential for using these components for dating samples older than possible using conventional luminescence dating, as Bailey (2000a) suggested.

One of the basic requirements for reliable dating of sedimentary materials is the complete zeroing of the OSL signal before deposition. Following incomplete resetting, a residual signal, most likely of unknown size, remains leading to an overestimate of the most recent burial period. Agersnap Larsen *et al*. (2000) recognised that LM-OSL may be a useful tool for identifying partial bleaching of sediments. They presented a study that assessed the effect of partial bleaching on the form of the linearly modulated OSL signal from previously heated

quartz. In this case, the partial bleaching was performed under controlled laboratory conditions using the same blue light stimulation. They fitted their LM curves, measured at 160°C, to three components, characterised by photo-ionisation cross-sections of $\sigma = 9.0 \times 10^{-17}$ cm^{-2}, $\sigma = 6.0 \times 10^{-19}$cm^{-2}, and $\sigma = 4.2 \times 10^{-20}$ cm^{-2} (similar values were obtained for sedimentary quartz by Kuhns *et al.*, 2000). In simulating known 'natural' (with various degrees of previous partial bleaching) and 'regenerated' doses, Agersnap Larsen *et al.* (2000) were able to identify partial bleaching by taking a ratio of the natural and regenerated LM curve data points. They also state that identification was more obvious, and hence advantageous, using LM-OSL than when the experiment was repeated using CW-OSL, as regions corresponding to the different traps were more distinct from the LM OSL measurements. The applicability of this method to a real dating scenario depends on many factors including the unknown size of the natural burial dose and the dose response of the different components. They also found, as expected, that for blue light stimulation the easy-to-bleach components were well zeroed in as short exposures as 10s at 160°C (20mWcm^{-2} CW-OSL), whereas the slower component required more than 1000s.

An extensive study, this time on natural sedimentary quartz samples, looking at zeroing of modern deposits was undertaken by Singarayer *et al.* (2002a). LM OSL was used in conjunction with SAR $D_e(t)$ plots (Similar to the better known 'shine plateau'; explained in detail in section 7.2.2 and Bailey, 2002b) to successfully identify young partially bleached sediments. The details of the study are presented in Chapter 7.

More recently, developments in luminescence technology have allowed the measurement of LM-OSL from single grains (Bulur *et al.*, 2002). CW-OSL measurements made on single quartz grains showed enormous variability in brightness and dose response characteristics (e.g. Duller *et al.*, 2000). Bulur *et al.* (2002) performed LM-OSL on 81 quartz grains. In this preliminary survey they found not only this variation in brightness, but in the relative proportion of OSL components (supporting previous findings of Adamiec, 2000a and 2002b). Some grains showed only a sharp initial peak, corresponding to easy-to-bleach components. Others showed only a hard-to-bleach component, and some a combination of all. Given the heterogeneity of the OSL traps, linear modulation of single grains may help to provide new insights into quartz luminescence properties. At present, however, only this preliminary study has been completed.

The linear modulation technique was initially slow to be used in luminescence dating research. It is now being increasingly used in a variety of diagnostic studies and is potentially a very useful tool especially in the areas of partial bleaching and thermal transfer (Watanuki,

2002). However, not many detailed studies have yet been published on quartz assessing more completely the behaviour of the OSL components.

3.4 Measurement of LM OSL

Risø readers R4a and R4b (as described in section 2.4.1), incorporated an automated ramping system for recording LM OSL. The details of the measurement system used are outlined in section 2.4.1. The linearity of the ramp was checked directly by replacing the emission filters with neutral density filters (Hoya ND0 + 3× Schott NG9) to reduce the light intensity to a suitable level and using the PMT to record reflected excitation light off a blank aluminium disc. Measurements were obtained over a number of different illumination times and temperatures, each time ramping between 0 and 90% (of full power, $18mWcm^{-2}$). The results in Fig. 3.5 illustrate that the output from reader R4a, used for many of the early measurements for this thesis, was non-linear in all cases. Such non-linearity will clearly affect the shape of the measured LM OSL, the severity of which depends on the extent of the non-linearity and the position of the OSL peaks.

Two aspects of the measurements on R4a required attention. Firstly, there were a number of dead channels (where the excitation intensity is (close to) zero, so only background levels were recorded) at the beginning of the measurement (see Fig. 3.5, insets). The number of dead channels depended on the total measurement time and the total number of channels, and occurred below a preset power threshold, set by a potentiometer within the system (to ensure that LEDs are not emitting at a low light level when not in use). These channels were simply deleted from any resulting data before any analysis was made. It would also have been possible to adjust the potentiometer to reduce the number but this was not undertaken for this study.

Secondly, the excitation intensity, although reproducible, did not ramp linearly through time, as illustrated by Fig. 3.6a, where the 7200s ramp has been fitted (unsuccessfully) to a linear function. The ramp was consistent at measurement temperatures between 20 and 250°C (see Fig 3.6b). The non-linearity results apparently from the method of signal intensity feedback built-in to the Risø reader. In each array of blue LEDs (see Fig.2.2) a single LED faces away from the sample chamber towards a detecting photodiode. The intensity from the backward-facing LED is used as feedback to achieve linearization of the ramp, assuming that the intensity is representative of the LED array as a whole. However, for the excitation unit R4a used for a considerable number of experiments in this study this proved not to be the case, hence, the significant non-linearity observed.
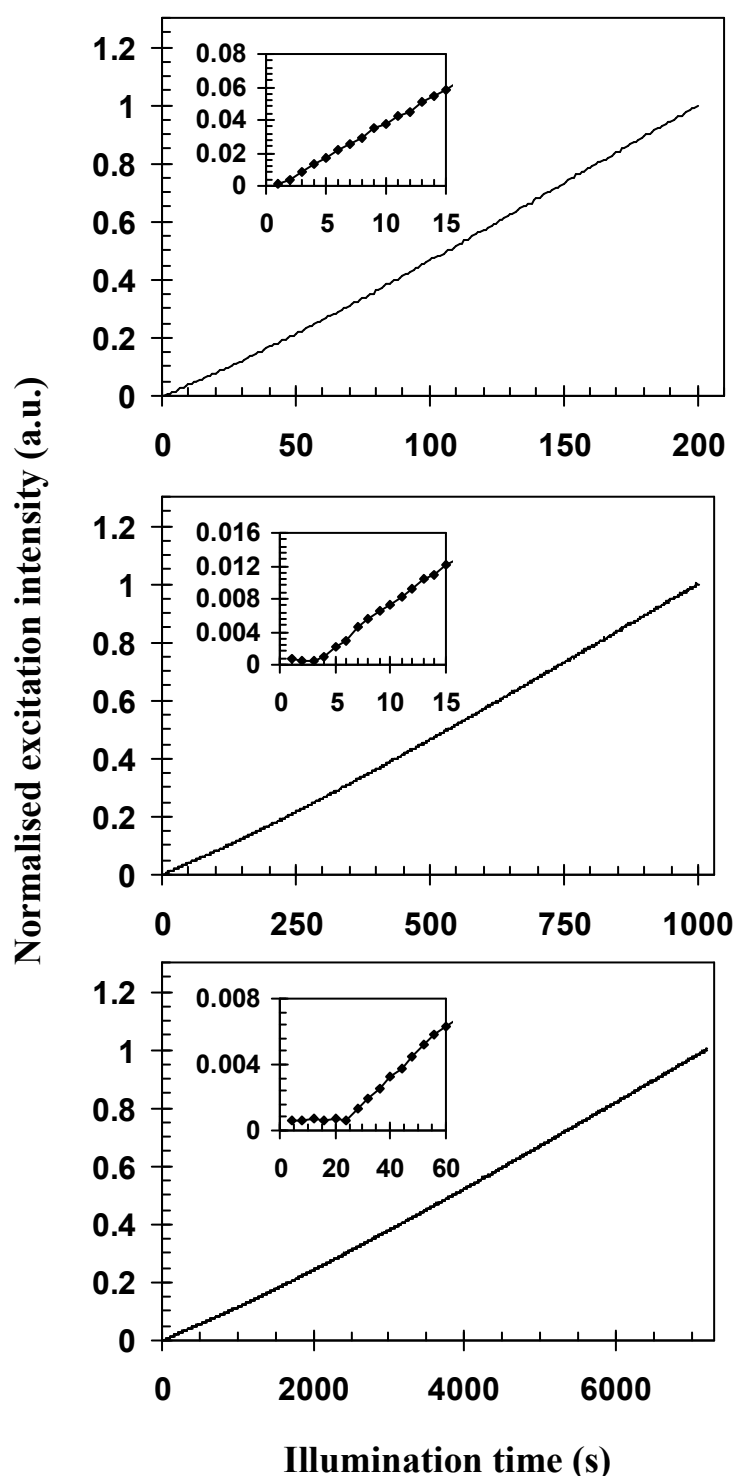
Fig. 3.5 Measurements of linearly modulated excitation intensity from 0 to ~18Wcm^{-2} over 200s (top), 1000s (middle) and 7200s (lower). Maximum signal intensity has been normalised to 1. Insets show in detail the form of the ramp over the first channels.
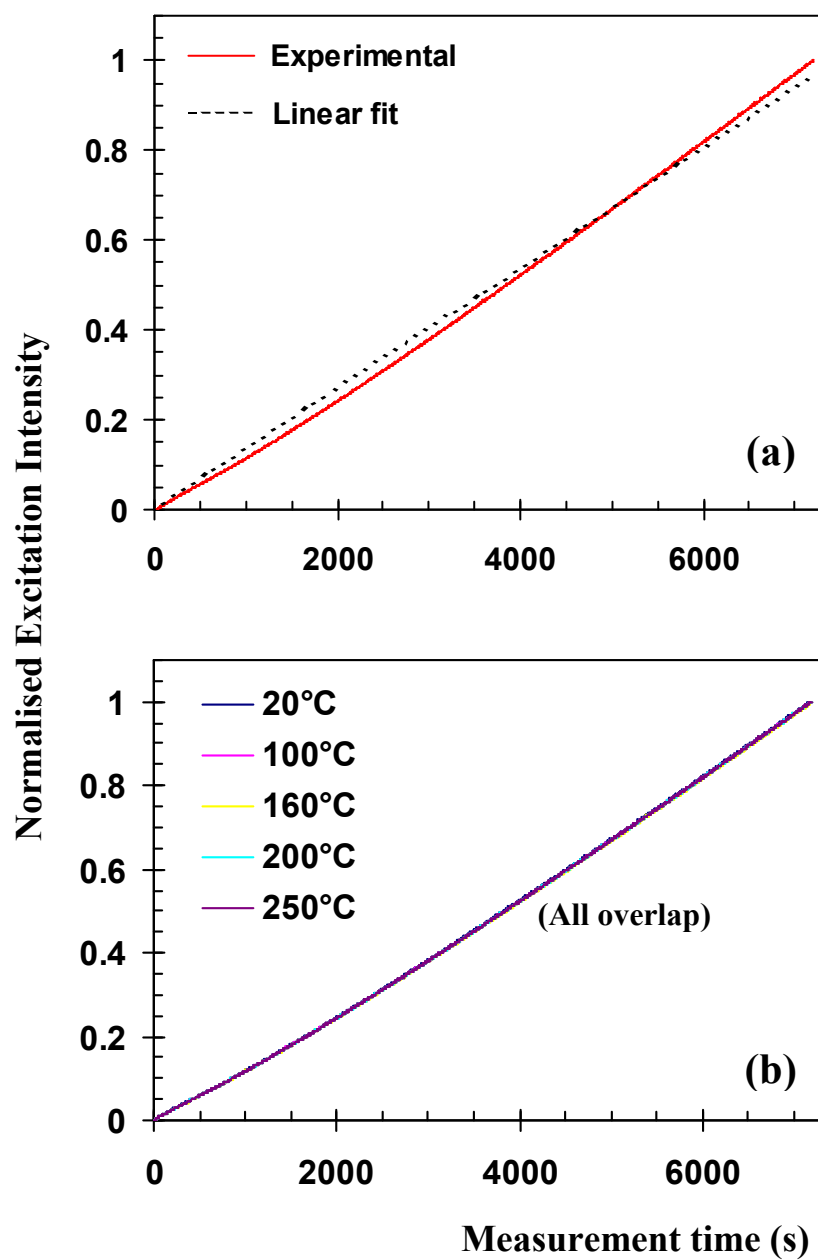
Fig. 3.6 (a) Ramped excitation light intensity vs. time, fitted to a linear function. (b) Comparison of the shape of the ramped excitation intensity measured at various temperatures.

3.4.1 Solutions for non-linear ramping

The analytical solutions to describe $I_{LM}(t)$ (section 3.2.2) are derived using a linear expression for the stimulation light intensity ramp. These equations were used in the deconvolution of experimental LM OSL curves to separate the contributing components (section 3.5). Unfortunately, the ramp of the Risø reader was sufficiently supra-linear to cause severe problems with fitting procedures (i.e. with the introduction of extra components, or ill-fitting results) without some modification. Several methods to try to circumvent this problem were tried with varying degrees of success as described below.

One approach used was to measure the OSL using constant stimulation intensity (CW OSL). The OSL decay curves can be transformed mathematically into the form that would be obtained using the linearly modulated technique. The transformation was first derived by Bulur (2000) and applied successfully to IRSL and green-stimulated OSL decays from K and Na feldspar samples. To convert a CW OSL curve into an LM OSL curve a new variable, $u(t)$, is introduced, defined as

$$u(t) = \sqrt{2tt_{max}} \tag{3.25}$$

where t is time in seconds and t_{max} is the total LM measurement time (this can be any value, but $t_{max} = 2t_{CW}$, where t_{CW} is the total CW measurement time, has been chosen here to equate the total incident light energy of CW and LM OSL). Then LM intensity is given by

$$I_{LM} = \frac{I_{CW}u(t)}{t_{max}} \tag{3.26}$$

By plotting I_{LM} vs. $u(t)$ one obtains the same form as experimentally recorded LM OSL curves. This transformation can be applied to convert first, second and general order kinetic OSL decays, provided the mechanism of the detrapping of charge is independent of stimulation power and the response is linear (as found by Spooner, 1994 and Bulur *et al.*, 2001b for quartz). This method can take advantage of the greater signal stability of CW OSL measurements and allows the transformed 'pseudo-LM OSL' to be fitted to derived solutions describing LM OSL.

Fig. 3.7 shows a comparison between transformed and experimental LM OSL for sample Van 2 that has been given a 20Gy dose and preheated to 260°C. There is good agreement between the actual and pseudo-LM curves, implying that the transformation is a valid approximation in this case. Similar comparisons have been made using several other samples and the same level of agreement obtained indicating that the assumptions made are appropriate.
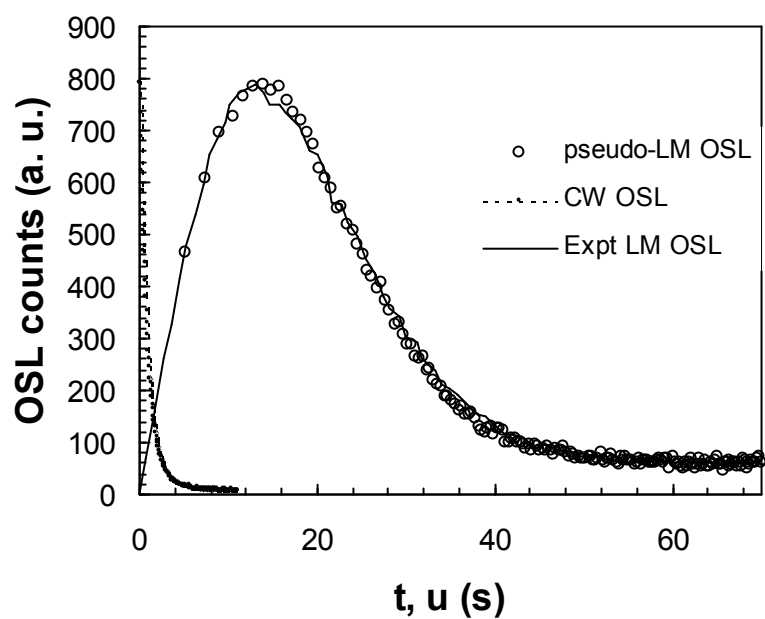
Fig 3.7 Comparison of experimental LM OSL and transformed 'pseudo' LM OSL for sample Van2 (given 20Gy dose and preheat to 260°C. OSL measured at 160°C). The experiment was performed at the Risø National Laboratory on a reader with a known linear ramp. The CW OSL used for the transformation is represented also.

The transformation has been used for a number of short LM OSL measurements made, in order to circumvent the non-linearity problem. However, where long measurements were required to observe all the quartz OSL components, due to the spread in peak position between the faster and slower components (over 3 orders of magnitude) and the maximum number of constant width data channels available (2000), sufficient resolution over the initial portion of the decay could not be obtained to make mathematical transformation a viable option (which could potentially be solved by introducing variable channel width measurement). In these cases, other methods had to be tried to solve the problem.

The mathematical transformation method involves modifying the way that the OSL is measured in order to solve the problem. Another way to solve the same problem entailed empirically measuring the LM OSL and subsequently accounting for the non-linear ramp in the fitting routine. This was attempted by two means. For both of these, the ramp excitation intensity was measured directly (using the procedure outlined at the beginning of section 3.4) under the same conditions as the LM OSL would be measured using (e.g. same measurement time, number of channels etc.). Then for the first method, the recorded ramp was then fitted to the most appropriate function that could describe the shape. In the case of Fig 3.8a, it was found that a reasonable fit could be obtained using a second order polynomial. The expression describing the ramp shape could then be substituted into equation 3.6 and used to derive a new equation for $I_{ramped}(t)$ (similar to the theoretical considerations given in section 3.2.4 concerning other forms of modulation).

(a) **(b)**

$$y = 3.06\text{E-}09x^2 + 1.18\text{E-}04x$$
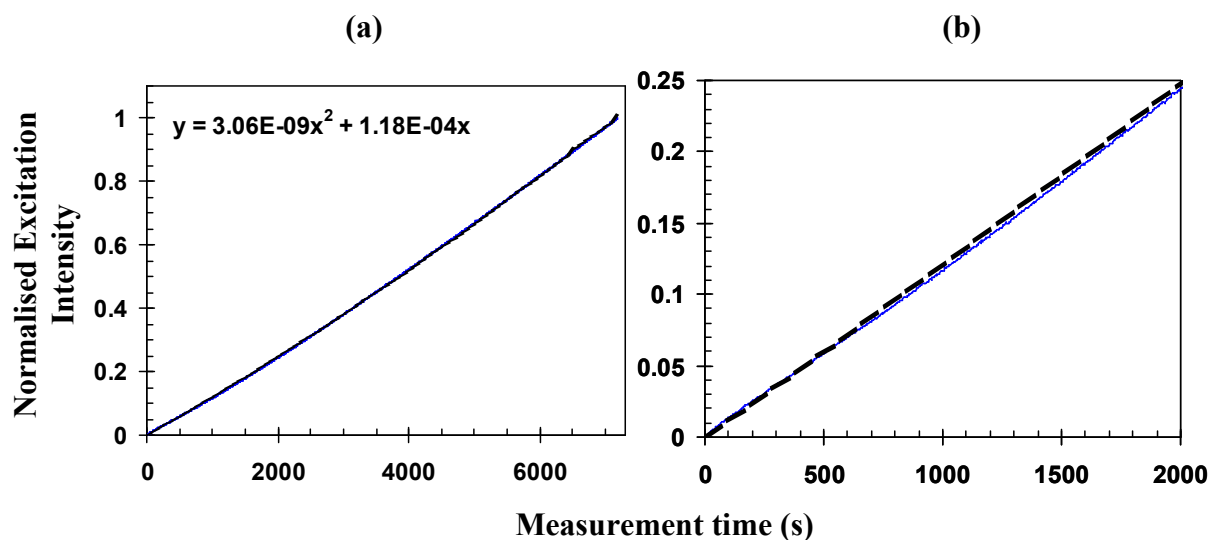
Measurement time (s)

Fig 3.8 (a) Excitation ramp intensity (see text for details) fitted to a second order polynomial. (b) shows the goodness of the polynomial fit over the initial 2000s of the measurement. (In both graphs: blue, solid line – data; black, dotted line – fit)

The derived solution for the LM OSL was then incorporated into the fitting routines described in section 3.5.2 to more appropriately fit the resulting LM OSL. This procedure and example results are described in more detail in section 3.5.4.

However, as well as being supra-linear on the whole, the ramp produced by the reader had some small non-linear features that were not well represented by the 2nd order polynomial equations used to fit the ramp (see Fig 3.8b), nor by higher-order polynomials. This had a bigger effect on the fits for the faster decaying OSL components. Another consideration was the effort of refitting the ramp data and reprogramming the LM OSL fitting routine for every different measurement condition used.

Consequently, a second method of accounting for the non-linear ramp was attempted. For this method, measurement of the ramp under the same measurement conditions as the LM OSL was required but no subtraction of dead channels or analytical description of the ramping function was needed. Instead, the trapezoidal rule for integrating the area under a curve was employed for fitting LM OSL curves.

In the absence of a definite mathematical description of the excitation ramp intensity the next best thing is to approximate. The approximation (using the trapezoidal rule) can then be used to derive a solution for the LM OSL curve as follows.

For the derivation of a first order solution equation 3.1 can again be used. Rearranging, and integrating this can be written

$$\int_{n_0}^{n} \frac{dn}{n} = -\int_{0}^{t} fdt = -\sigma \int_{0}^{t} P(t)dt \qquad (3.27).$$

Here, instead of explicitly stating $P(t)$ as in equation 3.6, the integration of $P(t)$ from 0 to t seconds can be approximated using the trapezoidal rule illustrated in Fig. 3.9. The interval for integration is divided into equal section of width Δt (for the excitation intensity Δt is the channel width). Each interval $P(t_i)$ to $P(t_{i+1})$ is simplified by a line passing through the endpoints. The areas of the resulting trapeziums are summed to approximate A, the total integral of the curve

$$A = \int_{t_1}^{t_n} P(t)dt \cong \Delta t \left(P(t_1) + P(t_n) \right)/2 + \Delta t \sum_{i} P(t_i) \qquad (3.28)$$

Following from equation 3.27 and using a similar method to that given in section 3.2 for the derivation, it is then possible to describe $I_{LM}(t)$ using

$$I_{LM}(t) = n_0 \sigma P(t) \exp\left(-\sigma A\right) \qquad (3.29)$$

Equation 3.29 approximates the 'linearly' modulated OSL from a single first order trapping state. The deconvolution routines described in section 3.5 were programmed to input the measured excitation intensity and use equation 3.29 as the solution with which to fit the LM OSL data. However, this is also a slightly inflexible solution, due to the ramp measurement required for each different condition used.

One further alternative that was tried was to build an external light source that incorporated a linear ramping function, and feed the output into Risø reader R2 (see section 2.4.1) using a liquid light guide. A unit was built that housed 91 Nichia light-emitting diodes (470nm; identical to those in the Risø reader). A photodiode was used to measure the total light output from the LED unit and use this as feedback into a circuit for the linear ramp. This is a more robust way to achieve the ramp than the method used in the Risø readers. The ramped output of the unit was found to be linear. However, the system of lenses that had to be used to focus the light from the LED array was ineffective and, coupled with the attenuation incurred in the light guide, the intensity at the OSL chamber was significantly less than the internal source, despite the fact that there were nearly three times as many diodes.

Also, attempted unsuccessfully, was plotting the LM OSL data vs. excitation intensity instead of time to try to obtain the form similar to that which would have been produced had the ramp been linear, consequently enabling fitting of the data to the equations assuming a linear ramp described in section 3.2.2. This method was tested and used by Singarayer *et al.* (2002b) to 'correct' the ramp of an IR laser stimulation source on a Risø TL-DA-15 model during a study of the LM infrared stimulated red luminescence (IRSRL) signal from feldspar. However, did not work as well as for Singarayer *et al.* (2002b) due to extent of non-linearity and position of component peaks. See Fig. 3.12 for example of fitting inadequacies using this method.
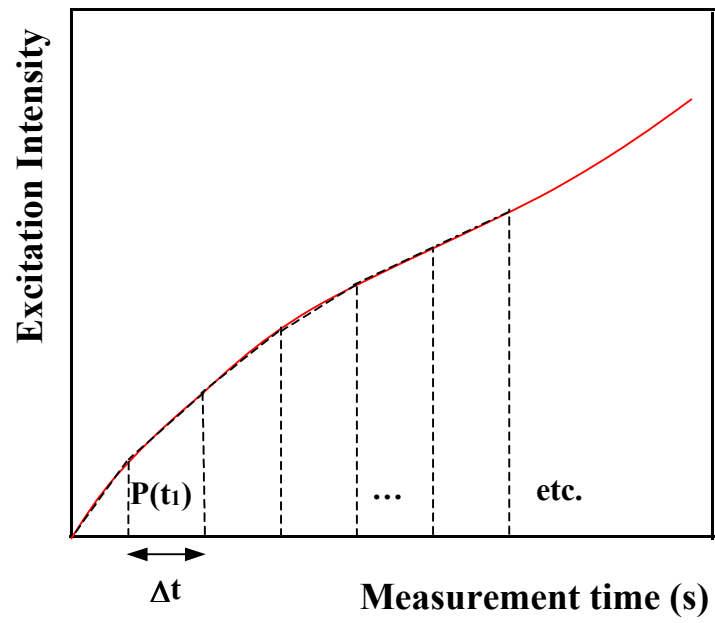
Fig. 3.9 Illustration of the trapezoidal rule for approximating the area under a curve.

As stated in section 2.4.1 the excitation unit on reader R4a containing the blue LED arrays was replaced during the last months of this study. The replacement LED arrays were more powerful, enabling stimulation intensities up to $\sim$36Wcm^{-2} at the sample position. Additionally, although the same method of obtaining feedback during ramping was used, the diodes were matched during the construction of the unit so that the feedback diodes more closely represented the light intensity into the sample chamber. Therefore, the ramp of the new unit (reader R4b) fitted well to a linear function (Fig. 3.10), allowing for more flexible LM measurements and more reliable LM OSL deconvolution. The problem of initial dead channels described previously was eliminated also.

Lastly, since Bulur *et al*. (2001a) acknowledged that this method of ramping can be beset with non-linearity and DC offset problems they developed a second method utilizing pulsed stimulation in order to combat the sorts of occurrences described in this chapter. A linearly modulated signal was produced by varying the repetition rate of a fixed width pulse of blue light-emitting diodes – termed frequency modulated pulsed stimulation. The stimulation power is controlled by varying the repetition rate. They noted that the pulsed stimulation might produce non-linearity at the beginning of the measurement, but this could be avoided by choosing an appropriate channel width for data collection. They demonstrated the linearity of the frequency modulated LED output and successfully applied the measurement system to samples of aluminium oxide, beryllium oxide and quartz. The frequency modulation technique is also practically easier to achieve than ramping of a continuous stimulation source, and has the advantage of possibly being incorporated in a fully digital system. This option was not available during the course of this study.
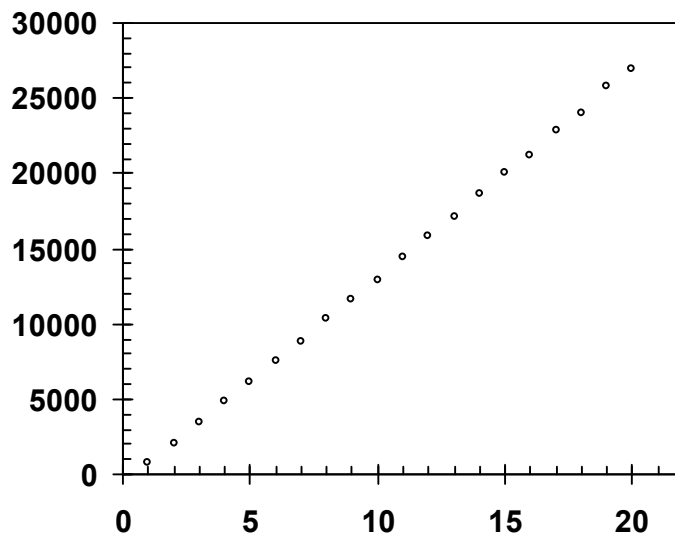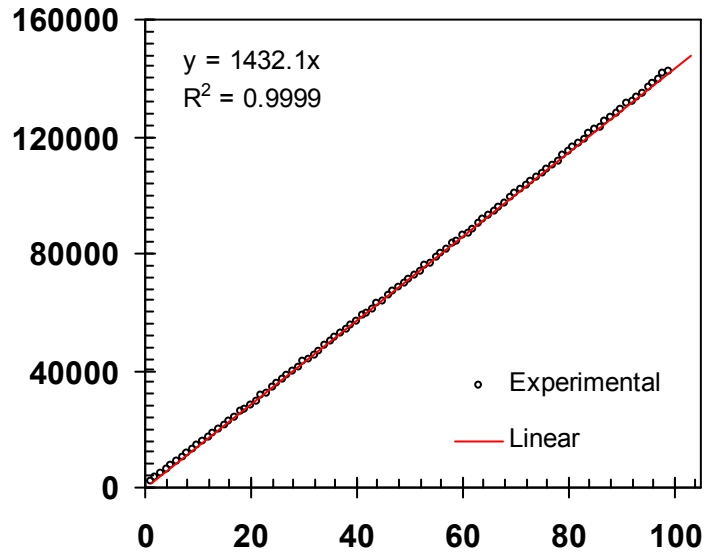
Fig. 3.10 (a) Measurement of ramped incident light intensity of reader R4b using neutral density filters in front of the PMT, from 0-95% full power over 100s. The experimental ramp has been fitted to a linear function (red line). (b) The same data as for upper figure has been plotted over the initial portion of the ramp.

3.5 Deconvolution of quartz LM-OSL curves

3.5.1 Formulation of the problem

The LM OSL data consists of intensity, $I(t)$, recorded at a discrete sequence of times [Note: the measured values, $I(t)$, are actually the summed counts over the interval $(t-\Delta t,\ t)$. This point will have more of an effect for the rapidly decaying components]. The LM OSL from quartz, stimulated at 470nm, is comprised of several overlapping component peaks (see Fig. 3.1). If the number of trapping states present is unknown then to resolve the LM OSL into its constituent components deconvolution techniques are required. The parameters that carry the wanted information, to be obtained from deconvolution, are n_0 and σ.

Assuming OSL is first-order one can model that each component with photo-ionisation cross-section, σ, produces $I(t)$ proportional to

$$K(\sigma,t) = \sigma \frac{P_0 t}{t_{max}} \exp\left(-\frac{\sigma P_0 t^2}{2 t_{max}}\right) \tag{3.30}$$

using the same nomenclature as in section 3.2.2. If there is a continuous distribution of σ the equation

$$I(t) = \int_0^\infty K(\sigma,t) g(\sigma) d\sigma \tag{3.31}$$

is used to describe $I(t)$, which is a Fredholm equation of the first kind. The spectral function $g(\sigma)$ determines the amplitudes. The problem is then reduced to a system of algebraic equations, which in a matrix notation takes the form:

$$\overline{I} = \overline{K}\,\overline{g} \tag{3.32}$$

where I is a vector that contains the LM OSL data, K is a set of LM OSL curves to deconvolve the data to, and g is the scaling factor, i.e. population of charge in that trap. The fitting then reduces to the problem of minimising

$$Q = \|I - Kg\|, \text{ subject to } g \geq 0 \tag{3.33}$$

On the other hand, for a known number of discrete constituents, n:

$$I(t) = \sum_{i=1}^n K(\sigma_i, t) g_i \tag{3.34}$$

which reduces to the straightforward problem of minimizing:

$$Q = \sum_t \left(I(t) - \sum_{i=1}^n K(\sigma_i, t) g_i \right)^2 \tag{3.35}$$

3.5.2 Curve fitting algorithms

As defined above this is a non-negative least squares problem for g_i. The algorithm used to solve for g_i is the non-negative least squares (NNLS) routine described in detail in Lawson and Hanson (1995). The code for the program used to deconvolve LM OSL data, incorporating the NNLS algorithm, is given in Appendix B. Matlab 5.1 was used as an environment for programming and plotting fits.

In equation 3.33, I is a vector that contains the recorded LM OSL data. K is a given matrix of (single) LM OSL curves distributed through time-space (i.e. each curve has different σ), and g is the amplitude vector, or spectral function, determined via minimisation, giving the scaling factor for the curves in K. It is ideal for the purpose of deconvoluting quartz LM OSL curves that in this method the number of constituent components is not a prior assumption. The matrix of LM curves is chosen to span the entire range of σ required for the measurement made. The vector g gives the number of components that give the best fit, and their magnitudes.

As stated above, Equation 3.31 is a Fredholm equation of the first kind; a class of equations that are known to be ill posed. An ill-posed problem, as defined by Hadamard (1902), is one for which the solution may not exist, may not be unique, or may not depend continuously on the data. In an example taken from exponential analysis (also classified in the same set of problems) Lanczos (1959) showed that a sum of two exponentials could be fitted by a sum of three exponentials with indistinguishable residual plots because a change in one parameter can be compensated for by adjusting the others. This problem becomes more serious for determining larger numbers of parameters. The same is true for analysis of LM OSL.

The level of noise in any measurement means that the data are not known accurately. It has the effect of letting the g_is vary, wildly in some cases (see Fig. 3.11). The procedure to stabilize the solution is called regularization. There are several methods to do this (Hofmann, 1986). The one used for this study is called Tikhonov regularization (Tikhonov and Arsenin, 1977). Here, equation 3.26 is modified so that an approximation is searched for, instead of an exact solution.

In matrix notation the initial problem is
$$\bar{I} = \bar{K}\bar{g} \tag{3.36}$$
which is the same as
$$\bar{K}^T\bar{I} = \bar{K}^T\bar{K}\bar{g} \tag{3.37}$$
Using Tikhonov regularization, this is replaced with

$$\overline{K}^T\overline{I} = (\overline{K}^T\overline{K} + \alpha\overline{D})\overline{g} \qquad (3.38)$$

where α is the regularization parameter, D is an identity matrix, I is the data, K is the kernel expressed in equation 3.35, and g is the solution vector. The optimum value for α can be found in several ways, most of them depending on the noise level in the data. For quartz, the spread of the cross-sections of the components is over at least three orders of magnitude. Because of the spread it was found that when a single valued-α was used if the value was large the solution was kept from creating too many LM peaks in the fit, but also fattened out the distributions, especially problematic for the more slowly decaying components (see Fig. 3.11). A small α value created a less stable solution (i.e. more peaks), especially for the faster decaying components. Consequently, the regularization parameter was modified so that for $K(\sigma, t)$, as σ_t varied α_t was varied in proportion.

Equation 3.35 (with the above modifications) could then be solved for g using the NNLS technique. Additionally, the problem can be solved for successively smaller overall values of α, and then the iterations should be stopped when the residual errors become comparable to the measurement error in the data to give the most appropriate result. However, this procedure is extremely time costly and was therefore only applied to a limited number of cases. Mostly, the overall regularization parameter was set for each LM curve manually to an appropriate value.

Another factor that affects the deconvolution process is the size of K. K ultimately depends on the perceived spread in the component cross-sections in the data (guess) and the resolution of the peak positions (i.e. cross-sections). The σ_i are calculated so that the LM curves in K are evenly distributed in time-space (i.e. using expression for t_{peak}, equation 3.9, this requires $\sigma_i \propto 1/t_{peak}^2$). The resolution, the maximum σ value used, and the spread required dictates the size of matrix K. In order to keep the solution as stable as possible, and to keep the fitting time as short as possible, the dimensions of K are kept to a minimum for the NNLS routine.

The advantage of the NNLS method of solution is that no prior assumptions are made about the number, or parameter values, of the OSL components. Conversely, the deconvolution of long LM OSL measurements, with up to 2000 channels and 1000 σ_is, was an extremely lengthy process (up to two hours per curve using Matlab).

For these reasons another fitting routine was employed also. The one found to be most convenient is the non-linear least squares Levenberg-Marquardt method. This is inbuilt into the Microcal ORIGIN 4.1 software package. A solution is found by minimising the Chi-squared value:

$$\chi^2 = \sum_{j=1}^{N} \left[I_{\exp}(t_j) - I_{fit}(t_j, n_0, \sigma) \right]^2 \tag{3.39}$$

(after Equation 3.28), where

$$I_{fit}(t, n_0, \sigma) = \sum_{i=1}^{n} n_{0i} \frac{\sigma_i P_0 t}{t_{\max}} \exp\left(-\frac{\sigma_i t^2}{2t_{\max}} \right) \tag{3.40}$$

Here N is the number of experimental data points and in this case, the number of components has to be assumed – given by n (deduced from previous NNLS fits and form of empirical data under various measurement conditions). The Levenberg-Marquardt algorithm (modified by ORIGIN to achieve more control and stability) finds the solution iteratively and alters between the steepest-descent method and the inverse Hessian method depending on how close the Chi-squared value is to the minimum. This makes it a more robust method than a lot of other iterative least squares techniques. A comprehensive description of the technique can be found in Press *et al.* (1992).

The advantages of the Levenberg-Marquardt fitting program (within the ORIGIN environment) are that it is a lot faster than NNLS, and through inputting the equation for fitting with each term being a separate component, it is easier to mix the kinetic order of the different components. Another advantage is that an error is given, in the ORIGIN software, for each fitted parameter. The standard error for each parameter is given by

$$\hat{\sigma} = \sqrt{\chi^2 C_{ii}} \tag{3.41}$$

where C_{ii} diagonal element of variance-covariance matrix C (for further details see Press *et al.*, 1992). The disadvantage is that the number of components and initial parameter values must be stated.

Other algorithms and software packages have been used but it was found that these were less robust and given poor initial parameter estimates they converged more often than not to local minima rather than the absolute minimum.

The two programs used routinely for the deconvolution of LM OSL data have been tested extensively using simulated data to assess their limits and robustness. The procedures for testing and results are briefly summarized in the next section.

3.5.3 Testing of curve fitting routines

When using any analysis tool, it is good practice to look at its general reliability and appropriateness. The fitting routines outlined in section 3.5.2 have been rigorously tested on computer-simulated LM OSL, from simple single component curves, to curves that have been constructed to resemble the LM OSL from quartz under a variety of conditions

(different component ratios representing e.g. partially bleached samples). A sample of the results is displayed here as it was thought that it is important to illustrate the method of testing but without displaying extensive results, as this would be tedious for the reader.

The simulated LM OSL used for initial testing was created assuming a linear ramp (unlike some of the experimental LM OSL). Four first order components were used, in general, with varying magnitudes and positions. Noise was added to the data to increase the relevance to experimental data. This was achieved by generating random numbers within a Poisson distribution. The *noise(i)* was added to the *data(i)* and the mean noise value subtracted from all data points.

Preliminary testing for the NNLS routine (given in Appendix B) was to look at the effect of regularisation. Fig. 3.11 shows the four-component stimulated LM OSL data fitted using NNLS under the same conditions (i.e. same matrix size etc.) but with different regularisation parameters. See caption for Fig. 3.11 for details of the simulated data and the fitting. 3.11a had no regularisation for the fitting, 3.11b had a single valued regularisation parameter and 3.11c had a varying regularisation parameter. Without regularisation the solution was unstable. The program fitted six components to the data as seen in Fig 3.11a. There was however, no structure to the residual plot from the fit, which would otherwise indicate a good/successful fit. When a single-valued regularisation parameter was introduced (Fig. 3.11b) of an appropriate size the number of components fitted reduced to four. As discussed above, the single-value regularization over constrained the smaller σ curves and resulted in a fattened distribution in the fourth component (see upper plot, G[i] vs. σ[i]). Consequently, there was some structure in the plotted residuals. Using a multi-valued regularisation parameter solved this problem (Fig. 3.11c). Four components were successfully fitted to the data.
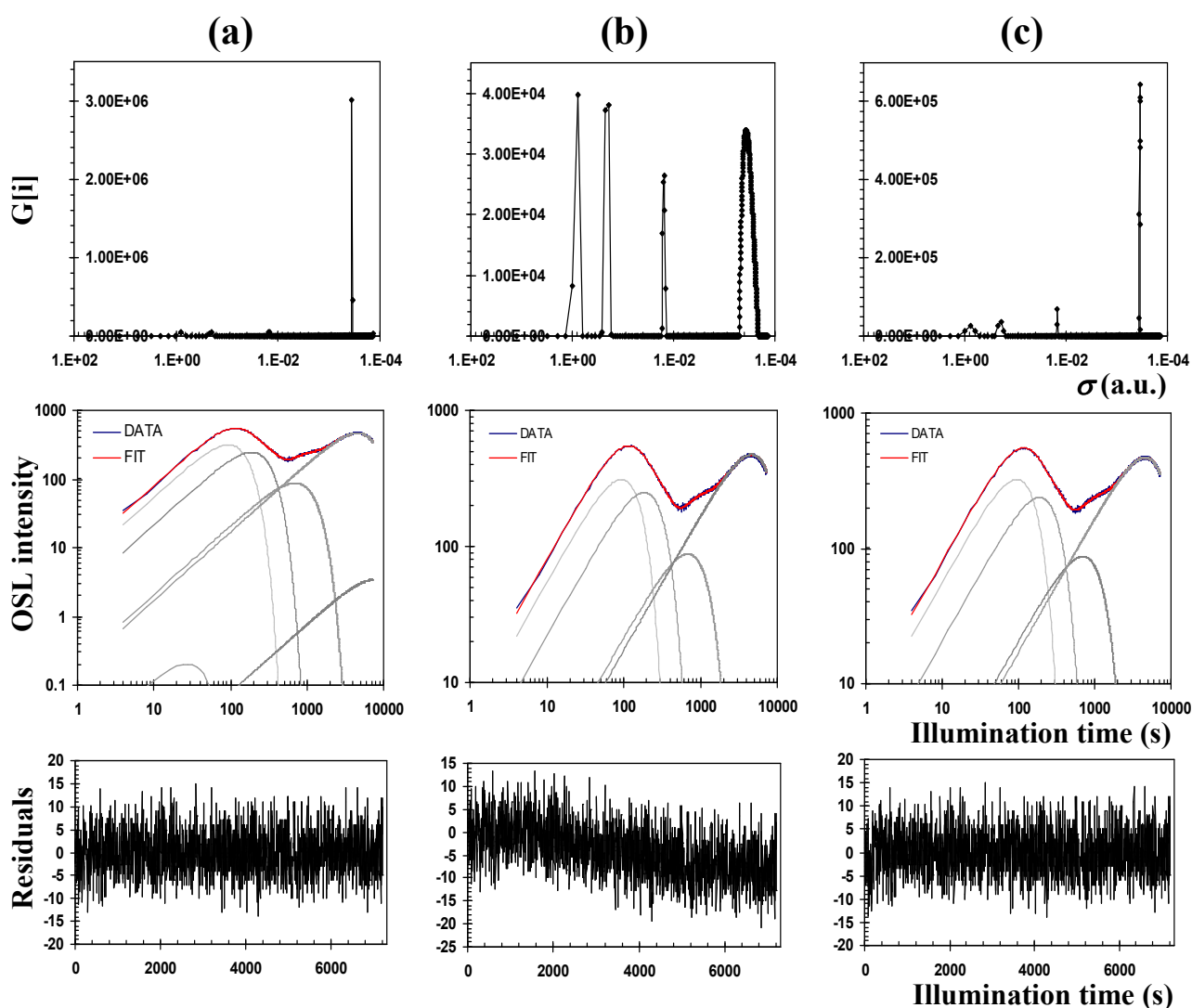
σ	n_0		σ	n_0		σ	n_0
9.75.1	9.12		0.822	48000		0.796	50900
0.814	48900		0.209	76100		0.201	74200
0.204	75900		0.156	98500		0.15	99400
0.151	99500		3.45e-4			3.5e-4	3500000
3.52e-4			3570000				
3470000							
1.39e-4							
40100							

Fig. 3.11 Results of fits to simulated data using the NNLS routine – without regularisation (a), with regularisation using a single parameter (b), and using a regularisation function (c). [Data simulation: σ - 0.8:0.2:0.015:0.00035, n_0 – 50000:75000:100000:3500000]

Using the ORIGIN program the number of components is specified initially. Therefore, considerations for testing are the starting values given to the n_i and $\square_i$ parameters. By starting the iterations with parameter values far from the actual values the program may be likely to converge at local minima, rather than the global minimum chi-square value. The likelihood was tested by using the same simulated LM OSL curve each time and varying the starting conditions of the fit, to see how sensitive the algorithm was to this, although this will be data-set dependent and so these results are not general. A sample result is illustrated in Table 3.2. For this simulated dataset there was little dependence of the fitted parameters on the initial input values.

Parameter	Actual values	Fit 1		Fit 2		Fit 3	
		Start	End	Start	End	Start	End
n_{01}	45000	20000	41153 ± 5473	90000	41044 ± 5478	5000	41152 ± 5475
σ_1	1	0.8	1.09 ± 0.1	2.0	1.09 ± 0.104	2.0	1.09 ± 0.1
n_{02}	45000	20000	49206 ± 4947	70000	49292 ± 4952	10000	49200± 4949
σ_2	0.26	0.2	0.27 ± 0.035	0.5	0.27 ± 0.035	0.1	0.275 ± 0.035
n_{03}	30000	20000	33986 ± 3433	600000	33999 ± 3431	100000	33979 ± 3452
σ_3	0.02	0.01	0.016 ± 0.0028	0.01	0.016 ± 0.003	0.0007	0.016 ± 0.028
n_{04}	1500000	2000000	150387 ± 13034	5000000	1503799 ± 13038	50000	1503795 ± 13038
σ_4	0.00037	0.0003	0.00037 ± 6e-6	0.00005	0.00037 ± 6e-6	0.00005	0.00037 ± 6e-6

Table 3.2 A summary of the fits produced using ORIGIN given three example different starting conditions

3.5.4 Testing modifications for dealing with empirical data

Using 2nd order polynomial power ramp, LM OSL data with 4 components (parameters given in Fig. 3.12 caption) have been created to simulate empirical LM OSL data collected from reader R4 using the old excitation unit. The simulated data have then been fitted using the various modifications suggested in section 3.4.

Fig. 3.12 Results from various methods of incorporating a non-linear ramp into the fitting process. Simulated data using a 2nd order polynomial ramp was created. The simulated data and total fit from each method are shown in the upper plots; residuals in the lower plots. See section 3.5.4 for further details.
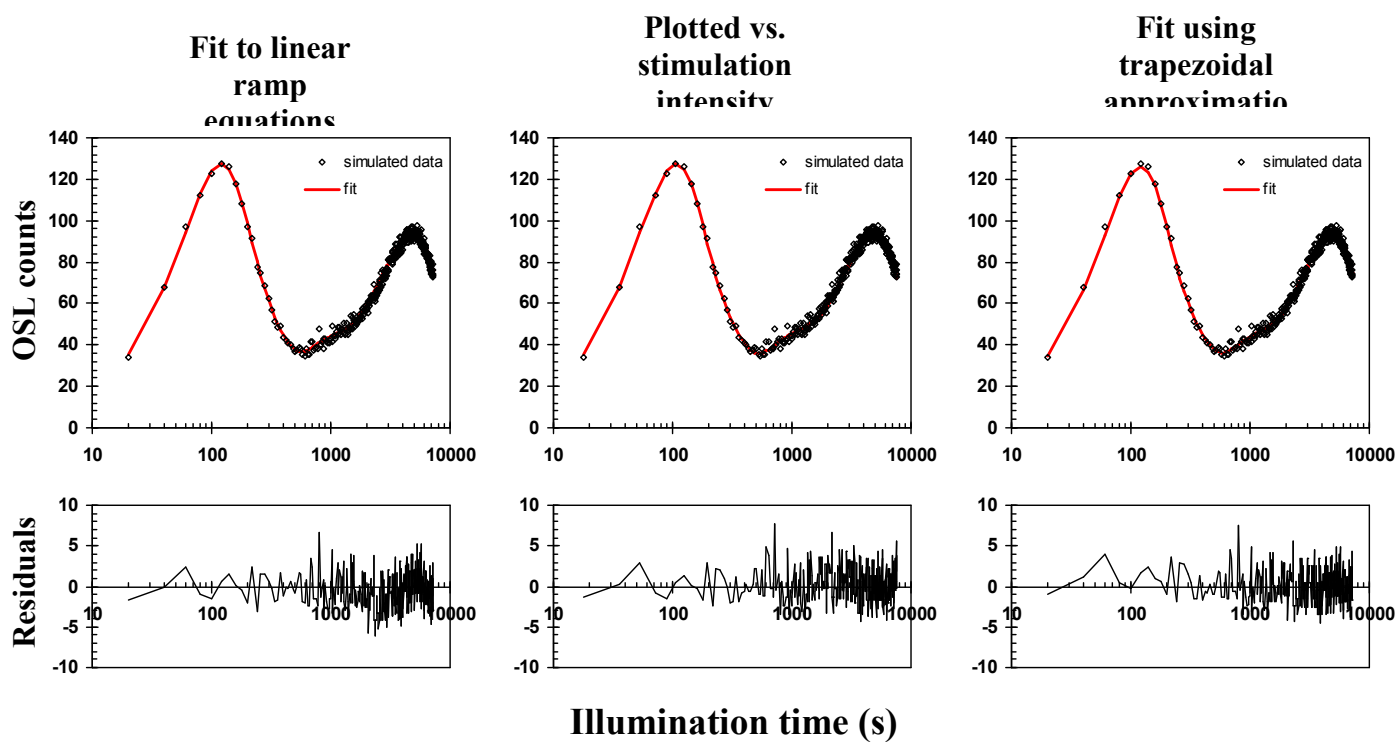
Parameter	Linear fit	vs. power	Trapezoidal fit	Actual
n_1	12906	12663	14161	15000
σ_1	0.725	0.87	0.806	0.8
n_2	15406	13705	14723	15000
σ_2	0.204	0.22	0.208	0.2
n_3	17889	19776	19772	20000
σ_3	0.0167	0.0149	0.0161	0.015
n_4	739985	758481	697526	70000
σ_4	0.00031	0.0003	0.00035	0.00035

The data were firstly fitted to the normal equations that assume a linear ramp. The results were compared with plotting the data versus stimulation intensity and then fitting the modified data to linear ramping equations and also fitting the data to equations that use the trapezoidal rule to approximate the actual ramp shape.

The data and the fitted parameters are shown in Fig. 3.12. Although there is not much structure in any of the residual plots, which might suggest that all the methods perform equally well during fitting, the fitted parameters shown below the plots indicate otherwise. From these it can be concluded that the trapezoidal method of approximating the stimulation intensity ramp gives the closest fit the given simulated parameters.

Fitting of experimental data measured using the reader system with a non-linear ramp (R4b) was performed using the trapezoidal method of approximation (which was incorporated into the standard NNLS software). This did however require subsequent measurement of the stimulation ramp for all the different measurement conditions/times used. The majority of experiments described in the following chapters were fortunately carried out using the replacement excitation unit that did display a linear ramp, which simplified the fitting process considerably.

3.6 Discussion

This chapter aimed to demonstrate the usefulness of the linearly modulated OSL technique for component-resolved measurements. By ramping the stimulation source peak-shaped luminescence is produced, instead of a monotonically decaying signal. This allows better visual identification of the OSL components.

Deconvolution techniques to separate the OSL components have been described for use with LM measurements. Confidence in the fitting routines has been achieved through a thorough testing process involving computer-simulated data.

There are several disadvantages to this system of measurement. Mainly, the measurement time is twice as long as CW OSL to impart the same energy (to record the first four OSL components on the Risø TL-DA-15 reader takes 3600s at 160°C). Fitting the resulting LM curves may also be a lengthy process. However, the advantages obtained through stimulating this way for observing the OSL component behaviour can be greater. Therefore, the majority of the empirical data collected and illustrated in the following chapters have been observed using the LM OSL technique.

Chapter | 4

4

INITIAL OBSERVATIONS OF QUARTZ LM OSL AND THERMAL PROPERTIES OF THE OSL COMPONENTS

4.1 Introduction

The technique of linearly modulated OSL and the methods of deconvolution described in Chapter 3 have been used to investigate the nature of the OSL from several sedimentary quartz samples. In the present chapter a survey of a number of samples is also reported to quantify both sample-to-sample and grain-to-grain variation in terms of the number of fitted components and trap parameters. Further experiments to characterise the luminescence properties of the OSL components were subsequently performed on a selection of the samples. Various pre-treatments and measurement conditions were employed to investigate the behaviour of the quartz OSL components, the results from which are discussed here.

Firstly, a discussion is undertaken to address in detail the issue of whether it is appropriate to fit quartz LM OSL curves to a sum of first-order components (as in Bailey, 1998b, and Bulur *et al.*, 2000). Analytically and numerically modelled data are presented in conjunction with empirical data to assess the kinetics of the OSL.

4.2 Basis for choice of kinetic order for deconvolution

The peak position of each LM OSL component depends on the photoionization cross-section of the trap and the maximum stimulation photon flux (see Table 3.1 for analytical expressions describing peak position, t_{peak}). Typical photoionization cross-sections, σ_i, of quartz OSL components, stimulated using 470nm light, produce overlapping LM OSL peaks (e.g. Fig. 3.1). The difference in σ_i is not sufficient to always allow one to see all individual component peaks, depending on pre-treatment and measurement conditions. In Chapter 3 the use of simplified analytical solutions and deconvolution techniques served as a means of separating and defining overlapping components was discussed. The deconvolution techniques described have been applied to all further experiments in this chapter, since this was the most convenient way to obtain component-resolved data using the available

equipment. Therefore it has been important to use relevant empirical and modelled data obtained to achieve an understanding of the degree of interaction between the traps, and hence, find appropriate analytical equations to use in the deconvolution process.

The models used are based on either *first-order* or *non-first-order* kinetics (Randall and Wilkins, 1945). As shown in Fig. 3.2a for the first order case, once an electron is freed from its trap, where trap charge concentration is n, the probability of it returning to the trap is much less than the probability of recombination. When there is no significant retrapping of charge into any of the OSL traps the peak position, t_{peak}, is independent of charge concentration (i.e. independent of laboratory dose/prior partial bleaching etc.). Conversely, non-first-order kinetics describes the situation where considerable retrapping occurs (Fig. 3.2b). Retrapping slows the rate of recombination and modifies the shape of the LM OSL curve. The probability of retrapping is charge concentration dependent; therefore, the peak position of a non-first order trap will depend on the charge concentration.

The effect on the position and form of the LM OSL of varying trap charge concentration for different possible systems has been investigated for this study, both analytically and using a numerical model. The results were subsequently compared to those obtained empirically.

Analytical models

Using the equations derived in Chapter 3 for $I_{LM}(t)$ LM OSL curves from a single trap with various initial trapped charge concentrations (i.e. different n_0 parameters) have been simulated. Fig. 4.1 demonstrates the difference between LM OSL from first and second order solutions. As is obvious from the equations describing t_{peak} (see Table 3.1) there is no dependence on n_0 for the first order case, but of $\sqrt{(N/n_0)^{b-1}}$ for general order solutions. Fig 4.2 illustrates the change in t_{peak} with initial charge concentration, n_0, for various order systems from first to third order. As the order increases the movement of t_{peak} with n_0 becomes more significant.
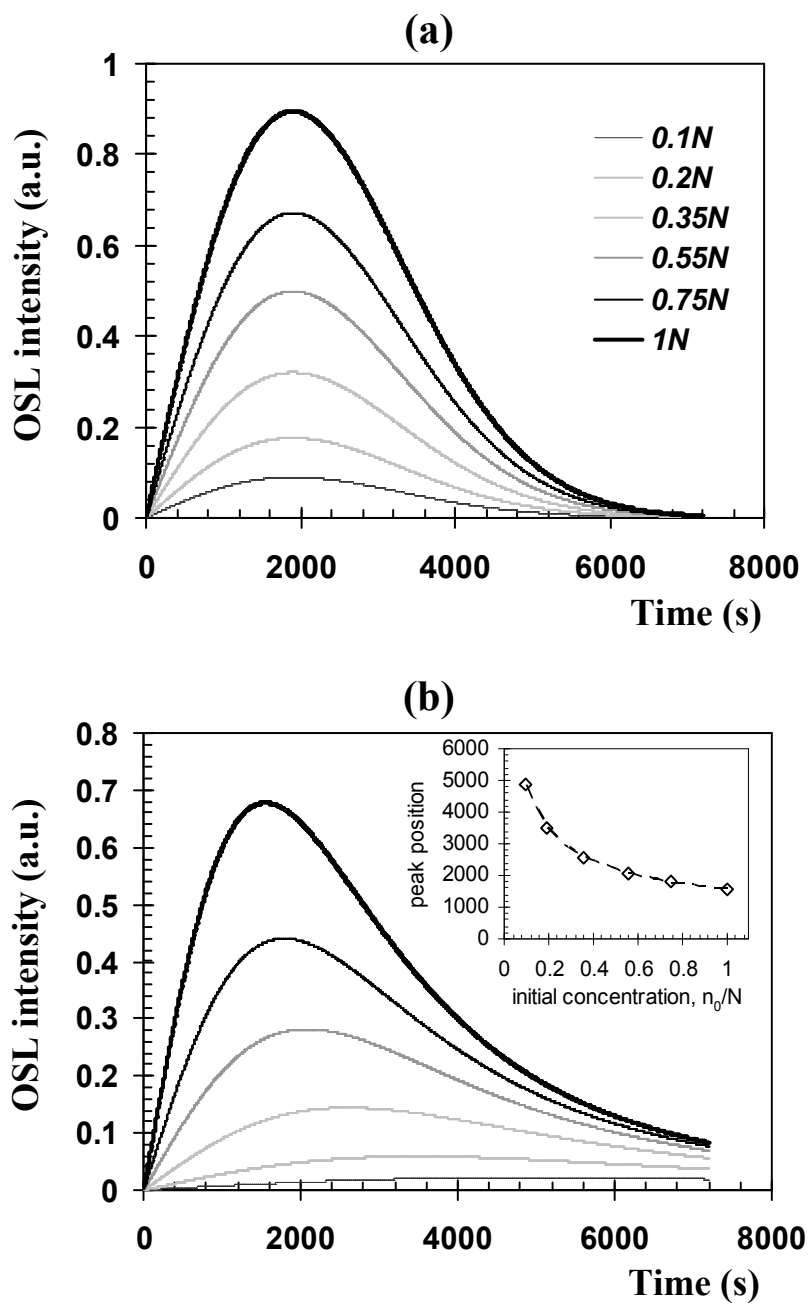
Fig. 4.1 (a) Simulated LM OSL from a single first order trap with various initial charge concentrations, n_0, given as a proportion of N, the number of traps. (b) Simulated LM OSL from a single second order trap with the same initial charge concentrations as in (a). Inset shows the trend in peak position with n_0 ($y=ax^{-0.5}$).
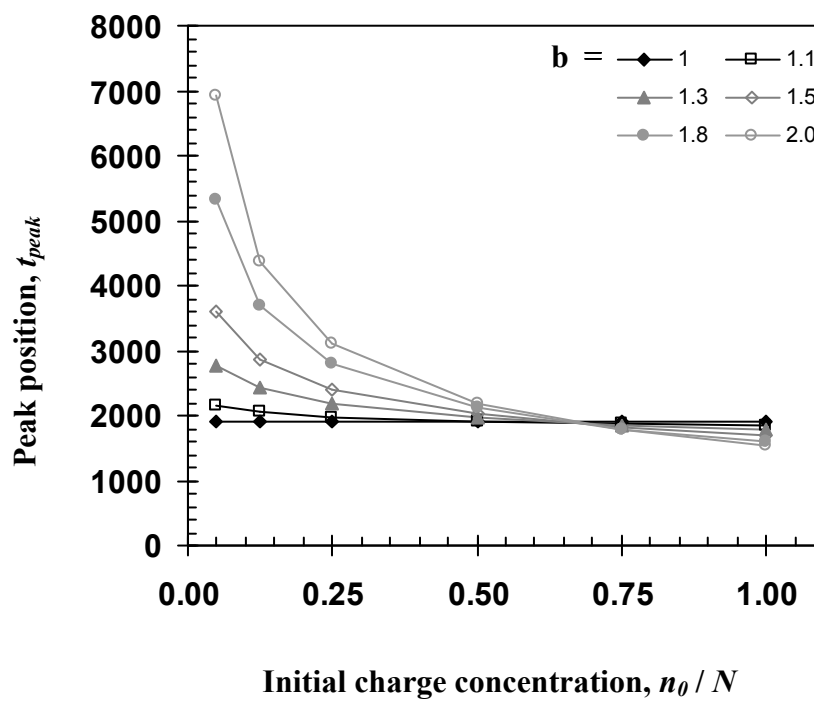
Fig. 4.2 Change in peak position, t_{peak}, with n_0 (as a proportion of N, trap concentration) for general order analytical LM solutions for b = 1…2

However, the derived solutions rely on potentially unrealistic assumptions and simplifications about charge transfer. The investigation of kinetics was continued using a simple numerical model, described below in which fewer assumptions are made.

Numerical model

The following rate equations were used to model the LM OSL from a simple system of a single electron trap and luminescence centre population. In this case only optical transitions were considered (since it is assumed that the OSL is thermally stable at typical measurement temperatures for the duration of the stimulation).

$$\frac{dn}{dt} = -nf(P) + n_C(N-n)A_n \tag{4.1}$$

$$\frac{dn_c}{dt} = -\frac{dn}{dt} - \frac{dm}{dt} \tag{4.2}$$

$$\frac{dm}{dt} = -n_C m A_m \tag{4.3}$$

where n is the trapped electron concentration, N is the concentration of electron traps, λ is the optical detrapping rate (dependent on stimulation power, and wavelength), A_n is the conduction band to electron trap probability, n_c is the concentration of free electrons in the conduction band, m is the concentration of trapped holes and A_m is the conduction band to hole probability (following McKeever, 1985). A thermally and optically disconnected electron trap, n_D, was incorporated for which

$$\frac{dn_D}{dt} = 0 \tag{4.4}$$

Trap n_D did not take part in the OSL process but was included to achieve charge neutrality in the system, i.e. $n + n_D = m$. See Fig. 4.3 for the energy band diagram of the simple system. The numerical model was run in Mathworks Matlab software.

Three scenarios are illustrated here to summarize the simulated effect of retrapping on the form of the LM OSL from different doses. The parameter values used for each are listed in Table 4.1. The simple model used here did not need to simulate the dosing/filling process and an initial value for parameters n, n_D and m the trapped charge concentrations, were declared at the start. To simulate different doses the initial value for n was varied up to saturation ($n = N$) while m was kept constant. Various degrees of retrapping were simulated by altering the conduction band to electron trap probability parameter, A_n. Fig. 4.4 shows the simulated LM OSL from the three models outlined in Table 4.1.

For model 1 (Fig. 4.4a) parameter A_n = 1e-8. This is comparable to the value used for the fast component in the general kinetic model of quartz produced by Bailey (2000b). In Fig. 4.4a (left) no change in peak position with n_0 is observed. This is strong indication of a first order system. The right hand plot shows that the normalized, numerically modelled data from this system (for all n_0) are in good agreement with the analytical solution for first order LM OSL. In the second model the conduction band to trap probability was increased, A_n = 4e-7. In this case retrapping was sufficient to modify the form of the LM OSL. One can see from Fig. 4.4b (left) the change in peak position with dose, characteristic of a non-first order system. In the right hand graph the modelled data have again been normalized to t_{peak} and I_{peak}, so all the peak heights and positions are equal. It can be seen that the form of the LM OSL up to n_0=0.2N is approximately first order. As the initial concentration of trapped electrons increases the form of the LM OSL progressively deviates away from the first order solution. For model 3 this effect is further amplified, due to the larger A_n parameter (see Fig. 4.4c).

At low concentrations models 2 and 3 give approximately first order LM OSL. It can be seen from equation 4.1 describing the rate of change in n, that when $n \ll N$ the second term in the equation giving the charge flowing into the electron trap from the conduction band is effectively constant (since $(N- n) \rightarrow N$). Therefore, since this term (i.e. amount of retrapping) does not vary significantly it is possible to get a first order shape from the model (described in more detail in Bailey et al., 1997). At higher doses the form increasingly deviates away from a first order shape especially for $t > t_{peak}$.

Fig 4.5 illustrates the movement of t_{peak} as n_0 is increased for models with various A_n values. At initial charge concentrations close to saturation, when retrapping is significant, t_{peak} occurs at shorter times than for the first order model. This trend was observed in both the numerical (Fig. 4.5) and the analytical (Fig. 4.2) models.
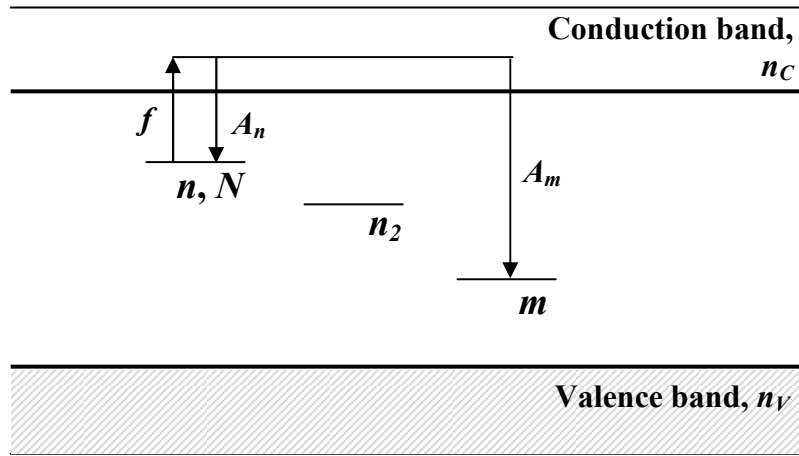
Fig. 4.3 Band diagram of the simulated single (effectively) trap/centre system. Charge transitions are indicated by the arrows. See section 4.2 for further details.

Parameter	Model 1	Model 2	Model 3
n	0.1 – 1e11	0.1 – 1e11	0.1 – 1e11
N	1e11	1e11	1e11
σ	0.2	0.2	0.2
A_n	1e-8	4e-7	8e-7
n_C	0.0	0.0	0.0
m	5e12	5e12	5e12
A_m	1e-8	1e-8	1e-8

Table 4.1 Initial parameters used to numerically model the LM OSL from a single trap/centre system. Three sets of initial values were used to provide different retrapping scenarios.
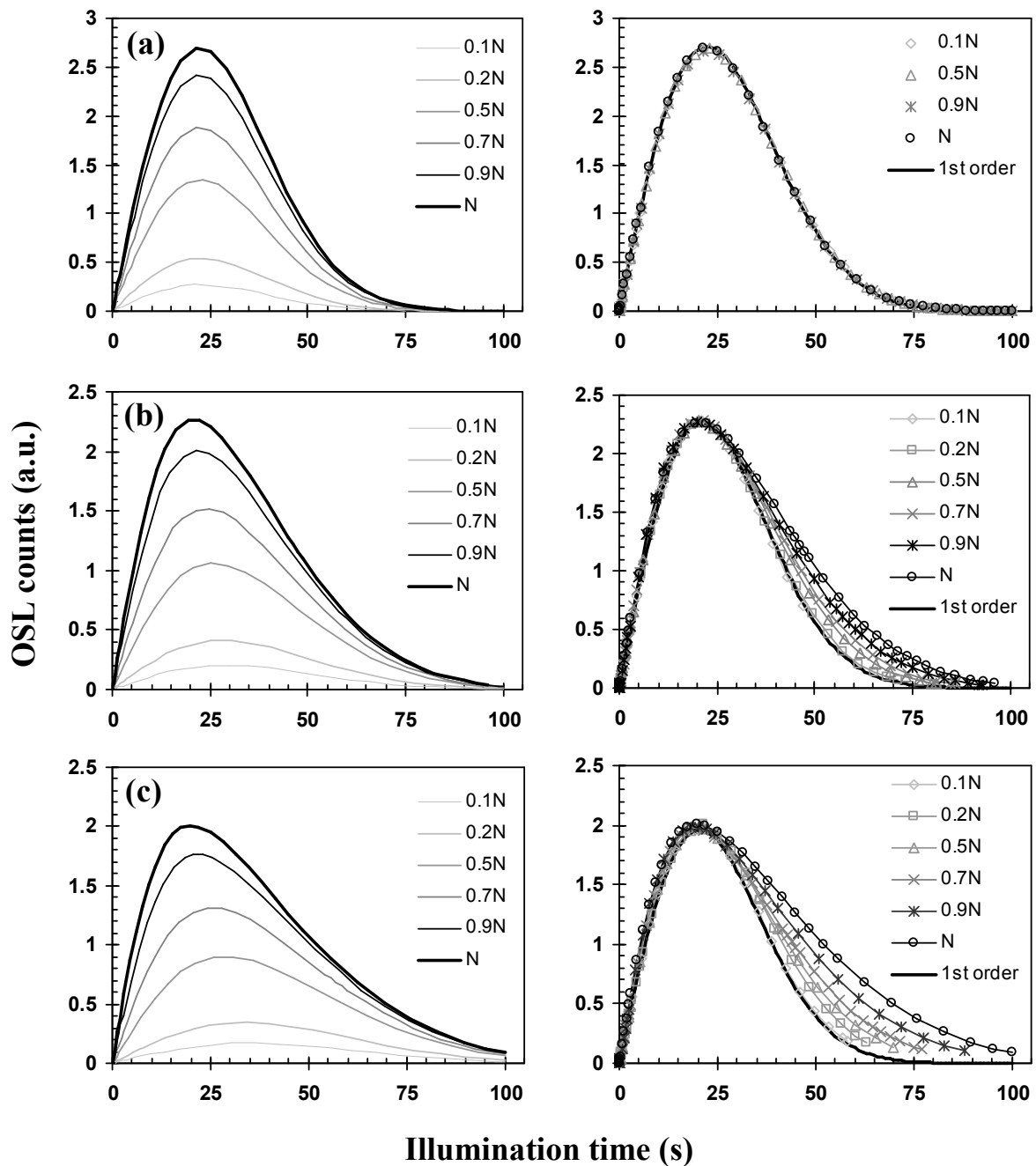
Fig 4.4 Numerically modelled LM OSL from a single trap/centre system. Left: LM OSL from various initial trapped electron concentrations up to saturation (*N*). Right: LM OSL modified from left data so that all LM curves have equal t_{peak} and I_{peak}, to illustrate the change in form with n_0. Plotted for comparison is the analytical solution for a first order LM curve. (a) Model 1 parameters used (see Table 4.1) (b) model 2 parameters (c) model 3 parameters.
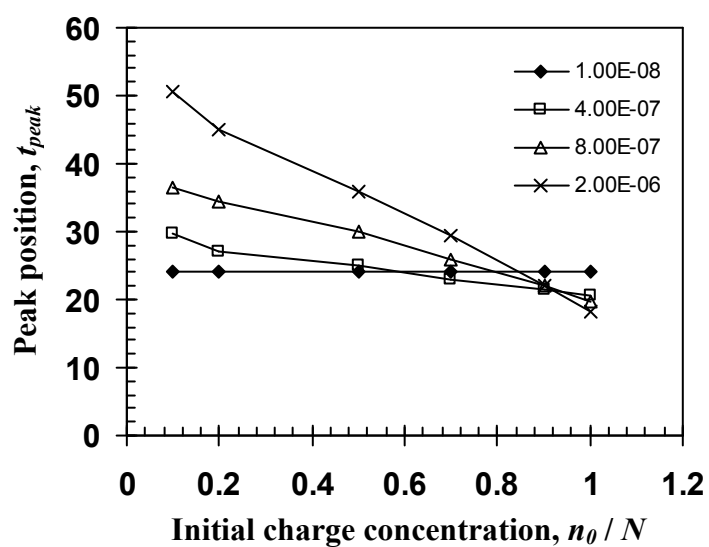
Fig 4.5 Peak position, t_{peak}, vs. initial electron trap concentration, as a proportion of N, for the single trap/centre numerical model.

In the model described above retrapping occurs into the same electron trap type. However, in minerals where there is more than one contributing trap, depending on the relative trapping probabilities, retrapping may occur into several different trap types. In view of the fact that there are several components contributing to the OSL of quartz (Bailey *et al.* 1997, Bulur *et al.*, 2000) one question that presented itself was whether, due to the interaction between traps, it would be physically possible to have a system where some components display first order properties while others display non-first order behaviour, and therefore would it ever be valid to attempt to fit the LM OSL from quartz to anything other than the sum of first order components? In other words, if one trap is non-first order does this imply that all the components will be, to some degree, non-first order, and if this is the case is it possible to fit the LM OSL to mixed order solutions, or does the interaction between the traps mean this is not feasible?

A two (interacting) trap numerical model was introduced to address this issue. The coupled equations governing charge dynamics were as follows:

$$\frac{dn_i}{dt} = -f(P)n_i + n_C(N_i - n_i)A_{ni} \tag{4.5}$$

$$\frac{dn_C}{dt} = -\sum_{i=1}^{2}\frac{dn_i}{dt} - \frac{dm}{dt} \tag{4.6}$$

$$\frac{dm}{dt} = -n_C m A_m \tag{4.7}$$

All terms have the same meaning as equations 4.1 to 4.3, and subscripts $i=1$, *2* denote the two different electron trap types. A disconnected trap, n_D, was again used in order to maintain charge neutrality.

The model was run with different A_{n2} values, each time for a number of different initial trapped charge concentrations (up to saturation, N). Fig 4.6 illustrates three different scenarios, for which the model parameters are given on the right of the plots. It is expected that for multiple traps recombining at the same centre, the components with larger σ (i.e. the faster components) are more likely to be first order, while smaller σ of the slower components may mean that retrapping is more significant (as $A_n(N-n) > \sigma$). Therefore, parameter values were chosen to try to simulate first order kinetics for component 1, by maintaining a small A_{n1}, and various order kinetics for component 2 by changing A_{n2}.

One can see from Fig. 4.6 that as A_{n2} is increased the shape of the second LM peak (component 2) becomes increasingly non-first order and change in t_{peak} is more evident. However, peak 1 (component 1) does not apparently change position with charge

concentration in any of the scenarios illustrated. These results seemed to indicate that component 1 was probably obeying first order kinetics even when component 2 was not. To further investigate this, the curve fitting techniques described in Chapter 3 were used to deconvolve the modelled data to see how successfully first- and general-order analytical solutions could describe the LM curves.

In model 1 (Fig. 4.6a) A_{n1} and A_{n2} were sufficiently small that the modelled LM OSL was characteristic of two first order components, in that there is no change in t_{peak} with dose. All LM curves fitted well to the sum of two first order components (see fit to saturated LM curve in Fig 4.6a – red line), verifying the visual indication of first order dynamics.

Model 2, Fig 4.6b, displayed slightly non-first order behaviour in the second component. The LM curves were fitted, initially, to the sum of first order solutions, and also to one first + one general order solutions. The results at low dose ($n_0=0.1N$) and high dose ($n_0=N$) are shown in Fig. 4.7. At the lowest concentration the LM OSL fits to the sum of two first order solutions to within 1%, as expected from the single trap modelling work. However, although the initial charge concentration, n_{02}, was within 1% of the model input, the fitted σ_2 was 15% smaller than the inputted value. At high concentrations the two first order solution no longer produced an adequate fit (see Fig. 4.7, lower). The 1st+general form produced a satisfactory fit to the data, estimating n_{02} to within 3%. Significantly, the LM OSL was also well fitted to the sum of three first order components. It is important to acknowledge that one can nearly always obtain good fits by summing many components. Therefore, it is critical to investigate the LM OSL using different measurement conditions (e.g. different stimulation photon energies or beta doses) to obtain some empirical basis for the fitting used, as described in the remainder of this chapter.

Also evident from the model was that a small proportion of the charge from component 2 is being retrapped into component 1. The residence time for the retrapped charge in component 1 was very small compared to component 2. Therefore the OSL from charge retrapped in component 1 was proportional to the total LM OSL from component 2 and allowed the resultant LM OSL curve to be fitted to two components (1st+general). This was possible only due to the difference in σ between the two components.

For model 3 A_2 was further increased. The non-first order behaviour of component 2 was more evident than in the second model. Fitting the data from model 3 resulted in a similar pattern to those explained above for model 2.
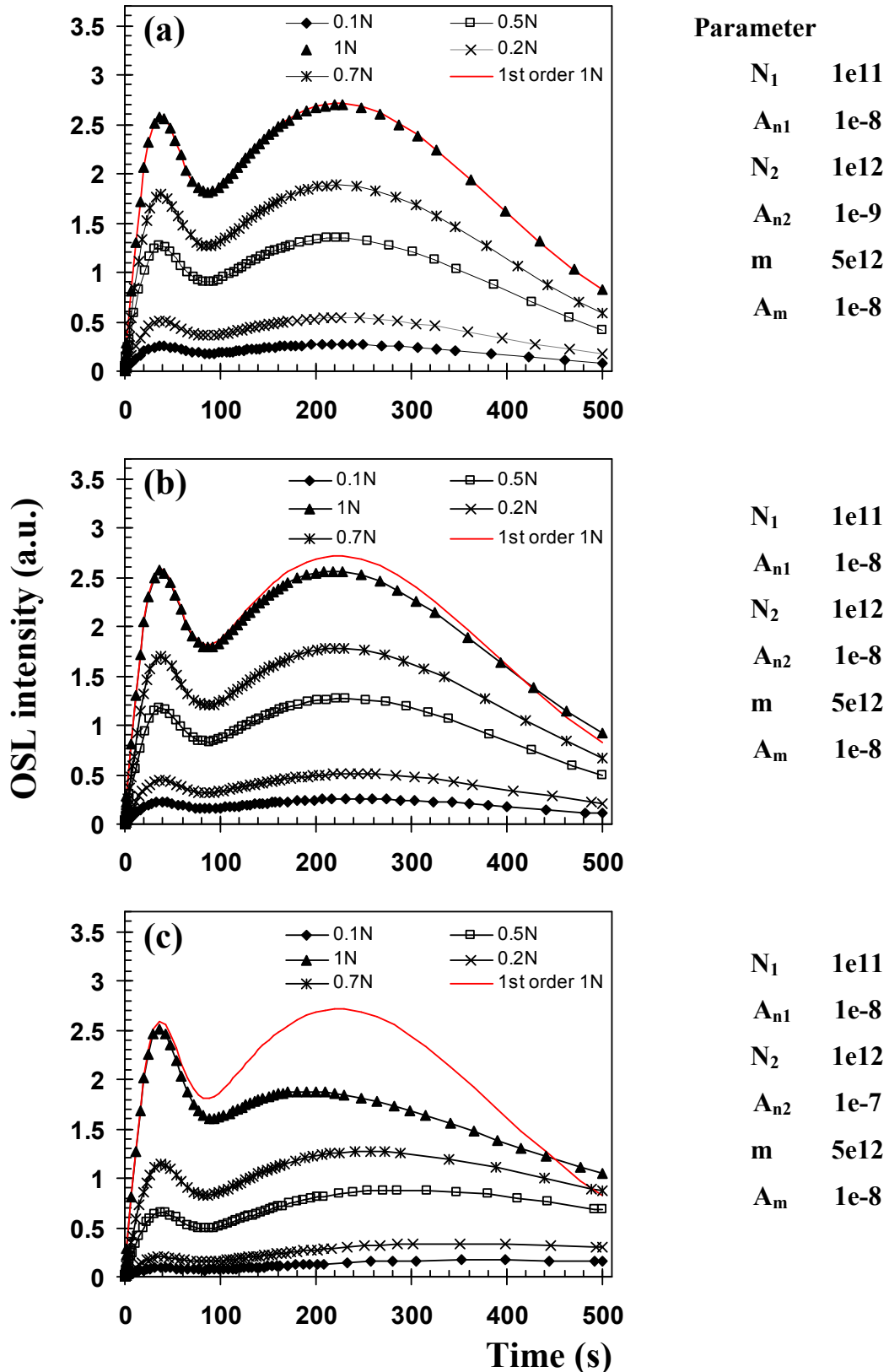
Fig. 4.6 numerically modelled LM OSL at various initial charge concentrations (as a proportion of N – saturation) for the two-trap model described in the text. Three models were used with model parameters of each listed on the right of the plot from each model (a) two first order components, (b) and (c) retrapping significant in the slower component.
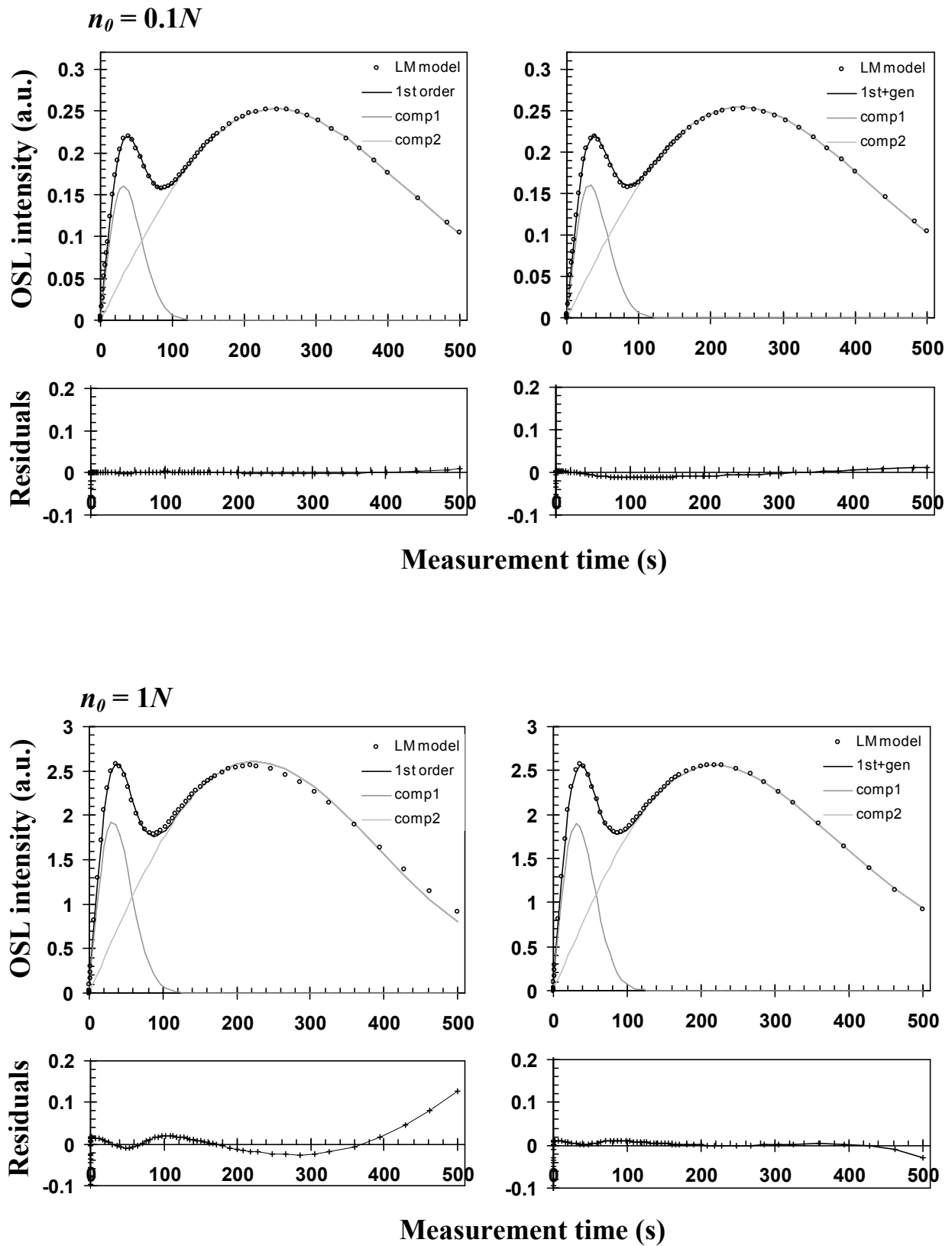
Fig. 4.7 Example fits to numerically modelled data from the two component system outline in Fig. 4.6b. LM OSL from low initial charge concentration (upper, $n_0 = 0.1N$) and saturation (lower, $n_0 = N$) have been fitted to two first order components (left plots) and first order +general order (right plots) for comparison. Absolute residuals are plotted underneath each.
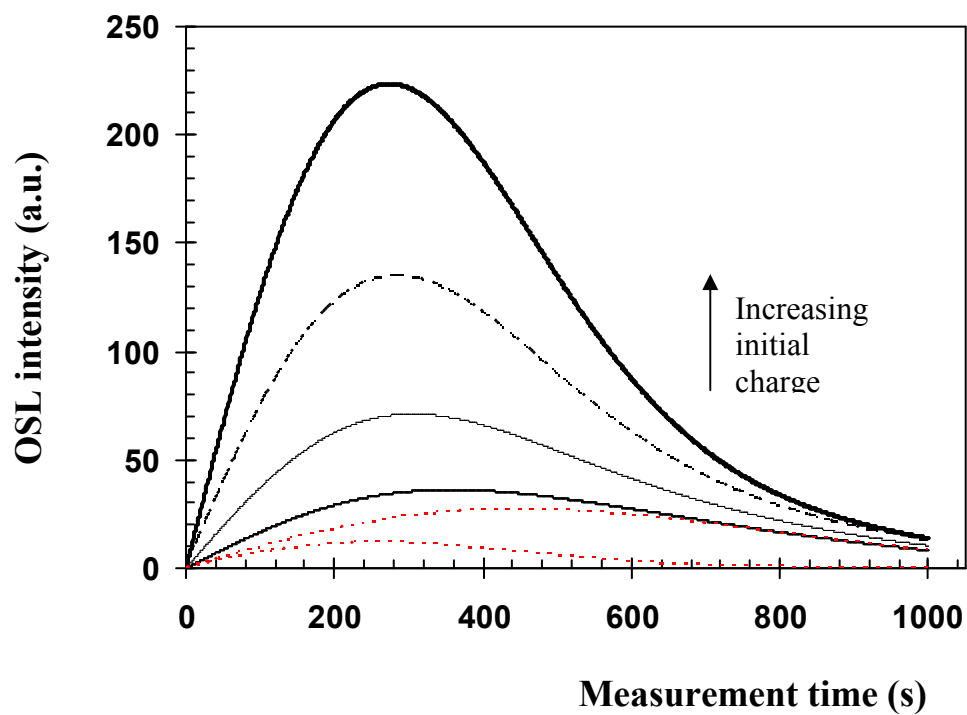
Fig. 4.8 Simulations using analytical model of a two first-order trap system (ratio of σ, 3:1). The contributions from each component at the lowest dose are plotted in red. The black lines represent the LM OSL from different doses. The peak position of the LM OSL shifts to shorter times at higher doses.

In summary, the response of the LM OSL t_{peak} to dose (i.e. trapped charge concentration) is a critical indicator of charge transfer kinetics. It is assumed that the LM OSL obeys first order kinetics if no change in shape or position of the LM peak with dose is observed. Through simple numerical modelling work it has been demonstrated that a spectrum of kinetic orders can be displayed in a single, multi-component LM OSL curve, depending on relative detrapping/retrapping parameters. The (modelled) data could be fitted to the sum of different kinetic order solutions. The information derived from the modelled system has been taken into consideration during the assessment of empirical LM OSL measurements on sedimentary quartz samples in order to gain some understanding of the charge dynamics and a theoretical basis for LM deconvolution in subsequent sections.

In a cautionary note, two first order components with different σ values and different dose responses may also, given the right conditions, produce a single LM OSL peak whose position is dose dependent. A simulated example is shown in Fig. 4.8 where the LM OSL (black line plots) is comprised of two first order components (dotted red lines). Due to the simulated different dose responses of the components the LM OSL peak shifts with dose similar to a single non-first order component. Ambiguity may be resolved through curve fitting, but as Whitley (2000) found it is possible to fit single second-order OSL to two first order components and vice versa under certain conditions. LM OSL measurement at different photon energies should allow conclusions to be drawn more easily (see section 5.3.1 for more details discussion of this).

An important finding from the model is that even if components display non-first order behaviour, at low initial charge concentrations the LM OSL can be fitted to first order solutions and can reasonably well estimate n_0. Therefore using doses well below saturation might simplify experimental investigations in such a situation and this was borne in mind throughout the work described in the following chapters.

Empirical data

Smith and Rhodes (1994) first noted that the quartz CW OSL decay at raised temperature could be described by the sum of three exponential (i.e. first order) decays. Further investigation by Bailey *et al.* (1997) found that these exponential signals were most like to be due to the presence of physically distinct trap types, although they observed non-exponential behaviour in the slow component. However, using the LM OSL technique on a heated quartz sample Bulur *et al.* (2000) identified four first order components. The curves showed no

recognisable peak shift with various given doses, indicating the validity of their first order assumption.

The remainder of this subsection contains a summary of experimental data on a variety of quartz samples. The data presented illustrates the charge concentration dependence of the LM OSL in order to further investigate charge dynamics in the quartz system and validate the fitting procedures used in the subsequent sections. Complete measurement details used to obtain the data outlined here will be described in the relevant sections.

All measurements have been made at temperatures > 120°C to eliminate contributions from a shallow trap identified as the 110°C TL peak. The 110°C TL trap is optically unstable (as demonstrated by Bailey, 1998b) and can be identified as a broad, intermediate component in LM OSL measured at room temperature (Bulur *et al.*, 2000). There is strong photo-transfer/trapping probability to the 110°C TL peak that will modify the form of the other OSL components. When measurements are made at temperatures in excess of ~120°C the residence time of charge in the 110°C TL trap is sufficiently short that it has a negligible effect on the LM OSL.

Fig 4.9 shows LM OSL from an aliquot of sample TQN, given different beta doses (20 to 500Gy) and preheated at 260°C for 10s. In 4.9a one can see the first peak clearly. There is no visible shift with dose. When fitted the first peak is 95% fast component and 5% medium component. The plot strongly suggests that the fast component is first order, as found by previous authors (Bailey, 1998b, Bulur *et al.*, 2000). Fig. 4.9b shows in detail the latter part of the dose response measurements. From this plot one can see that component 3 (at t_{peak}~1000s), which will be referred to as slow component 1, or S1, does not noticeably shift with dose either. There are two further slow components, as indicated on the plot as S2 and S3 (as first found in another sample by Singarayer and Bailey, 2002). The form of S2 is somewhat masked by S3 and the peak of S3 was not measurable using the experimental set up described in section 2.4.1. The peak of component S2 does not move significantly with dose, however, it is difficult to arrive at any conclusions concerning the kinetic order of component S3 from this sample using the present data.

In Fig 4.10 the LM OSL following different doses for three more samples is illustrated. The plots again focus on the latter part of the measurement to show in detail the slow components S1, S2 and S3. The response of S2 is unclear due to the overlap with S1 and S3 in sample CdT9 (Fig 4.10a), which is as a result largely featureless over this region. It is tentatively suggested that component S2 does not shift with dose in this sample. The LM curves for sample CdT4 show similar findings. Components S1 and S2 as indicated on the graph more

clearly maintain the same t_{peak} at all doses. Although the highest dose used in this case was only 90Gy, this covers a significant range of the dose response curve of component S2 (see section 6.3.2). Sample SL203, on the other hand, seems to show that S2 peak position shifts to slightly shorter times at high doses. This may suggest that S2 is not quite first order in this particular sample (somewhere between 1st and 2nd), but could also result from a change in relative magnitudes of S1 and S2, as the components have different dose responses. Similar data were obtained for an aliquot of SL203 using a 350°C preheat, presented in Fig. 4.11. In this case there was no shift in peak position of S2. However, this could be due to thermal erosion during preheat resulting in low concentrations post-preheat even though high doses were given initially since, as found in the modelling results, at low doses non-first order components can display first-order form.

Measurements could not be made at sufficiently high stimulation intensities to allow the recording of the S3 peak using LM OSL. Therefore no conclusions can be drawn concerning kinetic order using these data. However, data presented in section 6.3.2 indicated that S3 displays non-first order behaviour. This is discussed in more detail in the relevant section.

Singarayer and Bailey (2002) discovered that using infrared stimulation (7000s at 160°C using the laser described in chapter 2) one could completely bleach the fast component with negligible depletion of the medium (see Fig 4.12a showing near overlap of blue stimulated LM OSL following 6000s and 8000s IR). Various doses were given, followed by 8000s IR to bleach the fast component. In the LM OSL measured subsequently (Fig. 4.12b) the peak consists of primarily medium component. There is no observable shift in peak position with dose, implying that the medium component is first order.

In summary:

- The fast, medium and S1 components demonstrate first order response to dose. Component S2 also displayed first order behaviour in most samples. At low doses in all samples component S2 does seem to act as first order. The component S3 LM OSL peak is not measurable on the experimental setup used.

- For subsequent data, most experiments have been performed having given low laboratory doses (usually ~20Gy). At these doses components can be approximated by first order, and behave as such (see e.g. Fig. 4.12). For where high doses were required general order solutions for component S2 and S3 (see section 6.3) were used.
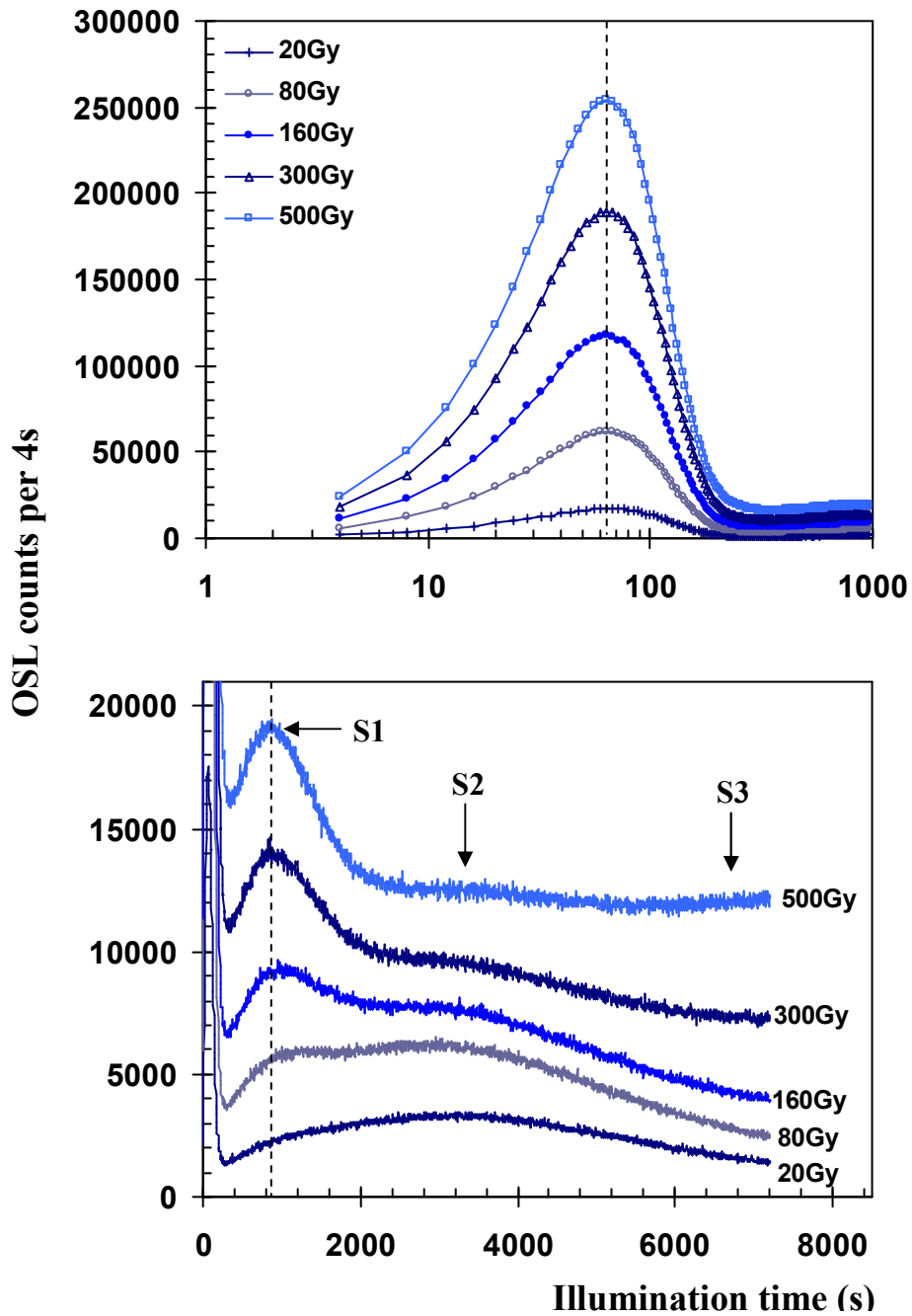
Fig. 4.9 LM OSL from a single aliquot of sample TQN following various added laboratory beta doses and 260°C preheat. (a) Data plotted on log (t) scale to show the first peak more clearly (primarily fast component) (b) data plotted on linear scale to show the form of the slow components more clearly.
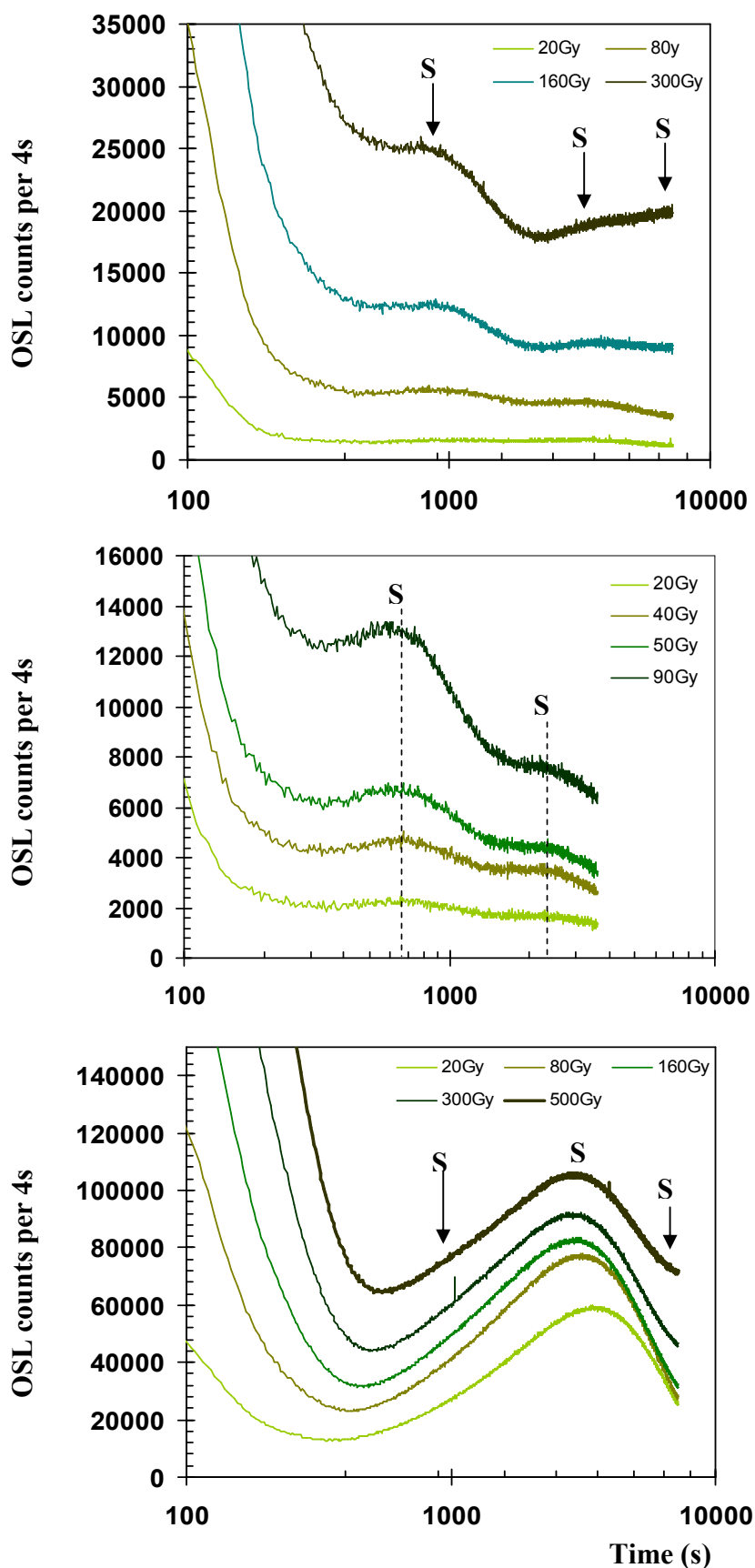
Fig. 4.10 Dose response of samples (a) CdT9 (b) CdT4 (c) SL203. Measurements were made on single aliquots. Following a beta dose the aliquots were heated to 260°C for 10s. LM OSL measurements were made at 160°C. LM OSL (a) and (c) were measured for 7200s using R4a. LM OSL (b) was measured on R4b for 3600s.
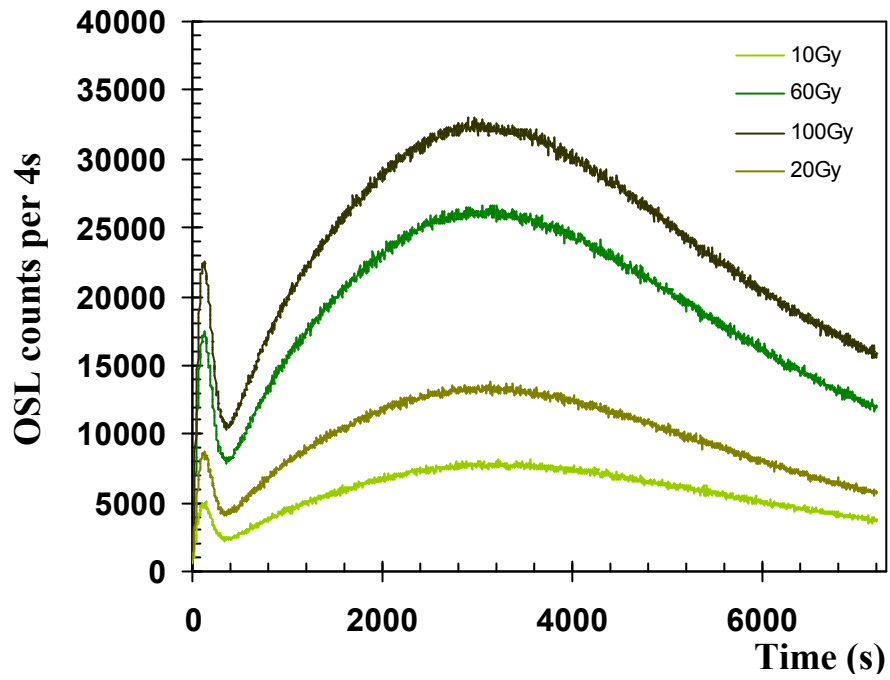
Fig 4.11 LM OSL on a single aliquot of sample SL203. Following laboratory beta dose the aliquot was heated to 350°C. LM OSL measurements were performed at 160°C.
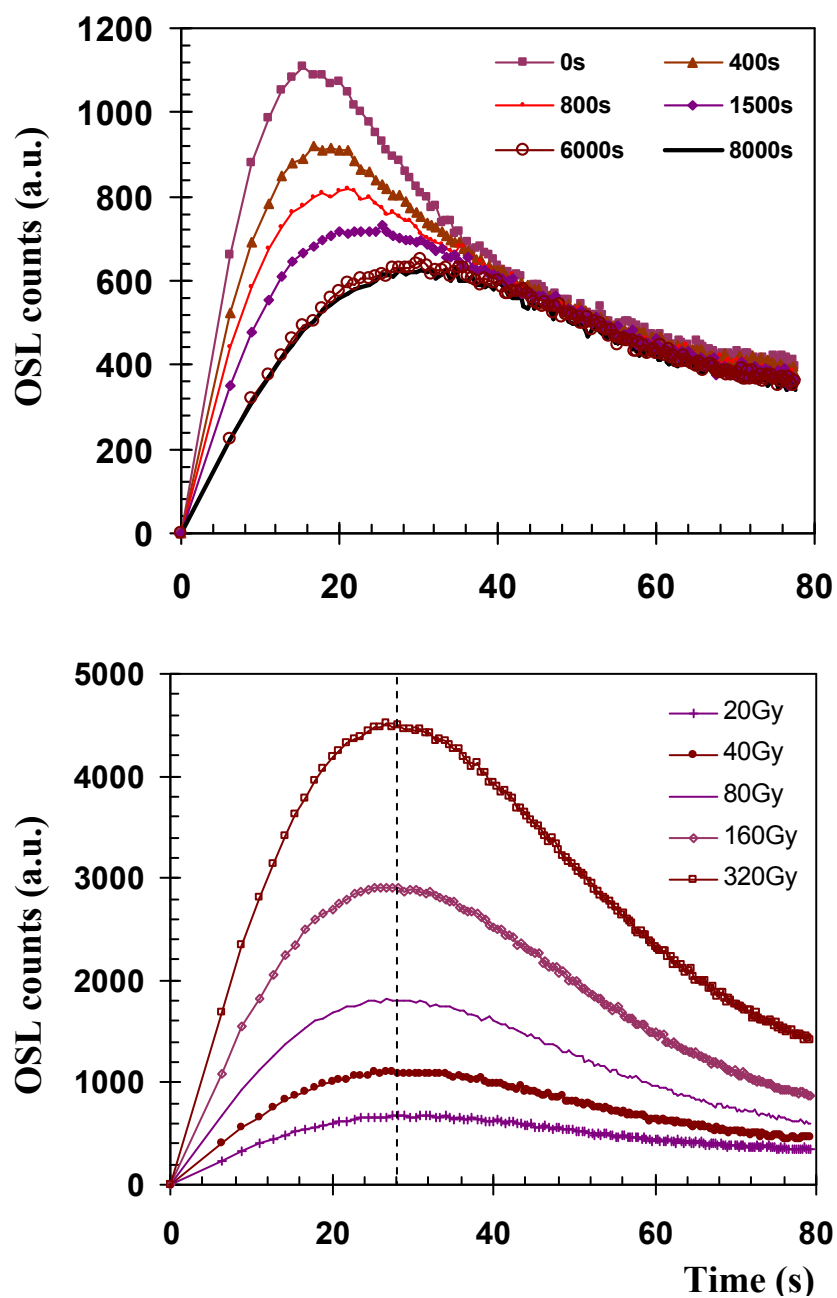
Fig. 4.12 (a) Pseudo-LM from sample SL203 following various durations of prior partial bleaching with IR at 160°C. (b) LM OSL from an aliquot of Sl203 following various laboratory beta doses and 8000s of IR exposure at 160°C, to remove the fast component (i.e. the peak is composed of mainly medium component).

4.3 OSL variability

4.3.1 Sample variability

It is important that the components being studied are represented in lots of different quartz samples from various locations, otherwise this study cannot be extrapolated to samples other than those used in the experiments. For the study to be worthwhile it should be applicable to a wide variety of quartz samples used for dating. Bailey (1998b) found that the CW OSL from seventeen out of eighteen sedimentary samples could be fitted to three exponential components. The half-life of the fast and medium components obtained through curve fitting were similar (within errors) in the various samples. They found that the decay of the 'slow' component was much more variable. This would be expected if it consisted of more than one component, as found by e.g. Bulur *et al.* (2000). The proportions of the components varied between samples.

Kuhns *et al.* (2000) investigated the form of the LM-OSL from several different types of quartz (sedimentary, natural rock crystal and synthetic quartz). Two samples from each type of quartz were used in the experiments. They noted that although there was similarity in the form of the LM OSL from the samples within each type, there was less similarity between the different types of quartz. Through curve fitting the photoionization cross-sections of the fast, medium and slow components fitted were found to be similar between the two samples of sedimentary quartz used. They observed no universal behaviour for quartz. However, their sample base was limited and they assumed only three constituent components.

For the purposes of this study only sedimentary quartz samples are relevant and the issues further investigated are done so in consideration of optical dating. Common components in various quartzes would be expected to arise from the same type of defect. Extensive studies (summarised in e.g. McKeever, 1985) have not been able to conclusively connect specific defects to OSL traps/centres. Therefore no discussion will be entered into to attempt to explain why sedimentary quartzes derived from spatially disparate locations might produce common OSL components.

However, it was deemed important to look at the form of the LM OSL from a number of quartzes taken from a variety of locations and depositional environments to explore how general the findings from further experiments will be. The details of each of the samples used are given in Appendix A. For 12 samples the natural LM OSL signal was measured (following preheat to 260°C, 10s) for 3600s at 160°C. The data resulting from these measurements are not shown here as the naturally absorbed dose varied enormously from sample to sample. Following the bleaching of the natural luminescence a 20Gy beta dose was

administered to each of the aliquots used. The LM OSL recorded from the 12 samples under the same conditions as the natural signal is displayed in Fig. 4.13.

The large variation in brightness/sensitivity is immediately apparent from the results. In general two peaks are observed and with the exception of MAL and SOT the position of these peaks does not seem to vary significantly between the samples. The position of the first peak is between 45 and 55s. This varies slightly because of noise and the relative size of the fast and medium components that make up the first LM OSL peak. The size of the slow components also will have an effect on the position of this peak to a smaller extent. The position of the second peak appears to be more variable. For several of the samples a second peak was observed at ~2500s. MAL peaks earlier (~700s) and in sample CdT9 two slow component peaks are observed (~850s and ~2500s). The position and number of slow components peaks depends on the number and relative size of the slow components.

The data from the 12 samples examined were fitted to first order components. In general four or five common components gave good approximations to the data, although not all components were present in all samples. A list of photoionization cross-sections of the fitted components for all samples is given in Table 4.2. The components have been called the fast, medium, (as in Bailey *et al.*, 1997) and slow components S1, S2 and S3. Similar values for each component were found between the samples, except for samples SOT and MAL. An average value for each component is given at the bottom of the table, with their standard deviation. That reasonable agreement of the component parameters was observed between samples indicates that the results from further experiments applied to a few samples to examine the behaviour of the OSL components (chapters 4 and 5) are more generally applicable to sedimentary quartz.

In sample RB3 a small 'ultrafast' component was also fitted. This has been observed by several authors (e.g. Dr M. Jain *Pers. Comm.*). In some of the aliquots of sample CdT1 the ultrafast component produced a clearly visible separate peak in the LM OSL (after a lower 220°C preheat) such as Fig. 4.14. However, no further experimentation was performed on samples displaying this component and it does not appear to be present in the majority of samples. It was noted that this component seemed not to be very thermally stable.
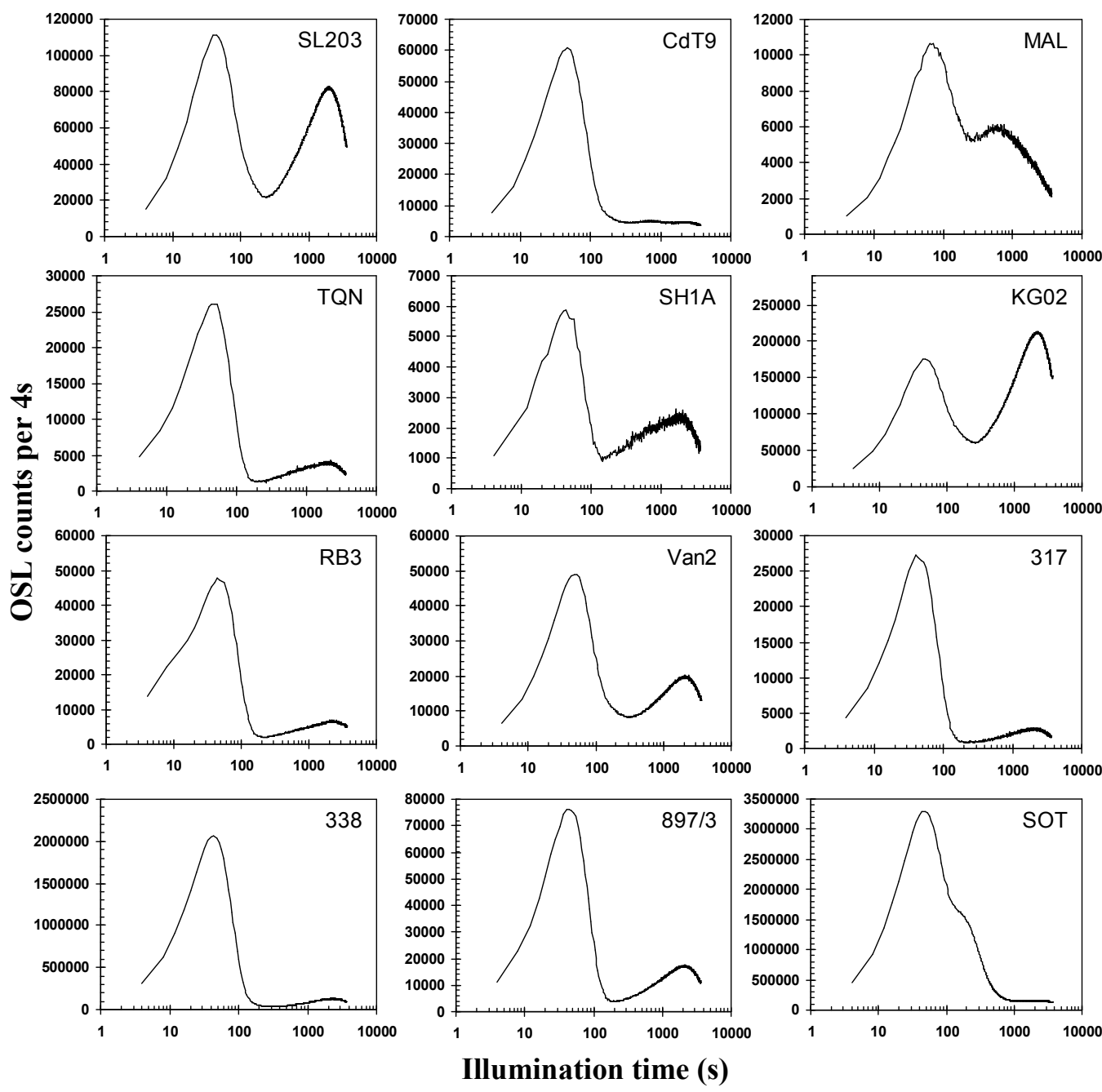
Fig. 4.13 LM OSL from 12 sedimentary quartz samples following bleaching of the natural signal, 20Gy beta dose and preheat to 260°C. LM OSL measurements were made for 3600s at 160°C from 0 to 36mWcm^{-2}.
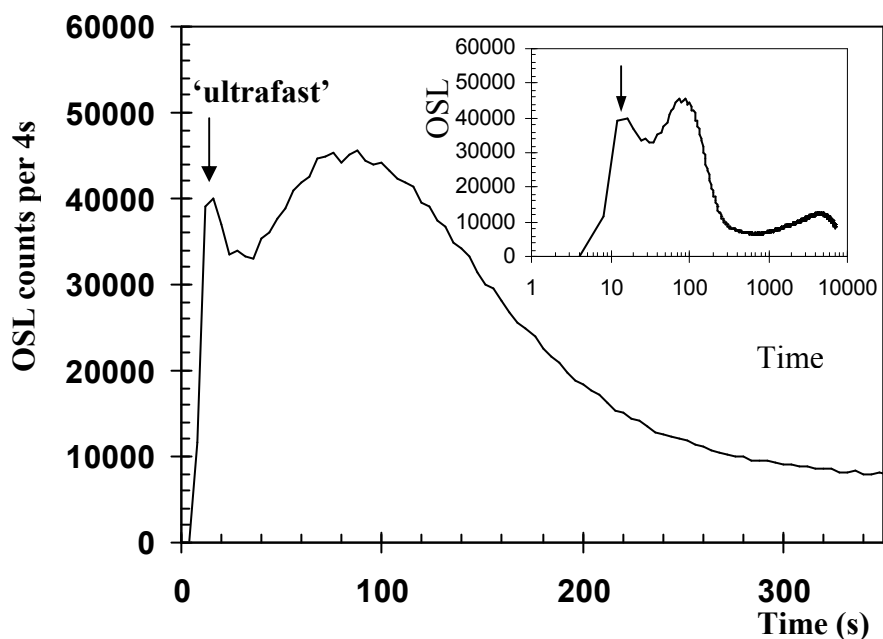
Fig. 4.14 LM OSL from sample CdT1 given 20Gy and preheat to 220°C prior to measurement. In this aliquot a very rapidly decaying component (indicated by arrow) was observed to produce an LM OSL peak at shorter times than the fast component. Inset shows the same data on log(t).

Sample	Photoionization cross-section					
	Fast	**Medium**	**S1**	**S2**	**S3**	**Ultra-fast**
CdT9	2.3×10^{-17}	3.8×10^{-18}	1.8×10^{-19}	1.7×10^{-20}	3.2×10^{-21}	-
SH1A	2.8×10^{-17}	5.9×10^{-18}	2.3×10^{-19}	1.6×10^{-20}	7.8×10^{-21}	-
SL203	3.1×10^{-17}	6.6×10^{-18}	2.6×10^{-19}	1.2×10^{-20}	6.3×10^{-23}	-
338	2.6×10^{-17}	5.2×10^{-18}	-	1.0×10^{-20}	-	-
317	2.5×10^{-17}	5.2×10^{-18}	1.8×10^{-19}	1.2×10^{-20}	-	-
TQN	2.4×10^{-17}	9.1×10^{-18}	1.6×10^{-19}	1.2×10^{-20}	1.2×10^{-22}	-
897/3	2.4×10^{-17}	8.1×10^{-18}	2.0×10^{-19}	1.1×10^{-20}	-	-
RB3	2.3×10^{-17}	8.1×10^{-18}	1.8×10^{-19}	1.1×10^{-20}	4.0×10^{-22}	7.0×10^{-16}
Van2	2.2×10^{-17}	2.8×10^{-18}	2.0×10^{-19}	1.2×10^{-20}	6.5×10^{-22}	-
KG02	2.6×10^{-17}	4.6×10^{-18}	3.1×10^{-19}	1.1×10^{-20}	7.8×10^{-22}	-
SOT	2.8×10^{-17}	6.4×10^{-18}	1.7×10^{-18}	2.7×10^{-20}	3.9×10^{-21}	-
MAL	1.2×10^{-17}	6.6×10^{-18}	1.9×10^{-19}	2.6×10^{-20}	1.7×10^{-21}	-
Average	$2.5 \pm 0.3 \times 10^{-17}$	$5.9 \pm 2.0 \times 10^{-18}$	$2.1 \pm 0.5 \times 10^{-19}$	$1.2 \pm 0.2 \times 10^{-20}$	$1.9 \pm 2.8 \times 10^{-21}$	-

Table 4.2 List of fitted component photoionization cross-section values for 12 different sedimentary samples. The list is grouped according to common parameters – fast, medium, S1, S2, S3 and ultra-fast. Average values and standard deviation from all except SOT and MAL are shown in at the bottom of the table.

4.3.2 Grain-to-grain variability

The variation of the OSL signal in quartz has been studied by several authors e.g. Duller *et al.* (2000), Adamiec (2000a, 2000b). In the study by Duller *et al.* (2000) large variation in the brightness of single grains from a sample, as given by the integrated OSL, was observed. In some samples 95% of the total OSL originated from 5% of the grains. The first single grain LM OSL results from quartz were published by Bulur *et al.* (2002). From 81 grains of a single sample three components were fitted, the third component visible as a rising edge only. Great variation was observed not only in the brightness of the grains but also in the relative proportions of the different components. They found that not all components were present in the OSL from all grains, but that the detrapping parameters of common components in different grains were very similar. This suggested that similar detrapping mechanisms were at work, and that interactions of the different traps are minimal. The observed heterogeneous distribution of traps on a grain-to-grain level led Bulur *et al.* (2002) to speculate that the same heterogeneity may be present within individual grains.

Extensive experiments examining the behaviour of the LM OSL from single grains different samples were not within the scope of this study. However, some measurements on single grains of a sample to investigate the variability were performed to provide insight into the single-aliquot experiments described in the following chapters. The single grain reader attachment on R4b outlined in section 2.41 was used. One hundred grains of bleached sample SL203 were mounted on a single disc. The grains were given a 52Gy dose and preheated to 260°C for 10s before recording the LM OSL at 160°C for 50s from 0-10mW. This was the longest measurement time possible with the current software and was unfortunately not long enough to allow recording of the second LM OSL peak (the slow components).

Unusually, a measurable signal was obtained from over 50% of the grains, a far higher proportion than observed by other authors (e.g. Duller *et al.*, 2000). The results from 17 example grains are shown in Fig. 4.15. The majority of grains exhibiting an OSL signal contained slow (hard-to-bleach) components, as given by the rising signal at the end of the measurement, and a significant number, 38% contained only slow component (e.g. grain 12 in Fig. 4.15). 26% of grains contained a fast component along with the slow, e.g. grains 7 and 8. A few of the grains displayed only medium and slow components e.g. grain 11. The rest of the grains with measurable signal contained fast, medium and slow components (e.g. grains 1, 9, 13). Due to the longer wavelength stimulation used for single grains (532nm) than multigrain aliquots (470nm) the peak positions of the fast and medium component are better resolved, i.e. pulled apart, making the distinction between fast and medium clearer. The

different response of the OSL components to photon energy is discussed in 5.3.1. The sum of the LM OSL from the 100 grains is shown at the bottom-right of Fig. 4.15. This represents the form of the LM OSL from a multiple grain aliquot.

The fast component has peak position of roughly 1.5 – 2s. This varies slightly from grain to grain due to noise, variation in the number of dead channels, and possibly the position of the laser light on the grain, affecting the stimulation intensity received by the grain. The peak position of the medium component from initial analysis is about 6 – 8s. By fitting the data to the sum of three exponentials detrapping rates for the fast and medium were found at be 10.5 and 0.97 (a.u.) respectively. The ratio of the photoionization cross-sections of the fast and medium is around 10.8. This is comparable to results from section 5.3.1 where the ratio of fast and medium components found by bleaching at 525nm (at room temperature) and measuring decay at 470nm was 9.9.

In order to illustrate further the distribution of the OSL signals, the initial integrated OSL (to represent the easy-to-bleach components) was ordered according to descending brightness and the cumulative light sum plotted as a function of the proportion of total grains. A similar plot was constructed using the integrated light sum from the end of the LM OSL measurements to represent the hard-to-bleach components. These plots are given in Fig. 4.16. In the upper plot the blue dotted line represents the result that would be obtained if all the grains contributed equally to the total OSL.

The plots in Fig 4.16 demonstrate visually the finding stated above that the easy-to-bleach components are distributed over a smaller proportion of the grains than the hard-to-bleach components, i.e. the lower plot is closer to the diagonal blue dotted line than the upper one. In the upper plot only five of the grains give 50% of the LM OSL from the easy-to-bleach components and around 40% of the grains show no significant easy-to-bleach components. In the analysis of the tail portion of the LM OSL (the hard-to-bleach components) only 10 of the grains displayed negligible slow component.

The main aim of this experiment was to demonstrate the heterogeneous distribution of components within grains of a sample that has been used for further studies as multiple grain aliquots. Although the number of grains studied was a small fraction of those in a multiple grain aliquot useful results concerning the grain-to-grain distribution of the OSL components were achieved. Similar experiments on more of the samples were not possible within the constraints of the present study but given that previous studies have shown vast differences in virtually all aspects of luminescence behaviour it is worthy of further study taking consideration of the distribution of components.
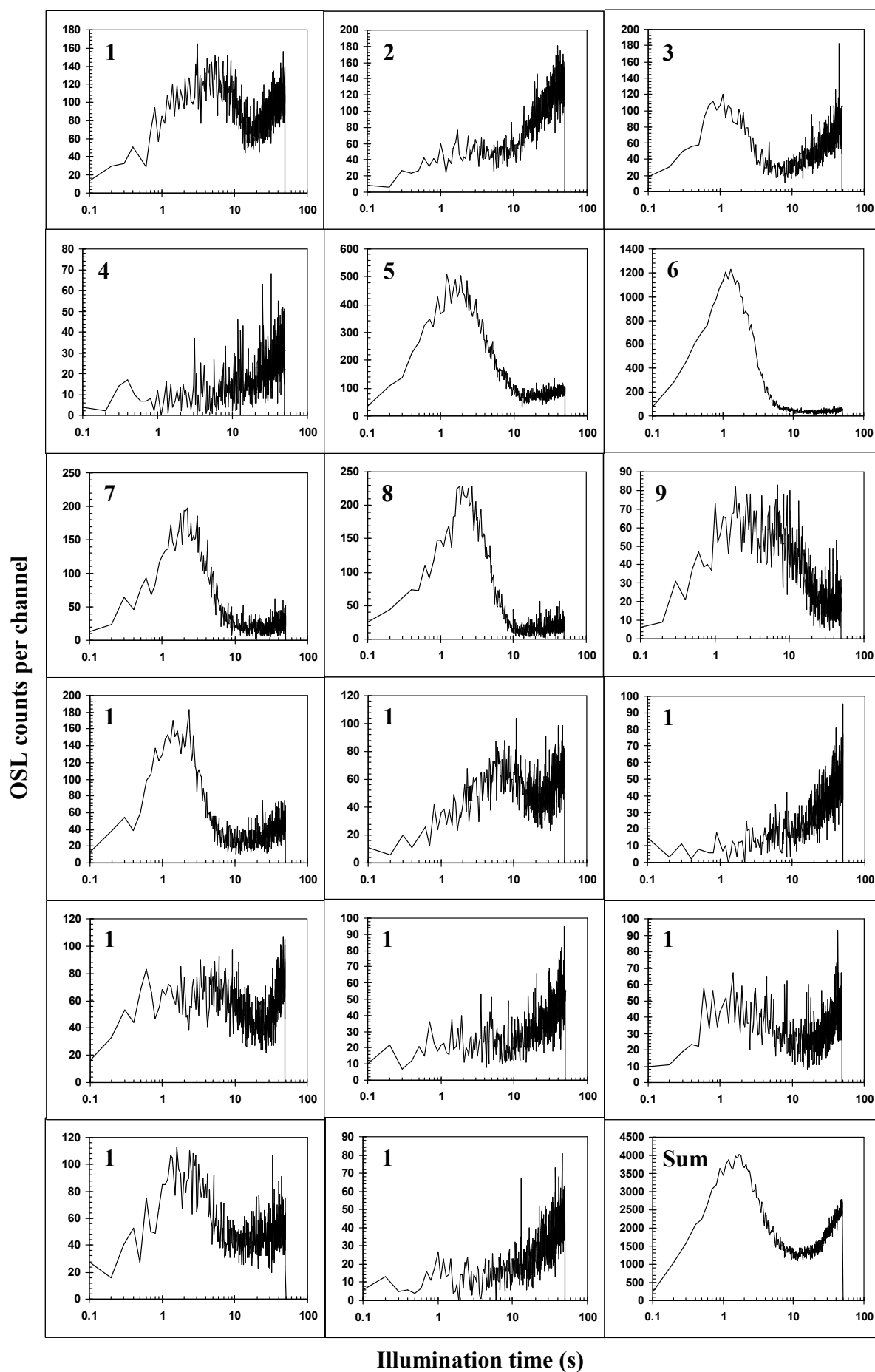
Fig. 4.15 LM OSL from 17 grains (from 100) of sample SL203 following 52Gy dose and preheat to 260°C, 10s. LM OSL measurements were made at 532nm for 50s from 0 to 10mWcm^{-2} at 160°C. The sum of the LM OSL from all the grains measured is displayed bottom right corner.
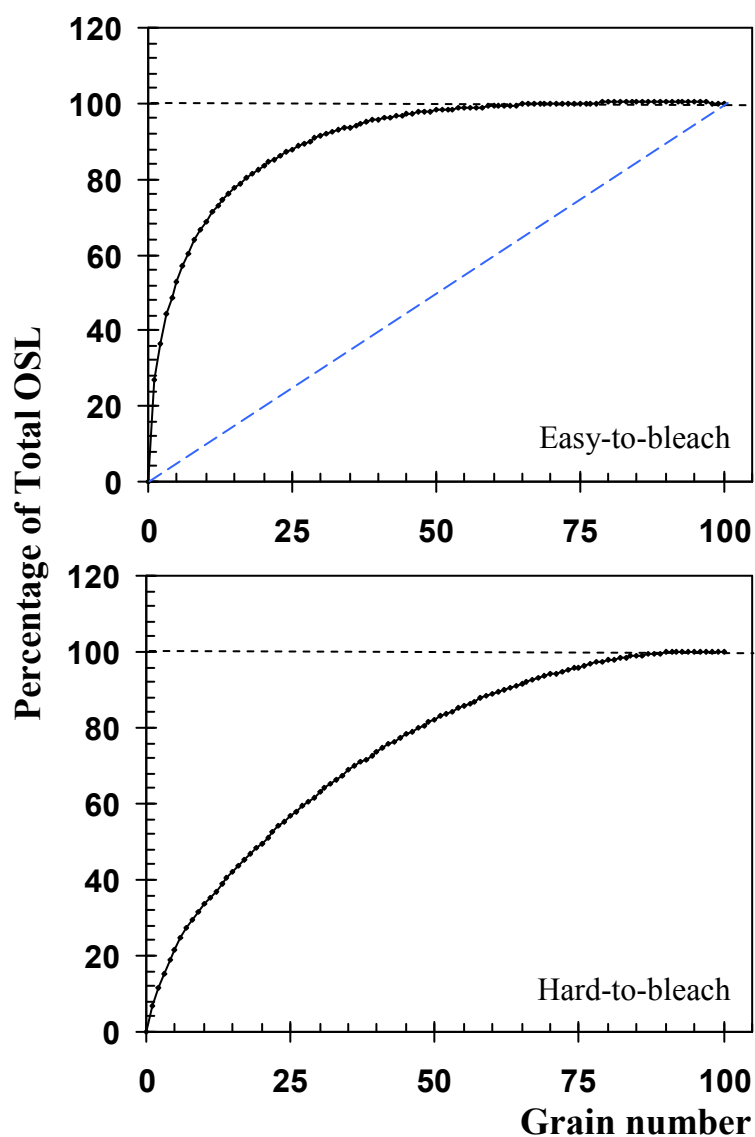
Fig. 4.16 A cumulative intensity plot showing the OSL signal from each grain as a percentage of the total OSL. The plots have been split into easy-to-bleach components in the upper plot (as given by the integral of the initial signal) and hard-to-bleach components (integral of the final measurement channels) in the lower. The blue line in the upper plot represents the plot that would be obtained if each grain contributed to the total OSL equally.

4.3.3 Implications for multi-grain experiments

LM OSL measurements on a number of sedimentary quartz samples have shown that there are at least five components that are common to most samples collected from a variety of locations and environments. Although not all components were observed in all samples the trap parameters of the present components were consistent between samples. Therefore it is concluded that the experiments described in the rest of the study on a few samples can reasonably be extrapolated to other quartz samples.

The single grain results showed that not all components are measured in all grains, and that the distribution of the total light sum between the grains was more equal for the hard-to-bleach components than the faster components. That the form of the fast and medium components does not seem to be significantly affected by the presence/absence of the other components suggests that they effectively don't interact, i.e. the first-order kinetic system is a good approximation.

Further, the results of this study should be taken into consideration when interpreting the results from multiple grain aliquot experiments investigating the interactions between different trap types, e.g. thermal and photo-transfer, since all traps are not present in all grains. There also may be potential implications for studying the OSL components using single grains without using complicated fitting routines. If single grains display single OSL components it could be possible to isolate and study the components this way in the future, although this is potentially an enormous amount of work given the small proportion of grains that give off a measurable signal.

The variability of single grains observed, in terms of which components are present and their brightness, may be related geochemical variations during rock formation, and to the number of depositional cycles a grain has undergone following separation from the parent rock. Given the mixed nature of sand-sized quartz in the natural environment it is perhaps likely that multiple grain aliquots are relatively homogeneous, in terms of the number of components, as shown by the results presented in section 4.3.1.

4.4 Thermal stability

4.4.1 Introduction

The retention lifetime of trapped charge, i.e. the length of time an electron is expected to remain trapped, is given by the following equation, assuming first order kinetics:

$$\tau = s^{-1} \exp(E / k_B T) \tag{4.8}$$

where τ is the lifetime (s), s is the frequency factor (s^{-1}), E is trap depth (eV), T is temperature (K) and k_B is Boltzmann's constant ($\sim 8.615 \times 10^{-5}$ eVK^{-1}). The lifetime presents one of the fundamental limitations to luminescence dating. To avoid age underestimation by more than 5% the lifetime at a given storage temperature needs to be at least 10 times the burial period (Aitken, 1998). Previously reported values for the lifetime of quartz OSL include 630Ma at 20°C by Rhodes (1990) and 850Ma at 20°C by Murray and Wintle (1999) for the initial decay of the OSL signal. Huntley *et al.* (1996) found evidence for four components with lifetimes at 20°C of 14ka, 2Ma, 28Ma and 4700Ma from isothermal decay analysis. Bailey (1998b) attempted a CW OSL, component-resolved isothermal decay analysis (using three exponential components). He obtained E and s values for the fast and medium components from which one can estimate lifetimes at 20°C of fast=210Ma, medium=1230Ma. From pulse annealing measurements on the slow component he also suggested that it was stable up to ~650°C, indicating that the slow component's OSL originated from a deep, extremely thermally stable trap.

Presented in this section are pulse annealing and isothermal decay experiments using LM OSL to obtain component-resolved thermal stability data on several sedimentary quartz samples. The influence of OSL measurement temperature and investigation into thermal transfer using LM OSL are also undertaken later in this section.

4.4.2 Dependence on preheating temperature: pulse annealing

For initial investigations into the thermal stability of the quartz OSL components a modified version of previous 'pulse annealing' experiments performed by e.g. Duller (1994) was used. The main modification was the long LM OSL measurement needed to obtain information for each OSL component at each preheating temperature as opposed to the strategy of 'short-shine' measurements previously employed. The experimental procedure used is outlined below in Fig. 4.17.

Following a low laboratory dose (20Gy) aliquots were preheated to temperatures between 250 and 450°C. LM OSL was subsequently performed for 7200s at raised temperature

(160°C). The long LM measurements were not sufficient to completely zero the slower components. Therefore, an additional CW OSL of 6000s at 170°C was carried out between each measurement to bleach the OSL to negligible levels (confidence in the level of bleaching was found by comparing the magnitude of the final part of the CW OSL measurement to the background from a 'dead' disc). The LM OSL from a test dose (10Gy) was used to correct for sensitivity change (see Fig 4.17 for details). The LM OSL from a 'dead' disc was used in background subtraction.

Pulse annealing was performed on three different samples. The data for sample TQN was collected using the replacement diode unit described in section 2.4.1 (Reader R4b), which ramped linearly, thereby allowing standard deconvolution methods to be used on the data. Fig 4.18 shows the LM OSL curves for sample TQN obtained from the pulse annealing experiment. From the upper plot, it can be seen that peak 1 is eroded completely by heating to >340°C. This is expected since it has been shown by Bulur (2000) that peak 1 consists primarily of the fast component, which has been found to originate from the 325°C TL region (Bailey *et al.*, 1997). Peak maximums, I_{peak}, of the later components are much smaller than the fast component. All the OSL components are eroded to undetectable levels by preheating to 400°C.

Fig. 4.18c shows the LM OSL measurements following a standard 10Gy test dose used to correct the pulse annealing data. The inset demonstrates that there is a linear relationship between I_{peak} of peak 1 (mainly fast component) and peak 2 (dominated by slow component 2) with the exception of the last point. That these components apparently sensitise together provides some evidence that they recombine at the same luminescence centre. This will be discussed in more detail in section 6.3.

The LM OSL curves have been fitted to the sum of five first order components. It was assumed that using laboratory doses well below saturation level (20Gy in the case of all components; see section 6.3) would ensure LM OSL was approximately first order and could be fitted as such (see section 4.2 for further explanation). Two example fits are shown in Fig. 4.19. The results illustrate that the fast component dominates peak 1, and component S2 dominates peak 2 at lower preheat temperatures (e.g. Fig 4.19a: 275°C). In both examples the absolute residuals are plotted. No structure is observed in the residuals, indicating that the fits are probably adequate.
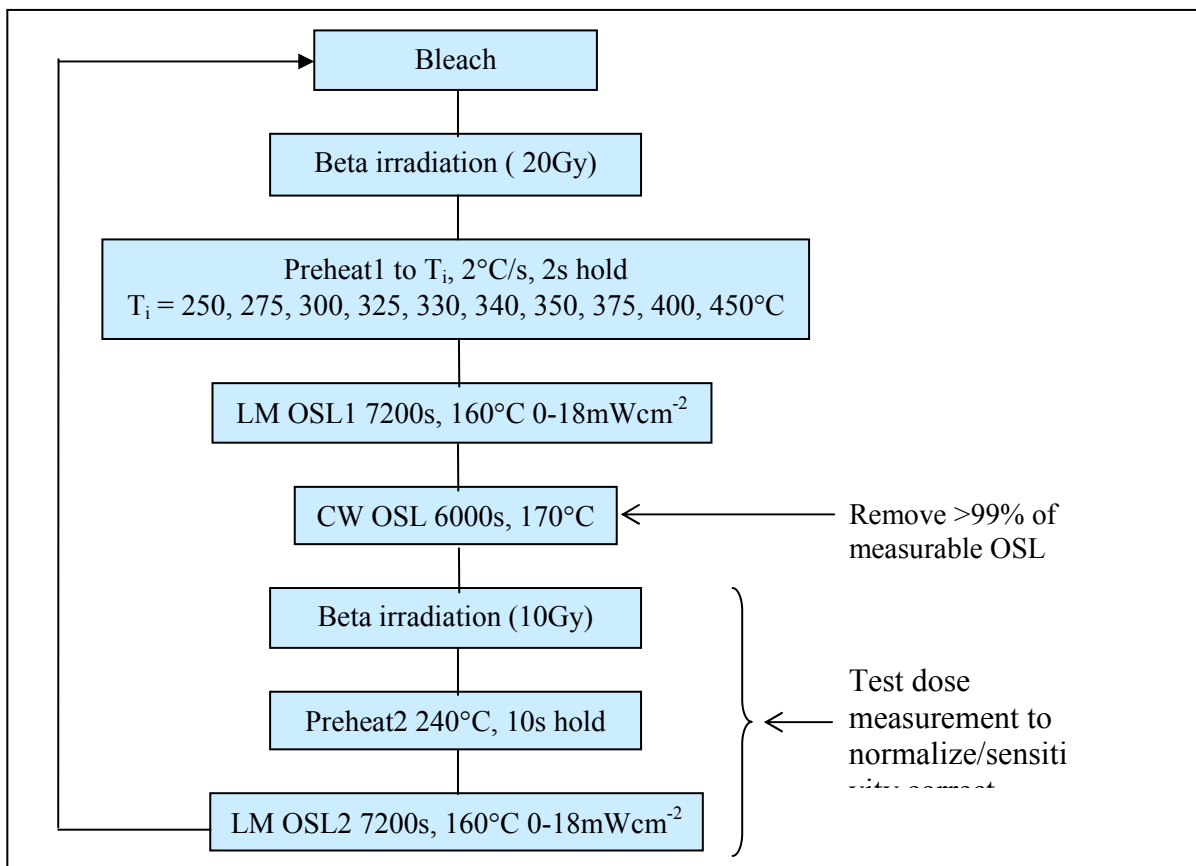
Fig 4.17 Experimental procedure for LM OSL pulse annealing using a single aliquot. Small variations on the procedure were used on different samples, e.g. the number of different preheat temperatures.
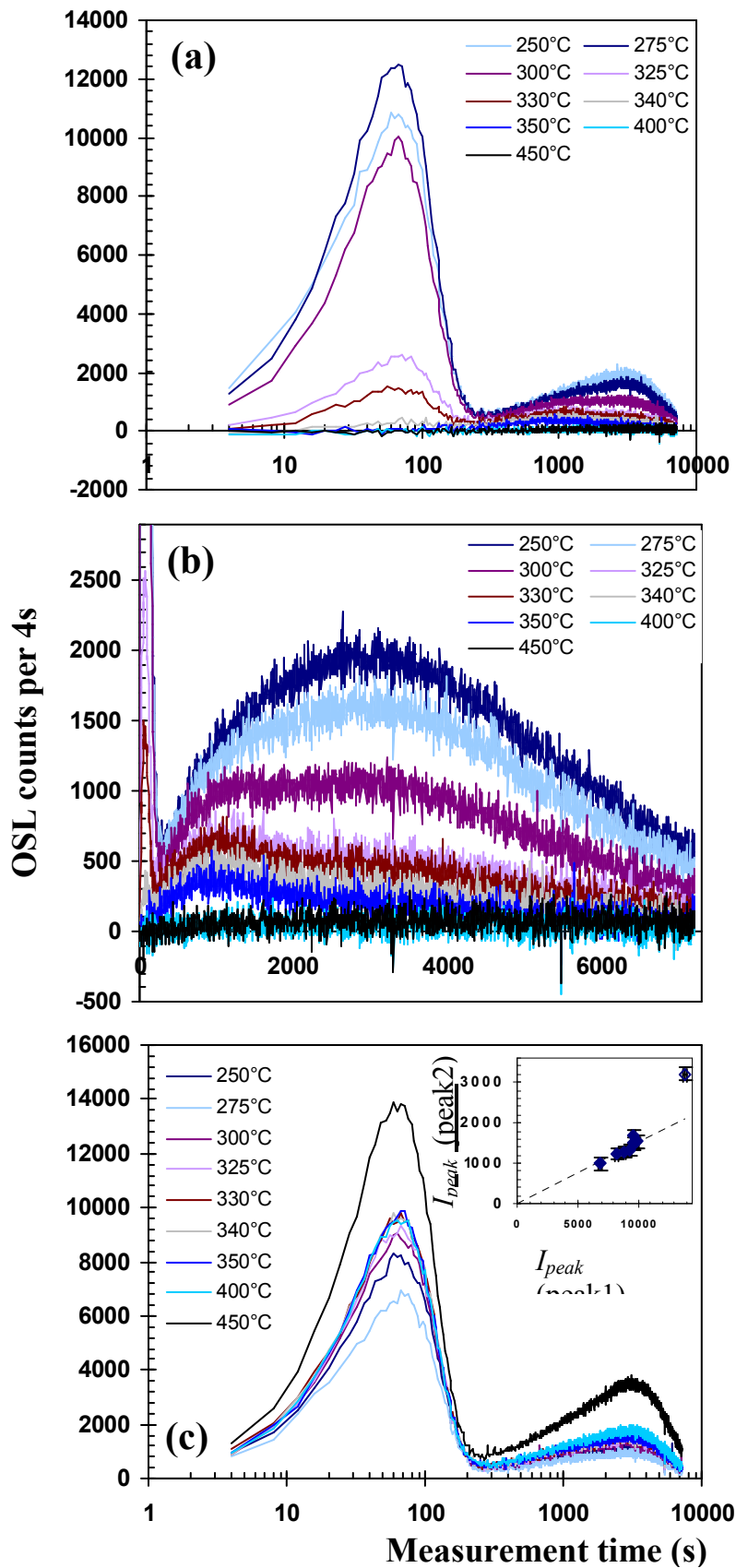
Fig 4.18 (a) LM OSL from a single aliquot of sample TQN following preheating to various temperatures plotted on log(*t*) scale. Plot (b) shows in more detail the latter part of the LM OSL on a linear *t*-scale. (c) The LM OSL from a test dose used to correct for sensitivity change due to preheat1.
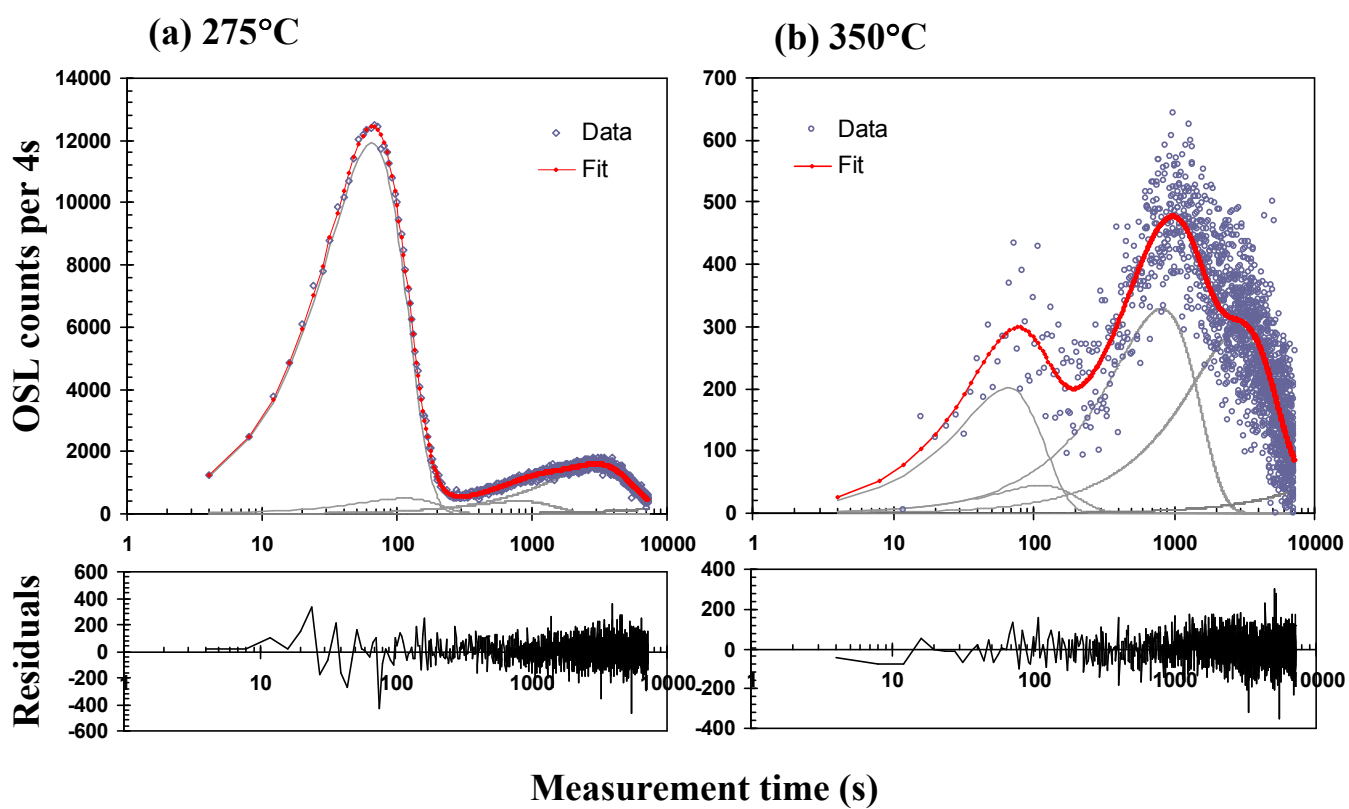
Fig 4.19 Example fitting of TQN pulse annealing LM OSL data to five first order components Preheat temperatures (a) 275°C (b) 350°C. Absolute residuals are also plotted.

Using the fitted component magnitudes, n_{0i}, it was possible to obtain sensitivity-corrected (by dividing $n_{0i}1$ by $n_{0i}2$, from the LM OSL following a standard dose), component-resolved plots of remnant OSL after preheating vs. preheat temperature. Separate plots for each fitted component are given in Fig. 4.21. The fifth component (S3) has not been plotted as measurements could not be performed at sufficient maximum stimulation intensity (and high enough dose) to allow enough of the component peak to be observed for consistent fits giving reliable data to be obtained.

The magnitude of the fast component drops sharply between 250 and 350°C. Previous authors, using CW OSL, integrating the initial portion of the decay (i.e. part dominated by the fast component), have observed a similar form for quartz. The shape of the medium component pulse-annealing curve is more ambiguous, partly because of the errors associated with the data obtained. It appears that a small proportion of the medium component is present after higher preheat temperatures than the fast (there is still medium component present after preheating to 350°C). However, substantial thermal erosion also appears to take place at lower temperatures than those that affect the fast component. Slow component S1 looks to be slightly more thermally stable than the other OSL components. It is relatively stable up to 300°C and reduces rapidly between 300 and 400°C. The pulse annealing data for slow component S2 show that it is the least thermally stable of the OSL components. Although a small proportion of the initial trapped charge is still present after preheating to temperatures in excess of 350°C, significant thermal erosion takes place at relatively low preheat temperatures (i.e. <250°C).

To attempt a more detailed analysis, the data have been fitted to expressions that assume first order kinetics during thermal erosion, derived below. Combining equation 3.1, describing the rate of change of n, and equation 4.8, describing trap lifetime, the following equation is obtained:

$$\frac{dn}{dt} = -ns \exp\left(-\frac{E}{k_B T}\right) \tag{4.9}$$

where n is the trapped charge concentration, T is temperature, n_0 is the initial charge concentration, s is the frequency factor and E is trap depth. Rearrangement of this equation gives:

$$\int_{n_0}^{n} \frac{dn}{n} = \int_{0}^{t} -s \exp\left(-\frac{E}{k_B T}\right) dt \tag{4.10}$$

But unlike the derivation for $I_{LM}(t)$, for pulse annealing it is the preheating temperature and heating rate that need to be used for integration. The heating rate, B, can be described by the following equation:

$$B = \frac{dT}{dt} \qquad (4.11)$$

that can be rearranged to give an expression for dt:

$$dt = \frac{dT}{B} \qquad (4.12)$$

Substituting this into equation 4.10 allows integration on temperature, T.

$$\int_{n_0}^{n} \frac{dn}{n} = \int_{T_0}^{T} - s \exp\left(-\frac{E}{kT}\right) dT \qquad (4.13)$$

Equation 4.13 can subsequently be integrated to obtain n as a function of preheating temperature. This will give an expression for the remnant trapped charge concentration following preheat to temperature, T_i (see Fig 4.20 for illustration), and hence, provide an analytical equation to describe the experimental pulse annealing curves (assuming that LM OSL is always proportional to the remnant trapped charge).
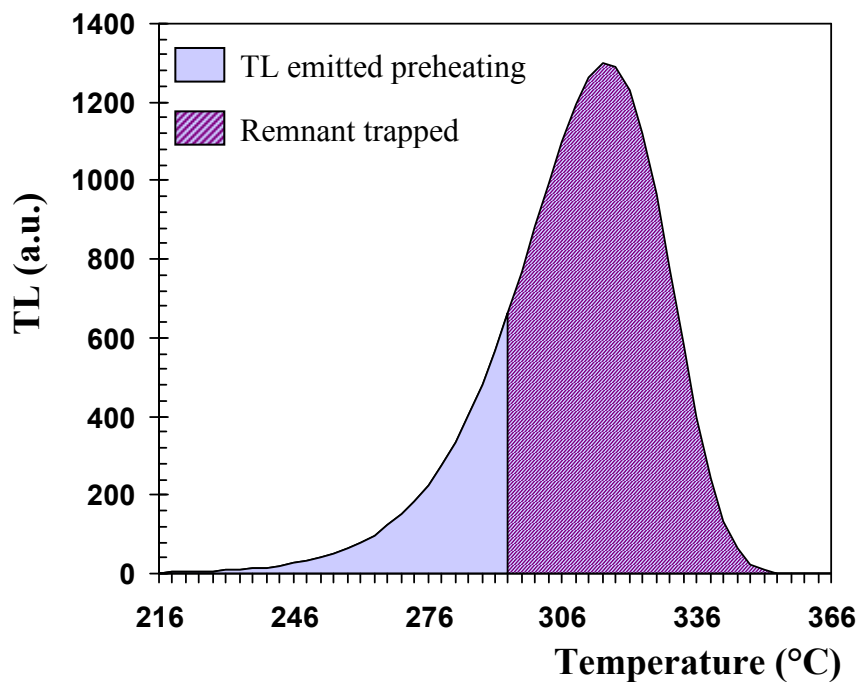
Fig. 4.20 Showing TL emission from a single simulated 1st order trap type during preheating to temperature T_i. In the pulse annealing procedure, the remnant trapped charge, n, is estimated from OSL measurements following the preheat.

The following equation for n is found through integration of equation 4.13:

$$n = n_0 \exp\left[\left(\frac{-sk_BT^2}{BE}\exp\left(-\frac{E}{kT}\right)\right) + \left(\frac{sk_BT_0^2}{BE}\exp\left(-\frac{E}{k_BT_0}\right)\right)\right] \qquad (4.14)$$

where n_0 is the initial trapped charge concentration, temperature is given in Kelvin, and T_0 is the ambient room temperature (~15°C = 288K).

Equation 4.14, giving the remnant trapped charge following preheating to temperature T_i, assuming first order thermal erosion, was used to fit the pulse annealing curves shown in Fig. 4.21. It was noted, however, that the 2s hold at T_{max} that was not accounted for in equation 4.14 may have the effect of making the components seem a little less stable than in reality. Successful fits were obtained from the fast component and component S1. Resultant E and s values from fitting are given in table 4.3. Relatively large errors on the data for the medium component were observed due to its magnitude found from curve fitting being relatively small compared to the other components, and therefore the LM OSL fits were less confident. This may have contributed to the less satisfactory fit of the pulse annealing data using equation 4.14. Slow component S2 could not be well fitted to the derived analytical solution using any combination of parameters. Several possible reasons for this were hypothesised:

1. Systematic errors in LM OSL curve deconvolution.
2. While the LM OSL from a non-first order component given a dose well below saturation may produce a first order peak-shape, thermal eviction during preheating may not have been first order (depending on the heating rate).
3. LM OSL2 'sensitivity correction' did not accurately represent the sensitivity of measurement LM OSL1.
4. There is a distribution of trap depths, E, having very similar photoionization cross-sections for optical eviction. Therefore, the OSL can be fitted to a single component, but the thermal eviction is broad due to the distribution and so the pulse annealing data will not fit to a single component.

To address the first possibility, additional analysis of the LM OSL curves using integrals rather than deconvolution was performed. By integrating from 3500-4000s a matching pulse

annealing decay shape as observed for slow component S2 using curve fitting was obtained, see Fig. 4.22a. It was assumed that the integral 3500-4000s was dominated by slow component 2 (and that since the peak position was not observed to move with preheat it was valid to use the same integration limits for all LM OSL), and that therefore the analyses using deconvolution and integration were equivalent. That each method of analysis produced the same resulting pulse annealing curve shape indicated that the main reason for the shape is not a systematic error from the curve fitting procedure.

In order to investigate option 2 (non-first order thermal eviction) analytical solutions, similar to derived first order solution 4.14, assuming general order kinetics were derived to examine the effect on the shape of the pulse-annealing curve. Substituting equation 4.7 into equation 3.12 and using a similar derivation to that described to obtain equation 4.14 the equation for general order kinetics is given as:

$$n = n_0\left[(b-1)\left(\left(\frac{-sk_BT^2}{BE}\exp\left(-\frac{E}{kT}\right)\right)+\left(\frac{sk_BT_0^2}{BE}\exp\left(-\frac{E}{k_BT_0}\right)\right)\right)+1\right]^{1/(1-b)}$$ (4.15)

where b, is the dimensionless parameter denoting the order of kinetics ($b > 1$), so that it is not confused with the heating rate, B.

The equation for second order kinetics (b = 2) is as follows:

$$n = \frac{n_0}{\left(\left(\left(\frac{-sk_BT^2}{BE}\exp\left(-\frac{E}{k_BT}\right)\right)+\left(\frac{sk_BT_0^2}{BE}\exp\left(-\frac{E}{k_BT_0}\right)\right)\right)+1\right)}$$ (4.16)

Comparison of the analytical solutions for pulse annealing from different orders of kinetics (b = 1, 1.5, 2) are shown in Fig. 4.22b [each with the same given initial parameters: E = 1.75eV, s = 1e13s^{-1}, n_0 = 250]. From the figure it can be seen that as retrapping becomes more significant, i.e. the order of kinetics increases, the pulse-annealing curve becomes increasingly flatter. It was found that the pulse-annealing data for component S2 could be well-fitted using equation 4.16 for second order thermal eviction (Fig. 4.22c shows both 1st and 2nd order fits for comparison).

If this result is reliable it requires that the thermal eviction of charge during heating is significantly non-first order, but that the optical eviction post-preheat can be either first order, or very close to it. It is currently uncertain whether this is physically possible. Numerical modelling of this phenomenon may be able to address this question. It is hoped that such a study will be carried out shortly.
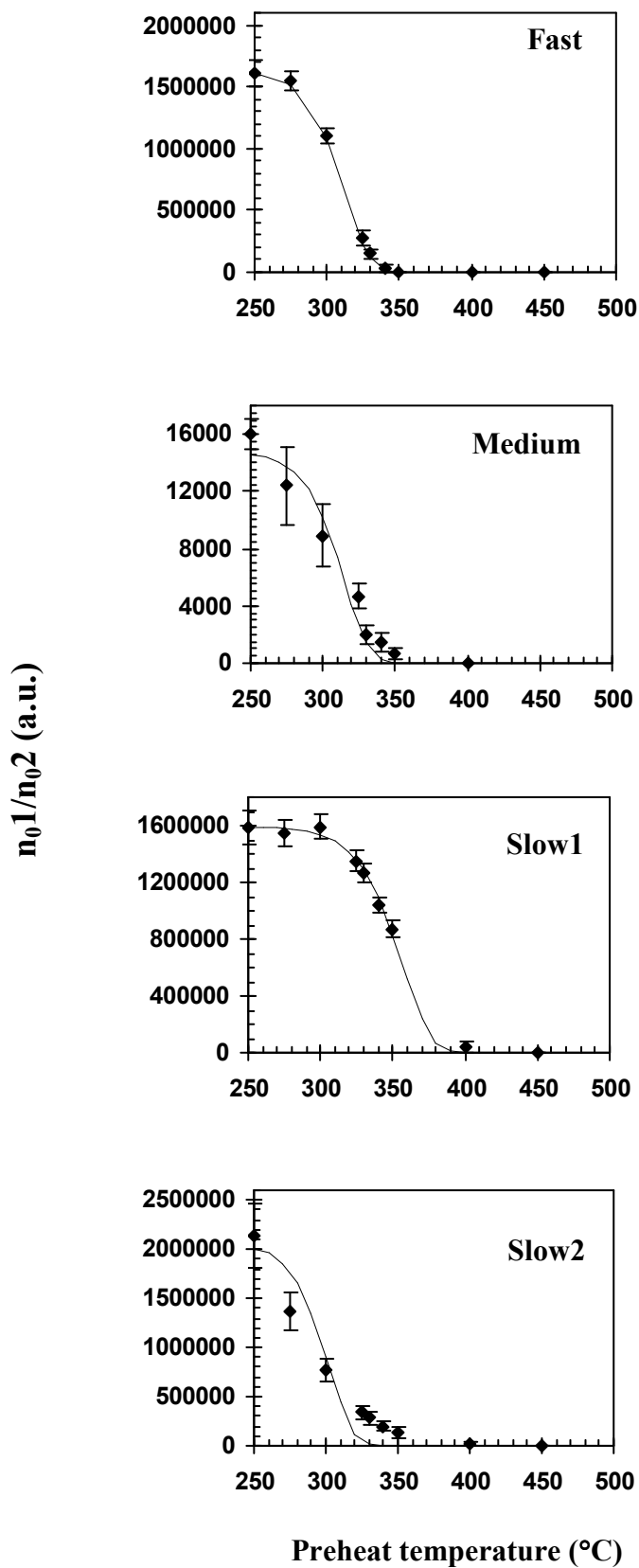
Fig 4.21 Plots of component-resolved sensitivity-corrected magnitudes from curve fitting vs. pulse annealing temperature for sample TQN. The data have been fitted to first order expressions given in the text (Equation 4.14).
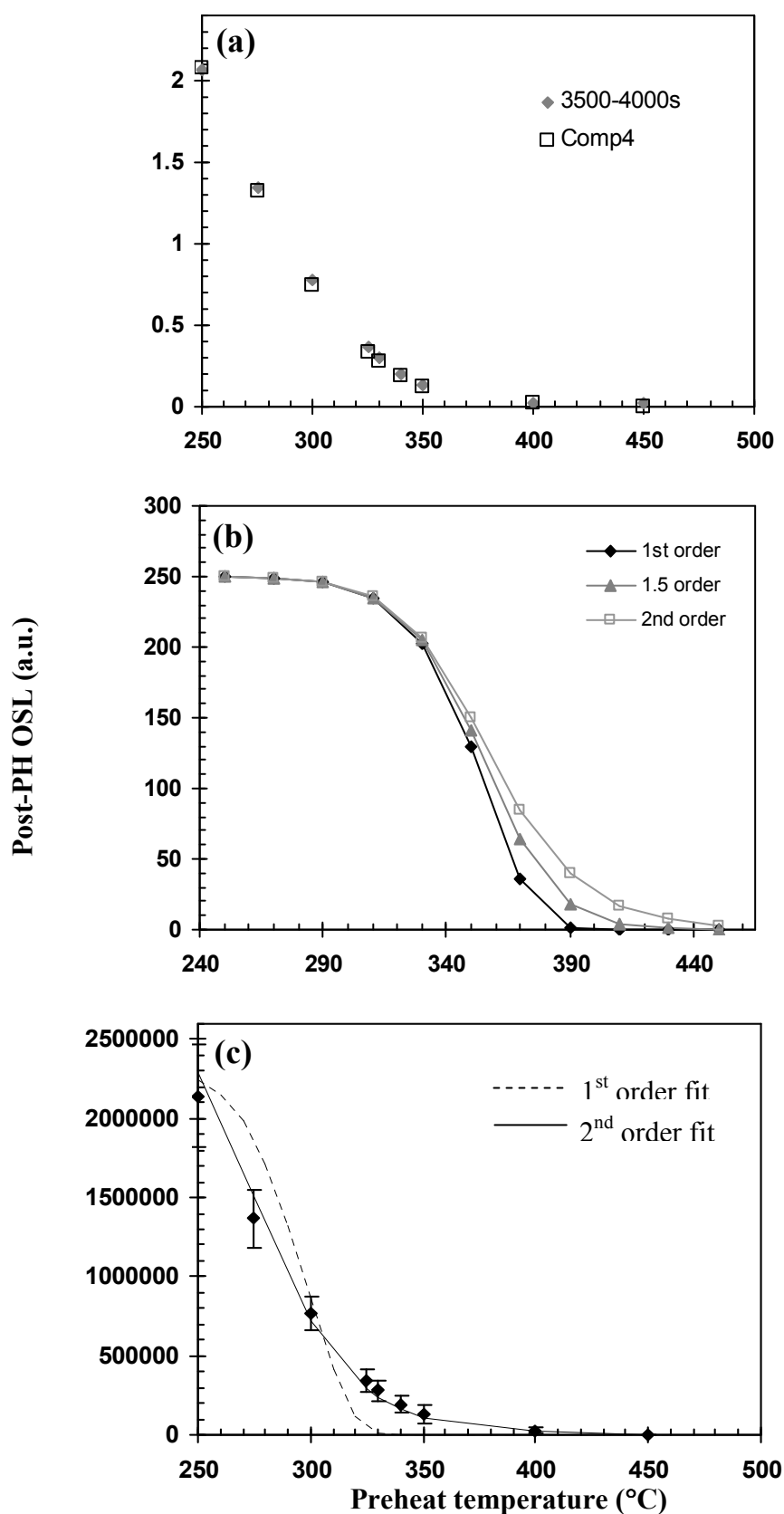
Fig. 4.22 (a) Comparison of pulse annealing curve shape obtained for slow component 2 (open symbols) and integration of LM OSL from 3500-4000s (filled symbols) for sample TQN. (b) Computer simulated pulse-annealing curves obtained using analytical solutions for 1st, 2nd and 1.5 order kinetics given the same trap parameters. (c) Pulse annealing data for component slow 2 fitted to a 1st order solution (dotted line) and a 2nd order solution (black line).

The third possibility, poor sensitivity correction, is a less likely main candidate for the non-first order form since the sensitivity corrected LM OSL produced pulse annealing curves for the fast, medium (tentatively) and component S1 could be well fitted to the first order equation 4.14. This indicated that the second LM OSL measurement adequately represented the sensitivity of the first, i.e. the sensitivity correction was satisfactory. It is possible that, perhaps sensitisation occurred during the LM measurement, resulting in the correction working less well for component S2 than the faster components. See section 5.4 for a full discussion of sensitivity change during LM OSL measurement. However, the plot of peak 1 maximum vs. peak 2 maximum in Fig. 4.18 shows proportionality between the two indicating that the fast and slow components sensitize together. Similar findings are presented in section 6.3 (Fig. 6.6) for all the fitted OSL components. It is not likely that this is the primary reason that the shape of the pulse-annealing curve of S2 is as non-first order as observed.

The last option listed was that a distribution of trap depths exist (as observed in TL for many materials, even quartz, Hornyak *et al.*, 1992) which have very similar photoionization cross-sections. This situation might produce a first order LM OSL shape but non-first order pulse annealing, since those traps with the smallest depth will recombine at lower temperatures whereas the deeper traps will thermally erode at higher temperatures. A simple simulation of such a system is illustrated in Fig. 4.23 where a uniform trap distribution of 30 first-order traps evenly spaced $E = 1.6…1.83eV$, with equal charge concentrations, and s-value, is shown in Fig. 4.23a. Pulse annealing curves were calculated for each of the traps (Fig. 4.23b) and summed to produce a pulse annealing curve that would be observed from such a system. The best fit to this data using the 2nd order solution given in equation 4.16 is shown by the dotted line, as also gave the best fit to the data for component S2. With the exception of the extreme high temperature end of the curve a reasonably good fit was obtained to the simulated data. Even with the relatively simple trap distribution system a wide range of shapes for the pulse annealing data could be obtained by varying only the width and spacing of the trap depths. Variation of charge concentration to give a Gaussian distribution and the number of different trap depths within the distribution would likely be able to produce pulse annealing curve shapes even closer to the second order solution.

Empirical testing of this idea might involve repeating the experiment at a variety of doses (initial charge concentrations). A distribution of trap depths would produce a constant pulse annealing shape at all doses, whereas a single trap evicting charge thermally by non-first order kinetics would be expected to result in curve forms that shift with dose.
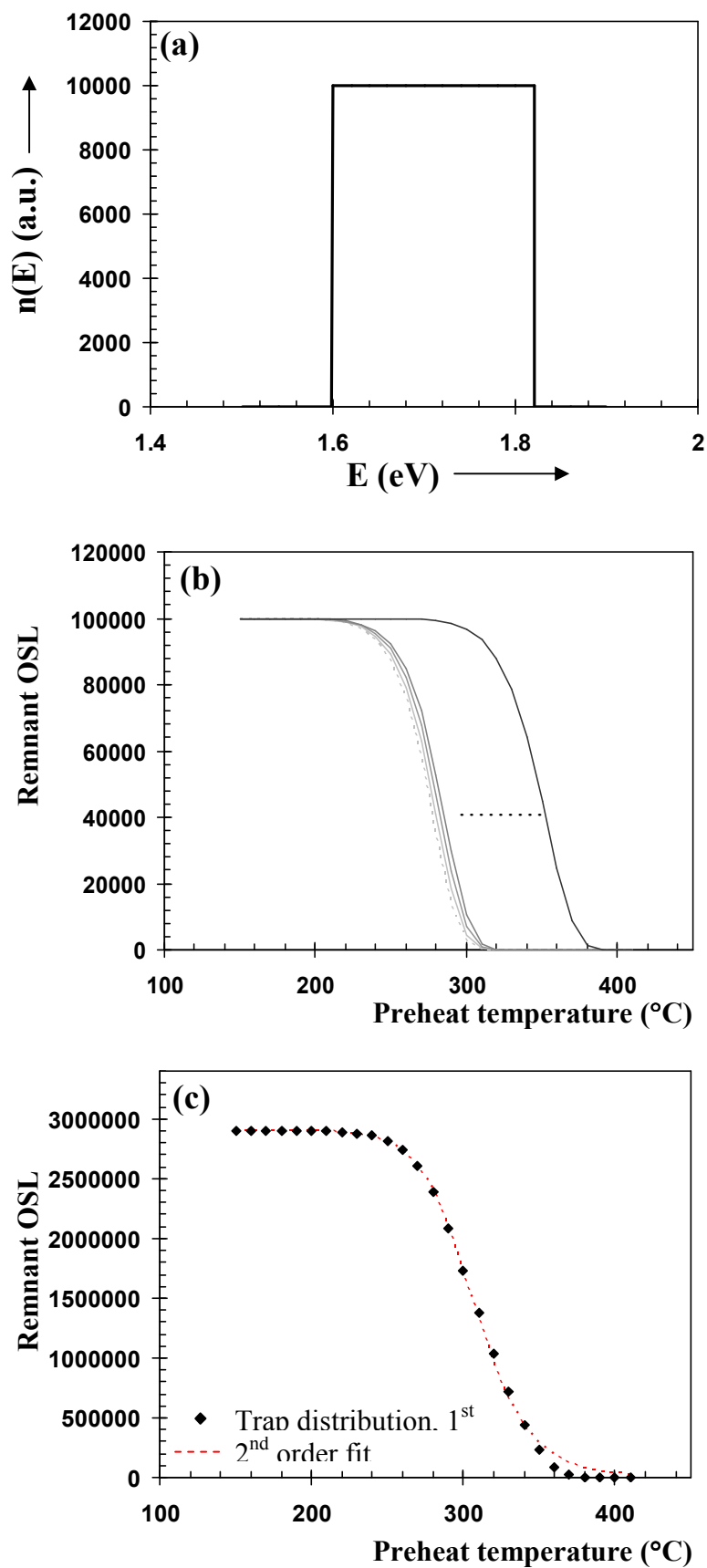
Fig. 4.23 (a) Diagram representing the uniform distribution of trap depths (30) created in the simulation. (b) Shows the simulated first-order shape pulse-annealing curves from the extremes of the distribution given in (a). (c) The filled symbols show the summed pulse annealing curve from the distribution. The red, dotted line is the best fit to the data using a second order curve.

No absolute conclusions could be drawn concerning the explanation for the broad pulse annealing shape of component S2 and further empirical investigation is needed to resolve between second order thermal eviction and the existence of a trap distribution. However, for the purposes of determining trap parameters for component S2 the second order fit shown in Fig. 4.2.2c was used directly to estimate E and s, assuming only a single trap.

The E and s parameters obtained for the first four OSL components from fitting the pulse annealing data for sample TQN are given in Table 4.3. A full discussion of these and results for other samples is undertaken at the end of this section. The s values obtained for the first three components are between $10^{13} - 10^{14}s^{-1}$. These are of the order expected (~the Debye frequency). The frequency factor, s, can be interpreted as the number of times per second a trapped electron interacts with the lattice phonons (multiplied by a transition probability), and therefore the maximum value expected is the lattice vibration frequency, $10^{12} - 10^{14}s^{-1}$.

The parameters have been substituted into analytical expressions for TL and the subsequent TL peaks have been plotted in Fig. 4.24c. For comparison, the percentage lost per annealing cycle for each component has been plotted below. This entailed calculating the percentage of the total OSL (from the fit) lost from one preheating temperature to the next and plotting the data versus preheat temperature, in Fig. 4.24a. This shows approximately where TL peaks for each component are expected during linear heating, and required one less level of approximation through curve fitting than 4.24a. Empirically measured TL is plotted in Fig. 4.24b for further comparison.

The derived parameters for the fast component give a simulated first order TL peak at ~325°C (B = 2°C/s). The simulated TL corresponds well to the 325°C TL peak observed in the empirically measured TL. It is well acknowledged that the fast OSL component originates from the 325°C TL region in quartz (e.g. Spooner, 1994; Bailey *et al.*, 1997). These results further corroborate this finding. The E and s values obtained for the fast component agree well with E and s values for the quartz 325°C TL peak found by Wintle (1975; E=1.69eV and s=1×$10^{14}s^{-1}$) and Spooner and Questiaux (2000; E=1.65eV and s=3.9×$10^{13}s^{-1}$).

The fitted E and s parameters from slow component 1 produce a first order TL peak at around 370°C. Assuming second order kinetics for slow component 2, the derived values produce a simulated TL peak at ~280°C. This correlates well with a measured peak 280°C TL region (also observed as common to many samples). The medium component gives a TL peak again close to 325°C. This was also observed by Bailey (1998b).

For all the components the TL peaks obtained from the three different methods: percentage lost TL, simulated TL and empirical TL all correlate well. This suggests that data collection by TL or OSL and all the levels of data analysis and curve fitting used are probably reliable and appropriate.

	E (eV)	s (s^{-1})
Fast Component	1.73 ± 0.15	$8.8(\pm120) \times 10^{13}$
Medium Component	1.67 ± 1.2	$2.1(\pm32) \times 10^{13}$
Slow Component 1	1.98 ± 0.3	$7.6(\pm40) \times 10^{14}$
Slow Component 2	1.47 ± 0.08 (1st order)	$9.1(\pm0.4) \times 10^{11}$(1st order)
	1.2 (2nd order)	1×10^{10} (2nd order)

Table 4.3 Trap parameters estimated for the OSL components of quartz sample TQN, derived from pulse annealing data described in 4.4.2.

Fig 4.24 (a) Percentage of total charge lost per annealing cycle vs. preheating temperature for sample TQN (derived from pulse annealing data). (b) Empirical TL measured from a single aliquot of TQN. (c) Simulated TL for the OSL components observed in TQN, derived from fitted parameters from the pulse annealing data.

The procedure used (Fig. 4.17) to obtain the pulse annealing results described above was also performed on sample SL203. The raw LM OSL data (minus background from a 'dead' disc) are plotted in Fig 4.25. The measurements were made using the older stimulation unit (R4a) known to have a slightly non-linear ramp. Fig. 4.25a shows the LM OSL data plotted vs. $\log_{10}$(power). The data for this sample have been fitted to 5 similar first order components to the previous sample using the trapezoidal approximation outlined in section 3.4.1. Dotted line (1) represents the position of the medium component. It can be seen from the LM OSL that at preheat temperatures >340°C the position of the first peak remains constant. The initial LM OSL following higher temperature preheats is assumed to consist of predominantly medium component signal, and the constant peak position of this part indicates first order behaviour. The same data is plotted on a linear time/power scale in Fig. 4.25b to show the second LM OSL peak (components S1, S2 and S3) more clearly. The LM OSL following test doses are shown in Fig. 4.25c. A significant amount of sensitivity increase took place in the course of the experiment on this sample.

Preheat temperatures lower than those used in the previous experiment were used in order to observe more accurately the thermal erosion of slow component S2. LM OSL measurements were made following preheats of 200, 220, 240, 260 and 280°C on sample SL203 (using reader R4b). The raw (background subtracted) LM OSL is shown in Fig. 4.26a. From the figure it can be seen that the LM OSL following 200°C preheat would have an origin significantly above zero counts (zero stimulation should produce zero OSL). It was thought that this could be due to a phosphorescence component still present after the low preheating temperature that decayed over a relevant time period during the LM OSL measurement at 160°C. Using the same aliquot a repeat measurement was made with the same pre-treatment conditions, but without optical stimulation during measurement at 160°C. The observed phosphorescence is plotted in Fig. 4.26b and was used as an approximation for the phosphorescence during the initial LM OSL measurement. The phosphorescence data was subtracted from the LM OSL data and the corrected LM OSL curves are plotted in Fig. 4.26c. The dotted line shown in Fig. 4.26c is intended to illustrate that there is minimal movement of peak 2 position following the various preheats. The test dose measurements are shown in Fig. 4.26d. Very little sensitivity change was observed during the experiment. However, the test-dose LM curves were still fitted and used to correct the pulse annealing data.

The high temperature (275-450°C) and low temperature (200-280°C) pulse annealing data were superimposed for further component-resolved analysis. The deconvolved pulse annealing data for the fast, medium, S1 and S2 components are shown in Fig 4.27. The results for sample SL203 were found to be remarkably similar to those for TQN. The fast component behaves as expected, sharp drop after 275°C, and all OSL depleted after 350°C. The form of the medium component pulse annealing data is ambiguous. The medium component is present up to 400°C, but at low temperatures some thermal erosion apparently also took place. Component S1 again seems to be the most thermally stable of the first four components. The initial portion of the data is noisy, but it is clear that S1 begins to deplete after preheating to ~340°C, and is still present after 400°C preheat. Using the low temperature preheating data the initial portion of the pulse annealing decay curve of component S2 could be observed, which was not possible with the range of preheat temperatures used on sample TQN. Similar to TQN the annealing curve for S2 of sample SL203 is much broader than expected from first order kinetics. Thermal erosion occurs at temperatures as low as 220°C suggesting that for this sample also component S2 is not thermally stable.

The fast component and slow component S1 were fitted to first order analytical solutions (equation 4.14). The fits are shown also in Fig 4.27 (thin lines). Component S2 was fitted to the second order kinetic solution. However, no expression could be found to adequately describe the shape of the medium component pulse-annealing data obtained by this method. Since this may arise from inadequate fitting of the LM OSL a second method was attempted to obtain pulse annealing data for the medium component without the need for curve fitting to separate it from the contribution of the fast component. Described in section 5.3.1.4 is using selected photon energy stimulation to isolate the OSL components. It was discovered that infrared stimulation (830nm) for 7000s at 160°C fully depletes the fast component with negligible loss of the medium component. The experiment outlined in Fig. 4.17 was repeated, but after preheating an extra step of IRSL (7000s, 160°C) was performed to zero the fast component so that in the subsequent LM OSL measurement the medium component was clearly visible. The peak height of the medium component was plotted versus preheat temperature, presented in Fig. 4.28. A repeat point following 275°C preheat at then end of the experiment was performed to show that the procedure used was appropriate, i.e. any sensitivity change was corrected for by the LM OSL following a test dose.

Using this method the pulse annealing data is markedly different to that shown in Fig. 4.27, especially at the lower temperatures, and now follows a similar form to the other

components. The data in Fig. 4.28 were fitted to the solutions given in equations 4.14 – 4.16. It was found that the data were well-fitted to the second order equation (the first order fit is shown also in Fig. 4.28 for comparison – dotted line).

The fitted *E* and *s* parameters for the fast, medium, S1 and S2 components are shown in Table 4.4. As for the previous sample, the percentage lost per annealing cycle from the deconvolution of the LM OSL vs. preheat temperature is plotted in Fig. 4.29a as a proxy for the TL from each component. The data have been compared to an empirical TL measurement (Fig 4.29b) and to simulated TL for each component derived using the fitted E and s values from the pulse annealing data (Fig 4.29c). Similar to sample TQN the fast component appears to correlate well with the 325°C TL peak. The medium component, as found from the modified post-IR experiment, seemed to correspond to a similar TL region as the fast component ~330°C, using the fitted E and s parameters, and would be difficult to distinguish from the fast component from the TL. Component S1 is the most thermally stable and possibly correlates to a TL region between 360 and 380°C (as can be seen from the experimental TL data). Slow component S2 appears to correspond to TL in the 280°C region and is the least stable of the components.
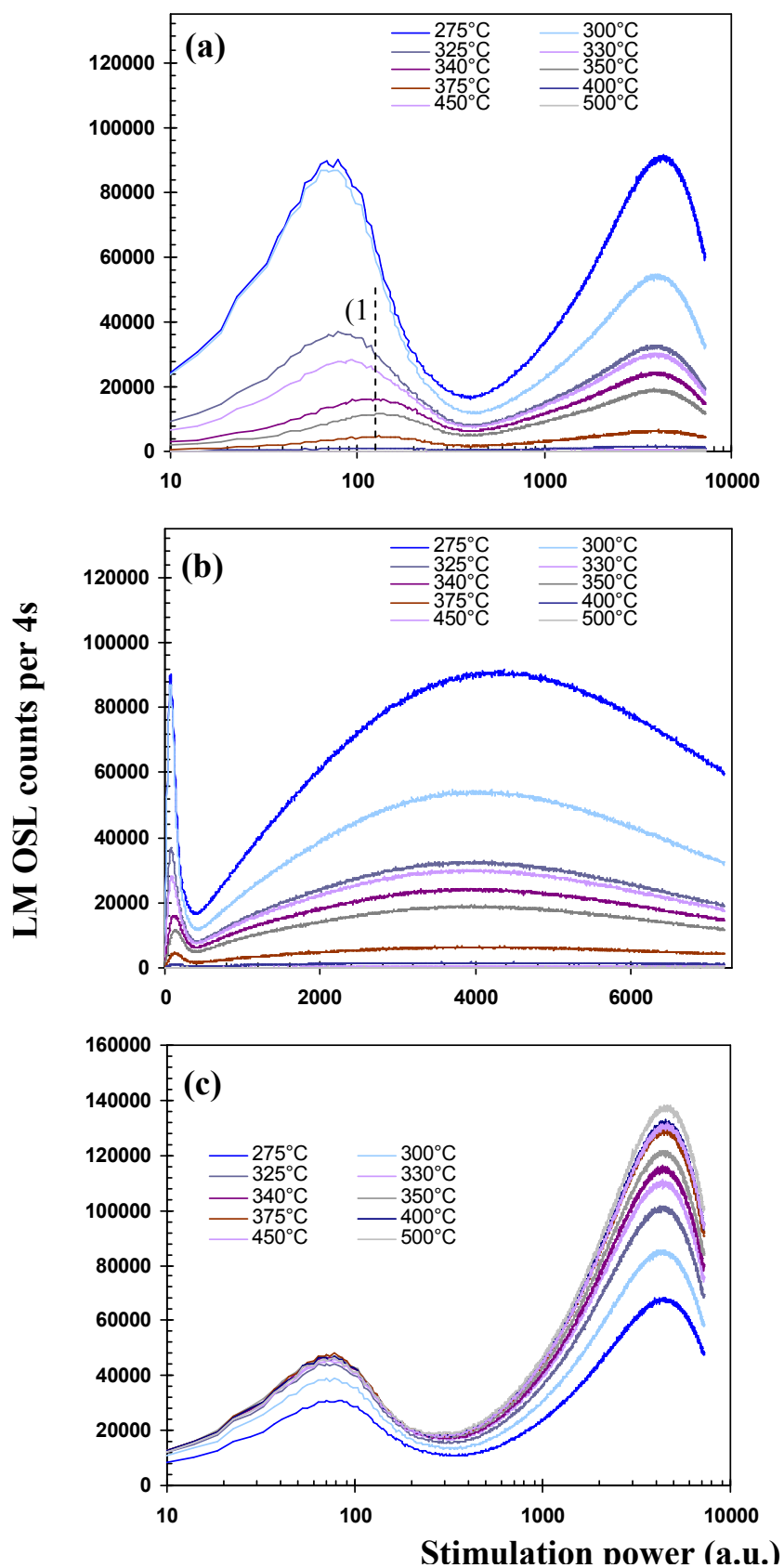
Fig. 4.25 (a) LM OSL from a single aliquot of sample SL203 following preheating to various temperatures plotted on log(t) scale. (b) shows the same data on a linear t-scale. (c) The LM OSL following the test dose, used to correct sensitivity changes during the course of the experiment.
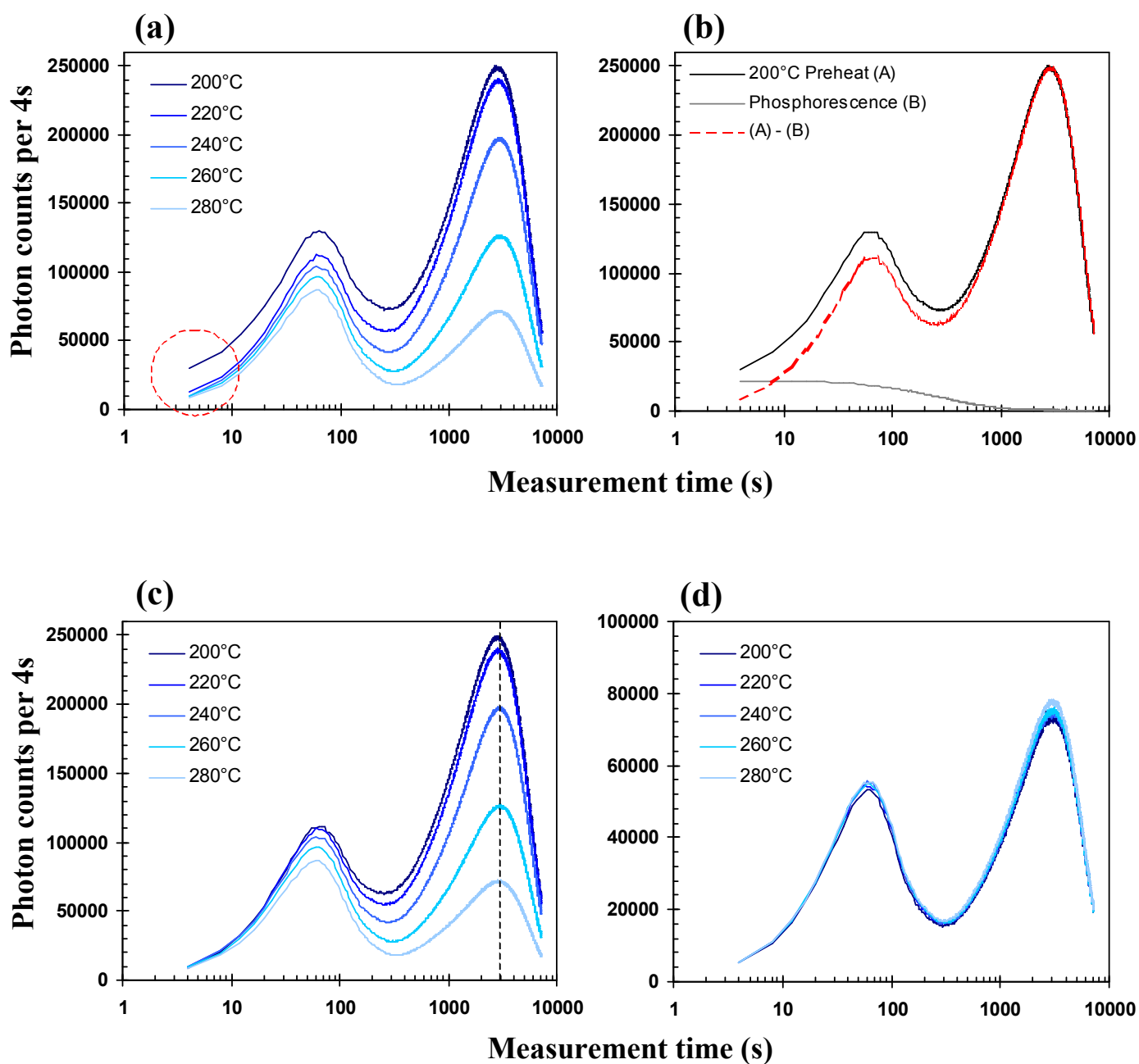
Fig. 4.26 (a) LM OSL measurements on a single aliquot of SL203 following preheating between 200 and 280°C. (b) Phosphorescence following preheat to 200°C was measured under the same conditions as used to obtain LM OSL. The phosphorescence data were subtracted from the raw LM OSL (post 200°C preheat). (c) The LM OSL with the phosphorescence component subtracted. (d) The LM OSL from a standard test dose used to correct for sensitivity change.
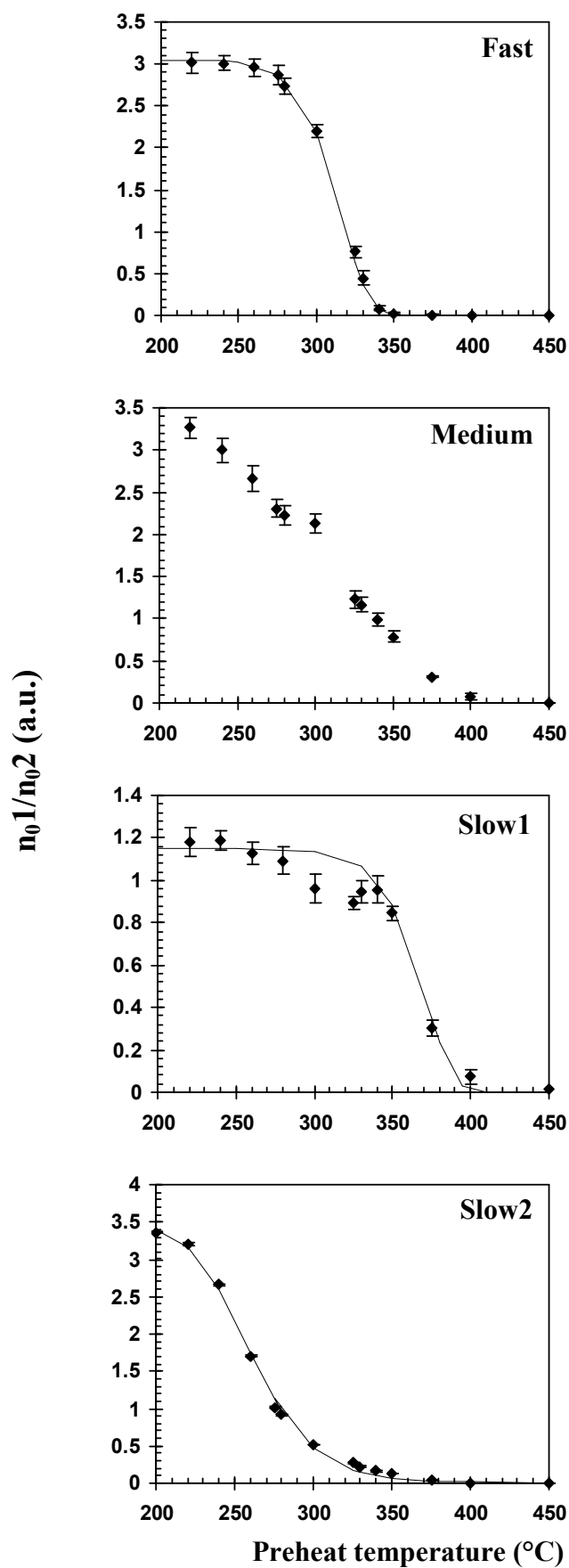
Fig. 4.27 Plots of component-resolved, sensitivity-corrected magnitudes from curve fitting vs. pulse annealing preheat temperature (filled symbols) for sample SL203. The data have been fitted to analytical solutions (black line), described fully in the text.
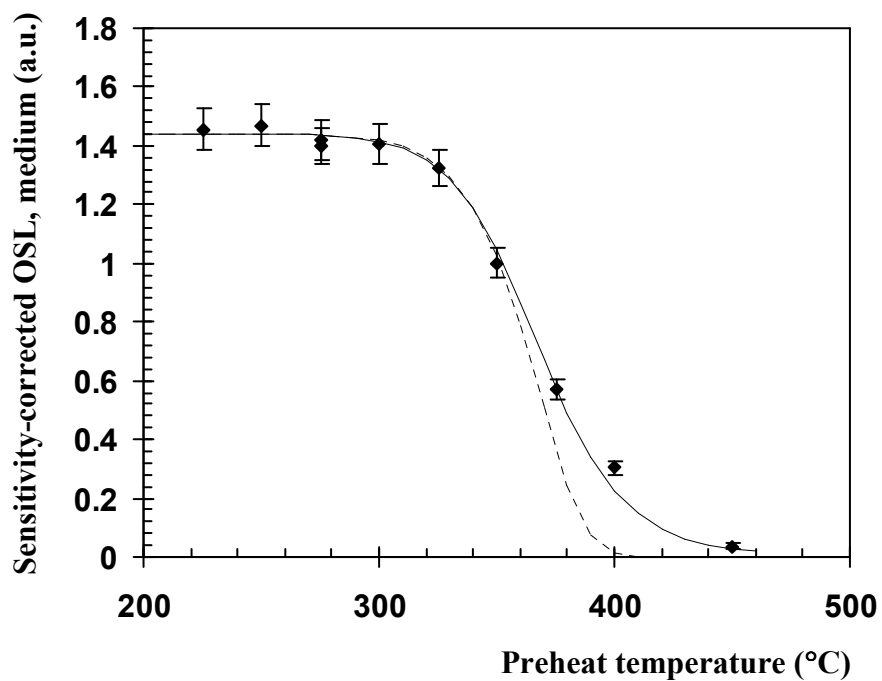
Fig. 4.28 Pulse annealing curve of the medium OSL component from sample SL203 (filled symbols). An infrared OSL measurement was used to deplete the fast component so that the medium component was clearer in the subsequent LM OSL measurement. The data have been fitted to a first order analytical solution (dotted line) and a second order solution (solid line).

	E (eV)	s (s⁻¹)
Fast Component	1.74 ± 0.5	$8.9(\pm 70) \times 10^{13}$
Medium Component	1.8 ± 0.4	$1.5(\pm 45) \times 10^{13}$
Slow Component 1	2.02 ± 1.2	$6.9(\pm 110) \times 10^{14}$
Slow Component 2	1.23 ± 0.1	$4.75(\pm 30) \times 10^{11}$

Table 4.4 trap parameters derived for the OSL components of quartz sample SL203, derived from pulse annealing data.
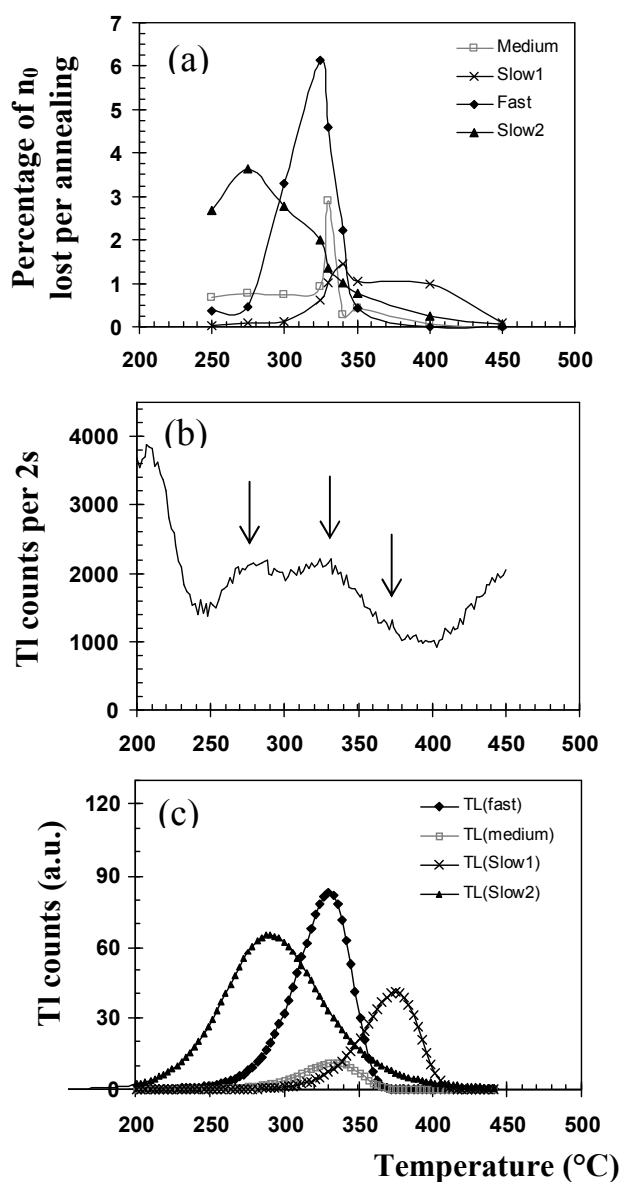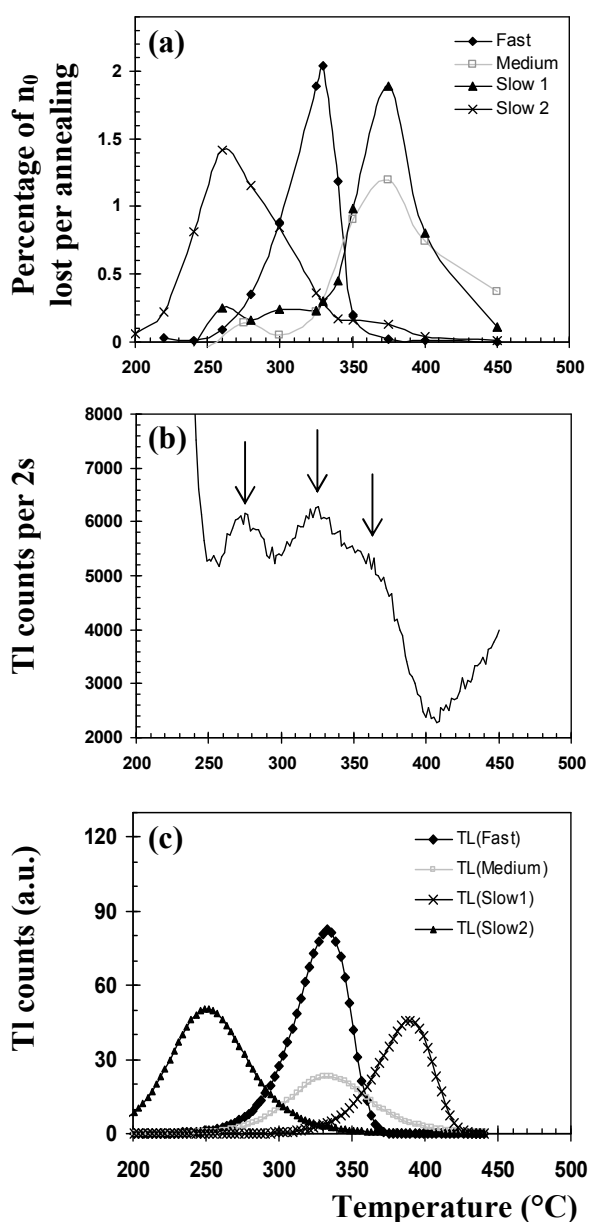

Fig 4.29 (a) Percentage total charge lost per annealing cycle vs. preheat temperature for sample SL203 (derived from pulse annealing data). (b) Empirical TL measured from a single aliquot of SL203. (c) Simulated TL for the OSL components observed in SL203, derived from fitted parameters from the pulse annealing data.

Discussion of pulse annealing results

Thermal stability is a crucial consideration for luminescence dating, as the temperature-dependent retention lifetime of a trap type (given by equation 4.8) places a fundamental limitation on the age range datable with that component. Attempts to characterise the thermal stability of the quartz OSL components have been attempted by Bailey (1998b) and Bulur *et al.* (2000 - on a single heated quartz sample only). In this pulse annealing experiment a similar procedure to that employed by Bulur *et al.* (2000), of preheating to increasingly high preheating temperatures, was used to look at the thermal stability of two different sedimentary samples in detail: TQN and SL203.

Five common components were fitted to the LM OSL data from the samples: fast, medium and slow components S1, S2 and S3. From the pulse annealing data obtained in this section the main conclusion is that the fast, medium and component S1 are of sufficient thermal stability for optical dating. Component S2 was found not to be adequately stable for dating sediments on Quaternary timescales. Consistent data could not be obtained from component S3 with this experimental procedure to allow conclusions to be drawn concerning thermal stability. Approximate lifetimes of the OSL components calculated from the fitted E and s trap parameters are given in Table 4.5.

The pulse-annealing data for the fast component were the most consistent between the samples. A sharp decay between 275 and 340°C was observed in all cases. Trap parameters, E and s, estimated from fitting of the pulse annealing curves to first order solutions confirm that the fast component is related to the 325°C TL region. The values obtained compare satisfactorily with those found for the fast component by Bailey (1998) using an isothermal decay analysis, and to those found for the 325°C TL peak found by e.g. Wintle (1975).

Results for component S1 suggest that it is the most stable of the first four OSL components (in the samples measured). The pulse annealing curve for S1 decays sharply between 350 and >400°C. Trap parameters estimated from fitting to a first order expression are within errors for the different samples. The results suggest that component S1 is associated with the TL region between 360 and 380°C.

The pulse-annealing curve for component S2 was found to be much broader than the fast and S1 components. Significant thermal erosion of the component occurred even at preheating temperatures as low as 220°C. However, a proportion of trapped charge still remains after heating to ~400°C (in sample SL203 - in TQN the data were too noisy at high temperatures to observe the structure of S2). This behaviour was unexpectedly non-first order, given the

apparent lack of dependence on charge concentration displayed in the LM OSL. The pulse annealing curves for component S2 could be fitted to a derived second order expression in all samples. The trap parameters obtained from this suggest that it may be related to TL between 260 and 290°C. Slow component S2 has previously been identified in quartz by Bulur *et al.* (2000). They found pulse annealing data for this component (which they called component D) showed a similar broad decay, starting at ~250°C, with 1% of the initial signal still present after heating to 400°C. They did not attempt any further analysis of the data except to note that two shoulders to the pulse-annealing decay curve were observed. Several hypotheses were constructed to attempt to explain the broad pulse annealing shape. These were discussed previously in this section. No firm conclusions could be drawn, however, without further experimental investigation. While the details of the kinetics involved may be uncertain it can be concluded that this component is not sufficiently thermally stable for dating of sedimentary samples.

From the raw LM OSL it was clear that the medium component was present after the fast component has virtually completely thermally eroded (at temperatures over 340°C). The pulse-annealing curve appears to have a similar broad decay to component S2. The size of this component and its peak position (when stimulated with 470nm) relative to the fast component made accurate fitting of the LM OSL inaccurate. A modified version of the experiment using IRSL to first bleach the fast component and observe the medium directly was more productive. The results suggested the medium is connected to TL ~330°C. Similar results were found previously by Bailey (1998b) who estimated that the medium component would give ~332°C TL peak from trap parameters found from isothermal decay analysis and suggested that it was slightly more thermally stable than the fast component. Bulur *et al.* (2000) were the only others to look at the thermal stability of this component using a pulse annealing experiment. They also observed a slightly broader decay than that which they measured for the fast component.

Although the LM OSL was fitted to five components no pulse-annealing data were derived for component S3. As explained previously, a sufficient proportion of the LM OSL peak could not be measured for this component to allow for consistent fits to be obtained at such low doses (only the initial rising part of the peak was observed). Nevertheless, from the raw LM OSL data for sample SL203 (Fig 4.25) a small rising limb of a very slowly decaying OSL component is visible just above background levels after preheating to 500°C. This though, taking into account the indications from component S2, is by no means evidence that this component is more thermally stable than the others components.

Bailey *et al.* (1997) and Bailey (1998b) observed one slow component that appeared to remain intact even after heating to 650°C, using CW OSL measurements. It is tentatively suggested that they have observed the small fraction of component S3 that may remain after such high temperature preheats. Conversely, Bulur *et al.* (2000) found that all OSL was completely eroded by heating to 480°C. Further experimental work to resolve the discrepancy between the different authors' findings was undertaken and is presented in section 4.7.

Component	Lifetime, τ, at 20°C for sample:	
	TQN	**SL203**
Fast	310Ma	210Ma
Medium	82Ma	19700Ma
S1	2610000Ma	480000Ma
S2	0.5ka	1ka

Table 4.5 Approximate lifetimes for the quartz OSL components at 20°C estimated from the pulse-annealing experiment described in section 4.4.2.

4.4.3 Isothermal decay analysis

4.4.3.1 Introduction

As stated at the beginning of section 4.4.1 the retention lifetime of trapped charge is given by equation 4.8, assuming first order kinetics:

$$\tau = s^{-1} \exp(E / k_B T) \tag{4.8}$$

where the terms have the same meaning as given previously, and the phosphorescence at constant temperature is given by:

$$I(t) = ns \exp(-E / k_B T) \tag{4.17}$$

for a first order system. In section 4.4.2 pulse-annealing experiments were described to estimate E and s, trap depth and frequency factor, by varying the preheat temperature prior to LM OSL measurement. Using equation 4.8 the trap parameters, E and s, can also be derived from the phosphorescence decay at a constant temperature using the following procedure. The method of isothermal decay analysis involves measurement of the OSL signal following storage at various temperatures for a range of times to find the lifetime of trapped charge at each temperature, τ. E and s can then be estimated from the following rearrangement of equation 4.7:

$$\ln(\tau(T)) = \ln(s^{-1}) + \frac{E}{k_B} \cdot \frac{1}{T} \tag{4.18}$$

From a linear fit to an Arrhenius plot of $\ln(\tau(T))$ vs. $1/T$ an estimate of trap depth, E, should be obtained from the gradient, and frequency factor, s, from the intercept on the y-axis.

This method works theoretically for traps that display first order kinetics. However, it may be the case that some of the quartz OSL components display some non-first order behaviour, as observed from the pulse annealing experiment described in section 4.4.2. For example, in a second order system the isothermal decay at constant temperature as given by Garlick and Gibson (1948) is as follows:

$$I(t) = \frac{A_n}{NA_m} n^2 s \exp(-E / k_B T) \tag{4.19}$$

where A_n and A_m are the trapping probabilities of the trap and luminescence centre respectively (and for second order $A_n = A_m$ can be assumed), and N is the concentration of electron traps. Trap parameters E and s can be found also using equation 4.18 providing the isothermal decays are fitted to equations appropriate to the order of kinetics.

4.4.3.2 Description of the procedure employed

Isothermal decay analysis was performed on sample TQN, mainly because the individual components are clearer in this sample than others due to the relative sizes of the components. A single aliquot procedure was used whereby a 20Gy dose was given followed by an initial preheat of 220°C for 10s. The aliquot was held for various times at a range of temperatures (see table 4.6). Following this LM OSL measurements were made for 3600s at 160°C, 0-36mWcm^{-2} (on R4b). Sensitivity was monitored using the LM OSL following a 10Gy test doses and 220°C preheat. The 0s hold measurement at each temperature was repeated at the end of the measurement sequence for that temperature to check the correction procedure.

The LM OSL were fitted and subsequent component-resolved, sensitivity-corrected (dividing the magnitude of the component OSL following holding at T_i by the magnitude of the test dose OSL) isothermal decays were obtained at each temperature. The decays were fitted to find the lifetime, τ, of each component at each temperature. The E and s values could then be obtained by the method described in section 4.4.3.1.

T_i (°C)	Holding time at T_i (s)			
270	0	70	250	600
290	0	40	80	150
310	0	10	40	100

Table 4.6 Durations of raised temperature storage used for isothermal decay analysis.

4.4.3.3 Results

The raw LM OSL following holding at 270°C is shown in Fig. 4.30 as an example of the data collected. In Fig 4.30b the slow components S1 and S2 have been magnified to demonstrate that there is negligible shift in the peak position of either with trapped charge concentration (i.e. size of the peak), indicating that first order kinetics were appropriate for curve deconvolution. The data for this aliquot of this sample were fitted to four components: fast, medium, S1, S2. No S3 component was observed.
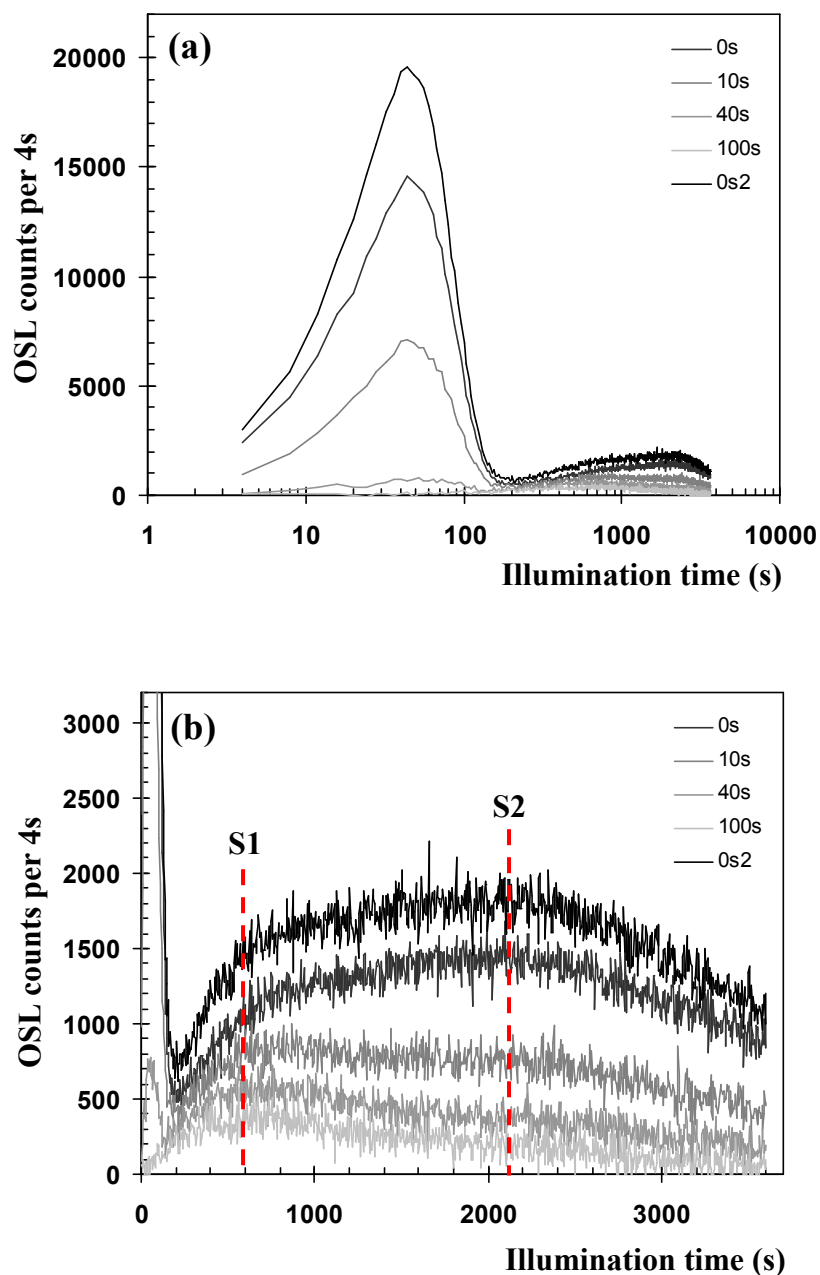
Fig. 4.30 (a) LM OSL plotted on a ln(t) scale from sample TQN measured at 160°C following holding the sample at 270°C for durations given in the plot legend. The same data are shown in (b) on a linear timescale to show slow components S1 and S2 more clearly. The dotted red lines show the peak positions of the components. There is no shift of peak position with charge concentration in either component.
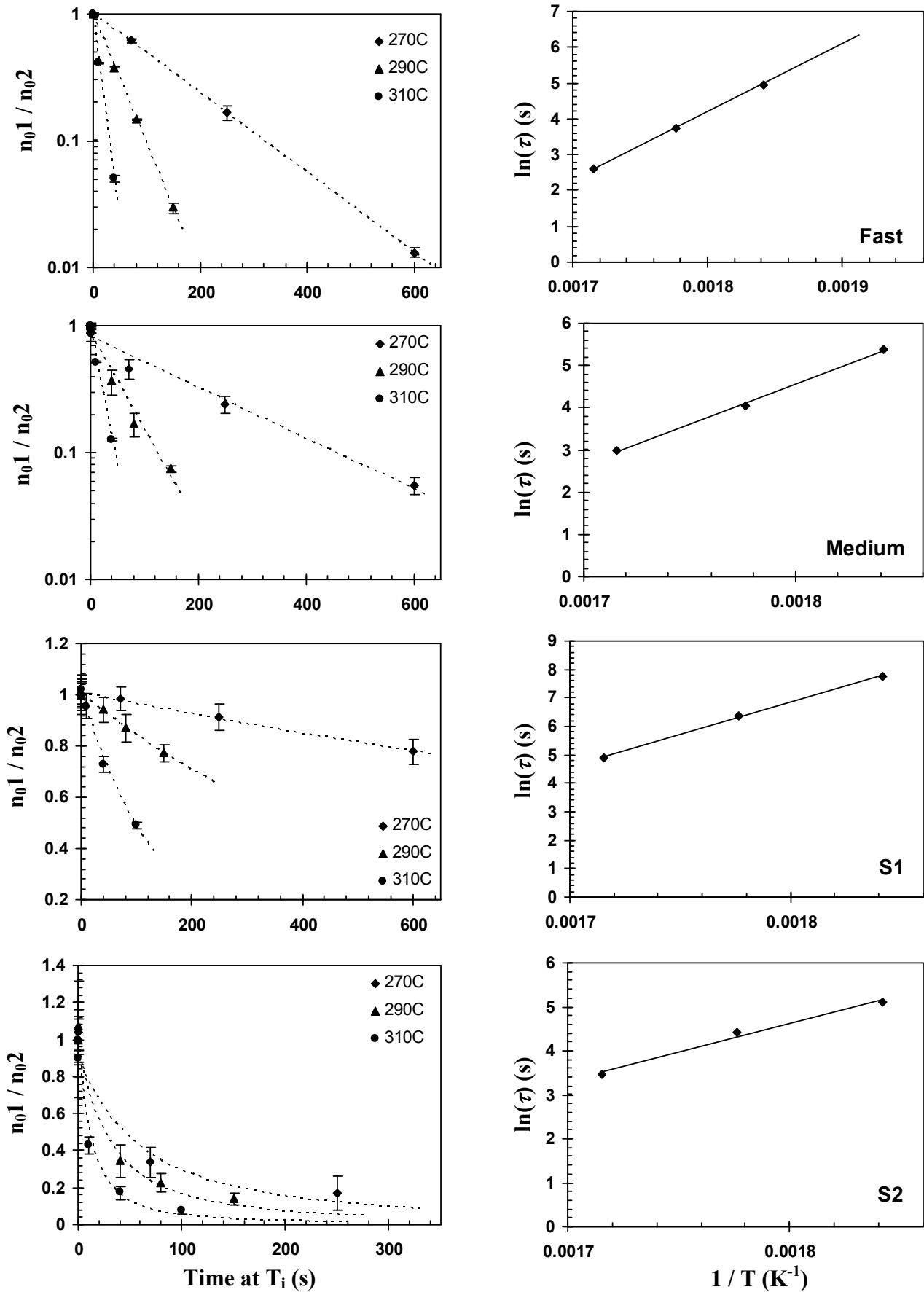
Fig. 4.31 (left) Component-resolved isothermal decay curves at 270, 290 and 310°C. The decays from the fast, medium and S1 components were fitted to exponentials to obtain the lifetime at each temperature. The data for component S2 was fitted to second order decays. (right) Arrhenius plots for each component to determine E and s.

The fitted sensitivity corrected magnitudes for each component, $n_{0i}1$ / $n_{0i}2$, are plotted in Fig 4.31 to observe the isothermal decays at each temperature. In a first order system the decay produced by holding at one temperature is expected to be exponential (as for CW OSL decay, Equation 3.4). Exponential functions gave good fits to the isothermal decays from the fast, medium and S1 components, and are represented in Fig. 4.31 by the dotted lines. The decays from component S2, however, could not be approximated with a first order solution. This may not be surprising if the results from the pulse-annealing experiments in section 4.4.2 are taken into consideration. The S2 component pulse-annealing curves from several samples could not be fitted to first order equation but were much better approximated with second order solutions. It was similarly found that the isothermal decays from this component fitted to second order equations, shown in Fig. 4.31.

The lifetime of each component at each temperature was obtained from the fitting process. Arrhenius plots of $\ln(\tau)$ vs. $1/T$ were subsequently created and are shown also in Fig. 4.31. Adequate linear fits were achieved for the OSL components to estimate trap parameters, E and s. These are given in Table 4.7.

	E (eV)	s (s⁻¹)	Lifetime at 10°C
Fast	1.64	1.1×10^{13}	430 Ma
Medium	1.77	1.2×10^{14}	8100 Ma
S1	1.95	5.1×10^{14}	3300000 Ma
S2	1.12	1.4×10^{8}	19ka

Table 4.7 Summary of the results from the isothermal decay experiment described in section 4.4.3. Values of E, trap depth, and s, frequency factor, are given for each fitted component. From these values the lifetime of each component at 10°C has been calculated.

4.4.4 Summary

The main aim of this section was to quantify the thermal stability of the OSL components in order to assess the limitations to optical dating of Quaternary sediments imposed on each component by the lifetime of trapped charge at ambient temperatures. This was achieved by two methods of analysis: the response of the LM OSL to varying preheating temperatures,

and analysis of the isothermal decay of the OSL components. From both values of trap depth, *E,* and frequency factor, *s*, for the fast, medium, S1 and S2 components were calculated and lifetime of each found using equation 4.8. The primary conclusion from these experiments is that the fast, medium and S1 components are of sufficient stability for optical dating. S1 was found to be the most stable of the first four OSL components. However, component S2, in which significant thermal erosion was observed during preheat temperatures as low as 220°C, is not stable over the required timescales.

The calculated lifetime of the fast component at 20°C was of the same order of magnitude as results obtained previously for the initial OSL decay (e.g. Rhodes, 1990; Murray and Wintle, 1999 – see section 4.4.1 for values). Huntley *et al.* (1996) found 4 OSL components by isothermal decay analysis, one of which gave a lifetime of 14ka. This is comparable to that found for component S2 in section 4.4.3 (19ka). However, results for this component varied considerably between the two methods used in this study.

With respect to assessing which of the two methods used is more reliable the number of levels of analysis required to achieve the wanted result (*E* and *s* values) might be considered. Although both methods should produce equivalent results the isothermal decay analysis entailed three levels of data fitting: deconvolution of LM OSL, fitting isothermal decay and fitting of Arrhenius equation. The method of pulse-annealing required only two levels of analysis: LM OSL deconvolution and fitting of pulse-annealing curves. Therefore, the inevitable errors introduced by each analysis would lead to the suggestion that the pulse-annealing results are somewhat more reliable than the isothermal decay.

4.5 Preliminary observations of thermally transferred LM OSL

Thermal transfer is defined here as the case where charge evicted from lower temperature TL traps is retrapped in the OSL traps, resulting in an increase in the measured OSL signal. Thermal transfer occurs in nature during burial as charge is thermally evicted from relatively shallow traps. Laboratory preheats are necessary in part to mimic the transfer that occurs in the natural environment. Some samples suffer from significant thermal transfer, and others not. If considerable, this may lead to overestimation of equivalent dose, which is especially problematic for young samples (e.g. Rhodes and Bailey, 1997).

Thermal transfer is most readily observed by measuring *recuperation* (Aitken and Smith, 1988). Recuperation refers to a 'double transfer' effect; where optical eviction of charge from the OSL traps at ambient temperatures results in a proportion of the charge being photo-transferred to lower temperature, optically stable traps. Some of the transferred charge is then

thermally transferred back to the OSL traps during preheating or storage. Studies concerning recuperation have found the most dramatic effect from retrapping in the 110°C TL peak. Aitken and Smith (1988) also observed strong thermal transfer from TL in the region of 250-300°C in several samples, which they interpreted as originating from the 280°C TL peak, that has been related to slow component 2 in the previous sections.

Bailey *et al.* (1997) investigated recuperation while studying the effects of partial bleaching on the form of quartz OSL. In this study thermal transfer following bleaching at room temperature was presumed to come mainly from the 110°C TL peak. They observed no difference in form between the natural signal and the recuperated signal (following a long bleach) and therefore suggested that recuperation occurred in both the fast and medium components in the same proportions as during irradiation. This would be expected given the accepted picture for quartz of delocalised charge transfer mechanisms (Bailey, 1998b) whereby electrons freed to the conduction band are mobile and may be trapped in any of the different trap types since they will have 'access' to all the OSL traps (for example, Bailey (1998b) found the photo-transfer ratio to be constant at all points in the OSL decay). Therefore some thermal transfer into all the OSL components is likely. Following some interesting observations during routine measurements on several samples (see example of sunlight bleaching on CdT9 at room temperature – section 5.2.2) that seemed to contradict this assumption, and other experiments where bleaching was performed at raised temperatures, it was felt that further experiments were required to test this. Experiments were undertaken on both single aliquots and single grains, as it was felt that (following discussion with Dr M. Jain) consideration of grain-to-grain variation in present components was also needed to allow conclusions to be made concerning the results of such transfer experiments, since not all the OSL components are observed equally in all grains; section 4.3.2.

In this experiment the form and preheat dependence of the recuperated LM OSL signal was investigated briefly on an annealed sample of Madagascan vein quartz (called EJR01an). In the first experiment a 50Gy dose was administered on multi-grain aliquots, followed by preheat to 280°C. LM OSL from 0-36mWcm^{-2} at 160°C for 500s was then performed to deplete the fast and medium components completely. Following preheat to temperatures between 220 and 280°C the LM OSL was again recorded. The second LM OSL measurement allowed observation of recuperation from TL traps >160°C to the fast or medium components. The results of this experiment are shown in Fig. 4.32a. Negligible charge is observed in the fast or medium due to preheating up to 220°C. Following higher temperature

preheats the magnitude of the medium component only is increasing. Additionally the magnitude of the slow component (tail) is observed to decrease as the preheat temperature is increased, and the magnitude of the medium increases. Through curve fitting of the LM OSL the medium and S2 signal sizes could be plotted versus preheat temperature. These plots are presented in Fig. 4.33.

The results are perhaps surprising given the accepted understanding of charge transfer processes in quartz, where recuperation would be expected to occur in both the fast and medium components, and is yet to be fully explained. Similar patterns have been observed in several samples where recuperation after bleaching at 160°C was found to occur only in the medium component. In a similar study by Watanuki (2002) recuperation using temperatures between 160 and 480°C was measured. All OSL data could be approximated by the three first order components (fast, medium and slow). After preheats of less than 200°C only slow component was observed in the LM OSL. However, following preheating to temperatures over 200°C the intensity of the medium component increased considerably, finally disappearing at 380°C. At all preheat temperatures no recuperation was observed to occur in the fast component.

The experiment described above for EJR01an was repeated but with the initial LM OSL measurement taking place at 20°C so that the 110°C TL peak could take part in the recuperation process. A 50Gy dose was given followed by preheat to 280°C. LM OSL was performed for 500s at room temperature followed by the second preheat to temperatures between 220 and 280°C. A second LM OSL measurement at 160°C for 500s was recorded to observe the recuperation. The results of the second experiment are given in Fig. 4.32b. This time a fast component recuperated signal was observed in addition to the medium (both visually and through curve fitting). The difference between the two results suggested that charge evicted from the 110°C trap could be retrapped in the fast component, but charge from higher temperature traps (probably mainly from 280°C TL peak) could not.

The empirical data at first glance suggest that the fully delocalised picture of charge transfer mechanisms in quartz is not correct. There are several possible explanations for the observations. For example, potentially clustering of certain defects could preferentially 'link' some of the components through spatial correlation. There could also be inclusions within grains giving rise to the medium component in those samples and therefore the same transfer could not take place into the fast component. Alternatively, the results could be a consequence of different trapping probabilities of the fast and medium component at various raised temperatures. The trapping probability (of an electron in the conduction band) is

related to the thermal velocity of carriers in the conduction band and capture cross-section, both of which are temperature dependent (McKeever, 1985). If the temperature dependencies of the fast and medium component trapping probabilities are sufficiently different then it would be possible to obtain the observed empirical results. It was also suggested that the result could be due to grain-to-grain differences in the constituent OSL components (Jain, *Pers. Comm.*). Therefore it may be possible that grains that display significant recuperation contain only or predominantly medium component traps and very few fast component traps.

Preliminary investigations of the recuperated 532nm stimulated LM OSL signals have been undertaken using single grains of quartz. Examples of six grains from a preliminary experiment on 100 grains of the same Madagascan quartz are shown in Fig. 4.34. A similar procedure of bleaching at 160°C followed by preheating to 280°C only was used. Grains 1,2,3,4 and 6 displayed fast, medium and slow components, while grain 5 contained only medium and slow components. The data represented by the black lines is the initial LM OSL (following dose and preheat). The data shown by the grey lines is the recuperated LM OSL signal. In all cases the result for the single grains is the same as the previous single aliquot experiment. The medium component displays a significant recuperated LM OSL signal following bleaching at 160°C that is not observed in the fast component. These results may indicate that the suggested grain-to-grain variation in contributing OSL components does not adequately explain the medium-only recuperation observations. However, more detailed experiments are required on more samples to investigate this further.

Whatever the explanation behind the medium component recuperation the result is that in samples that display this behaviour the effect on standard optical dates obtained may be significant, as discovered by Watanuki (2002). Dramatic age underestimates were obtained from sample with large amounts of thermal transfer. To circumvent this problem he separated the contributions from the fast and medium components via the application of curve fitting and achieved much more reliable results from the fast component, which apparently did not suffer from recuperation as the medium component did.

One noticeable trait of samples that display significant recuperation (in this study) is the slightly slower decay of the medium component relative to the fast than in samples that do not. For stimulation at 470nm and 160°C the ratio of the photoionization cross-sections of the fast and medium components is ~4.2 (see average values in Table 4.2). In these samples the ratio is ~6.1, as observed for EJR01an (and CdT9). Perhaps in this type of quartz sample the

trapping probability of the medium component is higher than usual, resulting in retrapping slowing the decay during LM OSL measurement. Feldspar contamination was not thought to be responsible having observed no significant IRSL decays at room temperature (see section 2.3).
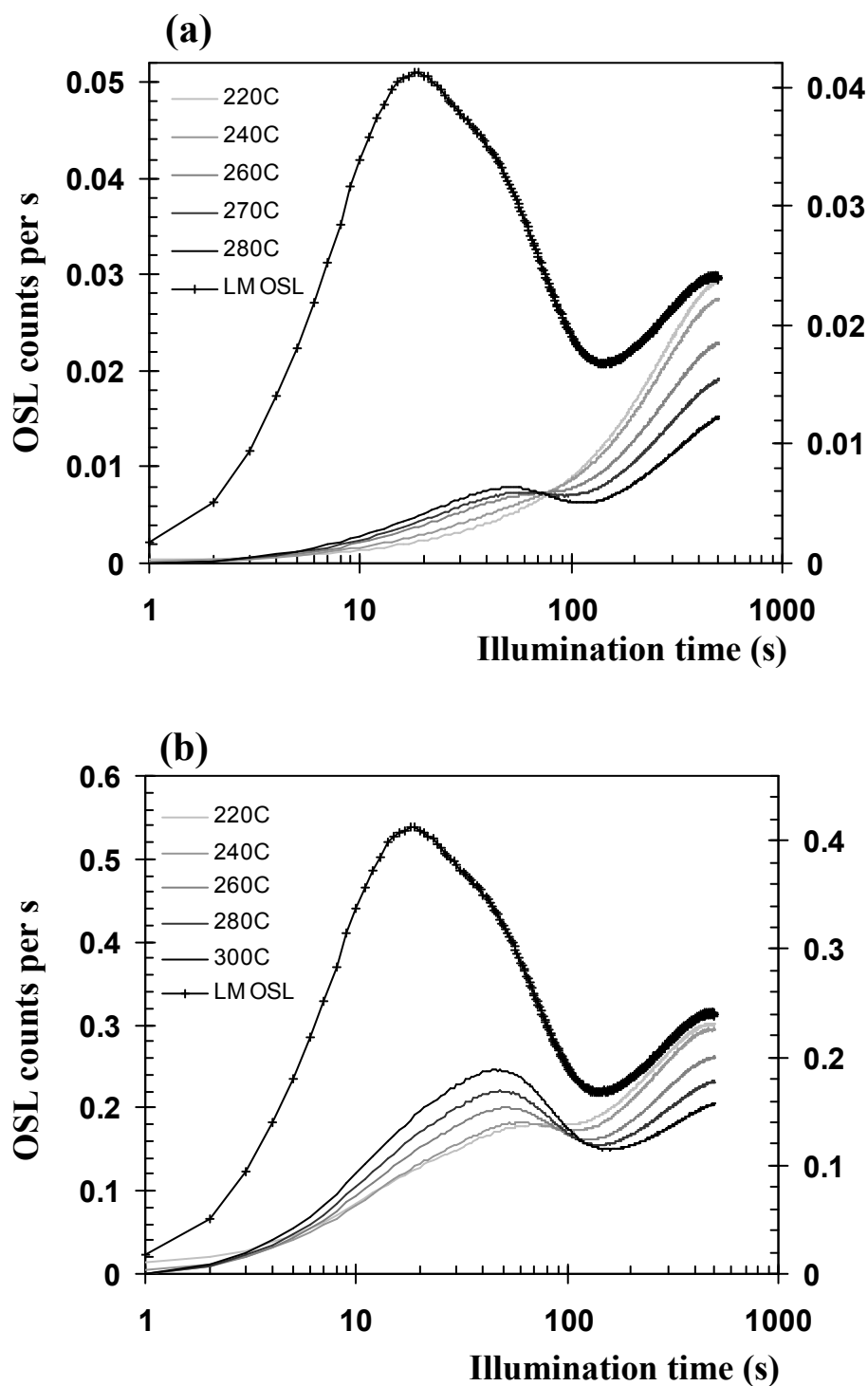
Fig 4.32 (a) Using sample EJR01an + 50Gy the LM OSL following preheat of 280°C for 10s is plotted in comparison to recuperated signals from bleaching at 160°C and preheating to temperatures given in the legend. (b) Similar data are plotted for the same sample, showing the recuperated signal following bleaching at room temperature.
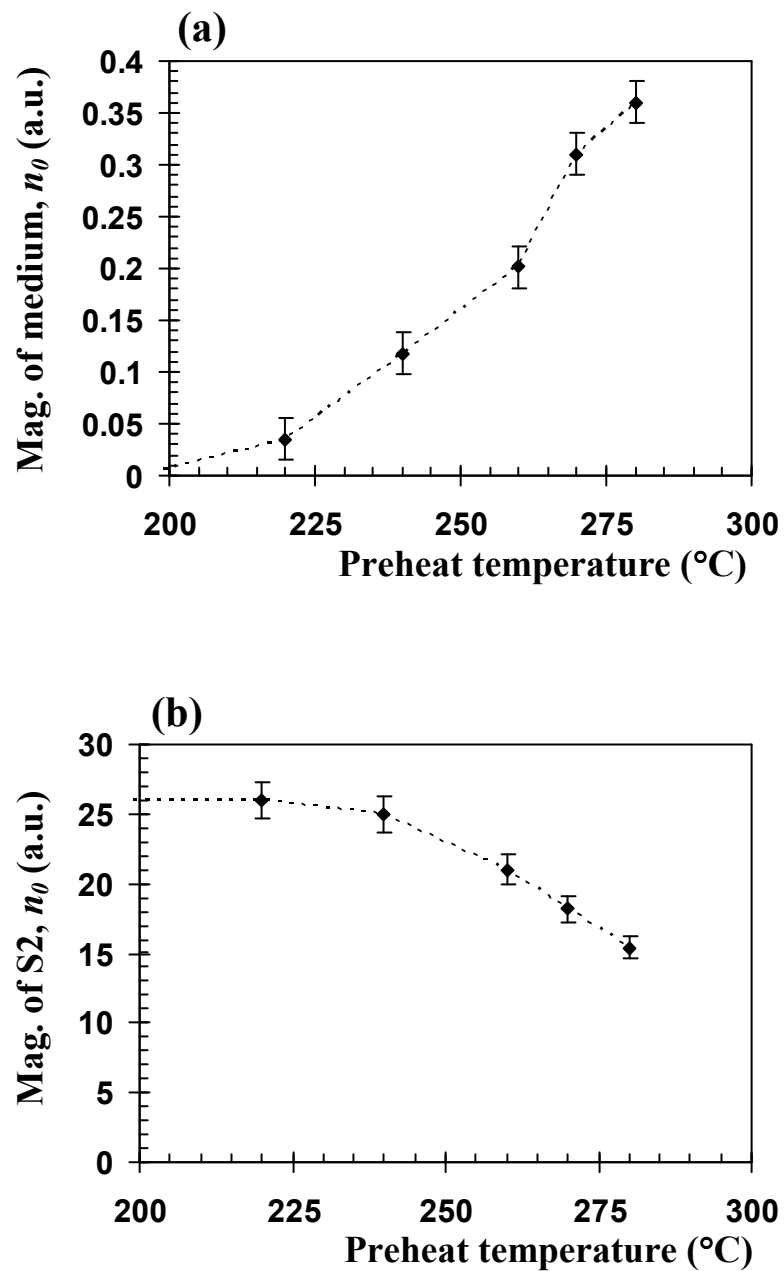
Fig 4.33 (a) Plot of the fitted magnitude, n_0, of the medium component recuperated signal versus temperature of preheat following bleaching at 160°C. (b) Similar plot for component S2 magnitude versus preheat temperature. The raw LM OSL used to obtain these plots is given in Fig. 4.32a.
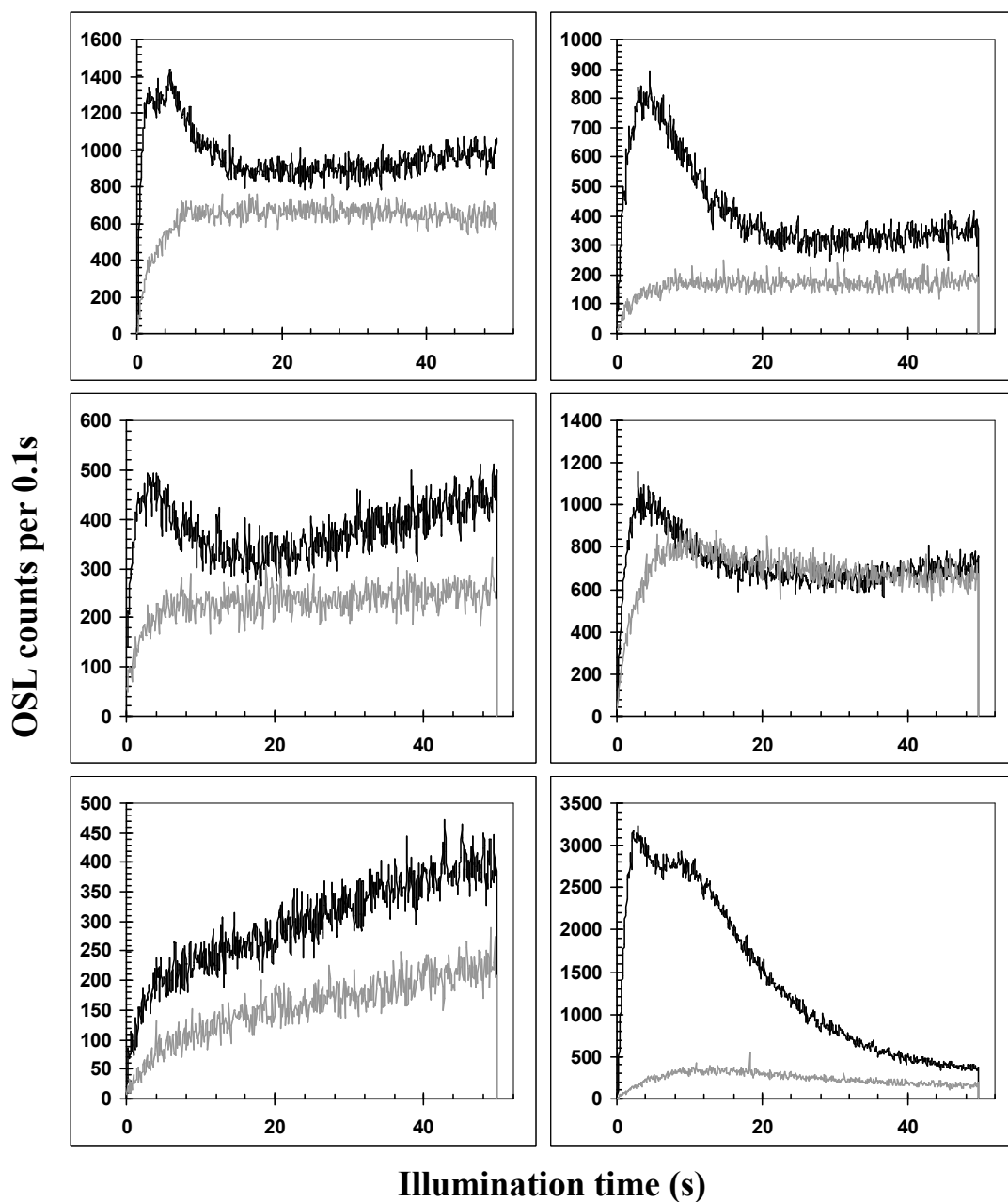
Fig. 4.34 LM OSL on six single grains of sample EJR01an measured for 50s at 160°C and 532nm. The LM OSL following preheat to 280°C is shown in black. The recuperated LM OSL signal following bleaching at 160°C then preheating to 280°C is shown in grey. Even on the single grain level the form of the recuperated signal differs drastically from the LM OSL signal, see section 4.5.

4.6 Reconciling the 'slow' CW OSL component with LM OSL measurements

The majority of the studies performed to understand the nature of the slow component are summarised in Bailey (2000a). Almost all previous work was done using CW OSL and using the assumption that there were only three OSL components (fast, medium and slow), an assumption which was backed up by adequate fitting of CW OSL decays to three first order components and other empirical evidence. Bailey (2000a) presented findings for the slow component that it displays extreme thermal stability, high dose response and other properties suggesting a sub-conduction band process may be responsible. Given the extraordinary nature of these findings it was felt necessary to try to see how they fit into the current picture of multiple 'slow components' using LM OSL. In the next subsection a summary of the most important results from previous behavioural studies is presented. In a further subsection the results of experiments designed to repeat some of these studies but with LM OSL replacing the standard CW OSL measurements are presented to try to reconcile the previous findings with current knowledge of the OSL components of quartz.

4.6.1 Previous studies on the slow component

The slow component was defined as that signal present after either optical wash (100s OSL to remove fast and medium) or thermal wash (to at least 400°C). These were assumed to be the same since only three components were believed to contribute to the OSL. Therefore, since the fast and medium were known to be depleted by both optical and thermal wash conditions what was left was assumed to originate from the same 'slow' component.

Pulse annealing experiments were performed, following optical washing to remove the fast and medium components. Initial decrease of signal size was observed between 300 and 400°C, then increase of signal size from 400°C and 600°C followed by decrease again. Results modified from Bailey (2000a) are presented in Fig. 4.35. Although thermal erosion and thermal sensitisation processes made interpretation of these results difficult, as acknowledged by the author, a fraction of the slow component was present after heating to over 600°C. The implication was that the slow component was extremely thermally stable.

The dose response of the slow component was found using N+β multiple aliquot techniques with a 500°C preheat to get rid of contributions from the fast and medium component. The data shown in Bailey (2000a) were not normalised. Single aliquot additive dose procedures were also used with 400°C preheat to deplete the fast and medium components (see also Singarayer *et al.*, 2000). It was stated that the chosen preheat was sufficiently low that minimal thermal sensitisation would take place, given the pulse annealing results. The slow

component measured using these methods was found to have a far higher dose saturation level than recorded for the fast or medium components, leading to proposal of the slow component for extending the datable age range of quartz OSL as introduced in Chapter 1, which was the main subject for investigation at the start of this project.

Dependence of the slow component signal form on initial charge concentration was observed. Faster slow component decays were observed following added doses (after 100s, 160°C optical wash). With successive illuminations at 160°C there was a trend to slower decays and an initial rise in signal whose time taken to reach maximum intensity increased with increased prior partial bleaching. Also, no optical desensitisation was observed to occur as the slow component was measured. These aspects of the slow component behaviour led to the hypothesis that a direct donor-acceptor (d-a) transition was involved (Bailey, 2000a). The probability of d-a recombination is dependent on separation distance, i.e. charge concentration, in a similar way as observed empirically for the slow component. See Bailey (2000a) for more details. The lack of optical desensitisation (and apparent lack of PTTL) suggested that the luminescence centre used by the slow component was different to that used by both the fast component and the 110°C TL peak, as did the apparent redder emission characteristics of the slow component than the fast and medium components (described by Spooner, 1994).

The above points will be addressed immediately below to correlate previous results with the current research on the quartz OSL components.

4.6.2 LM OSL observations

To address the first point, that the same slow component is observed after optical and thermal washing, the same optical and thermal wash conditions have been performed on four different samples prior to LM OSL measurement for 7200s at 160°C to see from what traps the remnant charge originates (Fig. 4.36). The LM OSL following a 'standard' type preheat is shown for reference, see Fig. 4.8 also. The samples were bleached and given 20Gy doses. After optical washing of 100s CW OSL at 200°C only component S2 and S3 were recorded in the subsequent LM OSL measurement. The signal from these components is negligibly reduced following the optical wash. After a thermal wash consisting of preheating to 450°C at $2°Cs^{-1}$ the signal levels are reduced by a factor of 100 in some of the samples. A very small fraction of component S2 remained, but mainly component S3 (hence no peak was observed in samples SL203, CdT9 and TQN after heating to 450°C). This is expected if S2 is

associated with TL ~ 280°C. The post-thermal wash OSL consists primarily of component S3.

In a previous pulse annealing experiment, CW OSL results by Bailey (2000a) showed the slow component signal increasing for increasing preheat temperatures up to 600°C, and were still present after heating to 650°C. A similar experiment was performed using LM OSL. A multiple aliquot procedure was used in this case. Bleached aliquots were given 50Gy followed by an optical wash of 50s at 200°C to remove the fast and medium OSL components. The aliquots were preheated to temperatures between 240 and 600°C, two aliquots were used to obtain data from each preheat temperature. The remnant OSL was recorded with 7200s LM OSL measurements at 160°C. The LM OSL from each of the two aliquots used for each temperature produced very similar LM OSL in terms of both peak heights and peak positions. Normalisation of the aliquots was achieved by dividing the LM OSL by the mass of the aliquot. The average LM OSL from the two aliquots was plotted. Fig. 4.37 shows the results on sample SL161.

Following the optical wash only the slow components S2 and S3 remain. The magnitude of the peak (S2) decreases between 240°C and 500°C until after 500°C preheat no component S2 peak is present, i.e. this component is near completely thermally eroded. The rising LM OSL signal observed after 500°C represents component S3. Between 500°C and 600°C a considerable increase in the signal is observed, as found by Bailey (2000a). An intermediate component peak is observed as well as the rising limb of component S3. This intermediate peak could be fitted to three first order components, none of whose photoionization cross-sections corresponding to the OSL components given in Table 4.2. It would anyway seem unlikely that transfer of charge to these OSL components would occur during cooling from 600°C given the residence time of charge in the conduction band (~30μs). This form of the LM OSL following preheating 600°C was found to be reproducible.

Integrating the LM OSL from 0 to 3600s gives the plot in Fig 4.37c of OSL vs. preheating temperature (Integration limits were not critical. Several different limits were tried with similar results). This figure is similar in form to those published in Bailey (1998b, 2000a), although temperatures up to 700°C were not used in this experiment.
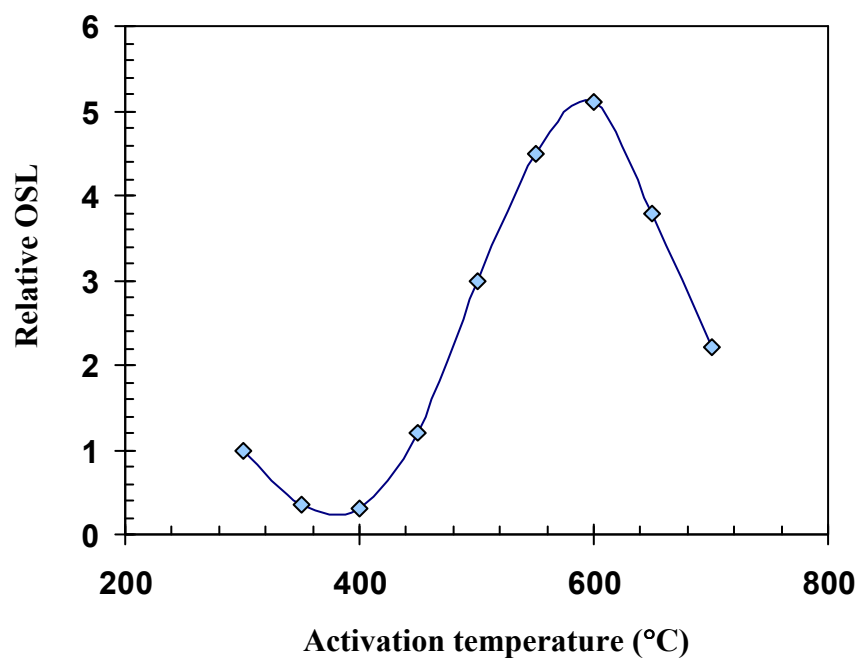
Fig. 4.35. CW OSL slow component pulse annealing curve, modified from Bailey (2000a). The fast and medium components were removed by 100s OSL at 250°C. Aliquots were heated to T_i with a 10s hold. The points in the figure are integrated from 100s OSL at 160°C.
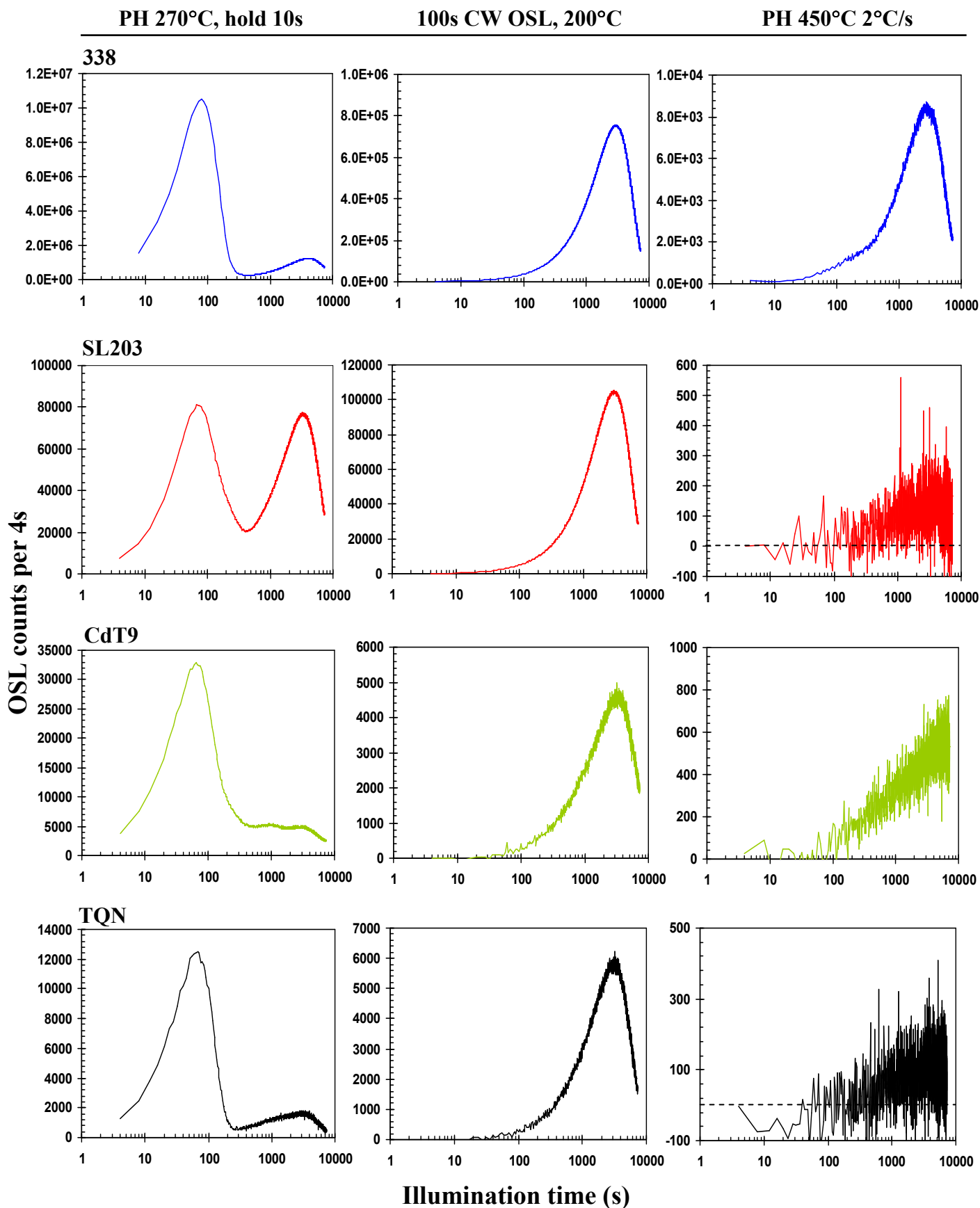
Fig. 4.36 shows the LM OSL at 160°C from four different samples (338, SL203, CdT9, and TQN) following various pre-treatment conditions given above the plots.

Through the application of LM OSL it has been shown that the initial decrease between 240 and 450°C can be attributed to loss of charge from component S2. At higher temperature the increase in signal size may tentatively be due to thermal sensitisation in component S3. Similar trends have been observed in some samples, but not all by any means. For example, sample SL167; taken from the same region as SL161, showed only a decrease in signal from 240°C until at 500°C no measurable LM OSL was recorded (identical trend to that observed for TQN, see section 4.4.2). For the samples that did retain some LM OSL signal after preheats >500°C the form of the LM OSL curves appeared to resemble that from SL161, with some charge being detrapped from an intermediate optical stability component and then a slow rising signal (attributed to S3).

Bailey (1998b) noted that the dose response of the slow component far exceeded that of the other components. The dose response of the components as found using LM OSL is discussed in section 6.3.2. To summarize the findings of current investigations, the fast, medium and S1 components were found to have similar dose responses. Component S2 appeared to saturate at relatively low doses ($D_0 \sim$ 30-40Gy). Only component S3 displayed the considerably high dose saturation levels observed by Bailey (1998b, 2000a). The observations of Bailey (1998b) would be therefore expected since the LM OSL results following thermal washing would chiefly consist of component S3. A more detailed comparison will be undertaken in the later chapter (6).

The findings listed in section 4.6.1 suggested a localised, sub-conduction band process for the slow component. Several of these experiments were repeated in this investigation. Bailey (1998) observed a dose dependent decay form, with decays being faster at higher doses. This may be explained by the fact that the slow component OSL derives from several traps with different dose responses and that component S3 displays significantly non-first order behaviour (see section 6.3 for evidence). The experiment presented in Bailey (1998b, 2000a) to observe the decay form as a function of prior illumination was repeated on sample 338, as used by Bailey, under the same measurements conditions (except for wavelength: 470nm) to check the reproducibility of the results. Bailey (2000a) interpreted the trend towards slower decay rates and an initial rise reaching maximum intensity at longer times following lengthier illumination times as possibly resulting from concentration dependent localised transitions (similar interpretations were made by Poolton et al. (1994) from a similar experiment on feldspar).

In the current experiment, an aliquot of sample 338 was given a 50Gy dose followed by preheating to 450°C at 20°Cs^{-1} to remove the fast and medium components. Four successive CW OSL measurements at 160°C were recorded, allowing the sample to cool in between. The results are presented in Fig. 4.38. In the main figure the OSL decays have been normalised to the same initial value to show more clearly the change in form (the inset shows the successive un-normalised decays). A similar pattern of slower decay rates after longer illuminations times was observed (between cycle 1 and 2 but not between 2, 3 and 4), as was the initial rise in signal. The reason for this became clearer when the experiment was repeated using LM OSL measurements. The LM OSL measurements of the remaining signal after various stages of the equivalent CW OSL experiment are shown in the lower figures (Fig. 4.38). The initial LM OSL [1] following preheating to 450°C showed that a proportion of the medium component (peak at ~100s) remains after preheating. Correspondingly, the sharper CW OSL decay [1] originates from the medium component, whereas the subsequent OSL measurements originate primarily from component S2 (see further LM OSL figures) Therefore the change in decay form is due mainly to contributions from multiple components.

Crucially, in contrast to Bailey (2000a) the peak position of the CW OSL initial rise was found not to depend on prior illumination time, i.e. a constant maximum intensity position was observed. The discrepancy between the results of the current study and the previous study on the same sample may perhaps be contributed to significant noise in the data leading to ambiguity in peak position, and difference in stimulating wavelength resulting in slower bleaching of the medium component over cycles [1] and [2] (see Fig. 4.38).

The phenomenon of photo-transfer is investigated in section 5.5. In contrast to Bailey (2000a), photo-transfer has been observed to occur in the 110°C TL peak from all of the OSL components as recorded using LM OSL. This and the other current results described above indicate that all the OSL components detrap charge to the delocalised band before recombination and that there is no substantial evidence for a direct d-a transition. It is suggested however that further experiments are carried out on component S3 to fully examine the possibility.
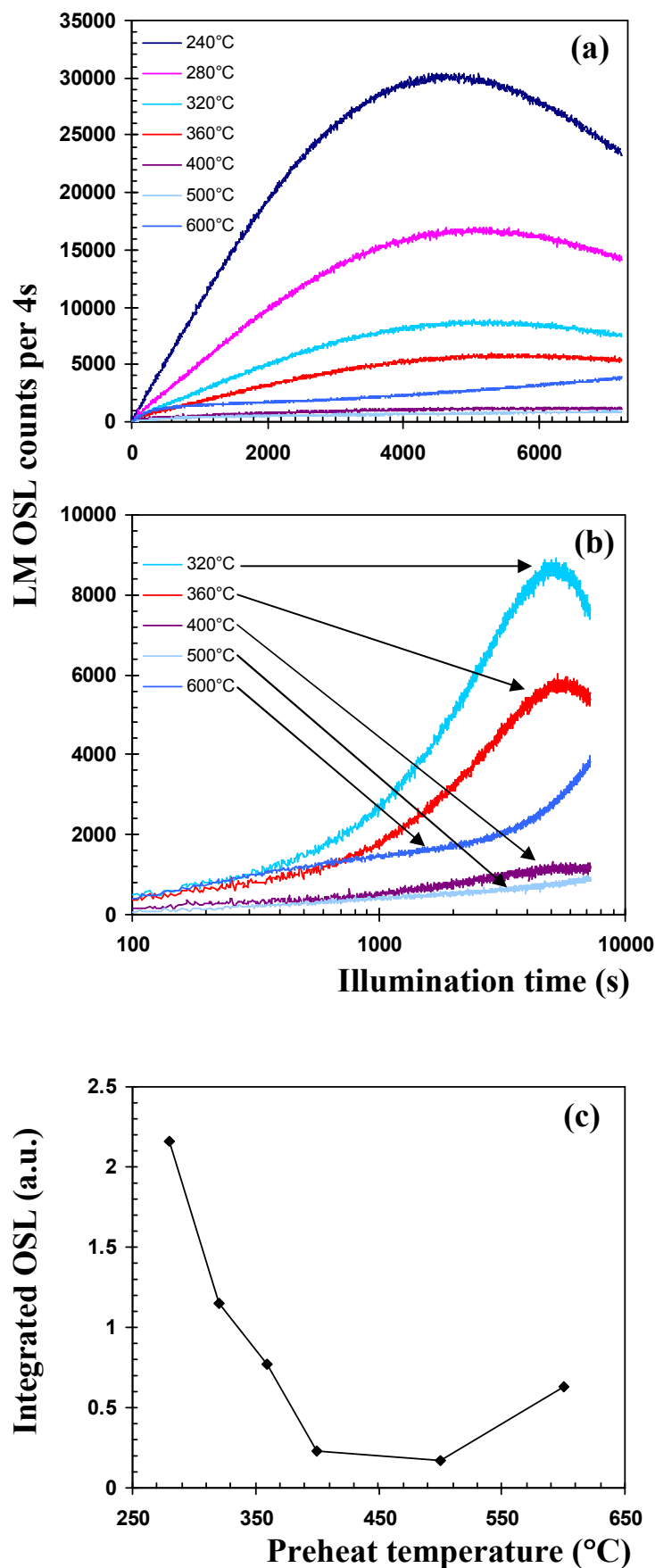
Fig. 4.37 (a) LM OSL from sample SL161 following various temperature preheats (between 240 and 600°C). (b) Same data as for (a), but on a log(t) scale and showing in clearer detail the LM OSL following the high temperature preheats (c) Integrated LM OSL data (0-3600s) vs. preheat temperature. Each data point is the sum of two similar aliquots.
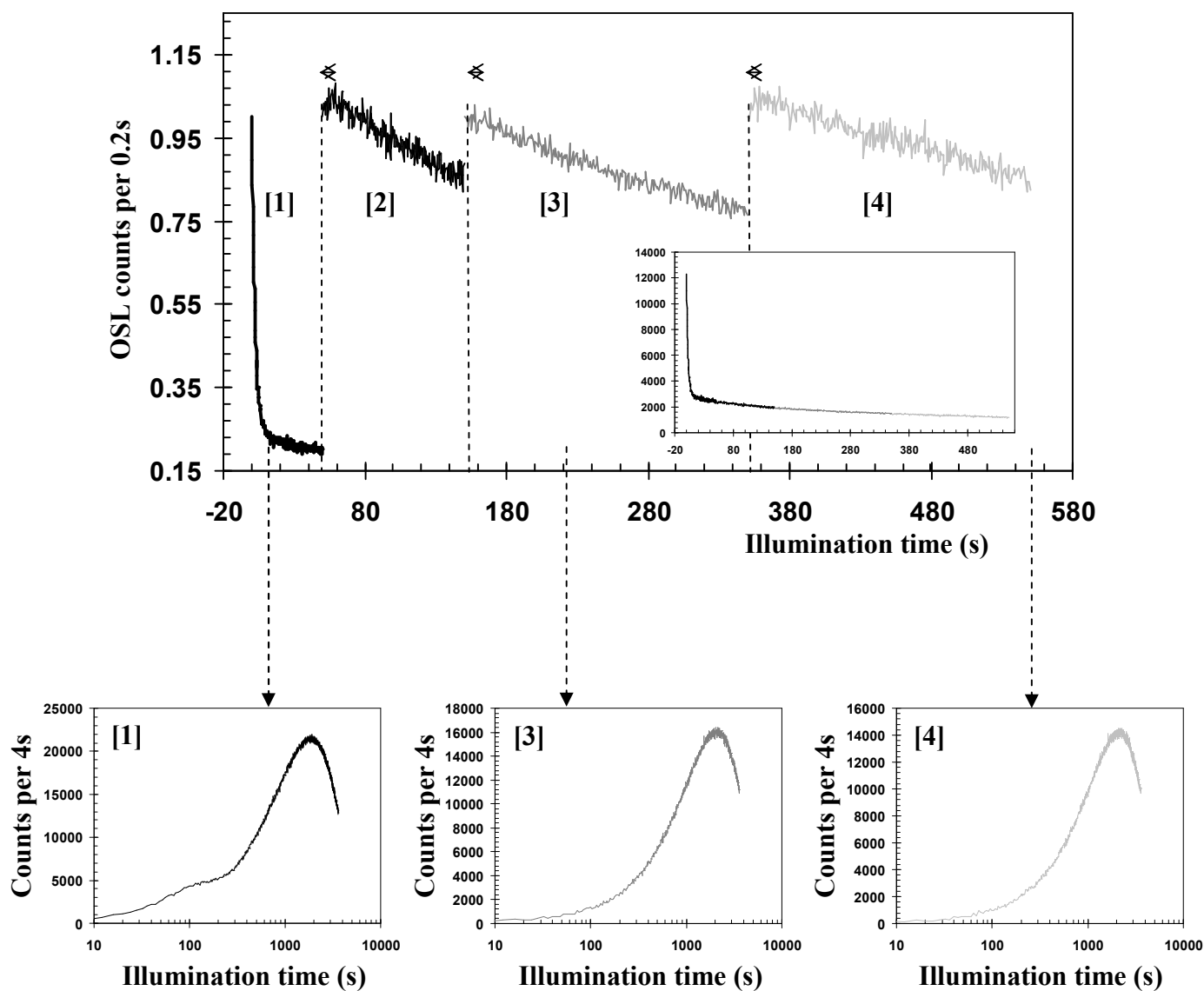
Fig. 4.38 (Main) interrupted OSL decay following preheating to 450°C. Successive measurements were made at 160°C on sample 338. In between each measurement the aliquot was allowed to cool to room temperature. The initial values have been normalised to unity. Arrows show the time taken to reach maximum intensity in OSL [2], [3] and [4]. (Inset) shows the successive un-normalised decays. (Lower) Equivalent LM OSL measurements to CW OSL measurements [1], [3] and [4] to illustrate which OSL components are contributing to the CW OSL.

4.7 Summary

Preliminary measurements on a number of samples have demonstrated, through deconvolution, that there are at least five OSL components common to most quartz samples. The most common components have been called fast, medium, S1, S2 and S3. This finding enables the results from further experiments on a smaller range of samples to be applicable to a wider number of quartz samples in general.

Following this, the main aim of this chapter was to explore the effects of temperature (preheating and measurement) on quartz OSL. The thermal stability of each component was assessed by two methods, giving similar results. Only component S2 was found not to be of sufficient thermal stability for application to optical dating (lifetime ~19ka by isothermal decay analysis). Data for component S3 was not presented due to ambiguity in LM OSL curve fitting for this component, since using the current measurement conditions the LM peak of component S3 was not observable at the low doses given (see section 6.3.2 for further observations of S3).

Finally, in the previous detailed study investigating the behaviour of the OSL components by Bailey (1998b, 2000a) three components were fitted to CW OSL decays: fast, medium and slow. The slow component was found to display behaviour indicative of a sub-conduction band recombination process. Given the strong degree of overlap between the previous study and the current investigations and the knowledge that there are several slow OSL components (S1, S2, and S3), experiments were repeated to reconcile the past observations using LM OSL. There were similarities in the data obtained, such as the dose saturation levels obtained for the CW slow component and LM OSL component S3 and dose dependent decay form. However, the data collected suggest that the previous results interpreted as a direct donor-acceptor transition are probably the result of the non-first order nature of component S3 (discussed in detail in section 6.3.2) and/or multiple trap contributions.

Chapter | 5

5 | OPTICAL DETRAPPING CHARACTERISTICS OF THE LM OSL COMPONENTS

5.1 Introduction

The present chapter is concerned with properties of the components with respect to optical eviction. The dependence of photoionization cross-section on measurement temperature and photon energy is discussed. Experiments have been undertaken to look at the bleaching rate of each component under the solar spectrum to estimate comparative bleaching potential in the natural environment.

Sensitivity changes during LM OSL measurement have been investigated and the effect on the form of the LM OSL is discussed. Photo-transfer of charge from each of the components to the 110°C TL peak is evaluated in order to assess detrapping of charge to the delocalised band.

5.2 Thermal dependence of optical detrapping

5.2.1 Introduction

The thermal dependence of OSL of quartz has been studied by several authors, e.g. Spooner (1994). Strong thermal dependence in the rate and magnitude of optical depletion has been observed. The first investigation on a component-resolved basis was performed by Bailey (1998b) to investigate possible differences between the components (this was partly to provide evidence for the multiple-component explanation for non-exponential CW OSL in quartz). Here the study is extended to several further samples and uses LM OSL to more clearly observe the OSL components. The main aim of this section is to examine the thermal dependence of the rate of optical depletion of the components in terms of:

(i)   Thermal assistance – the increase in the rate of optical depletion as the measurement temperature is increased.

(ii)   Thermal quenching – the decrease in the total measurable signal as the measurement temperature is increased, due to the increased probability of non-radiative recombination.

Thermal assistance of optical detrapping

Spooner (1994) found a roughly exponential dependence of the optical depletion rate on measurement temperature. Similar results were obtained by Huntley *et al.* (1996) over a range of photon energies. The data were fitted to Urbach-type expressions (Urbach, 1953) in both studies, given in equation 5.1. This describes the temperature and photon energy dependence of optical detrapping efficiency. However, it is an empirically derived rule for band-to-band transitions rather than centre-to-band and as such can only provide a rough approximation. Electron-phonon coupling of transitions from deep traps has been studied by many authors (e.g. Stoneham, 1979). Alternative expressions describing temperature and photon dependence of OSL will be discussed in more detail in section 5.3.1.2. The expressions used later on do, however, in most cases simplify to simple exponentials at high temperature. For this experiment simple exponential dependence is still assumed, since a single photon energy has been used:

$$I_0 = I_\infty \exp\left(-\frac{E^*}{k_B T}\right) \qquad\qquad (5.1)$$

where I_0 is the initial signal intensity, I_∞ is intensity at $T = \infty$, and $E^* = \phi(E_0 - h\nu)$ (ϕ is a constant, E_0 is the optical depth, and $h\nu$ is the photon energy). Spooner (1994) found that using 514nm optical stimulation the thermal assistance energy, E^*, needed was ~0.1 ± 0.02eV. Using various wavelength stimulation Huntley *et al.* (1996) were able to find $E_0 =$ 2.82eV and $\phi = 0.26$, although the photon energy dependence was not fully described by equation 5.1. The interpretation of E^* is not straightforward, as acknowledged by Huntley *et al.* (1996), but can be considered as the thermal component in the detrapping process that is expected from deep traps strongly coupled to the lattice.

To estimate E^* equation 5.1 can be rearranged to give:

$$\ln(I_0) = \ln(I_\infty) - \frac{E^*}{k_B} \cdot \frac{1}{T} \qquad\qquad (5.2)$$

Plotting $\ln(I_0)$ versus $1/T$ allows E^* to be found directly from the gradient of a straight line fit to the data. For component-resolved measurements I_0 is replaced by σ, the photoionization cross-section, a direct measure of optical detrapping rate, obtained through deconvolution of OSL.

Thermal quenching

Thermal quenching refers to the reduction in radiative intensity with measurement temperature, of the form described by Curie (1963):

$$\eta = \frac{1}{\left(1 + K\exp\left(-\dfrac{W}{k_B T}\right)\right)} \qquad (5.3)$$

where K is a frequency factor (s^{-1}), W is the activation energy (eV), k_B is Boltzmann's constant and T is temperature (K). Values for K and W were found for quartz TL by Wintle (1975): $K = 2.8\text{x}10^7\text{s}^{-1}$, $W = 0.64\text{eV}$. Spooner (1994) reported that the thermal quenching of quartz OSL corresponded to that found by Wintle for TL. Bailey (1998b) calculated similar quenching parameters, K and W, for the fast, medium and slow components also comparable to values from Wintle (1975).

The models suggested to explain the loss of radiative intensity (i.e. luminescence efficiency) with measurement temperature was investigated by Bailey (2001), from which the Mott-Seitz configuration coordinate model was found to be the most robust. In this model the probability of non-radiative recombination increases at higher measurement temperatures. Electrons captured from the conduction band to excited states of luminescence centres undergo a thermally assisted non-radiative recombination where energy is absorbed by the lattice (i.e. transfer of energy to phonons) instead of emitted as photons. Therefore experimental results of thermal quenching provide information concerning the recombination process.

As stated above, results from Bailey (1998b) showed similar quenching values for the fast, medium and slow components. Two possibilities were proposed: (1) all components use the same luminescence centre, which undergoes thermal quenching (2) components may use different luminescence centres, which all have similar quenching responses. Bailey suggested that the second option was more likely given results from Spooner (1994) where slow components were removed with red rejecting filters suggesting at least two different emission bands. However, no spectrally resolved OSL measurements have yet been undertaken.

5.2.2 Experimental method and initial results

Thermal assistance and thermal quenching can be quantified by a single experimental procedure involving measurement of OSL at various temperatures. The following procedure was applied to sedimentary samples SL203 and CdT9. Aliquots of the samples were bleached and given 20Gy laboratory beta doses followed by preheating to 280°C for 10s (sufficiently

high so that phosphorescence at the higher measurement temperatures should be negligible). The LM OSL was subsequently measured at temperature T_i for 7200s. Measurement temperatures used were: T_i = 100, 120, 140, 160, 180, 200, 220°C. The aliquots were bleached to negligible levels by CW OSL at 180°C for 6000s in between LM OSL measurements. A 10Gy test dose was given to the same aliquot, followed by preheat of 260°C, 10s. The LM OSL (7200s at 160°C) following the test dose was used to monitor luminescence sensitivity.

A multiple aliquot protocol was employed for sample CdT9, i.e. a fresh aliquot was used to obtain data for each measurement temperature. These results were obtained from the old non-linear ramping stimulation system (R4a). It was found that there was a significant aliquot-to-aliquot variation of fitted photoionization cross-sections of each component. Since these data were required to estimate thermal assistance energy, the experiment was repeated using a single aliquot procedure for sample SL203. The data for sample SL203 was collected using the more powerful, linearly ramping stimulation system (R4b).

The raw LM OSL for both samples is shown in Fig 5.1, (a) CdT9 (b) SL203. Shift of the LM OSL peaks to shorter times with increasing measurement temperature is visible, especially in the slow components. The *ln(t)* scale used for plotting disguises the effect in the fast component somewhat. The strong thermal quenching effect is more immediately obvious in sample SL203, where due to negligible sensitivity changes throughout the measurement procedure the LM OSL peak magnitudes are 'as seen'.

The LM OSL obtained at each measurement temperature was deconvolved to estimate n_0 and σ of each OSL component. The photoionization cross-section was used to quantify the thermal assistance energy for each component (described in section 5.2.1). The magnitude, n_0, was used to quantify the thermal quenching parameters for each component. Measurements made at 100°C were not included in the final analysis of the data due to broadening of the LM OSL form from photo-transfer to and optical eviction from the 110°C TL peak. Plots of n_0 vs. T and $\ln(\sigma)$ vs. $1/T$ are shown in Fig. 5.2 (sample SL203) and Fig. 5.3 (sample CdT9).
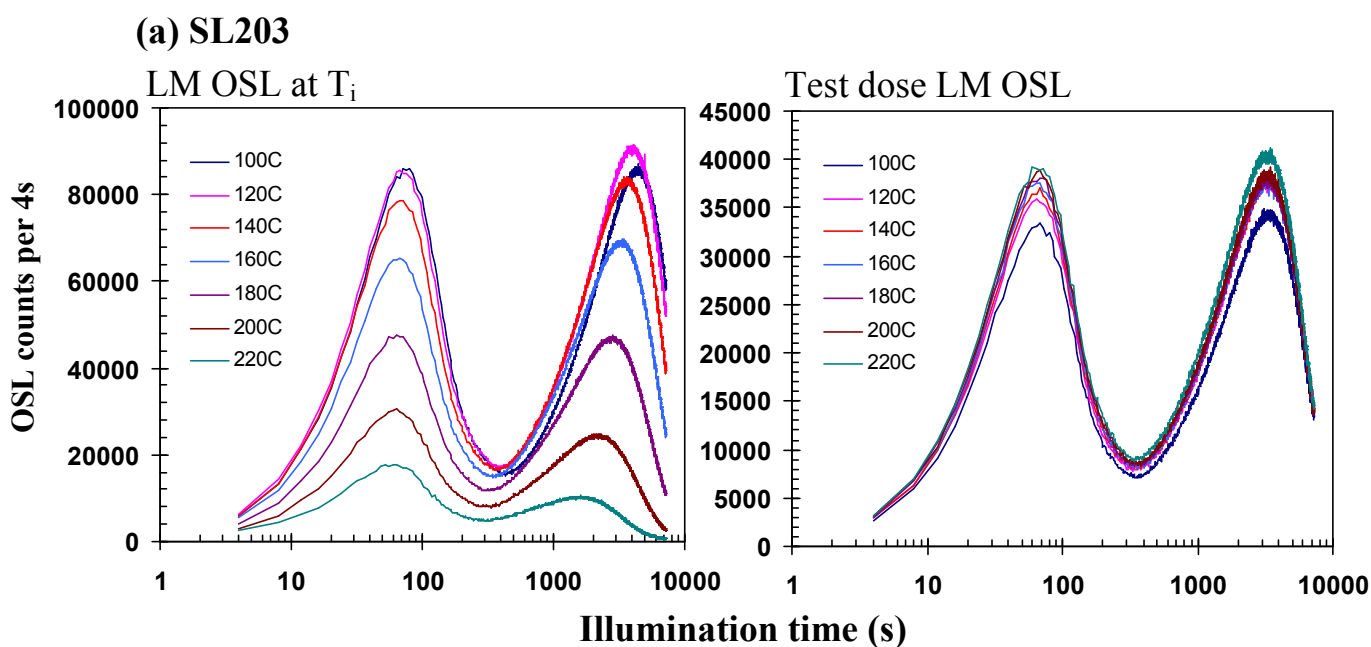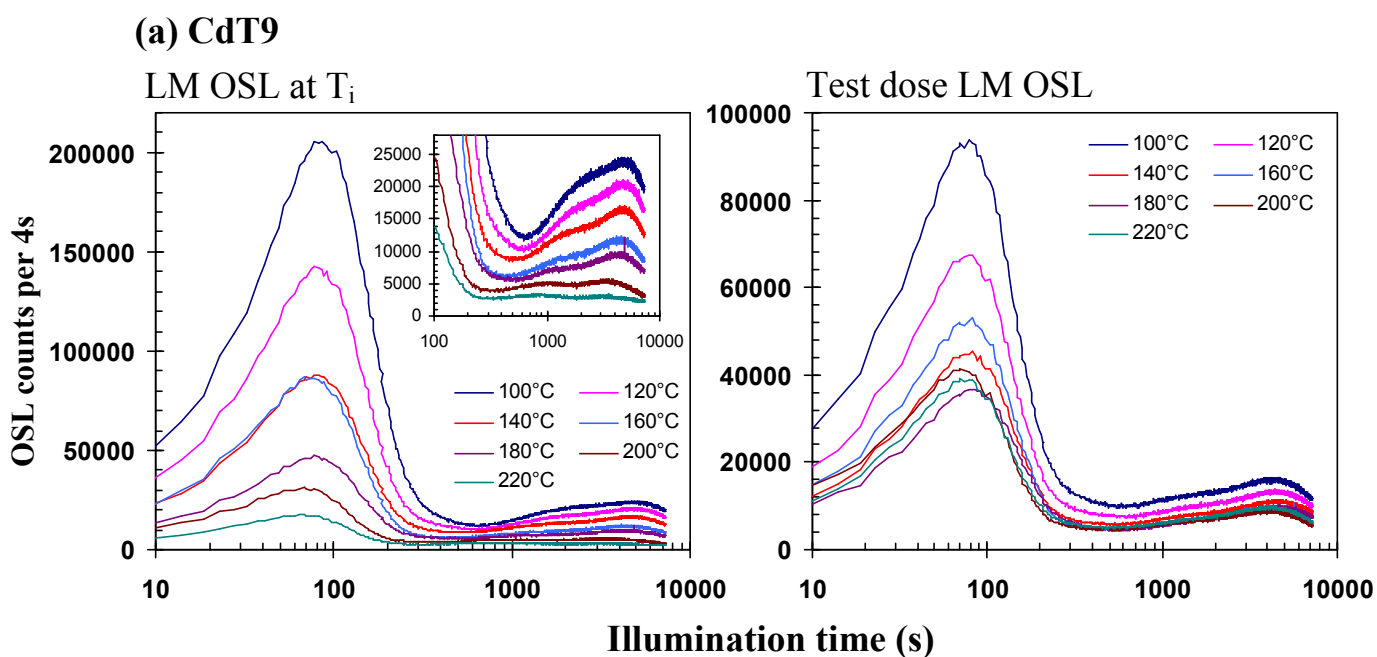
(a) CdT9

(a) SL203

Fig. 5.1 LM OSL measured for 7200s at various measurement temperatures, given in the legend, for samples (a) CdT9 and (b) SL203. The LM OSL (7200s at 160°C) following a test dose of 10Gy, preheat of 260°C for 10s is shown in the right-hand plots for each sample.
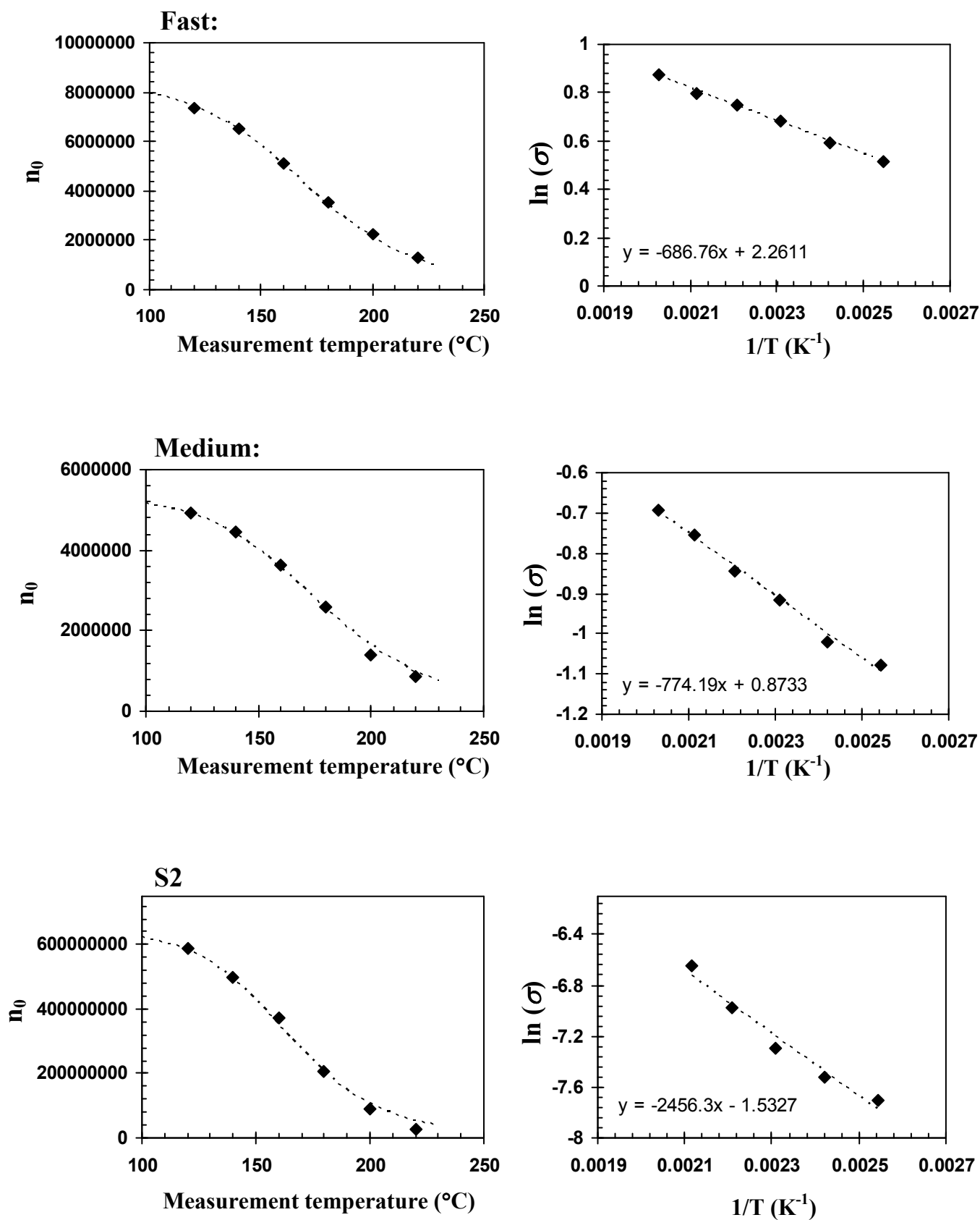
Fig 5.2 For the fast, medium and S2 OSL components of sample SL203 the component magnitude, n_0, vs. measurement temperature is plotted (left) to obtain information concerning thermal quenching. $\ln(\sigma)$ vs. $1/T$ is plotted also (right) to provide information about thermal assistance. See text, section 5.2 for further details.
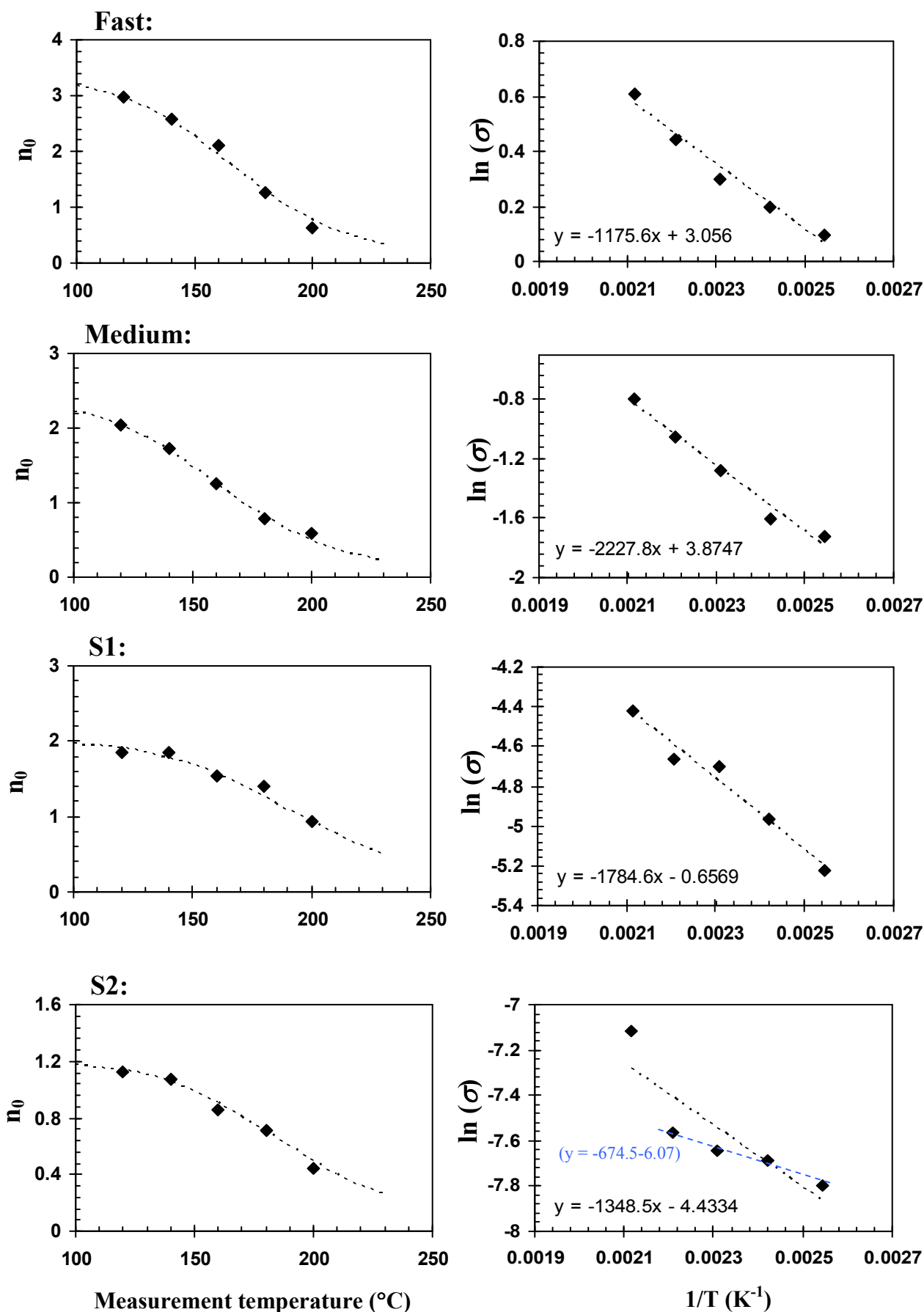
Fig. 5.3 For the OSL components of sample CdT9 the component magnitude, n_0, vs. measurement temperature is plotted (left) to obtain information concerning thermal quenching. $\ln(\sigma)$ vs. $1/T$ is plotted also (right) to provide information about thermal assistance. See text, section 5.2 for further details.

5.2.3 Analysis and Interpretation

The LM OSL from the one aliquot of sample SL203 used in this experiment was fitted to only three components whose fitted photoionization cross-sections matched the fast, medium and S2 components. Since other aliquots of this sample have been fitted to five components this illustrates the aliquot-to-aliquot variation in the relative proportions of the components. However, five components were fitted to all aliquots of CdT9, although consistent results were not obtained for S3.

Component magnitudes, n_0, versus measurement temperature plots for sample SL203 are presented in Fig. 5.2 (figures on the left). All three components display the same form of decrease in signal size with increasing temperature. The data have been fitted to equation 5.3 for thermal quenching, shown by the dotted lines in Fig. 5.2. Reasonable fits were obtained for each component. Similar data for sample CdT9 are plotted in Fig 5.3. Although the data collected for this sample are noisier than SL203 (probably due to the multiple-aliquot procedure used) reasonable fits to all components were again obtained. The fitted thermal quenching parameters, W and K for both samples are given in Table 5.1. A remarkable degree of similarity can be observed in the fitted values, both between the OSL components and between the two samples. This finding echoes results from Bailey (1998b), and are comparable to those found by Wintle (1975) for quartz TL ($K = 2.8 \times 10^7 \text{s}^{-1}$, $W = 0.64\text{eV}$). The observed similarity suggests that there is a common luminescence centre for all the OSL components, although the idea that there are several luminescence centres with the same thermal quenching characteristics cannot be ruled out without further spectral measurements.

Plots of $\ln(\sigma)$ versus $1/T$ for each fitted OSL component of sample SL203 are displayed in Fig. 5.2. If there is an exponential dependence on T (equation 5.2) then these plots should fit on a straight line, as was found to be the case for the fast and medium components. Component S2, while fitted to a straight line in the figure, arguably is slightly curved in nature at higher temperatures (lower $1/T$ values). The equivalent plots for sample CdT9 are shown in Fig. 5.3. The noise observed originates from the slight variation in fitted photoionization cross-section between the aliquots used. Straight line fits were obtained from all components. Again, component S2 produced the least satisfactory fits to the data, especially at higher temperatures. Reasons for the observed nonlinearity are not clear at this time.

		K (s⁻¹)	W (eV)
Fast	SL203	3.9×10^7	0.67
	CdT9	4.5×10^7	0.67
Medium	SL203	3.1×10^7	0.66
	CdT9	2.5×10^7	0.64
S1	SL203	-	-
	CdT9	6.0×10^7	0.63
S2	SL203	1.3×10^9	0.79
	CdT9	1.2×10^7	0.65

Table 5.1 Fitted thermal quenching parameters, *W* and *K*, from equation 5.3 for samples SL203 and CdT9. The fits performed to find these parameters are given in Fig. 5.2 (SL203) and Fig. 5.3 (CdT9).

		E* (eV)
Fast	SL203	0.05
	CdT9	0.08
Medium	SL203	0.06
	CdT9	0.15
S1	SL203	-
	CdT9	0.13
S2	SL203	0.17
	CdT9	0.10

Table 5.2 Fitted thermal assistance parameters, from equation 5.2 for samples SL203 and CdT9. The fits performed to find these parameters are given in Fig. 5.2 (SL203) and Fig. 5.3 (CdT9).

The results of the analysis, E^* values, are summarised in Table 5.2. The values are slightly smaller than the component-resolved values obtained by Bailey (1998b) as expected since a shorter stimulation wavelength (higher energy) was used (470nm rather than broad-band 420 – 560nm); therefore the amount of thermal assistance required is lower. Some variation between the two samples was observed. This is perhaps not unlikely given sample to sample variation in impurities and trap concentrations, influencing the local electronic environment. However, the result is that any differences in E^* between the components are outweighed by the scatter.

5.3 Dependence of optical stimulation on detrapping

5.3.1 Dependence of eviction rate on photon energy

5.3.1.1 Introduction

It is known that the energy of optical stimulation affects the rapidity of OSL signal depletion under constant illumination. Previous authors have found an increase in bleaching rate with increasing photon energy for quartz OSL (e.g. Spooner, 1994; Duller and Bøtter-Jensen, 1996). The thermal assistance energy, described in section 5.2, has been found to decrease with increasing photon energy (Spooner, 1994; Huntley *et al.*, 1996). The bleaching spectra of quartz have been obtained mainly in terms of integrated luminescence vs. photon energy (e.g. Duller and Bøtter-Jensen, 1996). No previous investigations on quartz have been carried out using a component-resolved analysis.

This section seeks to empirically investigate the dependence of the detrapping rate of each of the OSL components on photon energy to investigate the separation of the quartz components photoionization cross-sections, specifically the fast and medium, when under stimulation with different photon energies. The interest in this comes from previous work by Bailey (2002b) concerning the potential for identification of partially bleached samples using signal analysis methods (section 7.2). Studies by Bailey (1998b) and also Rhodes (1990) found that there was no change in signal form of CW OSL following bleaching with sunlight. This suggested that under the solar spectrum, where the majority of bleaching may be due to the UV portion, there was little difference in the detrapping rates of the fast and medium component. Therefore, it would not be possible to use signal analysis techniques to detect partial bleaching in aeolian samples.

5.3.1.2 Theoretical aspects

As previously stated in section 3.2.2 the detrapping rate from a single trap type stimulated with monochromatic light at a constant temperature may be expressed as:

$$f = \sigma(h\nu)P \tag{5.4}$$

where σ is the photoionization cross-section for the release of charge from the trap and P is optical stimulation photon flux. The rate of optical eviction of charge is therefore dependent on both the photon flux and the photon energy ($h\nu$). The hydrogenic model provides a firm conceptual basis for the characterisation of shallow traps in the absence of electron-phonon coupling (see Fig. 5.4, Böer (1992)).

$$\sigma(h\nu) \propto \frac{(h\nu - E_{i0})^{3/2}}{(h\nu)^5} \tag{5.5}$$

The assumptions made in this model breakdown as the localisation of a bound particle increases, i.e. for deeper traps, as phonon coupling increases also. The fast and medium have previously been found to be relatively deep trapping levels, $\geq 1eV$ (Bailey, 1998b). For such deep levels the photo-ionization cross-section, $\sigma(h\nu)$ has generally been described (e.g. Alexander *et al.*, 1997) with the following equation derived by Lucovsky (1965):

$$\sigma(h\nu) \propto \left[\frac{4(h\nu - E_{i0})E_{i0}}{(h\nu)^2} \right]^{3/2} \tag{5.6}$$

Here E_{i0} is the threshold energy for excitation. The forms of both the hydrogenic and Lucovsky photoionization cross-section spectra are illustrated in Fig. 5.4. The hydrogenic cross-section peaks sharply near the threshold whereas the Lucovsky cross-section is broader and peaks at roughly twice the ionization energy.

Spooner (1994) demonstrated the dependence of the rate of photo-eviction on both photon flux and photon energy experimentally from the intensity of OSL for different wavelengths. Optical depletion rate of OSL has been found by several authors (e.g. Spooner, 1994; Huntley *et al.*, 1996) to have approximately an exponential dependence on measurement temperature over the measured range of stimulation photon energies (1.84 – 2.73eV, Huntley *et al.*, 1996). The Lucovsky equation (5.6) does not account for the temperature dependence that has been observed in the rate of photo-eviction. As discussed in section 5.2, Huntley *et al.* (1996) found that the Urbach rule (Urbach, 1953) could be used to describe the temperature and wavelength dependence of the detrapping (this is an empirically derived rule for the temperature dependence of band-to-band transitions in indirect gap materials). The function is given below:

$$I_0 = I_\infty \exp\left(-\frac{E^*}{kT}\right) \qquad (5.7)$$

where I_0 is the initial signal intensity, with I_∞, at $T = \infty$, and $E^* = \phi(E_0 - h\nu)$, where ϕ is a constant whose physical meaning is not fully understood (Huntley *et al.*, 1996; Kurik, 1971), E_0 is the gap and $h\nu$ is the photon energy. Huntley *et al.* (1996) calculated E^* for different photon energies and found it decreased as photon energy increased. Spooner (1994) used the term 'thermal assistance energy' to describe this lattice vibration energy coupling component. He replaced E^* by E^{th}, to represent the thermal component in the detrapping process, as illustrated Fig. 5.5.

A considerable literature exists on the theory of temperature and wavelength dependence of detrapping. Many studies, both theoretical and empirical, have been undertaken to examine how the electron-phonon coupling modifies the photoionization spectra of impurities in semiconductors (e.g. Noras, 1980; Stoneham, 1979). In the event of strong coupling the electronic state is more sensitive to lattice vibrations that may give rise to additional broadening. This can be expressed following the theory of Huang and Rhys (1950). Using this model the photoionization cross-section at given temperature, T, is:

$$\sigma_T(h\nu) = \frac{const}{h\nu} \sum_{n,\mathbf{k}} \left| \langle \psi | \exp(-i\mathbf{k}_\lambda . \mathbf{r}) \varepsilon_\lambda . \mathbf{p} | \phi_{n,\mathbf{k}} \rangle \right|^2 J_{n,\mathbf{k}} \qquad (5.8)$$

where $J_{n,\mathbf{k}}$ contains the information about the vibrational states. ψ is the impurity wavefunction, $\phi_{n,\mathbf{k}}$ is the band wavefunction associated with reduced wavevector $\mathbf{k}$ and band n. For the model used J is given by:

$$J_{n,\mathbf{k}} = (4\pi k_B TS\hbar\omega)^{-1/2} \exp\left(-\frac{[h\nu - (|E_{io}| + E_{n,\mathbf{k}})]^2}{4k_B TS\hbar\omega}\right) \qquad (5.9)$$

In these equations $h\nu$ is the photon energy and $\hbar\omega$ is the phonon energy, E_{io} is the optical ionization energy, E_i is the equilibrium binding energy measured from the bottom of the conduction band and S_C is a coupling coefficient (stronger coupling: larger S_C value). Equation 5.9 provides a quantitative meaning to the phonon broadening of the optical spectra as a function of temperature, or in terms of typical OSL measurements, the increase in decay rate. Note that at high temperatures equation 5.9 is dominated by the exponential term, giving a similar form to that previously fitted to data from quartz for the temperature dependence of optical eviction rate (Equation 5.7).

Jaros (1977) simplified the Huang and Rhys equation to the following:

$$\sigma_T(h\nu) \sim \frac{1}{h\nu} \int_0^\infty dE \rho(E) \left| \frac{(1\pm\eta)E^{\frac{1}{2}}}{\left|E_{i0}^T\right| + E} + \frac{(1\mp\eta)(E_F)^{\frac{1}{2}}}{\left|E_{i0}^T\right| - E - (E_g + E_P)/2} \right|^2 \exp-\left(\frac{\left(h\nu - \left[\left|E_{i0}^T\right| + E\right]\right)^2}{4k_B T d_{FC}} \right) \quad (5.10)$$

where E_g is the band gap, E_P the optical gap, E_F is the Fermi level energy, d_{FC} is the Frank-Condon effect parameter, $E_{i0}{}^T$ is the optical ionisation energy, $\rho(E)$ is the density of states, $\eta=\exp(-2E/E_P)$ and $E = h\nu - \left|Ei\right|$.

The temperature dependence of the photoionization spectrum for a simulated system using equation 5.10 is plotted in Fig. 5.6. The spectrum becomes broader as the thermal energy becomes larger, i.e. photoionization can occur with smaller $h\nu$ at higher temperatures.
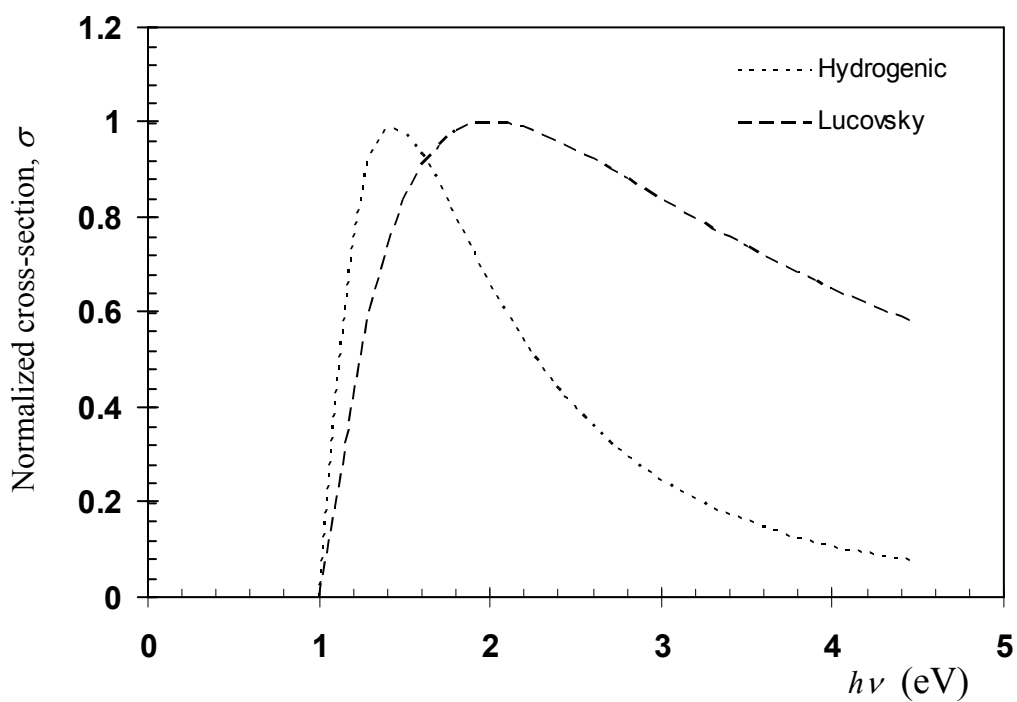
Fig. 5.4 Simulated, normalised photoionization cross-section, σ, as a function of normalised photon energy from the hydrogenic formula, Lucovsky formula (Lucovsky, 1965). See section 5.3.1.2 for details.
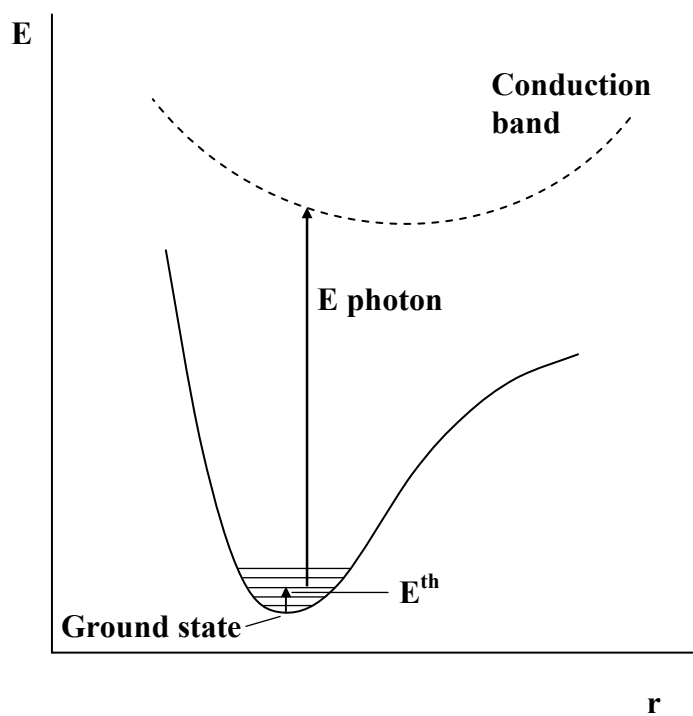
Fig. 5.5 Simplified configuration coordinate diagram of the photoionization process of quartz OSL. (Modified from Spooner, 1994)
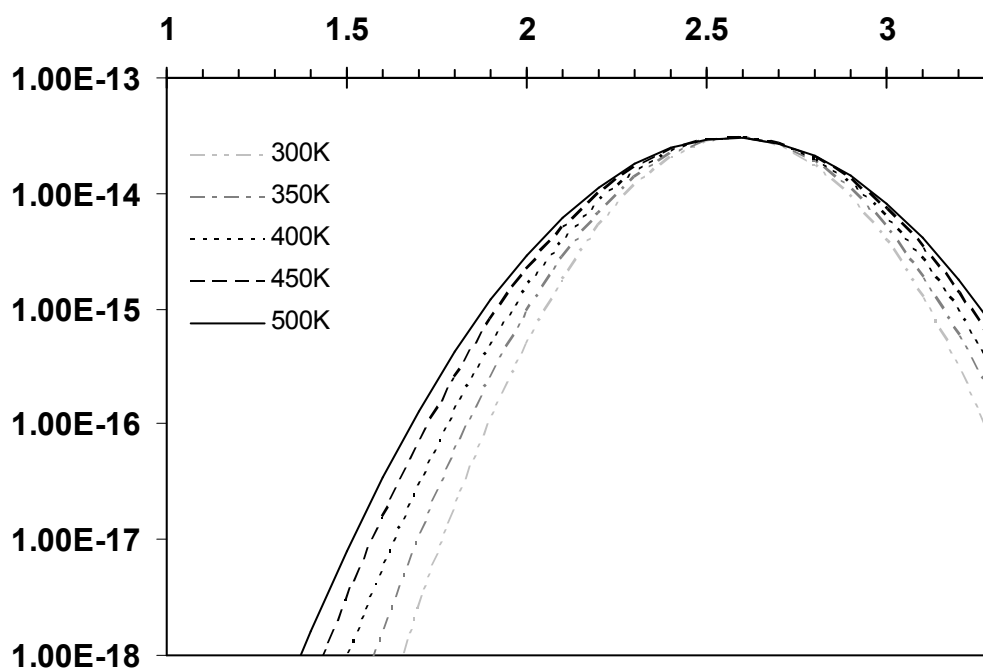
Fig. 5.6 Photoionization cross-section spectra simulated at various measurement temperatures using the Jaros (1977) equation 5.10.

5.3.1.3 Bleaching spectra of the fast and medium components: initial investigation

The simplest method of obtaining the photon-energy dependence of the detrapping rates of the OSL components is to stimulate aliquots with different optical stimulation energies while simultaneously recording the resulting luminescence. Unfortunately, sources of sufficient maximum intensity could not at the time be obtained to allow configuration of apparatus for simultaneous stimulation and OSL measurement. A more indirect approach to measurement was undertaken. Samples were bleached using an external bleaching unit with interchangeable LED clusters of a variety of wavelengths (photon-energies). The remnant OSL was subsequently measured in the Risø reader using 470nm stimulation. Light emitting diodes from UV to red wavelengths were available for bleaching. Details of each LED cluster used are given in Table 5.3. The sample and bleaching unit could be easily mounted on a heater plate to allow bleaching at raised temperatures. The 830nm IR laser-diode incorporated in several of the Risø readers (see section 2.4.1) was also used to extend the range of bleaching wavelengths available.

Even though the design of the present experiment is not ideal (i.e. indirect measurement) there are several advantages of this method of stimulation as opposed to direct OSL measurement at the different wavelengths. Firstly, fitting is possibly more reliable since the data are always collected from 470nm. Secondly, wavelengths within/near the UV emission band can be used without tackling issues concerning separation of excitation and emission light. Additionally, if two components decay at same rate at a particular wavelength (other than blue) then these would be observed as one component through direct measurement, but as two via an indirect method.

To obtain absolute data concerning the photo-ionisation cross-sections of the OSL components measurement of the power density at the sample for each of the photon-energy sources is needed. In the present case a Molectron PR200 pyroelectric radiometer was used. A quartz window was used for calibration and to provide a spectral range 230nm to 3.2μm with uniformity ±2% up to 200mW. The radiometer was placed in the position of the sample aliquot to estimate the light intensity of the LED arrays at the sample. The power density (in mWcm^{-2}), as measured by the radiometer, of each of the light sources is given in Table 5.3.

For initial investigations efforts were concentrated on the fast and medium component since, it might be argued, these are most relevant when considering issues of partial bleaching detection for optical dating. This enabled a shorter measurement sequence to be developed than for measurement of all the OSL components (which would be quite a feat, given the

methodology and number of different stimulation wavelengths used). In addition, the short OSL measurements required to observe the fast and medium allowed the use of mathematical conversion of CW OSL measurements to 'pseudo LM OSL' (see section 3.4 for detailed discussion of CW transformation) to take advantage of the greater signal stability achieved through constant intensity optical stimulation [this experiment was performed at a time when only a non-linearly ramping excitation unit was available in any of the Risø readers]. The good agreement between experimental LM OSL and converted pseudo-LM OSL observed in Fig 3.7 indicated that the transformation is a valid approximation.

The first experiment was to obtain the bleaching spectra of sample SL203 at ambient temperature (~20°C). Single aliquots were given 15Gy beta doses followed by heating to 260°C for 10s. The aliquots were then bleached at room temperature using the external LED unit described in the previous section. After a subsequent preheat the remaining OSL was measured with 470nm stimulation for 100s at 160°C in Risø reader 2 (a small amount of recuperation may have taken place during the second preheat, but it is not thought to have affected the results significantly). The cycle was repeated for various lengths of partial bleaching and different stimulation wavelengths. In between each cycle of partial bleaching the OSL was measured without bleaching to monitor sensitivity changes. The recorded OSL was converted into pseudo-LM OSL and fitted to the linear sum of first order peaks.

The converted LM OSL following bleaching at two of the wavelengths used is shown in Fig. 5.7 to illustrate the difference in the change of form of the LM OSL observed between partial bleaching with high energy and low energy optical stimulation. In Fig 5.7a the LM OSL following bleaching with UV (375nm) for various times is demonstrated. There is relatively little change in the form of the LM OSL following UV bleaching, i.e. no movement of peak position that would suggest preferential bleaching of the fast component. In contrast, bleaching with lower energy green light produces significant movement of the pseudo-LM OSL peak position. This indicates that, assuming the OSL from the fast and medium components is first order, the fast component is being depleted much more quickly by the optical stimulation than the medium component. Even without any more detailed analysis it is possible to conclude that there is a considerable difference in the response of the fast and medium components to stimulation with different optical energies. This is in complete agreement with earlier CW OSL results by Rhodes (1990) and Bailey et al. (1997).

Source colour	LED manufacturer	Peak wavelength (nm)	Incident intensity at sample position (mWcm^{-2})
UV	Nichia	375	0.20 ± 0.05
Violet-blue	RS Electronic	430	0.35 ± 0.1
Blue	Nichia, Risø reader	470	18 ± 0.5
Bluish-green	RS Electronic	500	1.40 ± 0.05
Green	RS Electronic	525	1.37 ± 0.05
Amber	RS Electronic	590	0.56 ± 0.05
Red	RS Electronic	640	Not measured

Table 5.3 Details of the sources used for bleaching. Except for the blue light source the bleaching sources were part of an external unit containing interchangeable LED arrays.
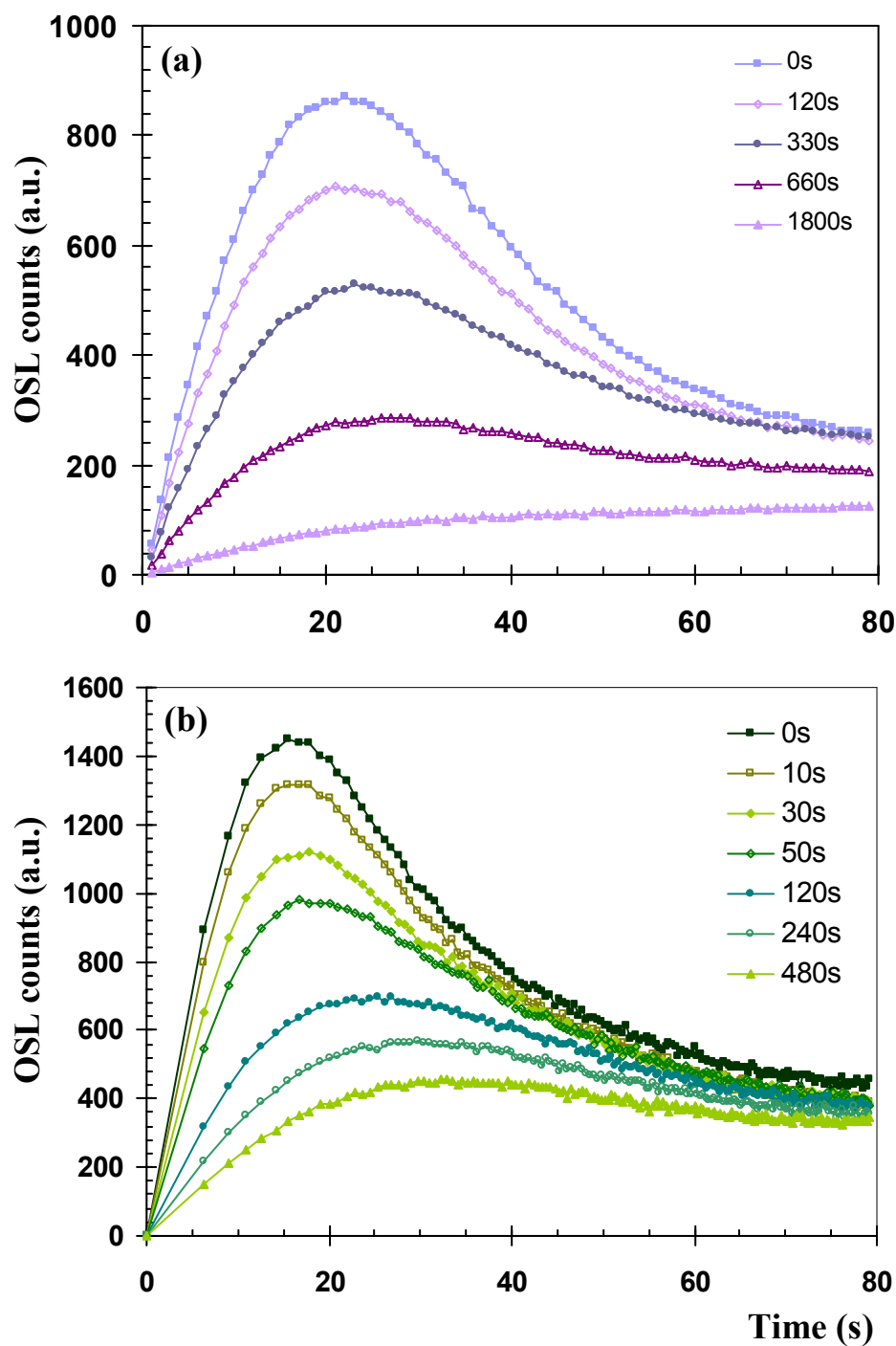
Fig. 5.7 Blue light stimulated LM OSL following various lengths of bleaching at room temperature with (a) 375nm UV (b) 525nm green light. See main text, section 5.3.1.3 for further details. Plot (a) was recorded using experimental LM OSL on R4b, plot (b) was recorded using constant intensity and mathematically transformed to pseudo-LM OSL on R2.

The data collected following bleaching with wavelengths from 430 to 590nm at room temperature were fitted and the resultant decays of the fast and medium component at each wavelength are displayed in Fig 5.8. The fitted magnitudes, n_0, for each component are plotted against the total number of incident photons (from the stimulation source) during partial bleaching. As found by previous authors (e.g. Spooner, 1994; Duller and Bøtter-Jensen, 1996) the decays rates increase as the stimulation wavelength decreases. This was observed in both the fast and medium components. Each decay was fitted to a single exponential function (of the form: $I(t) = I_0 \exp(-\sigma Pt)$ where P is the photon flux, and Pt is the total number of incident photons) to obtain a decay constant (i.e. photo-ionization cross-section) for each component at each wavelength. From this data it was possible to plot a bleaching spectrum in terms of photo-ionization cross-section, σ, vs. photon energy, $h\nu$. The spectra for the fast and medium components are plotted in Fig. 5.9. Using the experimental procedure it was possible to observe the form of the photoionization cross-section spectra at higher energies than possible through direct measurement.

The form of the σ-response to photon energy is similar to spectra found previously (e.g. Duller and Bøtter-Jensen, 1996). Not previously observed, however, is the difference in the responses of the fast and medium OSL components can be clearly seen in the lower figure. The ratio $\sigma_{fast}/\sigma_{medium}$ varies from 30.6 at 590nm to 3.7 at 430nm, i.e. there is a significant change in the form of the OSL with stimulation wavelength. At 375nm the ratio of the fast and medium component σ was only 1.4 ± 0.3. The similarity of the detrapping rates of the fast and medium components when stimulated with UV has implications for the identification of incomplete resetting using signal analysis methods. This is discussed further in section 7.2.

Attempts were made to fit the observed σ-spectra to an appropriate expression, knowing that the fast and medium are relatively deep trapping levels. The Lucovsky solution (Equation 5.3) for the case of a deep centre was used initially. This function fits the data for relatively high photon energies but fails to describe the data at low energy photon stimulation. As discussed in the previous section, the Lucovsky expression is not appropriate for deep levels where coupling to the lattice is strong, producing a broader spectrum. Noting this, the data were fitted to the Jaros expression (Equation 5.10), for strong coupling (Fig. 5.9 –lines 'a' and 'b'), which appears to be more appropriate for the quartz fast and medium components. However, the results presented are preliminary and similar measurements at a variety of temperatures are required to more accurately determine the nature of the photoeviction mechanisms. The values for the fitted parameters are given in Fig. 5.9.
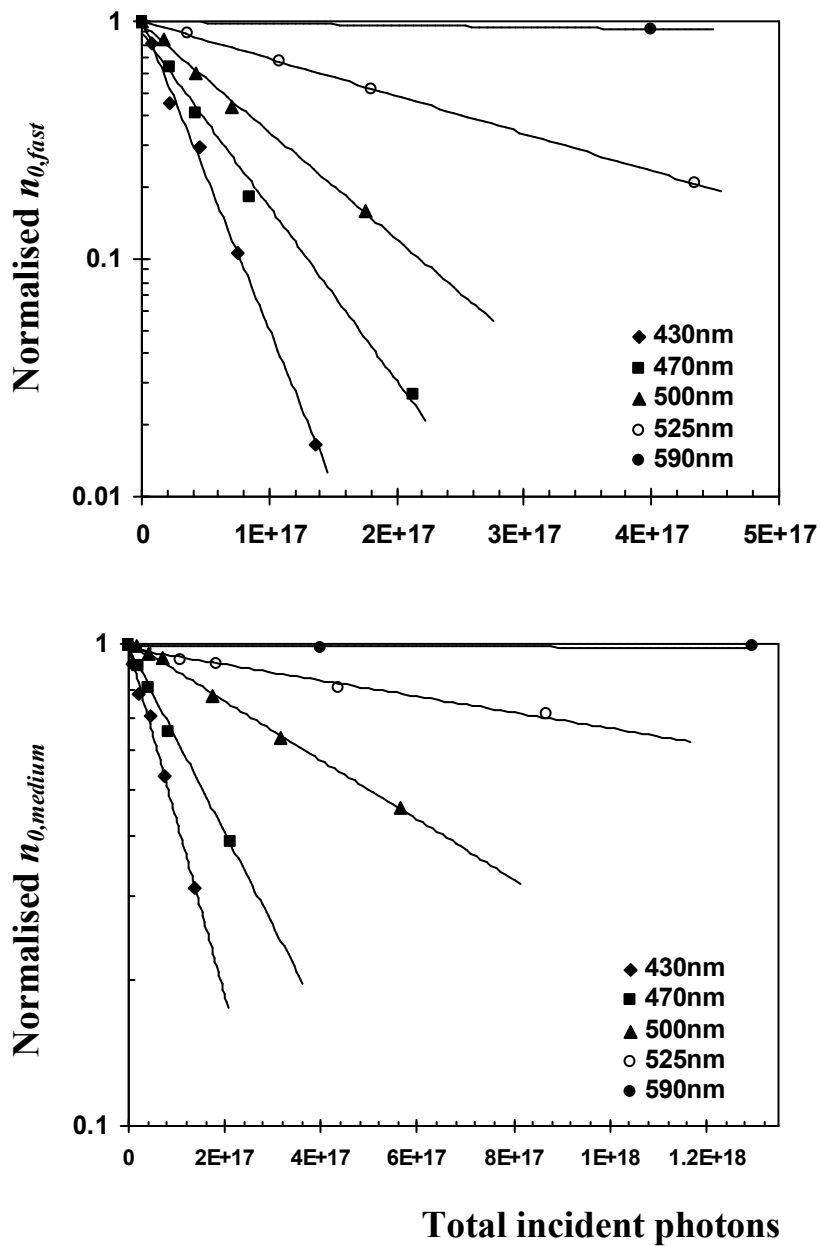
Fig. 5.8 Decays for the fast and medium components of quartz sample SL203 for various stimulation wavelengths (at ~20°C), fitted to exponential functions. For each point, $n_{0,fast}$ and $n_{0,medium}$ (proportional to the actual initial trapped charge concentration) were found from fitting the blue light pseudo-LM OSL after partial bleaching. See text for details, section 5.3.1.3.
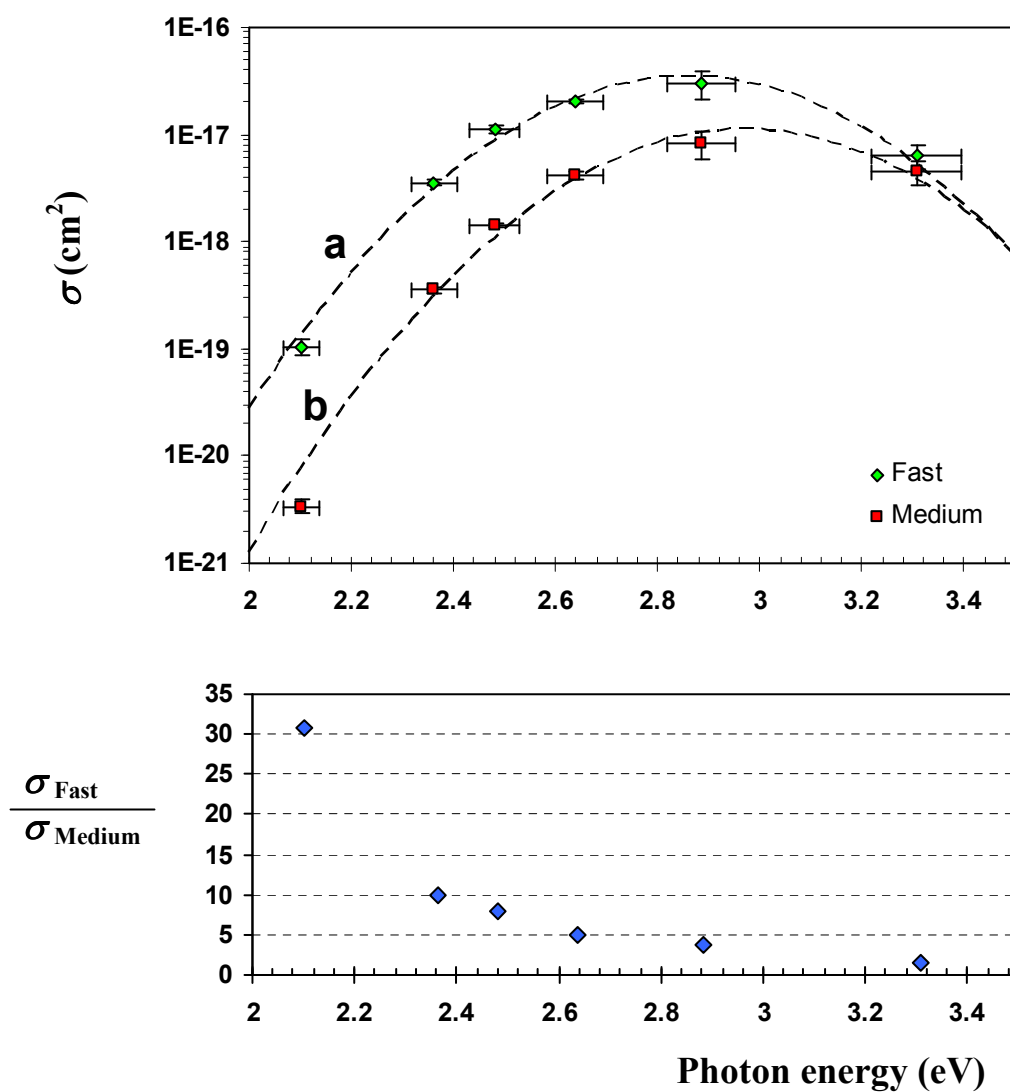
Fig 5.9 Calculated σ vs. stimulation photon energy for the fast and medium components of quartz, at room temperature. See section 5.3.1.3 for details of the fits to the data. A plot of the relative sizes of σ vs. photon energy is given (lower).

Fitted values: E_g=9.0eV, d_{FC}=1.0, E_F=4.5eV, E_0(fast)=2.88eV, E_0(medium)=2.99, E_P(fast)=10, E_p(medium)=20.

Using the calculated photoionization cross-sections for the fast and medium components at room temperature simulated LM OSL curves were created to illustrate the change in the form of the OSL with stimulation wavelength more clearly. The simulated LM OSL is presented in Fig. 5.10a. The photoionization cross-section of the fast component has been normalised to unity. At 375nm there is very little difference in the peak positions of the fast and medium components and therefore only a single peak is visible. At wavelengths of ~550nm or more the fast and medium components are seen as separate LM OSL peaks. The simulation demonstrates the importance of the selection of the most appropriate wavelengths for excitation.

Preliminary measurements have been performed to directly measure experimental LM OSL at different wavelengths. Measurements were made using an Argon-ion laser, which has several possible laser lines at wavelengths ranging from 457 to 568nm and was arranged to perform linearly modulated excitation. Aliquots of sample EJR01an were given 20Gy doses and preheated to 260°C prior to LM OSL measurement at room temperature. The LM OSL at 457, 478, 488nm are presented in Fig. 5.10b. Over this range of wavelengths the relative σ of the fast and medium components is expected to change by less than a factor of 2, given the bleaching spectra results in Fig. 5.9. Correspondingly, in the direct measurements (Fig. 5.10b) very little change in the form of peak 1 (composed mainly of the fast and medium components) is observed, i.e. there is very little change in the relative σ of the fast and medium components. However, the relative change in peak position of component S2 (i.e. LM OSL peak 2) is much more dramatic. This would suggest that component S2 is closer to the leading edge of its σ-spectrum at these wavelengths, resulting in a relatively larger change in σ with wavelength than the fast and medium components (cf. Fig. 5.9).

The data in Fig. 5.10b have not been fitted to separate the contributions from the signal components. Measurements were made at room temperature. Consequently, effects of retrapping into the 110°C TL peak would affect the accuracy of the results. Further measurements using a wider range of wavelengths at raised temperature are planned but were out of the scope of the current study.
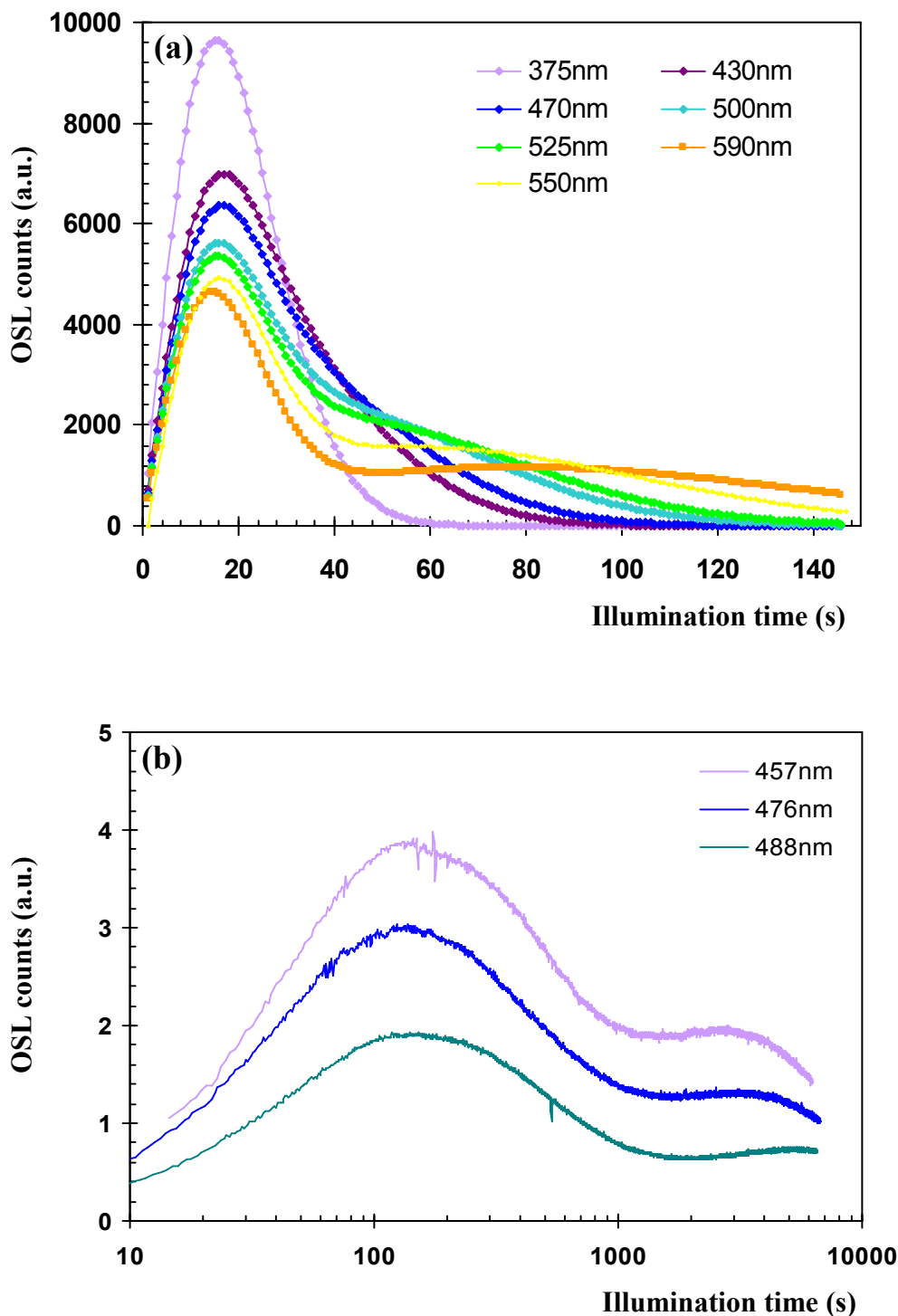
Fig. 5.10 (a) simulated LM OSL from the fast and medium components (using first-order solutions) at various stimulation wavelengths. The fast component photoionization cross-section has been normalised to unity. Values for the photoionization cross-sections taken from the measured room temperature bleaching spectra (see Fig. 5.9). (b) Measured LM OSL at various stimulation wavelengths at room temperature on sample EJR01an following 20Gy and preheating to 260°C. The positions of the first LM OSL peak have been normalised.

5.3.1.4 Isolating OSL components via selected photon energy stimulation

The first account of long wavelengths inducing luminescence in quartz was by Godfrey-Smith *et al.* (1988). For many studies including this one, the presence of IR stimulated luminescence at ambient temperatures has been attributed to feldspar contamination alone. However, Spooner (1994) found, during spectral measurements, that IR stimulation produced measurable luminescence in quartz at temperatures greater than 70°C. Bailey (1998a) reported requiring temperatures of at least 200°C when stimulating with low photon energies (880nm) to observe significant OSL above background levels. In that study, the luminescence from IR stimulation was found to correspond directly to the post–IR OSL signal measured in broadband (420-560nm) light, indicating that the IRSL and OSL signals are probably from the same traps. The initial IRSL decay and the post-IR OSL fitted well to single exponentials with indistinguishable decay rates.

Here a similar experiment was performed, using LM-OSL, to look at the component-resolved decay rates of quartz IRSL at raised temperature. Sample SL203 was again used for the initial investigation. A measurement temperature of 160°C was found to be sufficient to observe significant amounts of luminescence under 830nm illumination while low enough not to sensitise the sample during measurement. The procedure used was the same as described in the section 5.3.1.3. Various durations of infrared illumination were performed before measurement of the remaining blue light stimulated pseudo-LM OSL. Measurements of blue stimulated LM OSL without prior IR bleaching were performed in between to check and correct for sensitivity change throughout the measurement sequence.

Fig. 5.11a shows examples of the LM-OSL curves for blue-light stimulated OSL following various lengths of IR bleaching. Curve fitting was used to deconvolve the fast and medium components. The trapped concentration parameters obtained (n_0) were used to create the IR stimulated decay curves for the fast and medium OSL components (Fig. 5.11b). Interestingly, there appeared to be no significant decay from the medium component, while the fast component is depleted to negligible levels by 7000-8000s IR (830nm 0.4W) at 160°C. This is also nicely demonstrated in Figure 5.11a by the near-complete overlap of the 6000s and 8000s curves, indicating negligible further decay is occurring by increasing stimulation time. The fast component decay from the post-IR OSL fitted well to a single exponential (Fig. 5.12), and gave a very similar decay rate to the fitted IRSL (ratio ~0.96). This suggests that they are from the same OSL traps, supporting previous findings (Bailey, 1998a).

Similar experiments were undertaken on two further samples to substantiate the results. Unfortunately, measurement time was limited so it was not possible to obtain the whole

decay of the fast component using the method described above. Instead infrared bleaching durations of 0, 6000 and 8000s at 160°C were used only. Following the results for sample SL203, the LM OSL following the 6000s and 8000s illuminations would be expected to overlap completely, as the fast component should be fully depleted and the medium component should not decay noticeably. Another LM OSL measurement following holding the samples at 160°C for 8000s was used to compare with the 0s IR bleach measurement to quantify the contribution of thermal erosion (if any) during the long infrared illuminations. [Note that experimental linear modulation measurements were used in this part of the experiment]

The LM OSL results for samples CdT9 and TQN are presented in Fig. 5.11c and 5.11d respectively. Equivalent results were obtained for the two samples. Complete overlap of the LM OSL following no IR illumination and LM OSL after 8000s at 160°C was observed, indicating that there was negligible depletion due to purely thermal eviction in the infrared bleached measurements. The LM OSL following 6000s and 8000s IR also showed complete overlap. Following the results for sample SL203 this suggests that the fast component had been fully eroded while no noticeable reduction in the medium component had occurred. The LM OSL curves following 8000s IR were fitted and produced almost identical photoionization cross-sections for the medium component for all the samples (also derived from looking at the LM OSL peak positions, which occur at ~32s in both samples). The medium component of sample TQN appears to be much smaller, relative to the fast component, than either SL203 or CdT9. Its size may account for some of the ambiguity observed from fitting and the noise in the resulting fitted data for previous experiments (e.g. section 4.4.2, Fig. 4.21).

It is clear from these results that the fast component bleaches under IR stimulation. It is hypothesized that IR stimulation at 160°C is below threshold energy for the medium component, thereby allowing total depletion of the fast component signal with no measurable reduction in the medium. The results provide further corroborating evidence for the independent existence of the medium component (visible as the LM OSL peak in Fig. 5.11a, after 6000s and 8000s IR bleaching), and aid the determination of its peak position. Additionally, it offers a method of separating the fast and medium components for further research. Optical separation of the components is preferable to using complicated and possibly lengthy deconvolution procedures. The method of preferentially removing the fast component using infrared stimulation has been used to more clearly observe the medium

component in several experiments described elsewhere, and has proved more useful than curve fitting in several cases. For example, the errors from curve fitting to obtain the medium component pulse annealing curve of sample SL203 produced an ambiguous shape (Fig. 4.27) whereas repeating the experiment using IR stimulation to remove the fast component before measurement resulted in a much clearer pulse annealing form (Fig. 4.28).

For convenience, so that sequences could be automated in the Risø reader, IR stimulation (830nm) was used to separate the fast and medium OSL components. However, bleaching of single components may be possible using shorter wavelengths, provided that there is sufficient difference in σ. It is postulated that this method could be extended to separate the other components of quartz by finding, experimentally, the optimal wavelengths/temperatures to bleach successive components with negligible reduction of the next. Empirical measurements using 640nm at 160°C resulted in limited decay in the medium even when the fast component was full depleted. A speculative combination could be 640-850nm (fast), ~580nm (medium), ~540nm (S1), and ~500nm (S2). It is believed that a 'stepped wavelength' approach, where effectively a single component is stimulated during any measurement, could be a potentially useful method of measurement. There was, however, insufficient time to develop and experimentally investigate this idea at the time of writing.
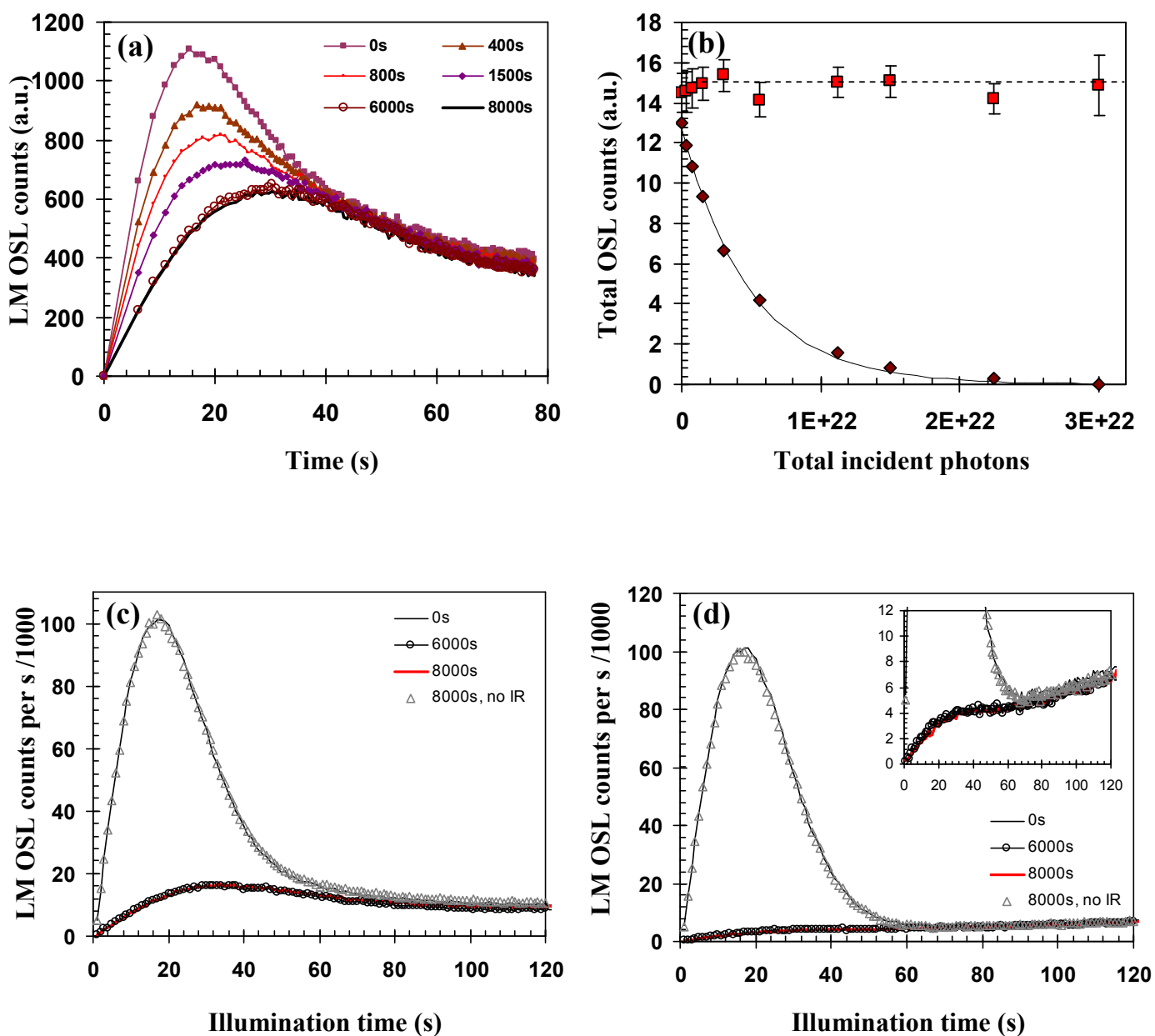
Fig. 5.11 (a) Pseudo-LM OSL curves stimulated at 470nm, 160°C after various durations of IR stimulation at 160°C on sample SL203. (b) The curves shown in (a) were fitted to separate the contributions from the fast and medium components. The fitted magnitudes, n_0, for each are plotted vs. total incident photons. (c) LM OSL curves stimulated at 470nm, 160°C after various durations of IR and raised temperature holds for sample CdT9. The same data is shown for sample TQN in (d), where the inset shows the data following IR in more detail.
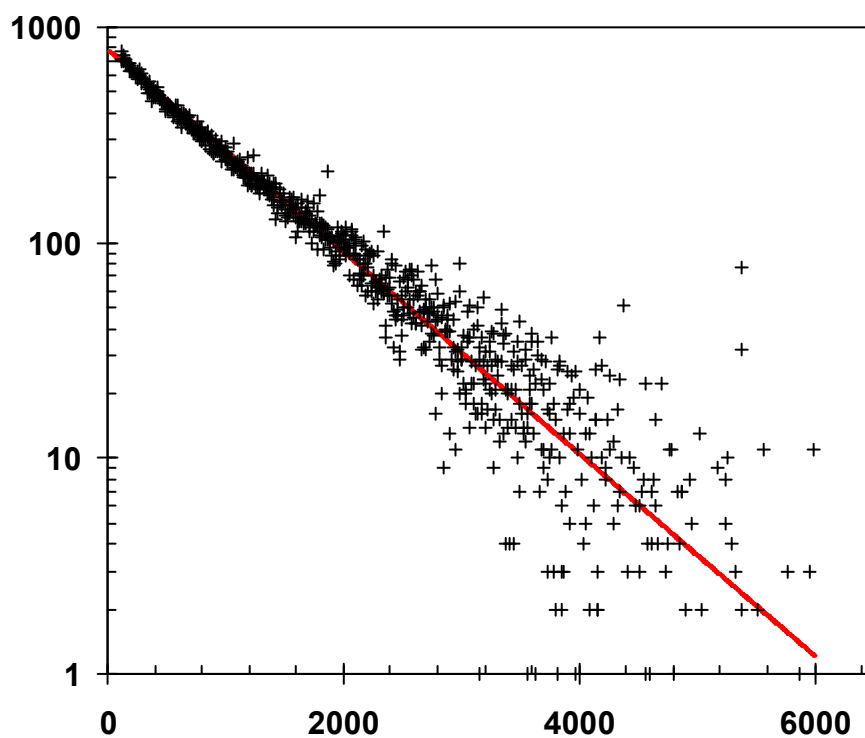
Fig. 5.12 IRSL decay of sample SL203 given 20Gy dose, preheated to 260°C for 10s and IR stimulated at 160°C, 830nm for 6000s. The data have been fitted to an exponential function (red line).

5.3.2 Bleaching quartz OSL components in the natural environment

The bleaching spectra obtained in section 5.3.1 are relevant when considering resetting of samples in the natural environment. The sun's spectrum extends from low energy infrared to ultraviolet. Fig. 5.13 shows the spectrum of sunlight at sea level (with the sun 48° below zenith, modified from the Oriel solar simulator handbook). The maximum intensity is in the visible region 450-600nm, but considering the decrease in efficiency of bleaching as stimulating wavelength increases, the part of the solar spectrum most relevant to resetting is from ultraviolet to green (Aitken, 1998).

The intensity and energy of photons contributing to the bleaching of sediments during transport depend on the depositional environment. For example, in fluvial transport systems there is considerable filtering of the high-energy part of the solar spectrum, more efficient at bleaching, by water (Berger, 1990). Also, when there is significant cloud cover attenuation occurs, which is stronger in the visible region, therefore daylight, rather than unfiltered sunlight is comparatively richer in UV (Aitken, 1998). The likelihood of full resetting depends both on the depositional environment and the duration of exposure to light in-transit and residence on the land surface (Stokes, 1992). (The form of the energy dependent optical eviction rate for the fast and medium OSL components was determined in section 5.3.1.)

The aim of this section is to assess the bleaching rate of each of the quartz OSL components when exposed to natural sunlight. Once the duration of exposure to sunlight required to reset the OSL to negligible levels is quantified this information can be extrapolated to assessing the likelihood of full resetting for each of the components in natural depositional environments. For this experiment an Oriel solar simulator was used rather than natural sunlight to produce a consistent spectrum throughout the measurement process. Only bleaching by the full solar spectrum, i.e. simulating bleaching of aeolian sediments, was considered. Examination of resetting in other depositional environments was undertaken through a study of the residual signals in samples of a variety of depositional types, discussed in section 7.2.

Previous values for quartz range from 2s, for the reduction of OSL by a factor of 10 (Godfrey-Smith *et al.,* 1988: sunlight overcast), to 130s for the same factor depletion (Rhodes, 1990: daylight). No component-resolved measurements of the bleaching rate under sunlight have been previously undertaken.
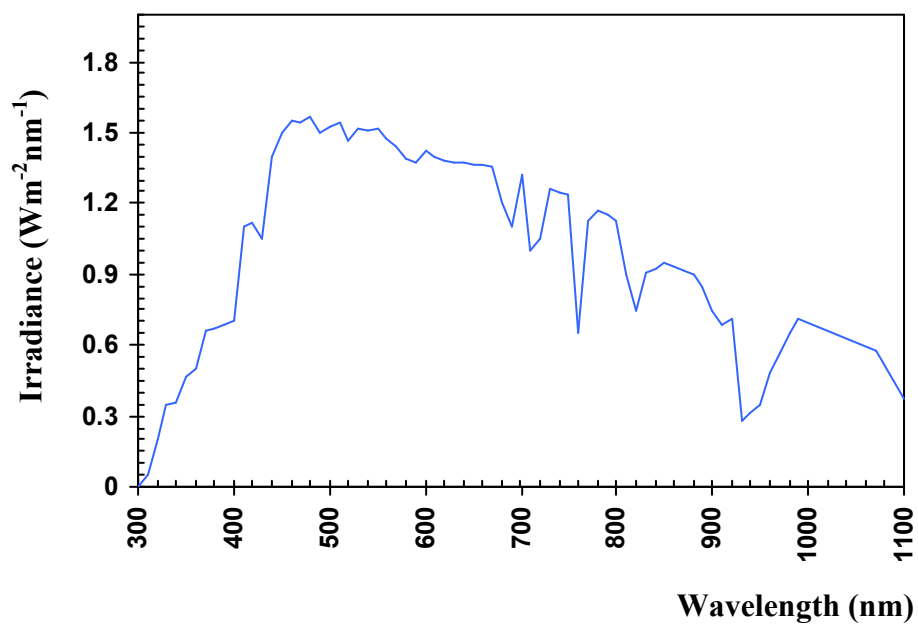
Fig. 5.13 The global solar spectrum for sunlight at 48° below zenith at sea-level (modified from the Oriel solar simulator handbook).

A single aliquot approach was used on sample CdT9. Aliquots were first bleached at high temperature with 470nm light to zero the natural signal (1500s at 300°C). Subsequent beta irradiation of 20Gy was followed by a preheat of 280°C for 10s. The aliquots were then exposed to solar simulator light for different durations at room temperature (exposure lengths used: 0, 10, 30, 100, 300, 1000, 3000, 10000, 52140, 239100s). A further preheat to 280°C was used to minimize possible phosphorescence during 160°C LM OSL from mid-range TL traps and also from the 110°C peak. The LM OSL from the single aliquots was measured for 3600s at 160°C. Measurements of sensitivity were made using the LM OSL following a 10Gy standard test dose and preheat to 260°C for 10s. In between each LM OSL measurement a full power 470nm CW OSL for 6000s at 180°C was used to completely zero the OSL signal.

An example of the raw LM OSL from sample CdT9 is shown in Fig. 5.14. Both the post-bleach LM OSL and test dose LM OSL are plotted. The fastest decaying components, when stimulated in 470nm, also deplete fastest under the solar simulator. There is, however, a measurable signal with peak position, t_{peak}, around 100s (mainly from the medium component) even following the longest solar bleach. This has been attributed to recuperation, which as found from experiments described in section 4.5 seems to occur specifically in the medium component. A proportion of charge detrapped during stimulation at room temperature becomes trapped in lower temperature but more optically stable traps. During preheating this photo-transferred population is evicted from the low temperature traps and some retrap in the OSL traps. Obtaining reasonable estimates for the bleaching rate of the component(s) affected by the recuperation in this sample is consequently more difficult, but also more realistic because bleaching would take place at <50°C in nature. Therefore, the 'effective' bleaching rate is that which includes recuperation.

The test dose LM OSL shows little change in sensitivity throughout the measurement sequence. However, all the LM OSL data were fitted to obtain sensitivity corrected magnitudes, n_0, after every solar bleaching and ultimately derive the optical detrapping rate of each component when exposed to the full solar spectrum at ambient temperature.
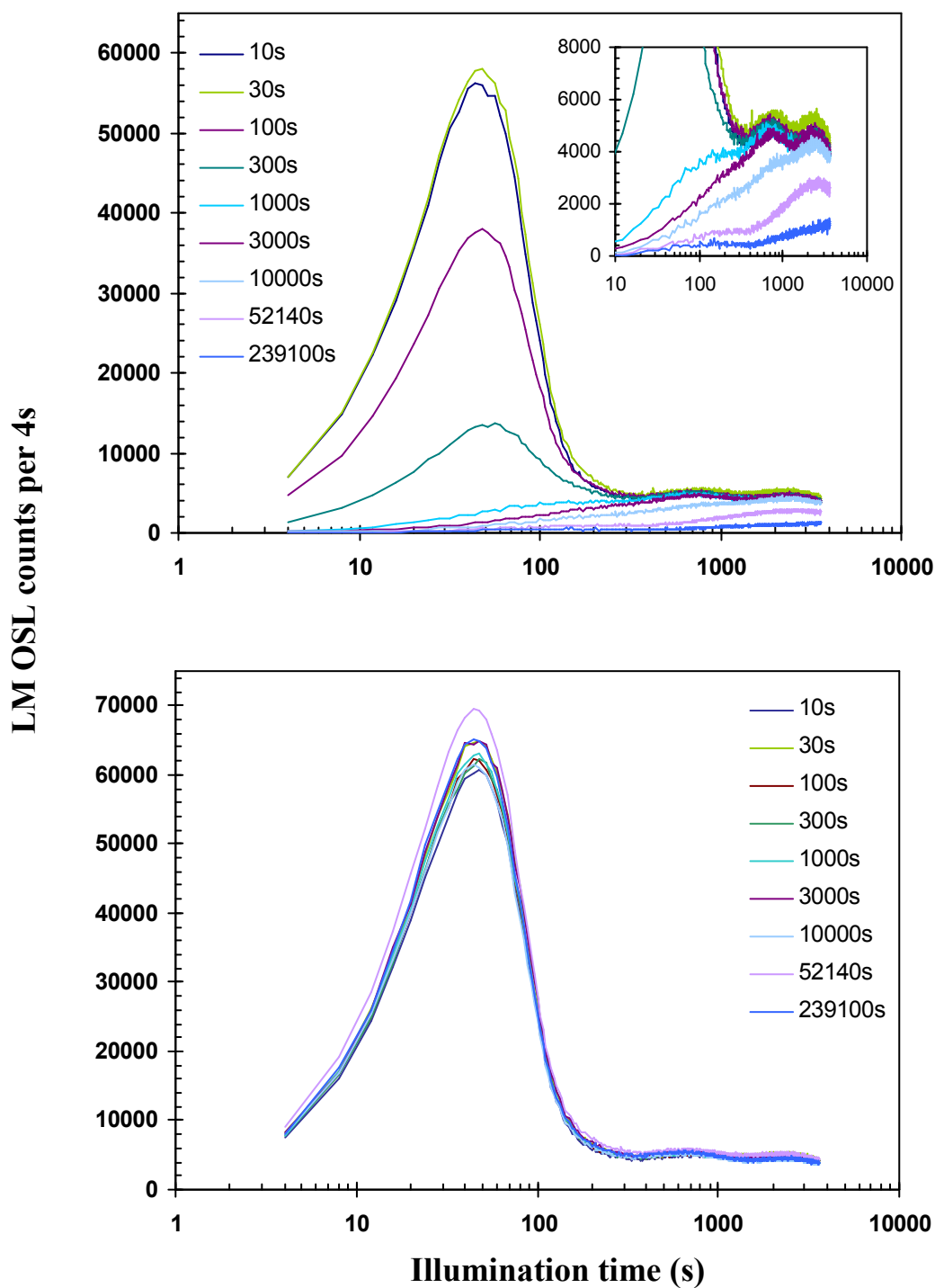
Fig. 5.14 (a) Raw LM OSL from sample CdT9 following 20Gy beta dose, preheating to 260°C and various durations of exposure to the solar simulator spectrum at room temperature. (b) LM OSL measurements following a test dose of 10Gy after each solar bleaching measurement. See section 5.3.2 for further details.

Plots of the component-resolved decay rates for sample CdT9, obtained through deconvolution of the LM OSL in Fig. 5.14, are displayed in Fig. 5.15. The data from each component were fitted to first order (i.e. exponential) functions to estimate the decay constants. A table of the calculated decay constants is also given in Fig. 5.15. Component S2 was fitted to both first and general order decay expressions (see Fig. 5.15). The spread of solar exposure durations resulted in only three reliable points in the decay to fit to the S2 decay. Therefore, it is uncertain whether the slightly non-exponential form of the decay observed was due to non-first order decay or noise from the fitting process. The decay constant for S2 given in the table is the non-first order value.

Using the solar simulator the length of exposure to bleach the fast component by a factor of 10 is ~380s. This is longer than observed by previous authors (for integrated OSL equivalent) and results from the lower intensity of the solar simulator in comparison to natural sunlight. The medium component incurred significant recuperation and therefore only the initial part of decay could be fitted to an exponential as after the longer bleaches a large proportion of the measured LM OSL is recuperation (although the bleachability of the 110°C TL peak means that the recuperation does not follow such a simple pattern exactly). The decay constant obtained gives only a rough value for the component. The ratio of the fast to medium component decay rates was calculated to be ~3.2. This relative value is more important than the actual decay constant with respect to assessing how feasible it would be to detect partial bleaching by sunlight (aeolian samples) using signal analysis techniques (described in more detail in section 7.2). Therefore a shorter experiment focussing solely on the fast and medium components was performed on another sample not suffering from recuperation to such a degree.

Using sample SL203 the same procedure was undertaken as in section 5.3.1.3 to obtain photoionization cross-section spectra. Raw pseudo-LM OSL following solar simulator illuminations of various lengths are shown in Fig. 5.16a. The LM OSL was deconvolved to enable OSL decay curves to be obtained for the fast and medium component (using n_0 parameters). The decays are shown in Fig. 5.16b. They have in turn been well-approximated by single exponential expressions. The ratio of the fast to medium decay constants for this sample is 2.9, as given in the figure. The value is marginally smaller than that obtained for sample CdT9. The small difference is assumed to arise from the recuperation observed in sample CdT9 slowing the apparent decay of the medium component, increasing the difference between the fast and medium decay rates.

All the components have been shown to be bleachable under the solar spectrum at ambient temperatures. If the intensity of the solar simulator is believed to correctly represent that of natural sunlight then the fast component would bleach by a factor of 10 in 377s, while for slow component S2 it would take 3.4 days to achieve the same level of depletion. It is speculated that the slow component S3 would take at least a week to bleach to the same level. For samples from an aeolian environment that are exposed to the full sunlight spectrum for lengthy durations of the order of days or weeks it is likely that all the OSL components will be fully zeroed prior to deposition.

Data from section 5.3.1.3 demonstrated that using 375nm UV light the difference between fast and medium component photoionization cross-sections is slight (ratio of 1.4). Using the solar simulator on two different samples the ratio of $\sigma_{fast}/\sigma_{medium}$ was found to be ~ 3 at the same temperature. This suggests that slightly longer wavelengths have a larger contribution to the effective bleaching under the solar simulator than 375nm. The ratio under the solar spectrum also implies that using signal analysis methods of detecting partial bleaching are not ruled out completely for aeolian sediments (the ratio $\sigma_{fast}/\sigma_{medium}$ must be significantly >1, so that the components have considerably different detrapping rates). However, under daylight rather than sunlight, that is when cloud cover obscures the sun, the attenuation of shorter wavelengths is less than longer wavelengths and so daylight is relatively richer in UV wavelengths. Under water the shorter wavelengths are preferentially filtered; thus the blue/green part of the spectrum becomes more important (Berger, 1990). The difference in detrapping rates of the fast and medium components is significantly different to potentially create signatures in partially bleached sediments that may be found using signal analysis techniques; ratio of $\sigma_{fast}/\sigma_{medium}$ ~ 8 at 500nm. Conveniently the nature of sediment transport via underwater processes makes the probability of partial resetting more likely in these environments.
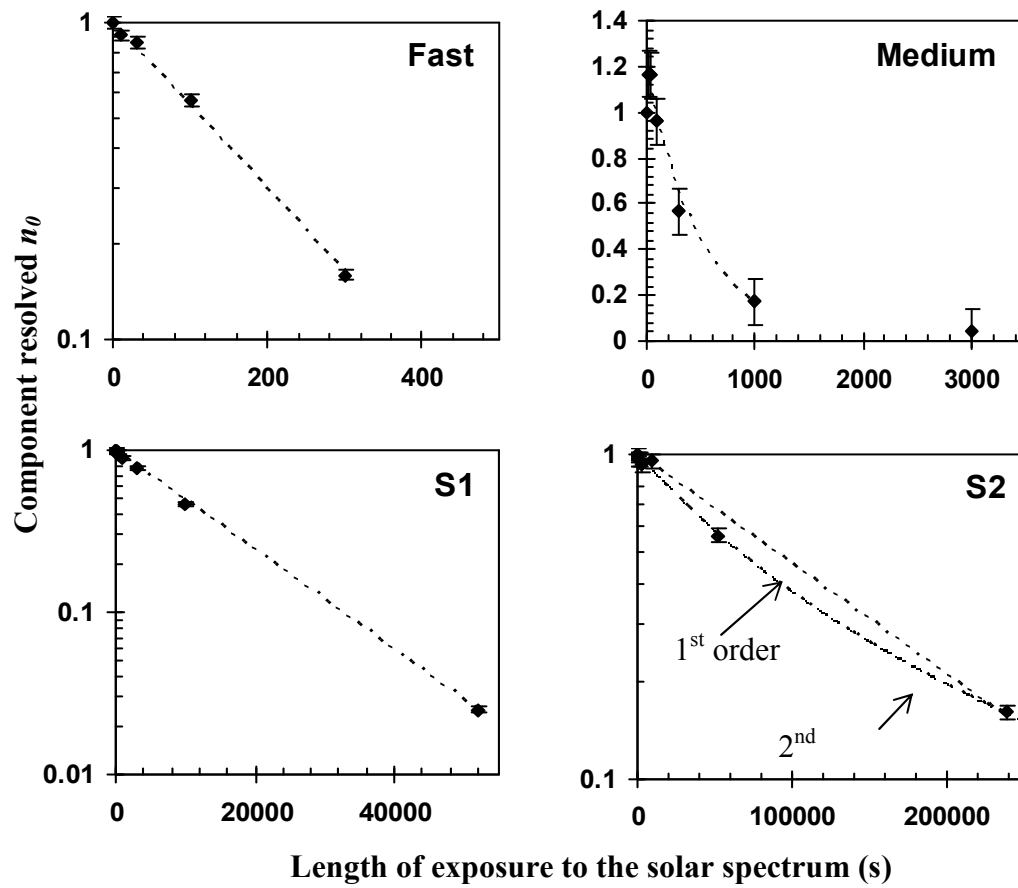
Fig. 5.15 Component-resolved plots of magnitude of each component stimulated at 470nm, 160°C versus prior length of exposure under the solar simulator at room temperature on sample CdT9. All decays have been fitted to single, first-order exponentials. S2 has also been fitted to a second-order expression. The decay constants calculated from the fits are given in the table.
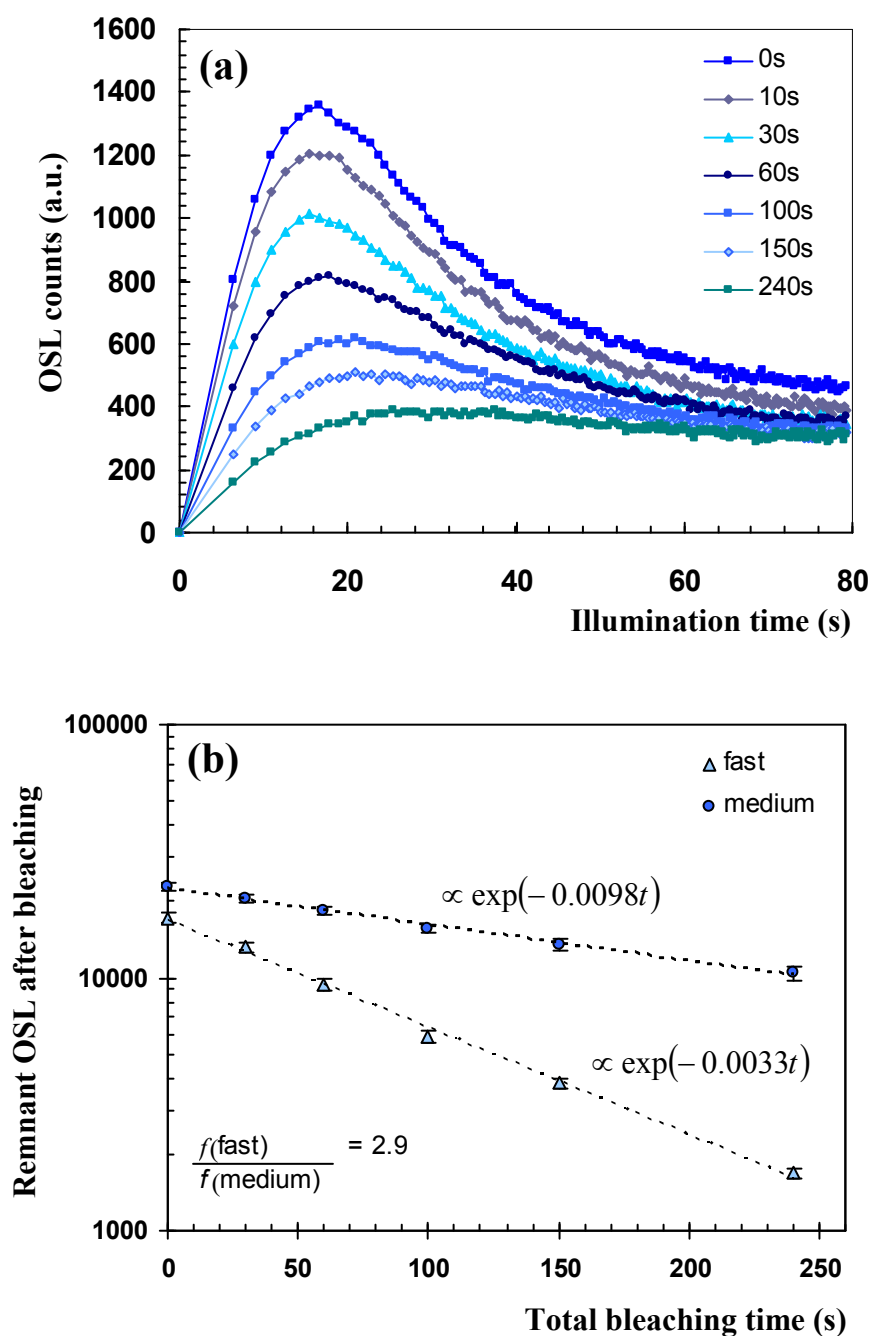
Fig. 5.16 (a) Pseudo-LM OSL stimulated at 470nm, 160°C following 20Gy dose, preheating to 260°C and various durations of solar simulator exposure at room temperature. (b) The LM OSL curves in (a) were fitted to separate the contributions from the fast and medium components, which are plotted versus bleaching time under the solar simulator. The data have been fitted to decaying exponentials. The ratio of the decay rates is given in the legend. See section 5.3.2 for further details.

5.3.3 Dependence of photon flux on eviction

One of the basic assumptions in the analysis of LM OSL using the equations derived in section 3.2.2 is that the detrapping probability is proportional to the stimulation light intensity, i.e. charge eviction involves a transition due to single-photon absorption. For the initial portion of the quartz OSL the dependence on stimulation power has been investigated by e.g. Spooner (1994; 514nm, 0.28 – 238mWcm^{-2}) and Bulur *et al.* (2001b; 0 – 25mWcm^{-2}) and a linear response observed. Bailey (2000a) looked at the dependence of quartz OSL following 500°C preheat and observed a similar linear dependence.

It was deemed essential to qualify that there is a linear dependence for all of the OSL components since the outcome would affect the form of the LM OSL, the results of curve deconvolution and ultimately affect the interpretation of the data. An example to illustrate this point comes from Bulur *et al.* (2001b) who measured the LM OSL from a sample of NaCl. The resultant LM OSL comprised a single observable peak but could only be well-fitted as the sum of two first-order components. However, the detrapping probability of this sample did not display a linear relationship with stimulation intensity but followed a saturating exponential form. Through incorporating this into a modified analytical solution for LM OSL the empirical data was found by Bulur *et al.* (2001b) to fit to a single first order component.

A simple experiment was performed to assess the linearity of the response to stimulation intensity from all the OSL components. Since by their very nature it would be impossible to use LM OSL measurements to obtain component-resolved data for this experiment, the response using CW OSL short-shines was recorded instead after partial LM OSL measurements to various intensities in order to get the main contributions to the OSL from the different components. Sample SL203 was used that was given a 20Gy dose and preheated to 260°C. Initial LM OSL measurements were made at 470nm and 160°C for:

0s (so that subsequent CW OSL originates primarily from the fast component)
0-5% in 200s (subsequent CW OSL mainly medium component)
0-21% in 800s (mainly component S1)
0 – 53% in 2000s (mainly S2)
0-95% in 3600s (S2 and S3)

Following each different LM OSL bleaching short-shine CW OSL measurements were made at 160°C at stimulation intensities of 0, 5, 10, 20, 40, 60, and 90% of full power (36mWcm$^-$^{2}). Short-shine measurements of 0.1s after 0s and 200s LM OSL were used to obtain a statistically significant number of counts with negligible depletion of the OSL with each measurement. Following the longer bleaches where only the slow components should have remained (800s, 2000s and 3600s) a longer short-shine measurement was required to measure sufficient counts. In these cases a 1s measurement was recorded at each stimulation intensity.

The results from sample SL203 are presented in Fig. 5.17. A linear response was observed following all the LM OSL bleaches. This can be interpreted as evidence that all of the OSL components display a linear response to stimulation intensity, i.e. the mechanism for photo-eviction is most likely single-photon absorption for each component at least up to 36mWcm$^-$^{2}. This suggests that the equations derived in section 3.2.2 used to describe LM OSL form assuming single-photon dependences are appropriate. It is similarly implied by the observation that the experimental LM OSL and mathematically transformed, pseudo-LM OSL (assuming linear dependence on intensity) agree, see section 3.4.
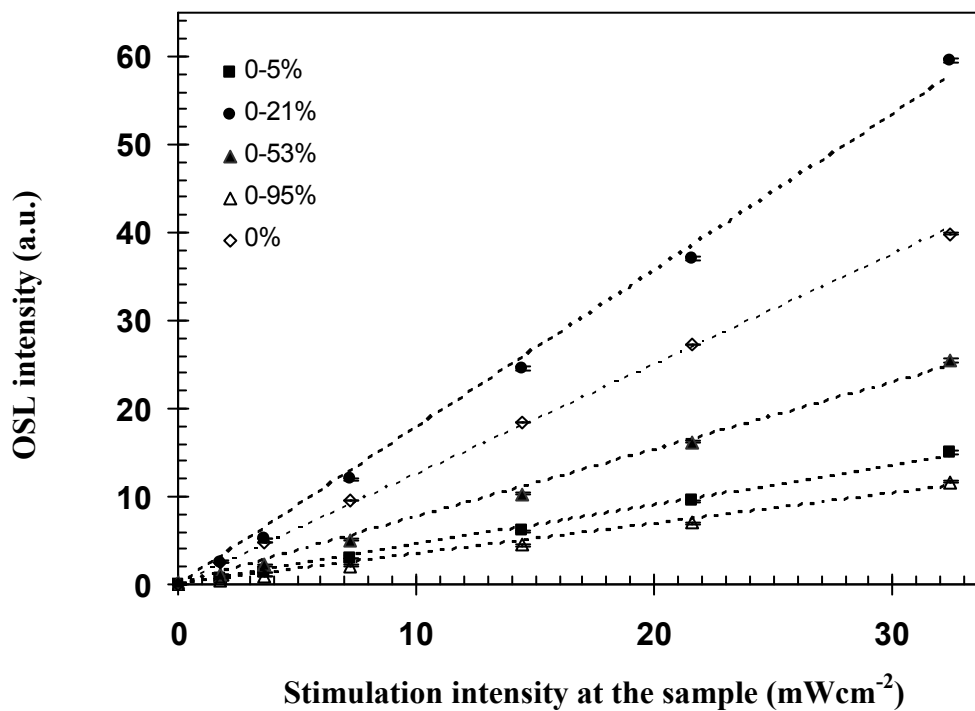
Fig. 5.17 The OSL intensity (from a short-shine measurement) plotted vs. CW stimulation intensity following different percentages (given in the legend) of a full LM OSL measurement of 3600s, 0-95% full power, 160°C. Sample SL203 was used that had been given 20Gy and preheated to 260°C for 10s.

5.4 Sensitivity changes during LM OSL measurement

During OSL measurement sensitivity changes may occur. This may be due to 'optical desensitization' where the idea is that during bleaching a proportion of the detrapped electrons recombine at available luminescence centres and consequently reduce the number available. The probability of an electron recombining with a luminescence centre is then reduced, possibly due to increased competition from empty electron traps or non-radiative centres (Zimmerman, 1971, Bailey, 1998b). The extent of this phenomenon will be dependent on the dose given, the severity of preheating, and the OSL measurement temperature. In a situation where following dosing a low temperature preheat was used then the majority of possible thermal sensitization (due to movement of holes from thermally unstable non-radiative centres to the luminescence centres) would not have taken place. Subsequently holding the sample at raised temperature during OSL may induce further thermal sensitization during the measurement. There are a wide range of possible responses that are sample dependent (numerical modelling by Bailey (2000b) has shown that changing the concentration of centres and to a lesser degree the traps produces very varied responses) and depend also on the measurement conditions used.

Throughout this study long measurements of LM OSL have been performed at raised temperatures of up to 7200s duration. Therefore, when it was clear that routine LM OSL measurements were required for most aspects of the study, there was concern about sensitivity changes during measurement that may affect the form of the LM OSL. For the purposes of this study it was necessary to examine possible sensitivity changes given typical preheating and measurement conditions since any considerable changes in sensitivity would affect the reliability of the deconvolution procedure, and therefore any further analyses and conclusions drawn.

Spectral information by Franklin *et al.* (1995) suggested the 110°C TL peak and OSL signal use a common luminescence centre. Using this information Bailey (1998b) monitored sensitivity as a function of illumination time using the 110°C TL peak. For several samples, optical desensitisation of maximum ~10% over 100-1000s at 160°C was observed.

In the current experiment the sensitivity must be monitored over a longer time period due to the extended standard measurement time for each LM OSL. Various preheating temperatures were used from 240 - 300°C to investigate the influence of preheating and what level of preheat might be most appropriate for use with LM OSL. A diagram showing the experimental procedure is given in Fig. 5.18. Multiple aliquots of natural samples TQN and SL203 were used. The initial sensitivity (χ_0) was monitored by giving a small test dose (1Gy)

and reading out the TL from the 110°C peak by heating to 180°C. This assumes that the 110°C TL response can be used to monitor the sensitivity of all the OSL components. Various preheats were given and the sensitivity after the preheat was measured, χ_1. Various durations of LM OSL measurement were undertaken at 160°C, as indicated in Fig. 5.18 to represent different stages along a single LM OSL measurement. One aliquot was used for each LM OSL measurement time. The sensitivity following the LM OSL was monitored by a third 110°C TL measurement, χ_2.

The amount of sensitivity change at various points during the LM OSL measurement was calculated using χ_2/χ_1. The sensitivity change from preheating could also be quantified using χ_1/χ_0.

The results for sample TQN are shown in Fig. 5.19. A significant amount of noise is observed in the data most likely due to the multiple-aliquot procedure employed. Following the lowest temperature preheat (240°C) considerable desensitization occurs up to a decrease of 17% at 7200s. There is a trend towards less desensitization after higher preheats. Only after very severe preheating does the sensitivity change during the LM OSL measurement become negligible. Sensitivity change during the preheat was in all cases greater than that during LM OSL.

Conversely for SL203, sensitivity increases were observed, see Fig. 5.20. In this sample the amount of sensitivity increase during measurement decreases with increasing preheat. At 210°C the final total increase in sensitivity after 7200s was ~12% whereas at 280°C this was reduced to only 2%. In this case the experiment was repeated but holding the samples at 160°C for various lengths of time rather than using optical stimulation, the results present also in Fig. 5.20. This was to highlight differences in the sensitivity changes induced from optical and thermal stimulation. Sensitivity increases of similar maximum magnitudes were observed, but occurred in the most part over the second half of the holding measurement. This suggests that the significant sensitisation observed over the first half of the LM OSL measurement is primarily optically induced.

There is a great deal of variation in the response of the samples used for this experiment. Following low temperature preheating sensitivity changes (increase or decrease) were over 10%. A simple model to examine the effect on the form of the LM OSL incorporated two OSL traps. Assuming linear change in sensitivity for simplicity the modelled LM OSL is plotted in Fig. 5.21 for maximum decreases in sensitivity of 0, 10 and 20%. The first LM OSL peak is relatively unaffected but considerable change in the form of the second peak occurs with both 10 and 20% sensitivity change.
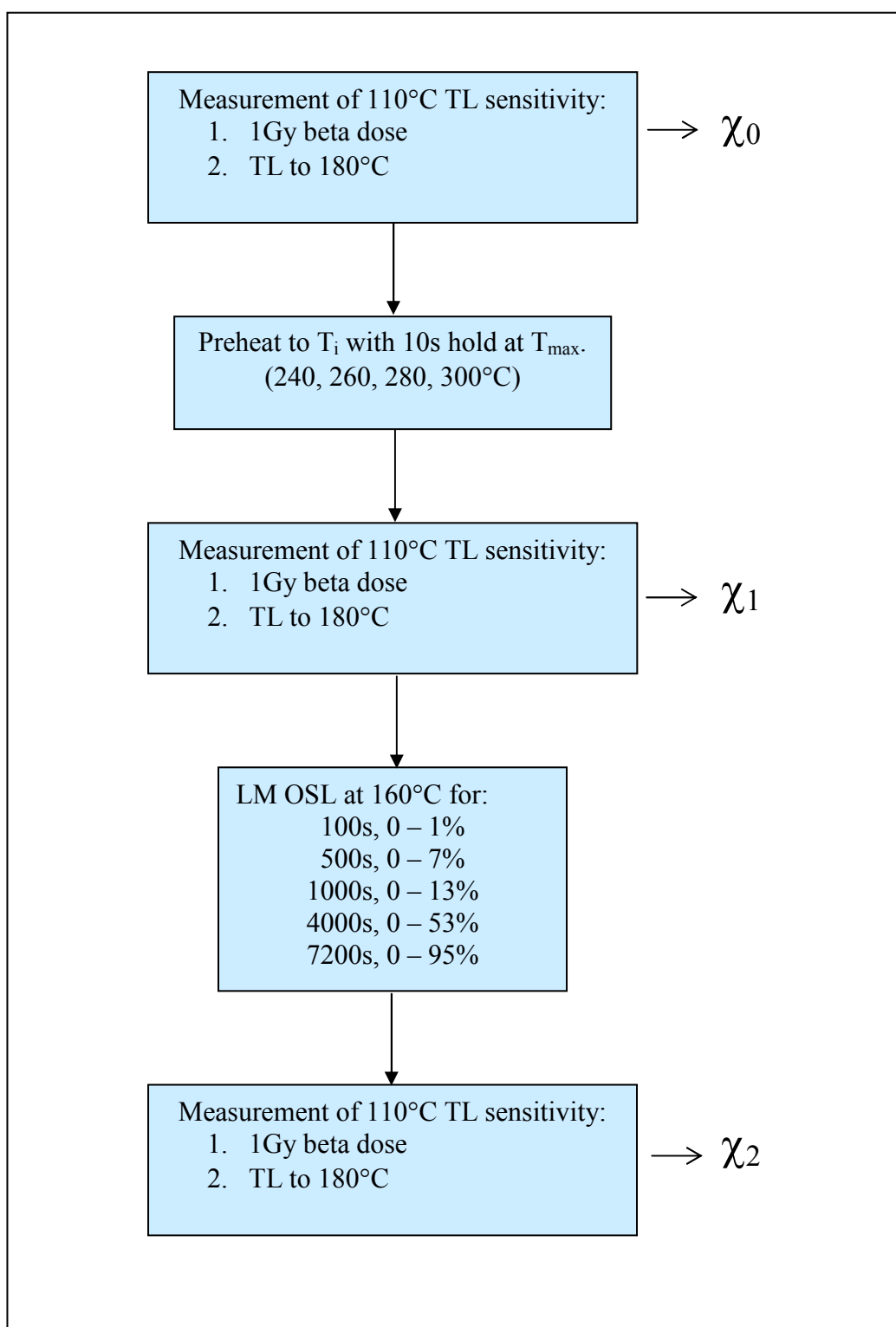
Fig. 5.18 Experimental procedure described in section 5.4 for assessing sensitivity changes during LM OSL measurement using the 110°C TL peak. The effect of preheating temperature is investigated. A single aliquot was used for each LM OSL time.
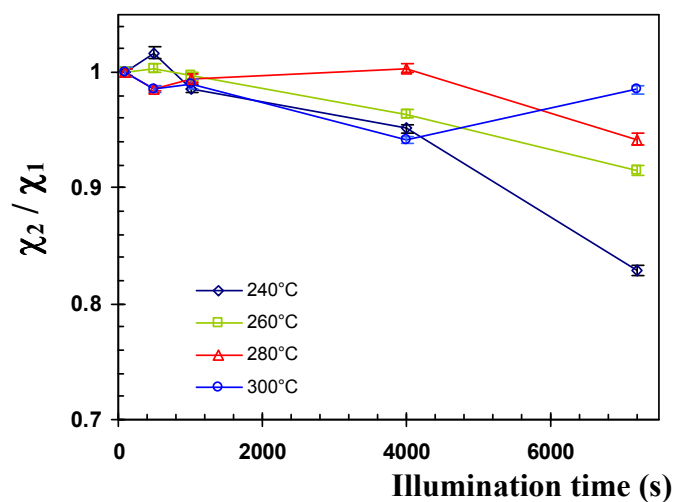
Fig. 5.19 Sensitivity change monitored using the 110°C TL peak due to linearly modulated OSL exposure at 160°C following different maximum preheat temperatures. Natural sample TQN was used. The 110°C TL response following a 1Gy standard dose was used to monitor sensitivity. See section 5.4 for details.
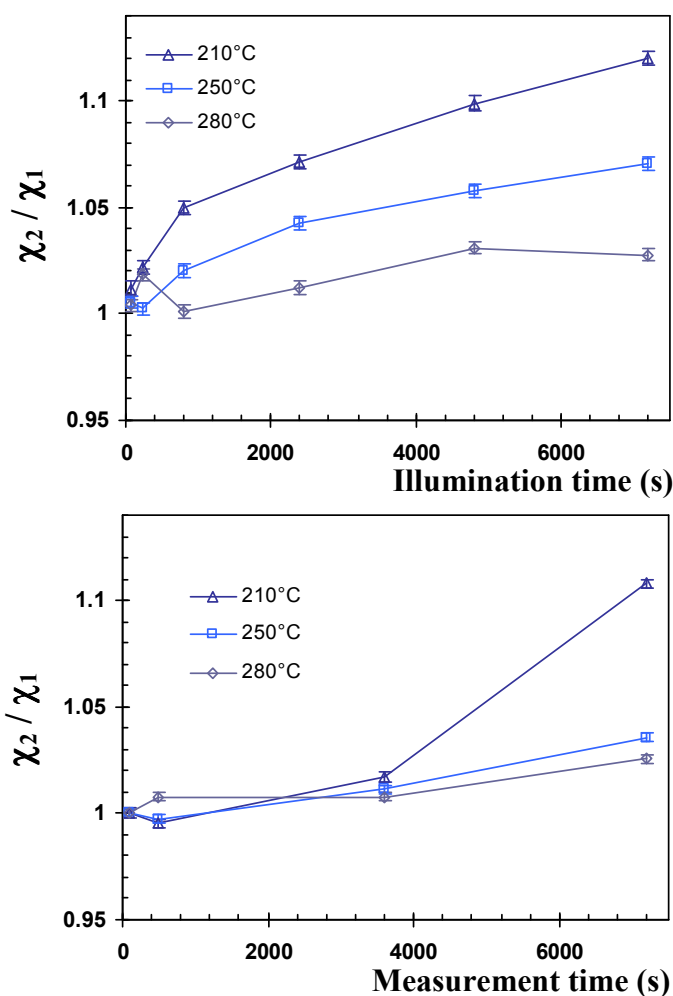
Fig. 5.20 Upper plot shows sensitivity change using the 110°C TL peak due to linearly modulated OSL exposure at 160°C following different initial maximum preheat temperatures for sample SL203. The lower plot shows the results repeating the experiment without illumination, but holding the sample at 160°C for equivalent durations.
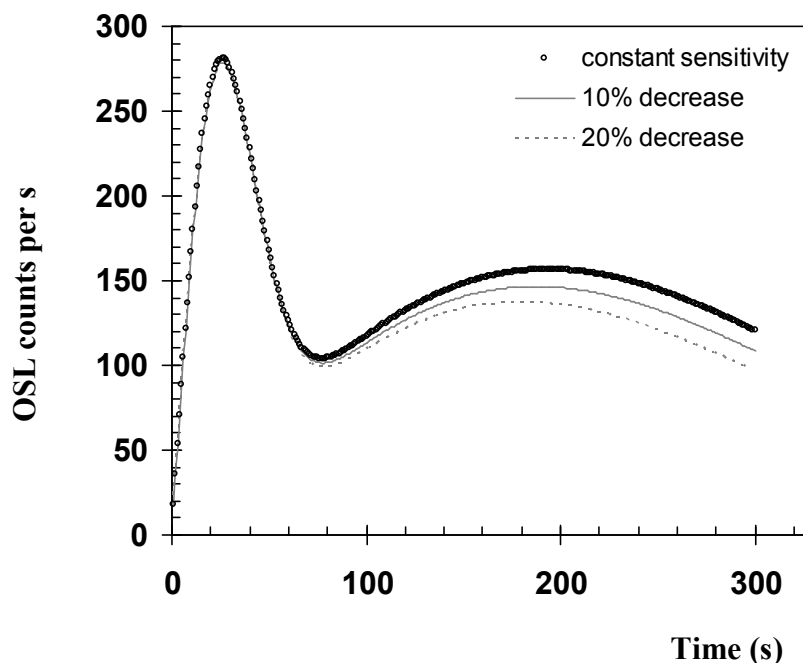
Fig. 5.21 Simulated LM OSL from a two-trap system to investigate the effect of sensitivity change during LM OSL measurement. Linear change in sensitivity is assumed. The details of the trap parameters are given in the table below.

	0% (actual)	10%	20%
n_{01}	10000	9941	9876
σ_1	0.5	0.501	0.504
n_{02}	50000	45421	41061
σ_2	0.008	0.00855	0.0092

Table 5.4 Details of the two-trap simulated system trap parameters (given in the 0% column) are compared to fitted parameters given maximum 10% and 20% sensitivity decreases during LM OSL measurement. See section 5.4 for details.

The apparent peak position is observed at systematically shorter times with increasing desensitisation. The results from subsequently fitting the LM OSL data are shown in Table 5.4. All LM OSL was adequately fitted by two components. Both the magnitude and the photoionization cross-sections fitted were affected by the sensitivity changes, e.g. n_{02} fitted from the 20% change LM OSL was 18% less than the actual modelled value. To obtain reliable results (< 5% error) the maximum sensitivity changes during LM OSL measurement must be less than ~ 7%. Although significantly sample dependent, using Fig. 5.19 and 5.20 the results suggest that preheating temperatures of at least ~250°C are required to achieve this level of stability when LM OSL measurement are made at 160°C.

Consideration of sensitivity changes during preheating to high temperatures must then be taken. Methods of monitoring and correcting for sensitivity changes are investigated in section 6.3 with respect to dating natural sedimentary samples.

This experiment makes the assumption that the 110°C TL peak can be used to monitor the sensitivity of all the OSL components, i.e. all components detrap via the conduction band and recombine at the same luminescence centre as the 110°C TL. The following experiment concerning photo-transfer of charge aims to investigate the validity of this assumption.

5.5 Photo-transferred TL

The currently accepted picture of quartz OSL involves detrapping of charge to the delocalised band so that charge has the possibility of recombination or retrapping at any site. In several minerals charge transfer can also take place via subconduction band processes (e.g. Poolton *et al.*, 1994, McKeever, 1985). These are localised transitions that occur following excitation of an electron to an excited state to allow recombination. Localised transitions have been proposed for feldspars (e.g. Poolton *et al.*, 1994).

It is therefore important to quantify charge transfer efficiency of all the OSL components. Bailey (1998b) used the photo-transfer to the 110°C TL peak (PTTL) to investigate transfer efficiency (given by PTTL / OSL) over the initial portion of the OSL decay. The results showed that the efficiency remained effectively constant at 0.39 ± 0.03 following 0.1s OSL measurements at room temperature to induce photo-transfer in the 110°C TL peak. However, Bailey (2000a) performed a similar experiment for the slow component following heating to 500°C to deplete the fast and medium components and observed no photo-transfer, which (in the context of a series of experiments concerning transport mechanisms of the slow component) was indicative of a localised transition.

The aim of this experiment is to quantify charge transfer efficiency of all the OSL components using a similar procedure to Bailey *et al.* (1997). Like the experiments described in section 5.4, using 470nm stimulation component-resolved measurements are not possible. Therefore the photo-transfer efficiency was measured at various points along the LM OSL curve.

The procedure used is presented in Fig. 5.22. In the development of the experimental procedure several factors were considered, such as the length of OSL measurement required to produce a statistically significant number of counts in the PTTL peak. The 110°C peak is also bleachable with a half life at room temperature calculated by Bailey (1998b) ~500s. Therefore the OSL duration used to induce PTTL is a compromise between these two factors. Sensitivity changes during measurement of LM OSL, as investigated in section 5.4, should not affect the results in this experiment since the subsequent CW OSL and PTTL measurements should have similar sensitivities and therefore division of PTTL/CW OSL ought to negate the effect of sensitivity change.

Sample SL203 was used which had been artificially irradiated with a 20Gy beta dose. LM OSL measurements were made from 0 to n% of full stimulation intensity at 160°C. This allowed correlation of the PTTL results with constituent component peaks more easily (as the rest of the experimental data concerning the components has been obtained in this way). The LM OSL was recorded at 160°C so that no charge could be transferred and reside for any significant length of time in the 110°C TL peak. The LM OSL lengths used were: 0s, 70s (0–2%), 200s (0–5%), 800s (0–21%), 2000s (0–53%), 3600s (0–95%). A CW OSL measurement of 50s at room temperature was made to induce a 110°C PTTL peak. Such a long OSL measurement, in comparison with previous studies, was used due to the low depletion rate and intensities of the hard-to-bleach components. The PTTL peak was measured by heating to 300°C at $2°Cs^{-1}$ although in the subsequent analysis only the TL from the 110°C peak was integrated. The photo-transfer efficiency, ς, was calculated as:

$$\varsigma = \frac{\text{Total CW OSL counts}}{\text{Total 110°C PTTL counts}} \tag{5.7}$$

The results are shown in Fig. 5.23 superimposed on an LM OSL curve from the same aliquot. A relatively constant photo-transfer efficiency was found by this method with a mean of 0.01 ± 0.0004. This is 10 times smaller than that observed by Bailey (1998b). The value obtained will be dependent on the OSL duration and also the stimulation wavelength used. However, the main conclusion of this small study is that, although the data are noisy, the transfer ratio remains roughly the same down the LM OSL curve, i.e. for first four components at least. No

significant change in the availability of recombination pathways occurs throughout the LM OSL measurement and that optical eviction of charge from these components is to the conduction band.

However, none of these measurements looks at photo-transfer from component S3 exclusively. This is the only component that is present following heating to 500°C, and as such is likely to be the component accessed in the observation by Bailey (2000a) that no photo-transfer to the 110°C TL peak occurred. In order to address this point aliquots were heated to 500°C followed by 50s CW OSL at room temperature to induce photo-transfer. A small 110°C TL peak was observed in the TL readout. The photo-transfer ratio was calculated at 0.022 ± 0.001, higher than that calculated in the previous measurements. This may be due to a change in the competition pathways following heating. Nonetheless, that photo-transfer was recorded indicates that trapped charge in component S3 is optically evicted to the delocalised band.
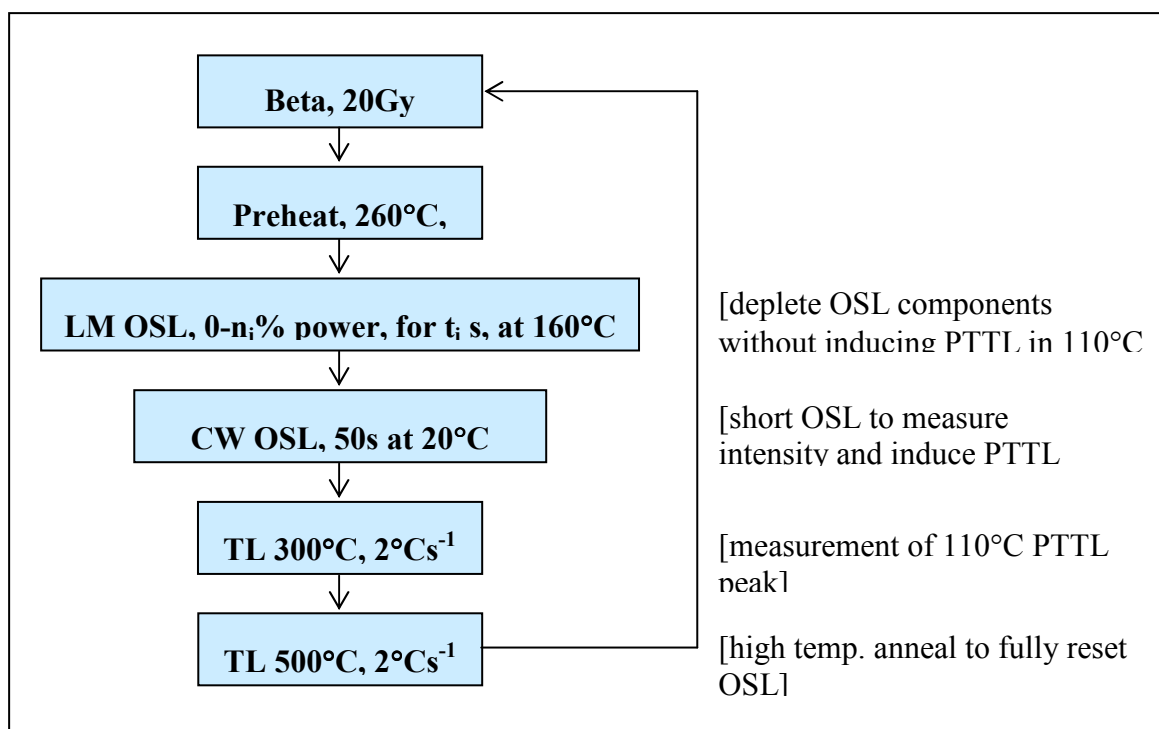
Fig. 5.22 Experimental procedure for measuring the amount of photo-transfer to the 110°C TL peak at various points along the LM OSL curve (i.e. from the different OSL components).
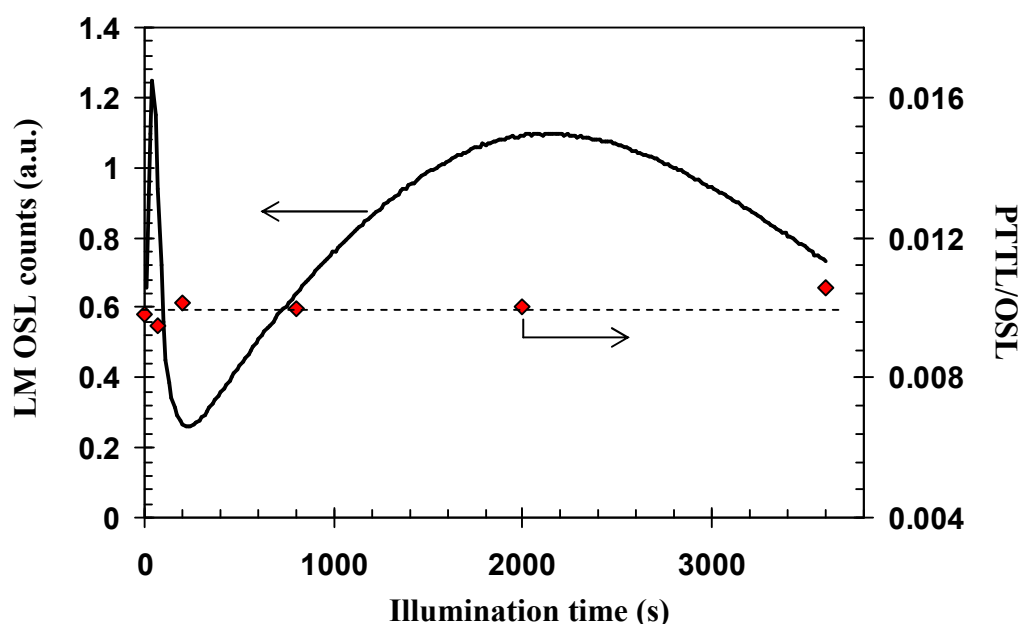
Fig. 5.23 Symbols in red show the photo-transfer ratio (PTTL/OSL) at various points during an LM OSL measurement. An example LM OSL curve is given for reference. Sample SL203 was used in this experiment. Mean $\zeta = 0.01 \pm 0.0004$.

5.6 Summary

In this chapter several aspects of the optical detrapping characteristics of the quartz OSL components were investigated. The dependence on temperature and wavelength of the photoionization cross-section of the components was quantified over a limited range of λ, T. By varying the measurement temperature of LM OSL thermal quenching and thermal assistance parameters were obtained. Similar thermal quenching behaviour was observed in each of the OSL components.

Narrow-band stimulation was used to obtain bleaching spectra for the fast and medium OSL components of quartz at ambient temperature. A significant dependence of σ on wavelength was observed for the fast and medium components. This finding has implications for the potential to identify partially bleached sedimentary samples using signal analysis techniques. IR stimulation enabled the selective removal of the fast component. A 'stepped wavelength' stimulation scheme was suggested as a means of optically separating the OSL components.

Given the lengthy LM OSL measurements required to observe all the OSL components sensitivity changes during OSL were investigated that may have adverse effects on subsequent analysis. It was suggested that preheat temperatures over 250°C should be used to avoid considerable sensitivity changes during the LM OSL measurement itself. This is most important to obtain reliable results from LM OSL curve deconvolution.

Evaluation of photo-transfer efficiency and luminescence efficiency with temperature (thermal quenching) support the current picture of quartz OSL that the components transfer charge via the conduction band and that all probably recombine at the same luminescence centre.

Chapter | 6

6

DEVELOPMENT OF A PROCEDURE FOR COMPONENT-RESOLVED D$_e$ DETERMINATION

6.1 Introduction

This section describes the development of measurement procedures for obtaining equivalent dose estimates from each of the OSL components. The relative merits of both multiple and single aliquot protocols will be addressed. Concerns relating to the illumination time required to reset the OSL signal completely and the measurement/correction of sensitivity changes throughout the procedures have been investigated. The aim of this section is primarily to determine the dose response characteristics of all the OSL components. The development of user-friendly and relatively time-efficient measurement protocols was also an issue in consideration of other users wishing to obtain similar component-resolved equivalent dose estimates.

6.2 Review of optical dating methods

6.2.1 Methods for obtaining standard dates

An introduction to estimating equivalent doses as part of the optical dating process was presented in section 1.1. The equivalent dose is obtained by comparing the natural OSL to laboratory induced OSL of known doses. OSL measurements have traditionally been obtained by either stimulating until the signal is reduced to a negligible level or from short duration illuminations, 'short-shines', where the duration of the illumination does not significantly deplete the OSL signal.

First OSL dating methods used the multiple-aliquot additive-dose protocol (MAAD), e.g. Huntley *et al.* (1985), Smith *et al.* (1990). A number of aliquots are prepared and divided into groups. One group is used to measure the naturally accumulated OSL signal while the other groups are given various added doses prior to measurement. All aliquots are preheated before OSL measurement.

Several problems are immediately apparent. One of which is that even though theoretically the same weight of grains is placed on each aliquot variations in sensitivity between grains

may result in inter-aliquot variation in brightness. Several methods have been employed by various users (Aitken, 1998) to normalise the OSL from each aliquot. For example, *natural normalisation* involves performing short-shine measurements on all aliquots immediately after preparation of the aliquots, to measure the natural sensitivity without significantly depleting the natural signal. Another method is *dose normalisation*, whereby following zeroing of the OSL signal during measurement a standard dose is given to each of the aliquots and the resulting OSL signal measured. The normalised OSL from each aliquot is plotted against the received dose, as in Fig. 6.1a. The resultant growth curve can be fitted and extrapolated to the intercept on the x-axis to find the equivalent dose (see Fig. 6.1a).

In the simplest case (i.e. a fixed number of traps and no sensitivity change) the growth of the OSL with dose can be described by a single saturating exponential function (Equation 6.1). This can be derived from equations 4.1 to 4.3. The following equation is used for the OSL intensity, *L*:

$$L = L_{max}\left(1 - \exp\left[\frac{-(\beta + D_e)}{D_0}\right]\right) \qquad\qquad [6.1]$$

where L_{max} is the OSL intensity at saturation, β is the laboratory dose, D_e is the equivalent dose and D_0 is the characteristic dose parameter defined as the dose at which the slope of the dose response is 1/e of the initial slope (see section 6.3.3 for further discussion). In reality, the situation is more complex. Factors such as normalisation not working perfectly due to aliquot-to-aliquot variation produce scatter and consequently uncertainty in the dose response. Coupled with the extrapolation required to obtain the D_e estimate, the level of uncertainty is in general not better than around ±5-10% (Aitken, 1998) and commonly at the 15-25% level. A multiple-aliquot regeneration method has also been used, which involves bleaching all the aliquots to zero, apart from those used to measure the natural signal, and then giving various laboratory doses. A regeneration growth curve like the simulated example in Fig. 6.1b can then be used for direct comparison with the natural OSL through interpolation. Equation 6.1 can be used to describe the regeneration growth with D_e set to zero. The elimination of extrapolation reduces the errors involved.

Similarly single-aliquot methods for obtaining D_e can involve either additive or regenerative protocols. One main advantage of using a single aliquot approach is that the need for inter-aliquot normalisation is circumvented. For the single-aliquot additive-dose technique, SAAD, (Duller, 1995) cumulative dosing is used in conjunction with short-shine OSL measurements, so that each measurement is the sum of the dose immediately prior to that measurement plus all the previously given doses. Preheating before each OSL measurement is still a

requirement, therefore the loss of signal due to successive preheating is greater in the later measurements. Methods of correction for observed decreases were investigated by Duller (1994). Unfortunately, the use of short-shines restricts the application of the SAAD to bright samples. Due to the cumulative nature of the protocol, measurements to correct for any sensitivity change occurring during the measurement procedure are unfeasible.

The single-aliquot regenerative-dose (SAR) protocol was first suggested by Murray and Roberts (1998) and further developed by Murray and Wintle (2000). In this method, following preheating the natural OSL is measured until effectively zeroed (sufficient to zero the fast/medium components only), then the same aliquot is subjected to further cycles of irradiation, preheating and OSL measurement to form a regenerated dose response. In order to monitor the sensitivity of the OSL measurements (the luminescence efficiency per unit trapped charge) the OSL from a small standard test dose (followed by low temperature preheat) is used to correct the natural and regeneration OSL measurements. Interpolation of the natural sensitivity-corrected OSL onto the regenerated growth curve (Fig. 6.1b) gives the equivalent dose.

The precision obtained from SAR D_e estimates can be extremely high; errors of ~2% are common (Murray and Wintle, 2000). A significant advantage of single-aliquot versus multiple-aliquot regimes is the possibility of obtaining many D_e estimates from several aliquots (whereas a number of aliquots are required to obtain a single D_e value in MAAD and MAR techniques) enabling investigations of populations of D_e estimates. Variations in dose between aliquots, and even between grains, can potentially provide new insights into dosing/bleaching heterogeneity and luminescence characteristics.

More detailed descriptions of the protocols outlined in this section and variants thereof can be found in e.g. Aitken (1998), Murray and Wintle (2000), Stokes (ed., 2002, in prep).
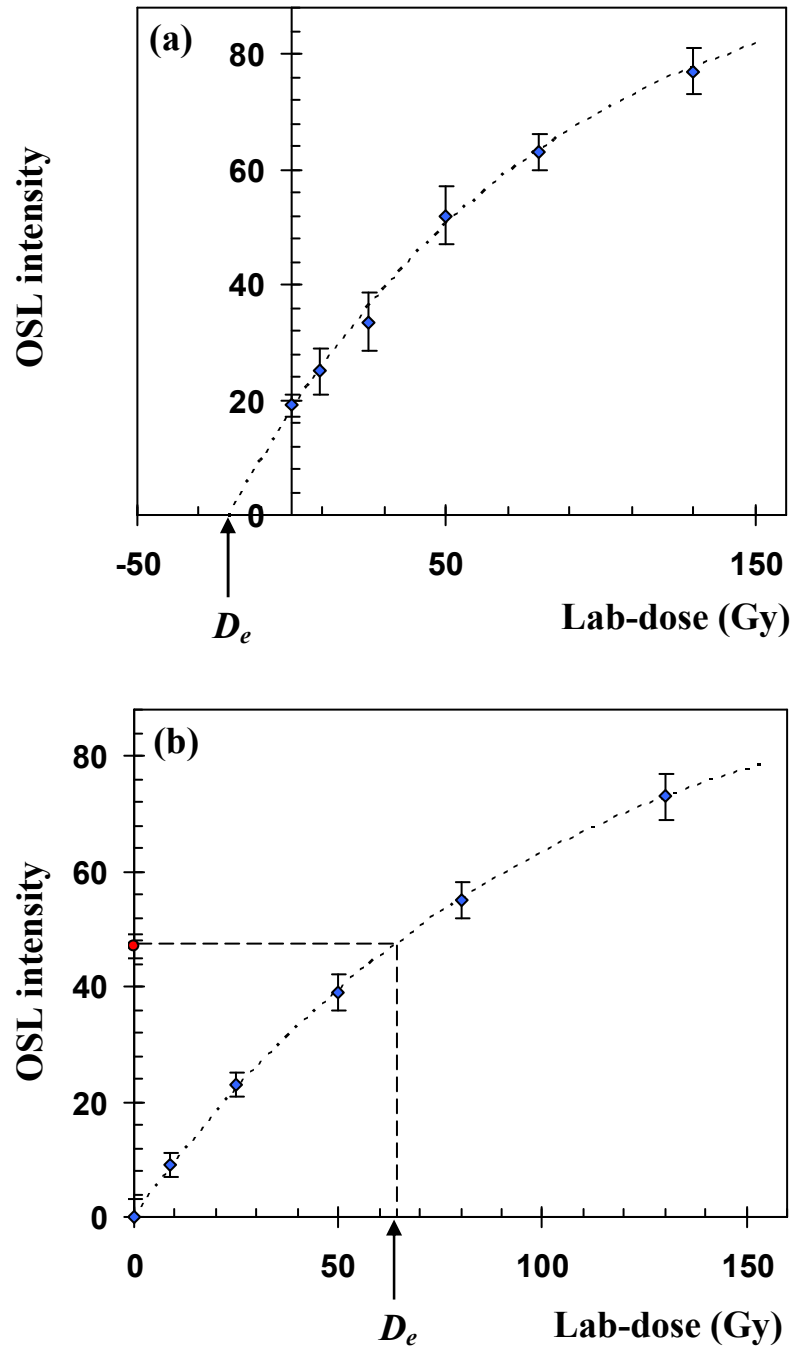
Fig. 6.1 Simulated growth curves for obtaining D_e estimates using (a) additive-dose protocol and subsequent extrapolation to find D_e, and (b) regenerated-dose protocol onto which interpolation of the natural point gives D_e. See text, section 6.2.1 for further details.

6.2.2 Previous component-resolved dating attempts

Bailey *et al.* (1997) published the first dose response curves for the fast, medium and slow components. They produced regenerated growth curves using a multiple aliquot technique (3 aliquots per dose point) by fitting CW OSL decays to three components. Data were normalised by 0.1s OSL at room temperature prior to starting experimental procedure. They observed the slow component to have growth characteristics far exceeding the fast and medium components. This approach (multiple-aliquot additive-dose, MAAD) was used by Bailey (1998b) where two exponentials plus a logarithmic decay (for the slow component) were fitted to find growth characteristics of the OSL components from several samples. He obtained D_e estimates from each component for several samples that were in agreement. In the majority of samples explored the slow component showed the highest dose saturation levels of all the components.

Bailey (2000a) developed slow component dating protocols to attempt to realise the idea of extending the upper datable limit suggested in Bailey (1998b). Due to the inter-aliquot scatter often observed with multiple aliquot procedures and the problems of normalisation a single-aliquot additive-dose procedure (SAAD) was preferably used. Each aliquot was taken through successive cycles of laboratory dose, heat to 400°C and subsequent 50s CW OSL measurement. The preheat temperature was chosen to be high enough to deplete the fast and medium components leaving the slow component, but low enough that thermal sensitisation was taken to be minimised. An OSL measurement of 50s was sufficient to obtain reasonable counting statistics with minimal depletion of the slow component (effectively a 'short-shine'). Results presented for several aliquots of one sample using this method were in agreement with standard optical dating SAR D_e estimates (also Singarayer *et al.*, 2000).

Bulur *et al.* (2000) presented preliminary results of LM OSL from quartz. In this study an additional slow component was identified, as discussed in previous sections. Using a sample that had undergone several cycles of dosing and heating to 450°C to stabilise the signal sensitivity, a single aliquot regenerative dose procedure (SAR) was used to obtain the growth curves from the four components by fitting the LM OSL following various laboratory doses. No sensitivity correction procedure was undertaken as this was taken to be negligible (estimated through repeating one of the low dose points). The growth curves were fitted to saturating exponential plus linear functions. It was found that the slow components both displayed higher dose responses than the fast and medium components for the sample used. This procedure was used only after extensive treatment on the sample in question to minimise sensitivity changes due to dosing and heating and is therefore unlikely to be

directly applicable to dating natural sedimentary samples due to the sensitivity changes likely to occur during the measurement procedure.

Given that no adequate correction/monitor for sensitivity changes during measurement was incorporated into either the MAAD or SAAD protocols outlined above or into the LM OSL SAR procedure used by Bulur *et al.* (2000), a thorough re-examination of the dose response of the OSL components of quartz was required. This necessitated the development of a methodology that could also be applied to dating natural sedimentary samples.

6.3 Obtaining dose response curves

6.3.1 Development of LM OSL dating protocols

It has been observed that there can be significant inter-aliquot variation in the relative proportions of the OSL components (e.g. Adamiec, 2000a). While considering the development of a multiple-aliquot dating procedure this variation was thought likely to be a potential cause of scatter between aliquots. A more involved normalisation procedure would be required to correct for this than that used by Bailey *et al.* (1997; see section 6.2) since the OSL from one component cannot necessarily be used to normalise all components as it may not be representative of the brightness of all components. In section 5.2.2 a multiple aliquot procedure for investigating the effect of measurement temperature of sample CdT9 was used. Normalisation was achieved by a second full LM OSL measurement following a standard (test) dose and preheat. A similar lengthy normalisation procedure would be necessary for a multiple aliquot dating protocol. Due to limits on precision arising from inter-aliquot variation the development of a single-aliquot procedure was attempted.

In developing such a procedure primary concerns relate to sensitivity changes at various points during the measurement procedure and complete bleaching of the OSL signal in between each cycle of measurement (due to the slow depletion rate of component S3).

The length of LM OSL measurement used to record all the components was ~7200s on the previous OSL excitation unit, R4a, and ~3600s on the new unit R4b. Due to concern about the magnitude of sensitivity changes resulting from such long durations of optical stimulation at raised temperatures, experiments were undertaken to investigate this; reported in section 5.4. The sensitivity of the luminescence was monitored throughout LM OSL measurement using the size of the 110°C TL peak following a 1Gy dose. The amount of sensitivity change observed was preheat-temperature dependent. Following low temperatures (240°C or lower) sensitivity increases/decreases of up to 17% were noted. This would significantly affect the form of the LM OSL. Through simulations it was found that the resulting modification

significantly affected the reliability of deconvolution. The results of this investigation suggest that stringent preheating (to 250°C or above) may be vital to minimise sensitivity changes during LM OSL measurement. Application to age constrained natural samples discussed in subsequent sections examines whether high temperature preheats are appropriate for application to dating natural sedimentary samples.

A second major consideration was bleaching all the OSL in between each measurement. Following low laboratory doses it was found that ~8000s at 160-180°C using full power was sufficient to bleach the OSL components to adequately low signal levels. This procedure was applied in preliminary LM OSL SAR protocols to bleach the OSL between the first LM OSL measurement and the measurement following a standard test dose (see Fig. 6.2 for full details). The method was tested on sample Van2 using doses up to 500Gy. The results are shown in Fig 6.3a. Following doses of 160Gy or over the method fails to bleach a substantial amount of residual component S3, which can then be clearly seen to affect the test dose LM OSL (Fig. 6.3b). Several different bleaching methods were tried such as those given in Fig. 6.4 (details in figure caption). Possibly the most 'natural' method to bleach would be to expose the aliquots with sunlight at room temperature for 24 hours or so, but this not realistic within the available time frame given the already lengthy LM OSL measurement time. Bleaching at high temperature was found to produce low residuals in shorter exposure times. The bleaching procedure of 1500s illumination at 300°C was incorporated into the LM OSL SAR protocol and tested on natural samples.

For several samples, D_es from the fast component agreed with those obtained from standard optical SAR dating procedures. For the majority, however, the D_e estimates were significantly lower. For example see Fig. 6.5 from sample TQN. The D_e from the normal SAR method on 6 discs was 188±27Gy. While the D_e estimates from all the components agreed (except S2, which was found to be thermally unstable in section 4.4) they were consistently too low; $D_e \sim 20$Gy. This is due to the very severe bleaching method in between measurements (1500s at 300°C), which fulfilled the criterion of resetting the OSL signal from observation of the level of a 0Gy measurement, but the long hold at such a high temperature seemed to cause significant sensitivity change so that subsequent LM OSL measurement after a standard dose did not represent the sensitivity of the initial measurement. It was initially considered that if the same bleaching procedure was used before each dose, as long as the sensitivity change was in proportion that reliable corrections could be obtained. The results suggest otherwise. However, the lowest dose point was repeated at the end of the measurement sequence and was found to be within 10% of the

initial dose point. This may suggest that the regeneration curve is reliable, and the majority of un-measurable sensitivity change occurred in the first cycle (the natural point).

In view of this, and for developing a user-friendly protocol, it was considered that if the sensitivity change was the same for all the OSL components this may be advantageous. It may be expected since empirical evidence from previous sections (e.g. thermal quenching, section 5.2) suggests that recombination from all the components takes place at the same luminescence centre. Therefore following an initial LM OSL measurement the OSL from the fast component after a standard test dose could be used to correct for each of the components. This would mean that no lengthy illuminations would be needed in between each measurement as the fast component would be zeroed and that only a short second LM OSL measurement (or even early integration from a standard CW OSL measurement) would be required thereby drastically reducing the total time per measurement cycle. Consequently, experiments were performed to look at the effect of sensitivity changes on the OSL components.

Results from one sample SL203 (that had been previously bleached for 1500s at 300°C) are shown in Fig 6.6. The measurement sequence used involved giving various laboratory doses up to 500Gy and then performing CW OSL at 300°C for 1500s to induce sensitivity change and completely bleach the OSL signal. The aliquot was then given a 20Gy dose and preheat to 260°C. Measurement of LM OSL was for 7200s at 160°C from 0 to 32.5 mWcm^{-2}. The LM OSL was fitted to separate contributions from the different components. The fitted magnitude (n_{0i}) of the medium, S1, S2 and S3 were plotted versus the magnitude of the fast component. Large uncertainties were obtained in component S1 due to its small size relative to the other components. Proportionality between components S2 and S3 and the fast component was observed indicating that it may be possible to use the fast component to correct for sensitivity changes in these components. The medium and S1 components were found to fit better to a linear relationship with small non-zero intercept. This may result from errors in the fitting or perhaps differently-competing non-radiative centres. The intercept is small in both cases; therefore the possible error introduced by this will be minimal.

Given the above results, experiments were undertaken to try to recover given doses using the fast component for sensitivity correction within a single-aliquot procedure. The procedure used is outlined in Fig. 6.7 (LM OSL SAR protocol B). The first LM OSL measurement is the same as in protocol A. However, there was no full power illumination to zero the OSL after LM OSL1. Instead, the sensitivity correction measurement following a standard test dose was immediately carried out using a much lower preheat than previously of 220°C for

10s. LM OSL 2 of 120s at 160°C allowed recording of the fast, medium and rising limb of the slow components. The fast component was initially used for sensitivity correction of all the components separated by deconvolution of LM OSL1. By this procedure the length of each measurement cycle in protocol B compared to protocol A (Fig. 6.2) is more than halved. In Fig. 6.8 an example is presented of one such dose recovery experiment on an aliquot of sample TQN that had been bleached and given a 15Gy beta dose to try to recover using the above measurement procedure. Regeneration doses of 5, 10, 20 and 50Gy were used to construct a regeneration growth curve. The LM OSL 1 curves were deconvoluted to give the magnitude of each component. Once sensitivity corrected the growth curves for the OSL components were plotted as seen in Fig. 6.8. No data could be obtained from this aliquot for component S3, either because the doses used were too low for the fitting to recognise it over noise, or because none of the grains composing this aliquot displayed this component in measurable quantities. For the four components that were fitted the regeneration curves could all be approximated to single saturating exponential functions. Similar to Fig. 6.5 component S2 saturated at much low doses than the other components. Good recycling ratios were obtained for all components (component S1 displayed the worst recycling ratio ~15% decrease), suggesting that the sensitivity correction was appropriate. The D_e obtained from each of the components was in agreement with the given dose within errors. The medium component gave the least accurate D_e. It is postulated that the small magnitude of this component relative to the others produced some error, systematic and random that contributed to this.

That a given dose could be recovered from each of the components indicates that the procedure described above (protocol B) may be suitable for natural deposits. Further tests were performed on samples that had been collected from sites previously dated by independent dating techniques. These experiments are described in the section 7.2.
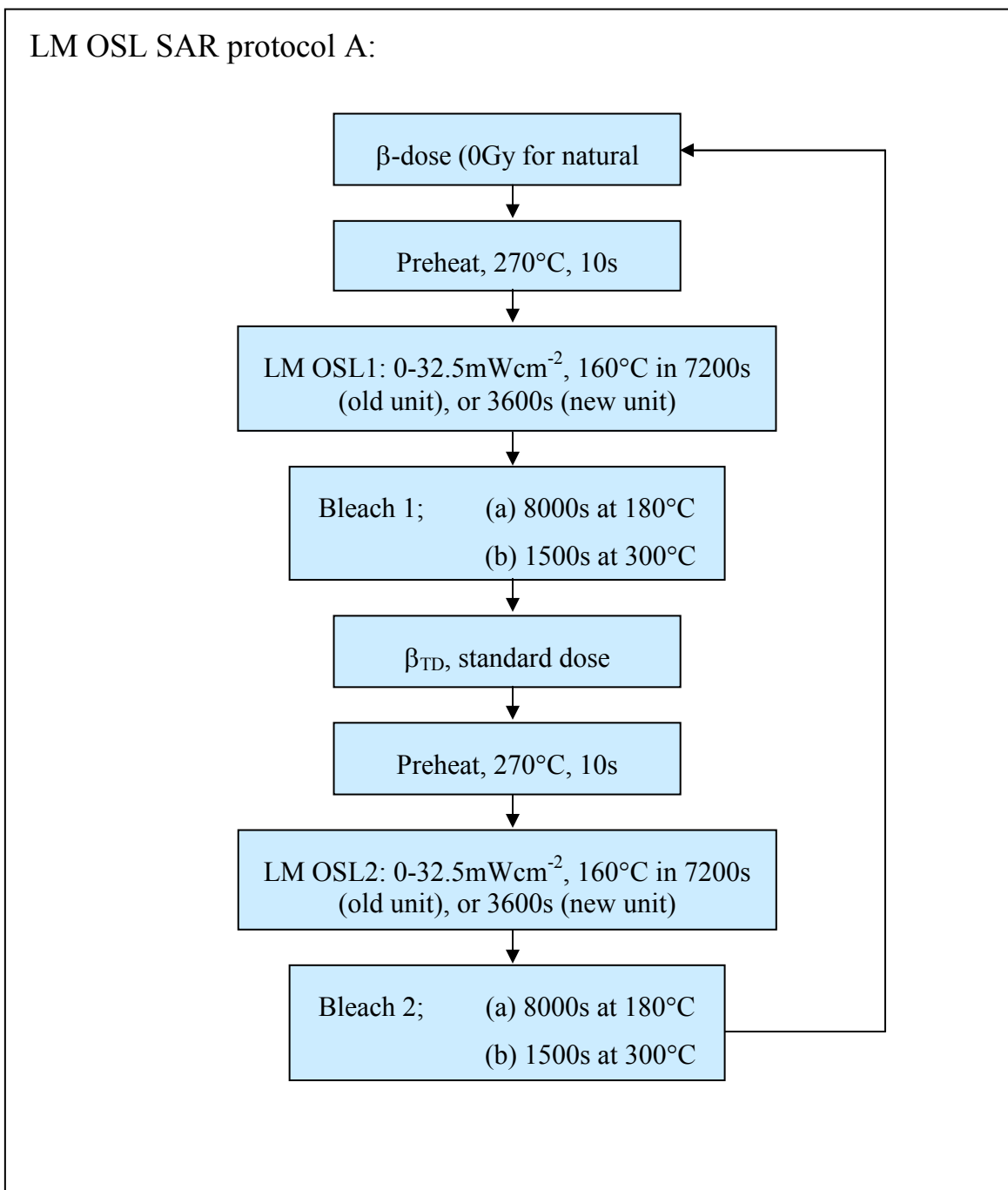
Fig. 6.2 Flowchart outlining procedure A for an LM OSL single-aliquot regenerative-dose, SAR, protocol to obtain equivalent doses from each of the OSL components.
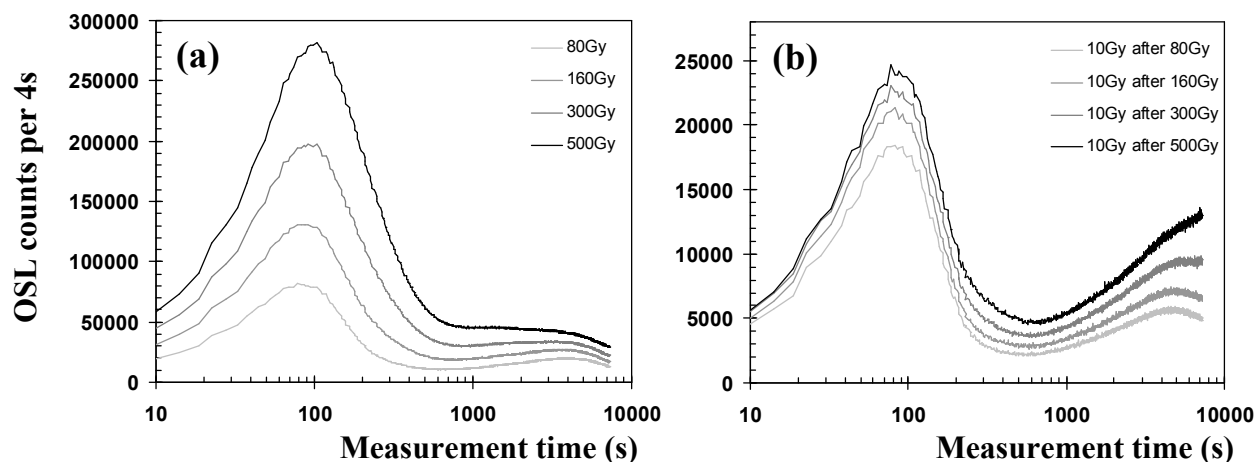
Fig. 6.3. (a) LM OSL from a single aliquot of sample Van2 following various beta doses, given in legend. (b) Following initial LM OSL and 8000s at 180°C to attempt to bleach the OSL signal before measurement of a 10Gy test dose LM OSL. Following doses above 160Gy the test dose LM OSL is clearly affected by residual OSL not zeroed during bleaching.
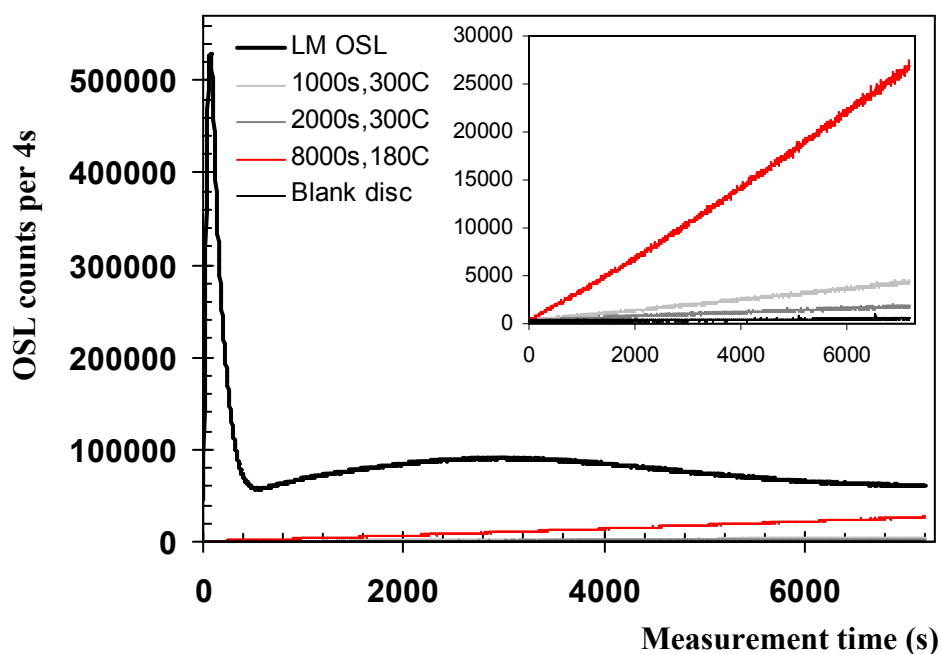
Fig. 6.4. The degree of zeroing achieved using various bleaching techniques. An aliquot of SL203 was given 400Gy dose and 7200s LM OSL measurement at 160°C. Various bleaching procedures, given in legend, were used followed by further LM OSL measurement to test the effectiveness of each technique. Comparison to LM OSL from a blank disc is shown.
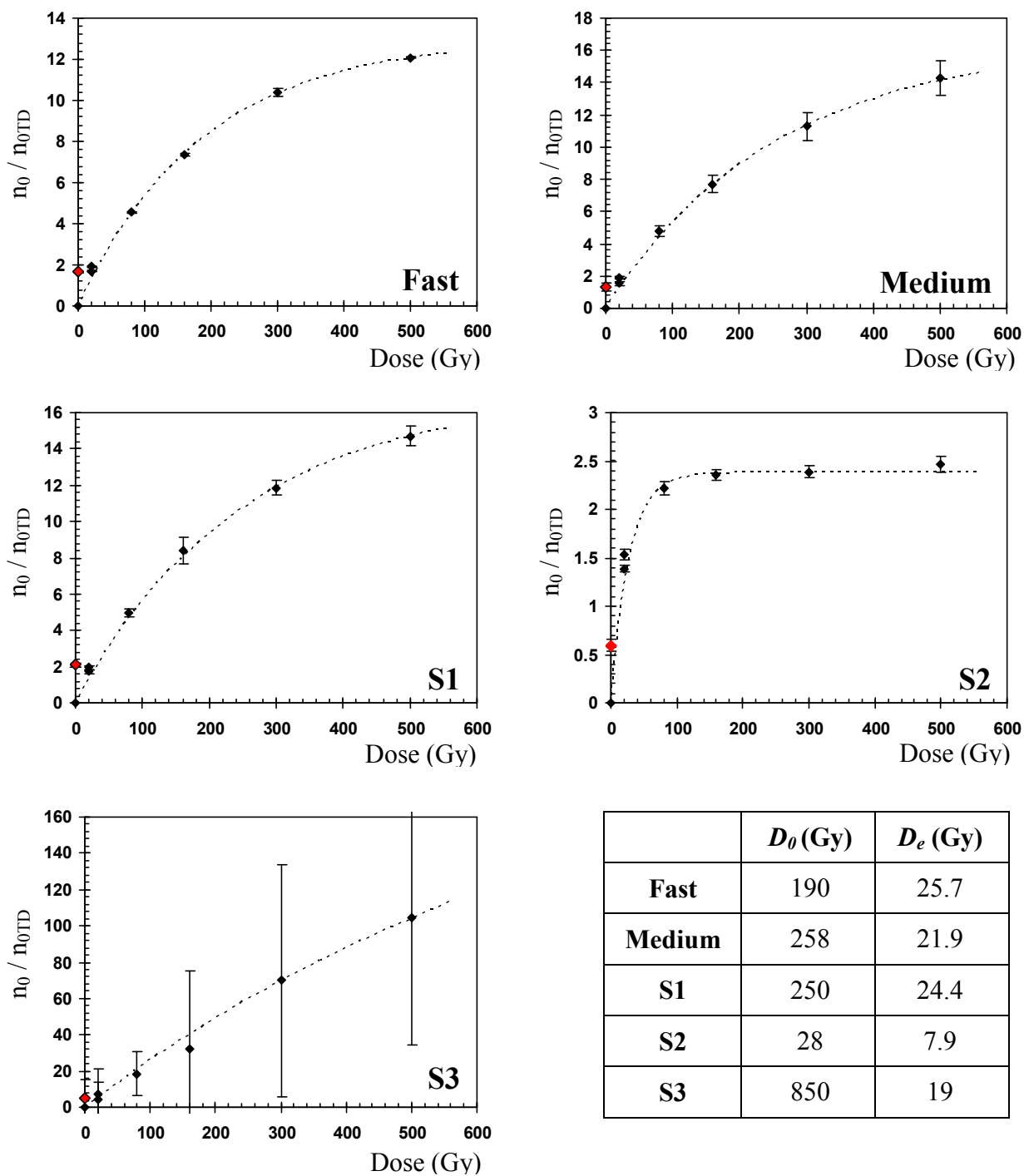
Fig. 6.5. Regenerated growth curves and D_e estimates from a single-aliquot of sample TQN. The data were obtained using LM OSL SAR protocol A with 1500s at 300°C CW OSL bleaching in between measurement cycles. [Standard SAR D_e = 188 ± 27Gy]
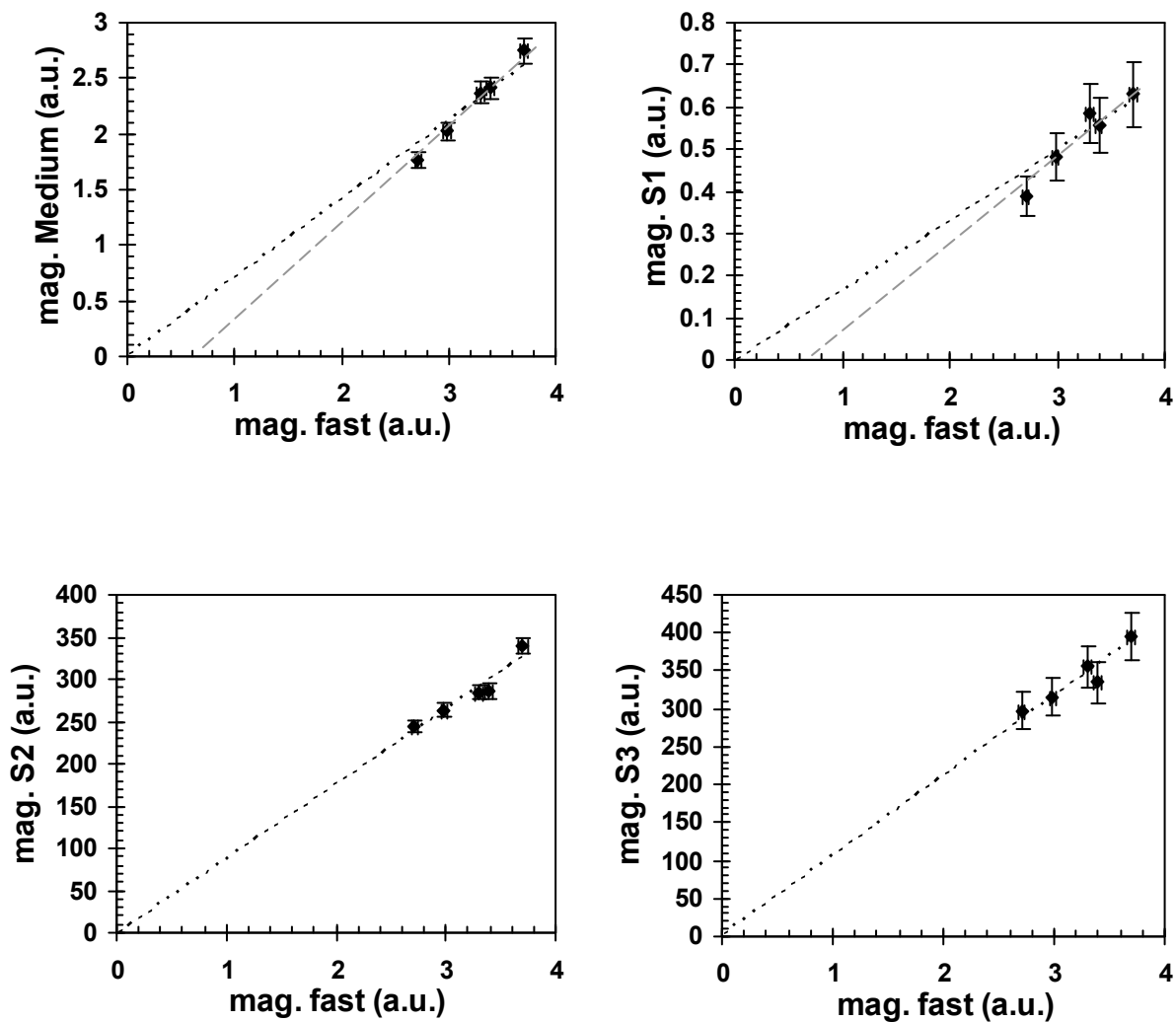
Fig. 6.6. Relationship between the fast component and other OSL component fitted magnitudes (medium, S1, S2, S3) from sample SL203 given the same dose at each measurement. Sensitivity changes were induced by giving large doses and bleaching in between each LM OSL measurement. Black, dotted lines indicate the best fit to a proportional relationship. Grey, dotted lines indicate linear fit.
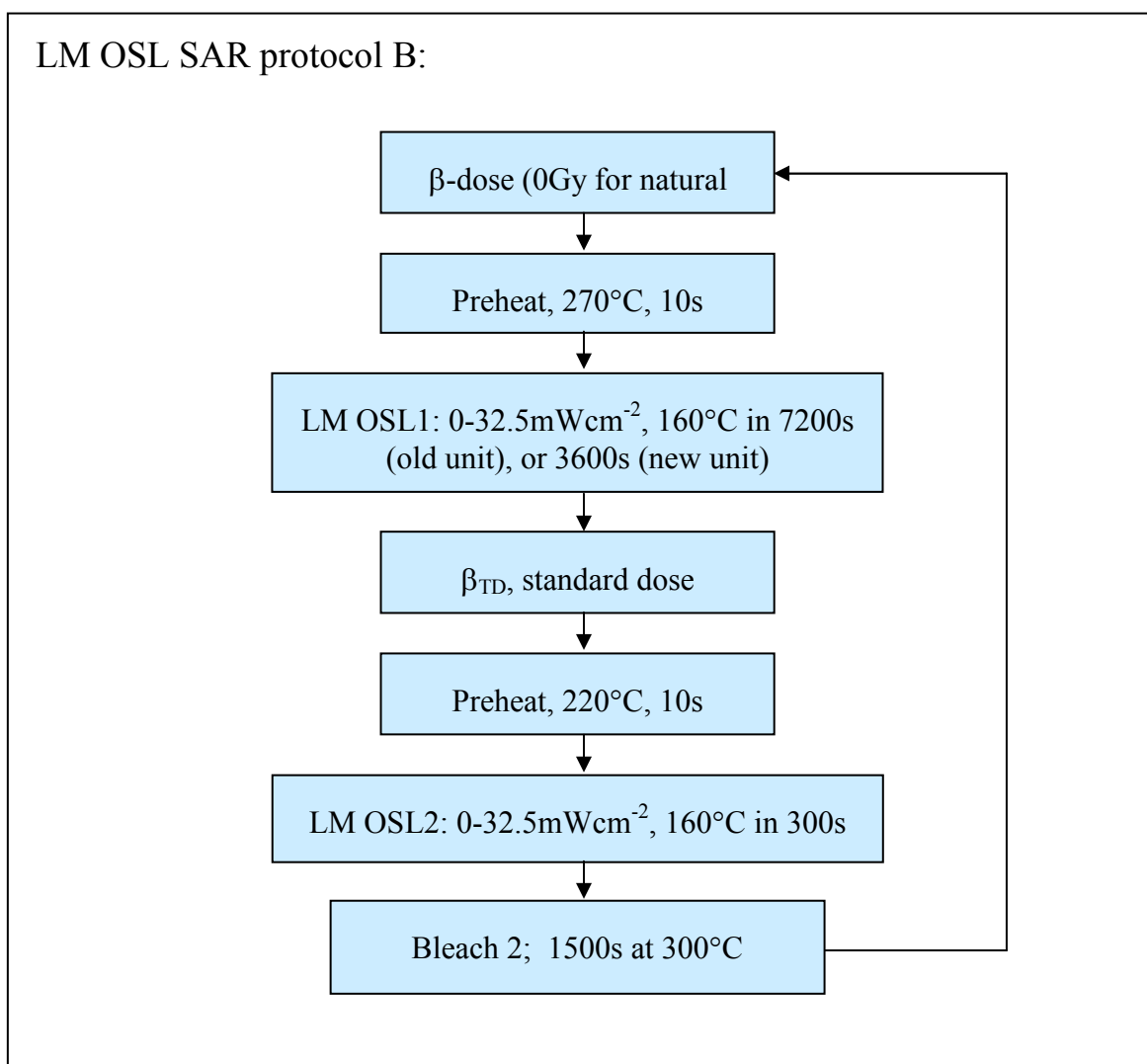
Fig. 6.7 Flowchart outlining procedure B for an LM OSL single-aliquot regenerative-dose, SAR, protocol to obtain equivalent doses from each of the OSL components.
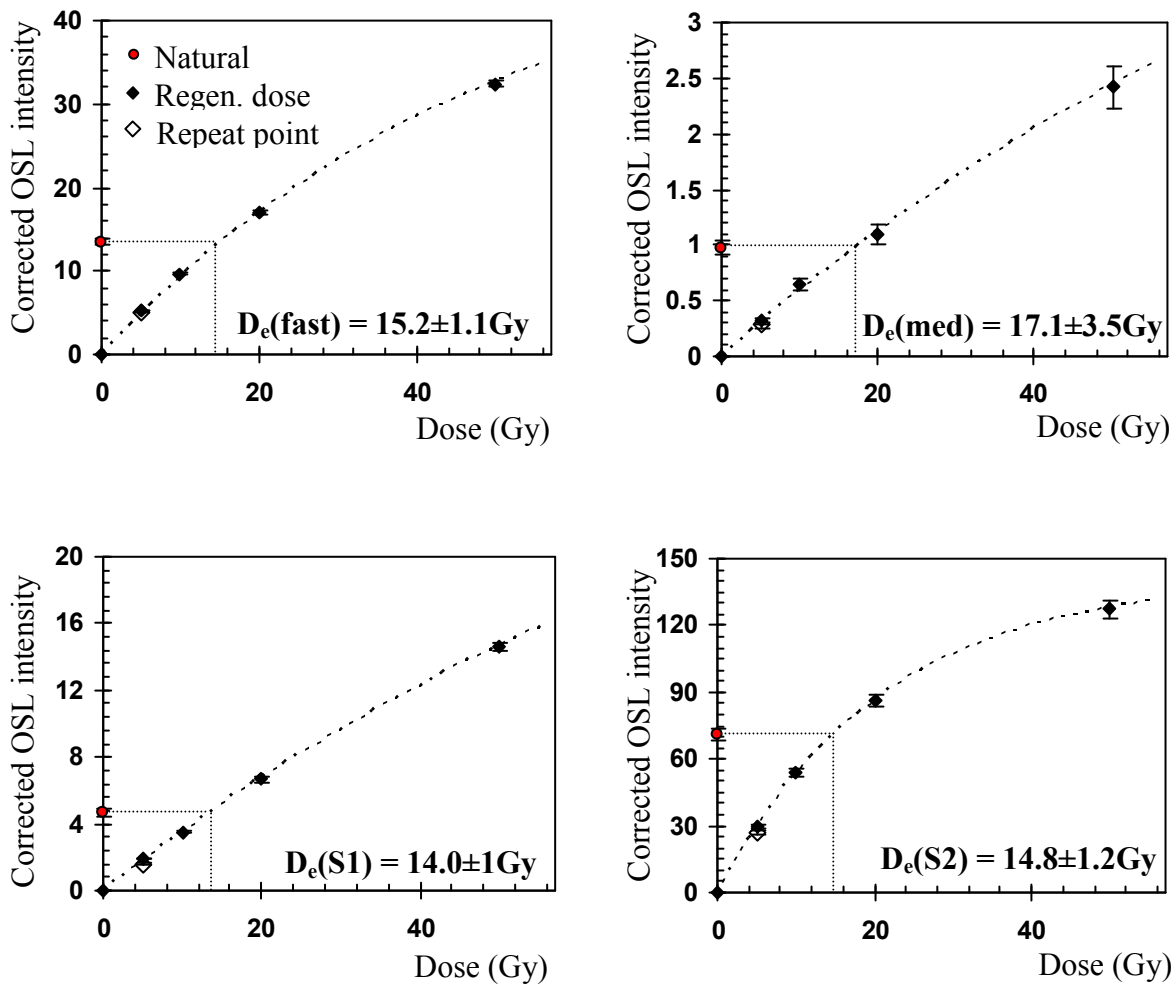
Fig. 6.8 Component-resolved SAR growth curves and D_e estimates for an aliquot of sample TQN that had been previously bleached and given a 15Gy dose prior to SAR measurement. The doses given were too low to obtain a D_e from component S3.

6.3.2 Dose saturation levels

Although unable to obtain accurate equivalent doses for the aliquot of TQN presented in Fig. 6.5 the agreement of the repeat dose points in the regeneration curve suggested that after the first (natural) cycle the sensitivity correction method was adequate and therefore the forms of the regenerated dose responses are reliable. The results show that the fast, medium and S1 components have very similar dose saturation levels, as indicated by their D_0 values (shown in the figure). Component S2 was found to have an extremely low saturation level with D_0 = 28Gy and full saturation reached at ~160Gy. The only component to apparently show dose response significantly higher than the fast component was S3. The D_0 for this sub-sample was 850Gy which given a typical dose rate of 1Gyka^{-1} equates to nearly a million years of growth. However, large errors were obtained from the deconvolution process due to the fact that the peak of component S3 cannot be recorded with the stimulation power and measurement times available. Therefore it may not be that the fits were appropriate but this can only be investigated through measurement past the component peak (see later).

Similar patterns were observed for several other samples. The dose response of the components from sample TQL was obtained up to saturation for all except component S3. The regenerated growth curve data and estimated D_0 values from approximations to single-saturating exponential functions are shown in Fig. 6.9. The relative saturation levels follow roughly the same pattern as previously observed in TQN. The medium and S1 components display slightly higher dose responses than the fast. Component S2 saturates at very low doses (~160Gy) and S3 again apparently has a dose saturation level far exceeding all the other recorded OSL components. The large uncertainty observed for the D_0 values of component S3 results from the fact that at the maximum doses applied there is still very little sub-linearity in the dose response and therefore little information on the overall shape of the growth curve. Therefore errors of around ± 90% are not unexpected.

Since this work is a continuation mainly from the findings of Bailey et al. (1997) and Bailey (1998b) it was thought that a direct comparison of the dose responses of the fast, medium and slow components found on one specific sample by Bailey (1998b) using CW OSL (MAAD) and the LM OSL SAR protocol employed here should be made. For this sample 319 (from Chebba, Tunisia; see Appendix A for further details) was used. Bailey (1998b) used a multiple-aliquot additive dose technique, fitting the OSL decays to the sum of three components to get D_e estimates from each component. The author observed that the fast and medium components displayed linear growth for added doses up to at least 150Gy. The data from the slow component appeared scattered and was apparently saturated. The LM OSL

SAR protocol B was employed on a single aliquot of 319, the results of which are presented in Fig. 6.10. The data could only be approximated by the sum of five components, as observed in many other samples using LM OSL (see section 4.3.1). The growth from each component again is very similar to the other samples investigated. The medium and S1 components have slightly higher responses than the fast (S1 in this sample was three times larger by D_0 value). The fast and medium components saturate at slightly lower doses than found by Bailey (1998b). This is possibly due to the fact that no sensitivity correction was used in the MAAD approach. Component S2 displayed a very low dose saturation level, and appeared to be fully saturated by ~150Gy. When compared with the growth curves found by Bailey (1998b) it may be that, although only three components were fitted to the CW OSL decays, the 'slow' component growth may have been dominated by component S2, hence apparent saturation observed. The regenerated growth of component S3, on the other hand, was fitted to give a D_0 value of 981± 792Gy. However, it is likely that due to the relative signal sizes of components S2 and S3 the large dose response of S3 was not been detected in this sample via CW OSL analysis. For other samples the CW slow component was found to have an extremely large dose response. See section 7.3.3 for component-resolved age determination of sample 319 using LM OSL.

As suggested by Bailey (1998b), the fact that the quartz OSL components display different dose response characteristics strongly indicates that they originate from physically distinct trap types. This argument is perhaps now less critical as the component peaks have been observed separately using LM OSL. There is some sample-to-sample variation in the relative saturation levels (given by D_0 value) of the components. Such variations may be due to variation in the proportions of the components, and concentration of luminescence centres or other traps competing for charge. Further investigation of the causes and magnitude of variation could involve employing a general kinetic model (such as that developed by Bailey (2000b)). Investigations of this nature have been done previously by e.g. Chen *et al.* (1988), Bailey (2000b, 2002a).

Sample TQL
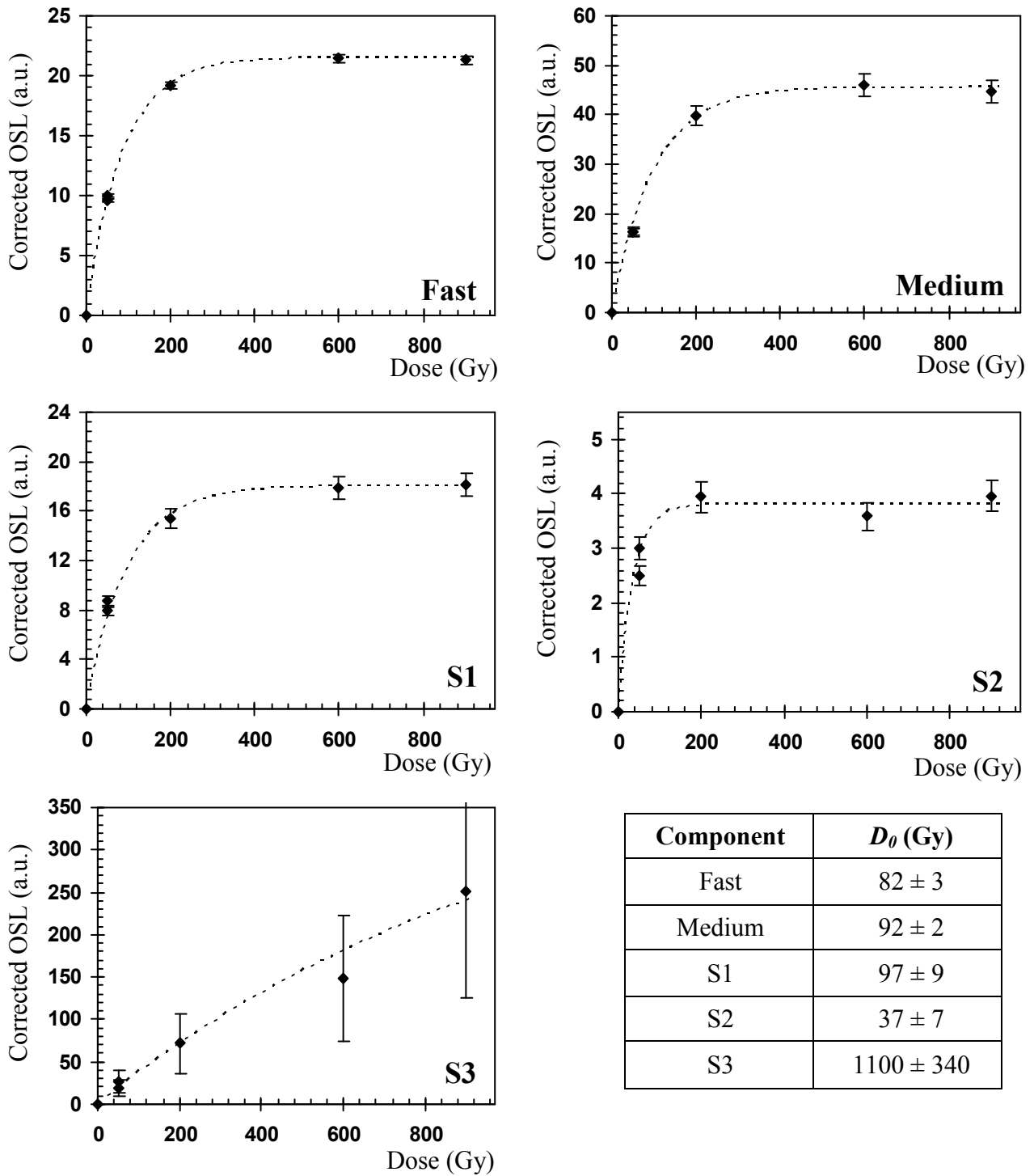
Fig. 6.9 Component-resolved single-aliquot regeneration growth curves for sample TQL. The data were collected using LM OSL SAR protocol B and deconvoluting the LM OSL to separate the components. The growth curves were fitted to single-saturating exponential functions to obtain D_0 values for each component listed in the table.

Sample 319
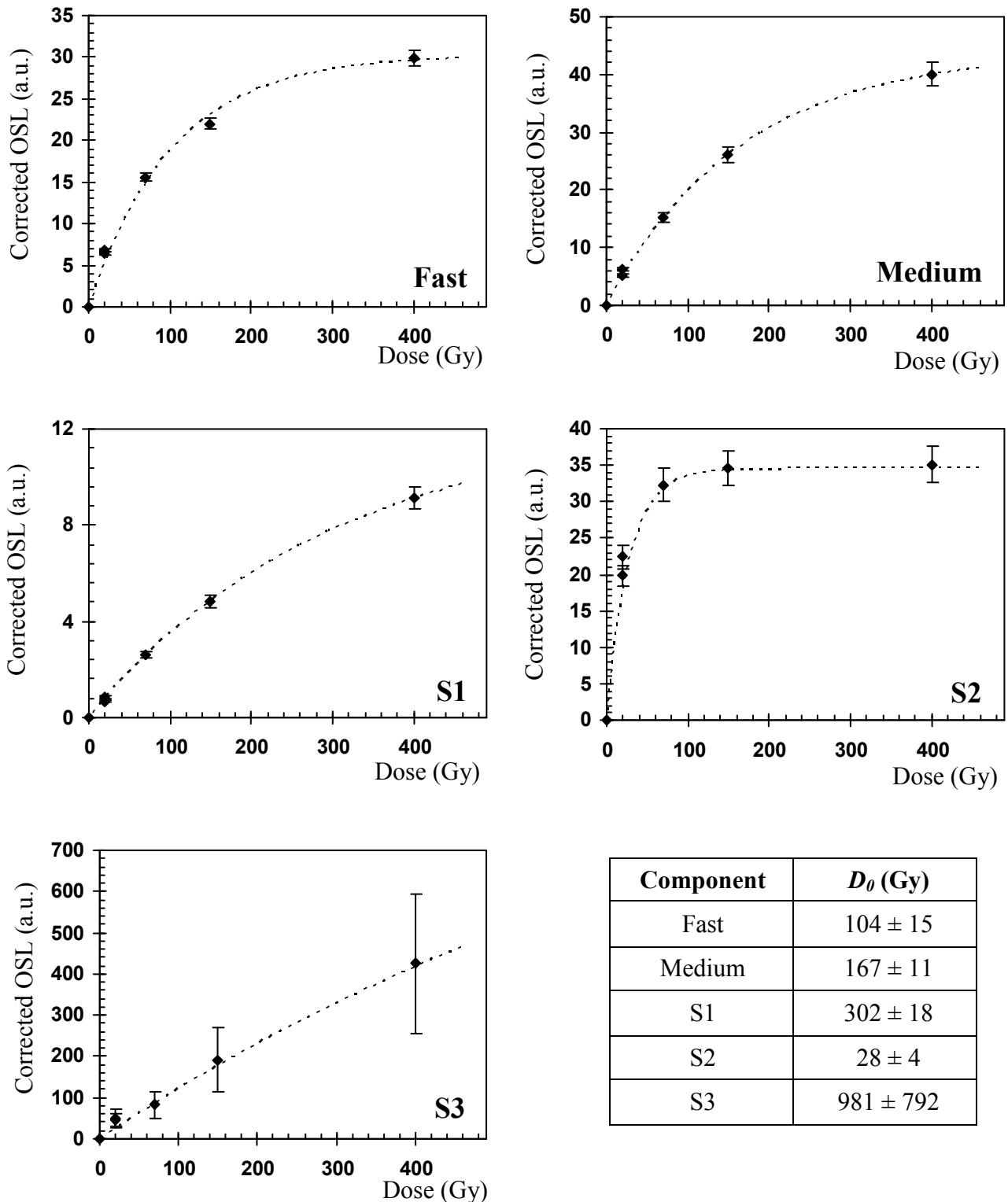
Fig. 6.10 Component-resolved single-aliquot regeneration growth curves for sample 319. The data were collected using LM OSL SAR protocol B and deconvoluting the LM OSL to separate the components. The growth curves were fitted to single-saturating exponential functions to obtain D_0 values for each component listed in the table.

With respect to the possible extension of the datable range of quartz, the only component with a dose response significantly larger than the fast component is S3 from the above results. It is also the only component to retain some of its OSL signal after preheating to 500°C (see section 4.7 for further details), suggesting that this component is possibly highly thermally stable. This component, in fact, displays several properties extremely similar to those found by Bailey (2000a) for the 'slow' CW OSL component. The use of component-resolved dating for dating samples beyond the range of the fast component will be discussed in section 7.3.

One concern is that the measurement conditions (LM OSL to 36mWcm^{-2}) did not allow the peak of component S3 to be recorded. This may have an effect on the appropriateness of the deconvolution. Due to the measurement duration required, the LM technique is not the most convenient method of observing this component. Additional measurements were made by CW stimulation, which was subsequently converted to pseudo-LM OSL (as outlined in section 3.4) to attempt to observe the peak of component S3 and investigate the response of the peak position to various given doses. [Component S3 had been previous fitted to a general order equation and it was expected that the peak position of component S3 should shift to shorter times, i.e. display non-first order behaviour]

A bleached single aliquot of sample SL203 was given a laboratory dose and preheat to 280°C for 10s. A short LM OSL measurement (100s, 0 to 32.5 mWcm^{-2} at 190°C) was performed to deplete the fast and medium components immediately followed by 10 000s CW OSL at full power at 190°C. The CW OSL decay was subsequently transformed to a pseudo-LM OSL curve equivalent to LM empirical measurement of 20 000s. The pseudo-LM OSL following doses of 200, 517 and 1000Gy are shown in Fig. 6.11a. Components S2 and S3 are clearly labelled. The peak of component S3 was visible at the doses of 500Gy or higher. Significant movement of the S3 peak was observed, indicating that non-first order kinetics is involved.

The data were fitted to general order equations to obtain magnitude of component S3 and to obtain a rough regenerated growth curve (components S1, S2, S3 fitted to data). Fig. 6.11c shows the change in peak position of component S3 calculated from the fits (using equations for t_{peak} from table 3.1. The peak position variation with dose could be approximated to a power law (as expected from equation 3.23 for t_{peak}), equation given in the figure. The magnitude of component S2 was used to correct for sensitivity change. Since it was known that S2 would be fully saturated at doses higher than 150Gy (as observed for all the samples investigated) any change in magnitude of this component was assumed to be due to

sensitivity change only, and therefore it could be used to correct the sensitivity of component S3, assuming that the sensitivity of both components changes proportionally. [However, it is also possible that the fitting of S2 is influenced somewhat by the size of S3 – therefore some error may be present due to this]

The growth curve calculated is shown in Fig. 6.11d. The dose response was approximated by a single-saturating exponential function. The D_0 value obtained for this sample appeared slightly lower than for the other samples, using LM OSL measurements where the peak of S3 was not observed. However, $D_0 = 408$Gy is still considerably higher than found in general for the other components, and this component appeared to still display significant growth at 1000Gy. Unfortunately, various constraints dictated that no repeat points or higher doses could be obtained at the time of measurement that could validate the method of sensitivity correction used. Therefore the dose response obtained using this method is currently provisional.

Further investigation of component S3 is required, especially in terms of quantifying thermal stability and developing some measurement protocol for obtaining D_e estimates more easily. In respect of the non-first order nature of this component it is noted that it will not be possible to take integrals to obtain the dose response (as done for normal SAR dating methods, see section 6.2, and by Bailey (2000a) using the slow component) unless the total light-sum of the OSL component measured to full depletion is used, due to the change in the detrapping rate with given dose. This would result in misleading information if a constant integral width and position was used, as the proportion of the total OSL summed would vary with dose.
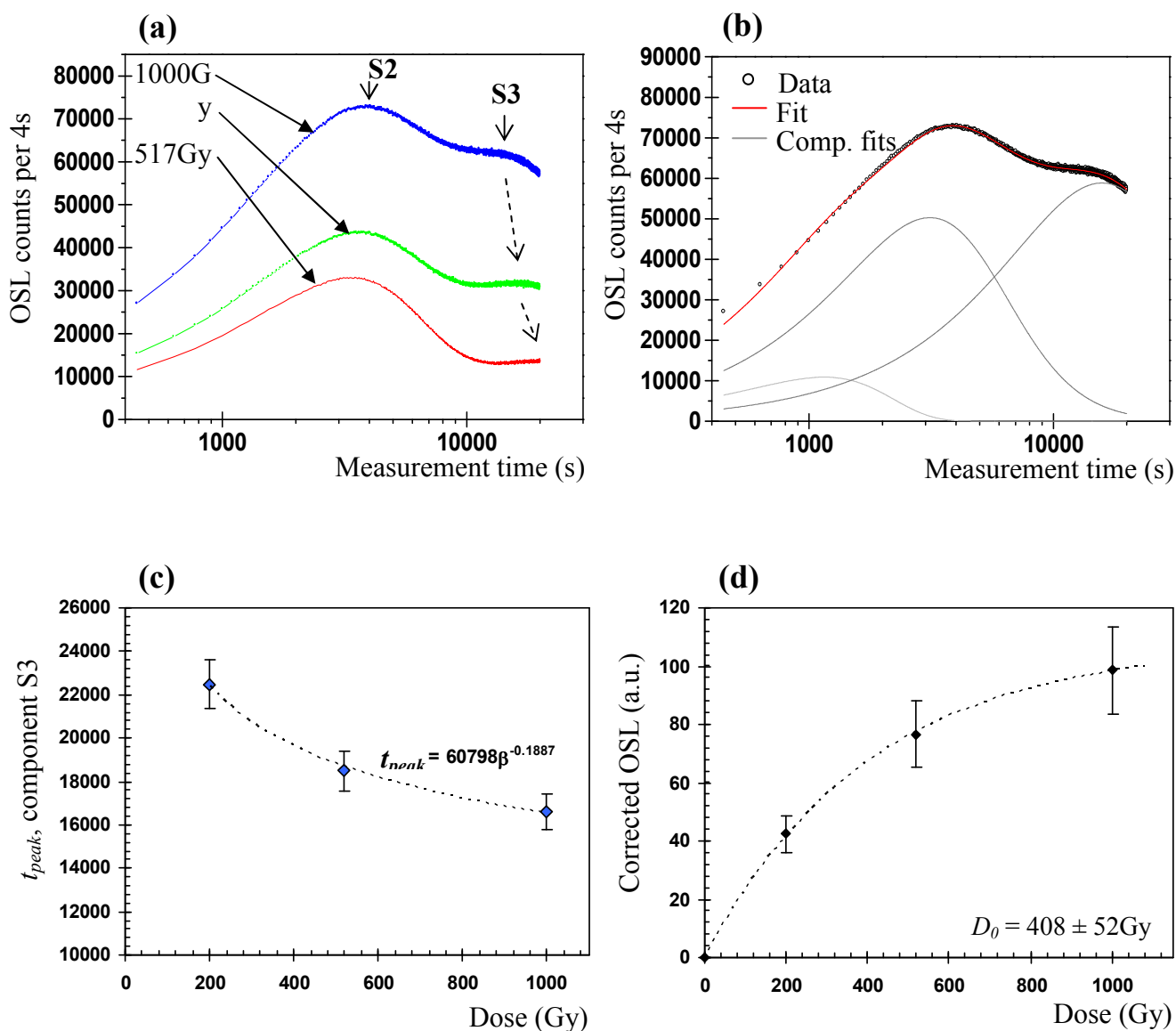
Fig. 6.11 (a) Pseudo-LM OSL curves for components S2 and S3 from sample SL203 following various doses. CW OSL measurements were made at 190°C, full power and transformed using the method described in section 3.4. Component peaks of S2 and S3 are labelled. The peak of S3 shifts to shorter times at high doses. (b) Example fit of 1000Gy data to three components S1, S2 and S3 (general order) (c) graph showing the fitted peak position of component S3 vs. given dose (d) Regenerated growth curve for component S3 sensitivity corrected using the magnitude of component S2. The growth curve was fitted to a single saturating exponential to find the D_0 value given in the figure. See section 6.3.2 for further details.

6.3.3 Trapping probability

In order to obtain quantitative information concerning the relative trapping probabilities of the quartz OSL components the regeneration dose response within the initial linear response range was used. The equation for the rate of change of trapped charge, n, during trap filling is given as:

$$\frac{dn}{dt} = A_n(N-n)n_C \qquad [6.2]$$

using the same nomenclature as given in equations 4.1 to 4.3. If the maximum irradiation is limited such that $N \gg n$, i.e. the maximum dose is limited to well below saturation level, within the linear dose response range, equation 6.1 can be simplified to:

$$\frac{dn}{dt} = A_n N n_C \qquad [6.3]$$

And therefore,

$$n_R = A_n N n_C t_R \qquad [6.4]$$

where n_R is the final trapped charge concentration after dosing and t_R is the total irradiation time. Given that t_R is proportional to the total dose, D, it follows that

$$n_R \propto N A_n D \qquad [6.5]$$

assuming that n_C is constant. Consequently, from a plot of regenerated growth (effectively plotting n_{max} vs. D) the slope of the dose response within the linear range is proportional to $A_n N$. Dividing the slope by N, proportional to the saturation level, should give relative trapping probability.

To investigate this for the quartz components the regeneration growth curve data from Fig. 6.8, was re-examined using only maximum dose of 20Gy (10Gy for component S2). The procedure to obtain these data was described in the previous section, 6.3.1. The data from Fig. 6.5 were used to obtain the trapping probability from Component S3 for the same sample, as the doses used in Fig 6.8 were not high enough to get data from S3. The trapping probabilities of all the components relative to the fast component are shown in Table 6.1.

The initial slope of the dose response curve can also be related to D_0. The definition of D_0 is the dose at which the slope of the dose response curve is 1/e of the initial slope. By differentiating equation 6.1 with respect to dose, β, one obtains the rate of change of intensity of OSL signal:

$$\frac{dL}{d\beta} = \frac{L_{max}}{D_0} \exp\left(-\beta / D_0\right) \qquad [6.6]$$

If, once again, the linear range of the dose response is used only then $\beta << D_0$. Following this the exponential term tends to the value 1, i.e.:

$$\frac{dI}{d\beta} = \frac{L_{max}}{D_0}$$

[6.7]

The rate of change within this dose range is a constant (therefore equation 6.7 is the slope of the linear response). Using equations 6.3 to 6.5 it follows that:

$$A_n \propto \frac{1}{D_0}$$

[6.8]

Consequently, since for most of the samples on which the LM OSL SAR procedure was applied the doses used were not within the linear range, the D_0 values obtained from the fits to the data have hitherto been used instead to obtain the relative trapping probabilities of the OSL components. These values are included in Table 6.1.

Sample	A_{Fast} (s⁻¹)	A_{Medium} (s⁻¹)	A_{S1} (s⁻¹)	A_{S2} (s⁻¹)	A_{S3} (s⁻¹)
TQN	1	0.55	0.48	2.10	0.22
319	1	0.62	0.35	3.71	0.11
TQL	1	0.88	0.89	2.22	0.08
SL203	1	0.67	0.45	2.51	0.17

Table 6.1. Empirically obtained relative trapping probabilities of the OSL components from several samples. See section 6.3.2 for further details.

With the exception of sample TQL the relative trapping probabilities of the OSL components from the different samples used are similar. Reiterating discussion from section 6.3.2, variation in the relative trapping probabilities between samples may result from differences in the proportions and total concentrations of the OSL component traps and centres in different samples.

Numerical modelling should provide further insight into the magnitude of the effect on variations of trapping state concentrations. The calculated data from table 6.1 can be used to

empirically constrain general numerical models such as the one developed by Bailey (2000b), as can the other trap parameters estimated from empirical data described in previous chapters. In the first general kinetic model for quartz OSL and TL by Bailey (2000b) the fast and medium OSL components were incorporated, as being the most relevant for normal OSL measurements relating to dating. The trapping probabilities of these components were not measured directly as above due to lack of precision in MAAD data, but through constraints given by a series of other OSL measurements (e.g. photo-transfer, dependence of form on prior partial bleaching). Through an iterative process the absolute values obtained for the trapping probabilities of the fast and medium components were 1e-9 and 5e-10 respectively. The ratio of these values is approximately what has been observed in table 6.1. The trap parameters found from this experiment and those described in previous chapters are included in further refinements of the Bailey (2000b) general model to produce an even more widely applicable model. The next generation model is described in Bailey and Singarayer (2002) but further discussion relating to this is outside the scope of the present study.

6.4 Effect of ionizing radiation type

The main ionizing radiation types in the natural environment relevant to dating are alpha particles ($_{2}^{4}He(\alpha)$), beta particles (electrons), and gamma rays. The penetration range of each type of radiation within quartz crystals was discussed briefly in section 2.3. As well as the difference in penetration, the efficiency of luminescence production varies with radiation type, depending on the LET (linear energy transfer) of the radiation. In general high LET radiation is found to be less efficient at inducing luminescence than low LET radiation (McKeever, 1985). For example, the energy from heavy alpha particles is deposited in dense, localised, pseudo-cylindrical volumes along the track of the particle. The traps within the path of the particle may become locally saturated, reducing the sensitivity of the grains. In comparison, the beta particles and gamma rays are lightly ionising in nature (low LET), producing more continuous, uniform ionization.

When considering irradiation with alpha particles, the low efficiency is accounted for by incorporation of a multiplication factor, a-value, which gives a ratio of OSL per unit of alpha radiation to OSL following beta or gamma radiation. In this section the characteristic a-value for each of the quartz OSL components was investigated briefly.

Previously annealed sample EBSan that had been given an alpha dose of 10Gy was preheated to 260°C for 10s before LM OSL for 3600s at 160°C to measure the OSL induced by the alpha dose. The aliquot was bleached at 180°C for 8000s, which was noted to reduce the

OSL to background levels. A 10Gy beta dose was then given, followed by further preheat and LM OSL measurement. To obtain the a-value for each component the LM OSL from the alpha and beta dosing were fitted and $n_0(\alpha) \, / \, n_0(\beta)$ = a-value, was calculated. No sensitivity correction was performed for this experiment. The sample had been annealed and sensitized previously so sensitivity change was likely to be small. Moreover, the absolute values obtained were not of as much interest as the relative a-values of the OSL components.

The recorded LM OSL is presented in Fig. 6.12a. That induced by the alpha dose is significantly smaller than the beta dosed LM OSL. The inset shows the same data having normalised the first peak heights to be equal. In doing so the difference in the form of the second peak (component S2) is immediately apparent. This suggested that the dose received by component S2 is smaller than the easy-to-bleach components. The LM OSL for this sample was approximated to only three components – fast, medium and S2 (indicated by peak positions). Even though no component S1 was observed in this sample the trap parameters of the other components present are unaffected (i.e. approximately the same as for other typical samples), demonstrating that the signals are relatively independent. The interaction between the components is minimal.

Fig. 6.12b shows SAR growth curves for each component with the alpha dosed LM OSL as the natural (zero dose) and the beta 10Gy as the regenerated curve with assumed zero point at zero dose. Such low doses were assumed to be within the linear range for all components, and therefore a linear fit to the data was used. From this the a-values estimated, as given in the figure, were 0.073±0.005, 0.077±0.008 and 0.058±0.01 for the fast, medium and slow components respectively. The fast and medium components produce values in agreement, within errors. The slow component a-value is lower. The reason for this is at the moment uncertain. It may be due to the alpha dose responses being different to the beta dose responses, and more significantly different in component S2.

In a study of optical dating applied to British archaeological deposits, Rees-Jones and Tite (1997) calculated a-values for a number of fine-grain quartz samples. Values between 0.032 and 0.043 were obtained; considerably lower than found here. This may result from some sensitivity change that may have occurred despite annealing and sensitizing the sample prior to measurement. A more detailed study using a full SAR procedure with sensitivity correction performed on various samples would be necessary in order to resolve this issue.

(a)

(b)
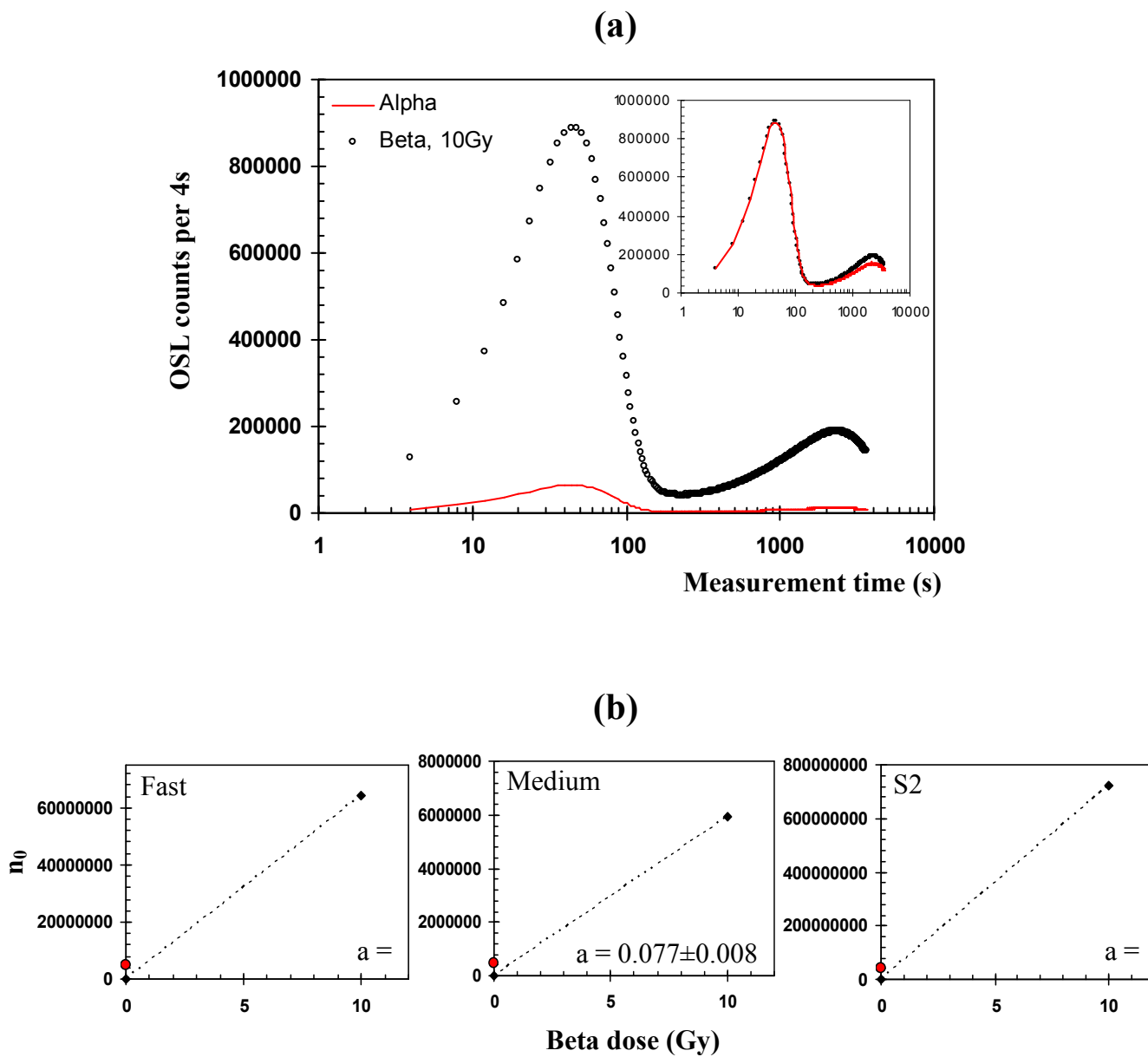
Fig. 6.12 (a) LM OSL measurements at 160°C following 10Gy alpha and 10Gy beta doses and preheat to 260°C on previously annealed sample EBSan. Inset shows the same data with the first peak maximums scaled to be equal in both LM OSL curves. (b) Regenerated growth curves from each OSL component. Red point is the alpha dose intensity; black points are beta dose intensity with a linear fit. This data was used to find the a-value from each component, given in the legend. See text section in section 6.4 for further details.

6.5 Summary

In chapter 6, attempts to develop a measurement protocol to obtain equivalent doses from each of the OSL components were discussed. Ideas were drawn in and considered from the various approaches used for normal optical dating, as well as the few attempts made previously to obtain component-resolved D_e estimates. The problems of complete bleaching of OSL, given the extremely slow depletion rate of component S3, and sensitivity correction were investigated. A single-aliquot regenerative-dose procedure incorporating LM OSL measurements produced reasonable results, and was tested via dose recovery experiments described in the text.

A subsequent aim of this section was to observe/record the saturation and dose response characteristics of the components. In all cases regenerated growth curves were well approximated by single-saturating exponential functions. The saturation doses of the fast, medium and component S1 were found to be fairly similar (medium and S1 slightly larger than the fast). Component S2 saturated at very low doses whereas the S3 was found to still be growing after doses as high as 1000Gy. Similar responses were observed in all the samples investigated. However, due to the exceedingly lengthy measurement protocols the number of aliquots used from each sample was limited. Therefore, the representativeness of the sub-samples used was perhaps not tested sufficiently, although the degree of similarity even between samples suggests that dose response characteristics may be fairly consistent between samples.

Component S3 is the only OSL component to show potential, in terms of dose response, for significantly extending the upper dating limit of quartz, as first suggested by Bailey *et al.* (1997). However, due to its slow optical depletion rate and non-first order kinetics it is difficult to measure. The thermal stability of this component needs to be quantified and the likelihood of bleaching in the natural environment investigated to fully assess the feasibility of its use for this purpose. The issue of bleachability is discussed in section 7.2.

Chapter | 7

7 | APPLICATIONS OF COMPONENT-RESOLVED OSL TO OPTICAL DATING

7.1 Introduction

This chapter reports a series of measurements aimed at using the properties of the OSL components (described in previous chapters) to address certain problems in optical dating. Several different applications will be discussed. The properties with the greatest potential are the difference in response of the components to stimulating photon energy, dose and thermal transfer, having possible applications for identification of incomplete resetting, extending the datable upper limit of quartz and correcting samples suffering from recuperation.

7.2 Identification of incomplete resetting

7.2.1 Introduction

A critical assumption for the reliability of OSL dating is that optical resetting of the OSL signal to zero or negligible levels occurs during sediment transportation. The likelihood of full resetting depends on several factors that vary considerably with depositional environment, including both the duration of exposure to light and the natural stimulating spectrum (as discussed in section 5.2.1). For depositional environments that have short transport durations (e.g. colluvial), and/or where there is considerable attenuation and filtering of the solar spectrum, the assumption of complete resetting becomes increasingly difficult to accept. For example, in fluvial environments the higher photon energy part of the spectrum, more efficient at bleaching, is strongly attenuated through water (Berger, 1990).

The presence of unknown residual signals following incomplete resetting would result in age over-estimation. The severity of the overestimate depends on the relative sizes of the residual and true burial dose and therefore, the younger the sample (smaller burial doses) the greater the effect of incomplete resetting.

A number of authors have obtained evidence for satisfactory resetting of aeolian sediments in studies where young sediments have been dated, e.g. Huntley *et al.* (1985), Stokes (1992), Berger (1995) and Duller (1996). Similar studies of various recent deposits from fluvial environments have produced mixed results. Evidence for poor bleaching has been found in several studies, e.g. Rhodes and Pownell (1995), Rhodes and Bailey (1997), Berger (1990)

and Olley *et al.* (1998). Encouragingly, results reported by Stokes *et al.* (2001) from a study of modern fluvial sediments from the Loire River system (France) indicated that resetting in fluvial environments is possible.

Methods to assess the extent of prior bleaching currently available are based on either analysis of OSL signal form (using the principle that the components bleach at different rates and hence the form of the OSL will be modified by prior partial bleaching), e.g. Bailey *et al.* (1997), Bailey (2002b), or interpretation of D_e distributions, e.g. Olley *et al.* (1998). Distribution methods rely on the heterogeneity of bleaching to produce recognisable D_e distribution shapes from a number of aliquots or grains (Lepper *et al.*, 2000). However, D_e distributions can also be influenced by several other factors, such as beta micro-dosimetry effects, bioturbation or grain-to-grain differences in OSL characteristics (see e.g. Murray and Roberts, 1997) and subjective interpretations of distribution shapes are required. Signal analysis methods, on the other hand, may provide means of distinguishing partial bleaching and micro-dosimetry/mixing effects (e.g. Bailey, 2002a).

7.2.2 Principle of signal analysis methods of detection

A fundamental assumption, in order for this method of analysis to work, is that partial bleaching in the natural environment results in systematic modification of the form of the OSL signal, i.e. the main stimulating photon energies are such that the photoionization cross-sections of the components (critically the fast and medium) are significantly different, so that preferential bleaching of the fast component takes place. Following partial bleaching the residual signal in the medium component (and other harder-to-bleach components) would be expected to be larger than in the fast component. Therefore, the medium should yield a greater final age than the fast component (age(fast) < age(medium) < age(S1) etc.), from thermally stable traps, and is a trend that can be formed only through partial bleaching. Only after complete resetting will the age obtained from all the OSL components be equal.

The 'shine plateau' technique was first suggested by Huntley *et al.* (1985) and applied to multiple-aliquot additive-dose data by several authors since (e.g. Stokes, 1992). The idea being that if all components were completely reset, the D_e obtained from all portions of the OSL decay should be the same. Hence, plotting D_e obtained from successive portions of the OSL decay vs. illumination time should yield a flat D_e 'plateau'. If partial resetting has occurred prior to deposition then a rising plot should be observed, since the D_e from the later portions of the OSL decay will be relatively richer in medium component, which retains a larger residual dose (provided the components are thermally stable). More recently Bailey

(2000a) concluded that the interpretation of shine-plateaux obtained using multiple-aliquot methods is not straightforward and may give results that cannot be correctly interpreted to obtain information about resetting. However, Bailey (2002b) found that shine-plateaux analysis applied to single-aliquot regenerative-dose (SAR) was indeed sensitive to partial bleaching and may be useful for identifying partially bleached sediments. For plots of D_e as a function of measurement time the new term $D_e(t)$ plot was introduced to replace 'shine-plateau', and will be referred to as such henceforth. The principle of $D_e(t)$ analysis is demonstrated in Fig. 7.1.

Using $D_e(t)$ analysis each integral remains the sum of several OSL components but similar information concerning the degree of resetting can be obtained from D_e estimates from each OSL component, using similar measurement protocols to those described in Chapter 6. Through measurement of LM OSL, and deconvolution to separate the contributions from the components, a D_e from each can be obtained. Following the same principle as above, if D_e (fast) = D_e (medium) etc. indicates that the sediment had been previously fully reset. On the other hand, D_e (fast) < D_e (medium) etc. suggests incomplete resetting of the sediment. The components most relevant to optical dating are the fast, medium, i.e. incomplete resetting in these components would result in age overestimations using standard (SAR) techniques.

The dependence of depletion rate of quartz OSL on illumination wavelength has been reported in several studies (e.g. Spooner, 1994; Huntley *et al.*, 1996) and in section 5.3.1. Faster depletion is observed at higher photon energy (shorter wavelength). Further, as shown in section 5.3.1, the <u>relative</u> bleaching rate of the fast and medium components is also dependent on photon energy. Therefore the bleaching wavelengths, which vary considerably in different depositional systems, will have an effect on the efficacy of signal analysis techniques to detect partial bleaching. Under the solar spectrum from a solar simulator the ratio of optical decay rates of the fast and medium components was found to be ~3 (see section 5.3.2). Using solely UV (375nm) then the ratio calculated was closer to 1.4 (section 5.3.1). Since under most conditions the daylight spectrum is richer in short wavelengths the experimental data obtained in previous sections suggests that for bleaching due to daylight, as occurs for aeolian transport, the fast and medium components will have very similar bleaching rates. This may reduce the ability of the signal analysis methods described above to detect partial bleaching. However, in the aeolian environment optical resetting is highly likely to be complete prior to deposition (e.g. Stokes, 1994) as sediment transport times are in general at least of the order of minutes to hours.

Grains transported and deposited under water (e.g. 'fluvial' sediments) are much less likely to be exposed to strong daylight and therefore adequate bleaching can not be assumed (Aitken, 1998). Reduction in the absolute intensity of the light reaching sediments underwater and filtering of the daylight spectrum due to the stronger attenuation of shorter-wavelength light (by solid particulates and chlorophyll, according to Berger, 1990) are expected in such environments. In a study of the effect of submersion on the natural daylight spectrum, Berger (1990) found that in turbid conditions the higher-energy part of the incident solar spectrum (<400nm) was effectively removed by >30cm of water. Severe reduction in the 400-500nm band of the daylight spectrum was also observed at depths of 30cm and by a depth of 2m this part of the spectrum was almost entirely removed. Therefore fluvial sediments are more likely to be partially bleached prior to deposition. Coincidentally, the long-wavelength bleaching spectrum should mean the bleaching rates of the fast and medium quartz components are considerably different. The ratio of fast to medium detrapping rates varies from ~3.7 at 430nm to 31 at 590nm at ambient temperature (section 5.3.1). Therefore, signal analysis methods of investigating partial bleaching should be more applicable to such depositional environments.
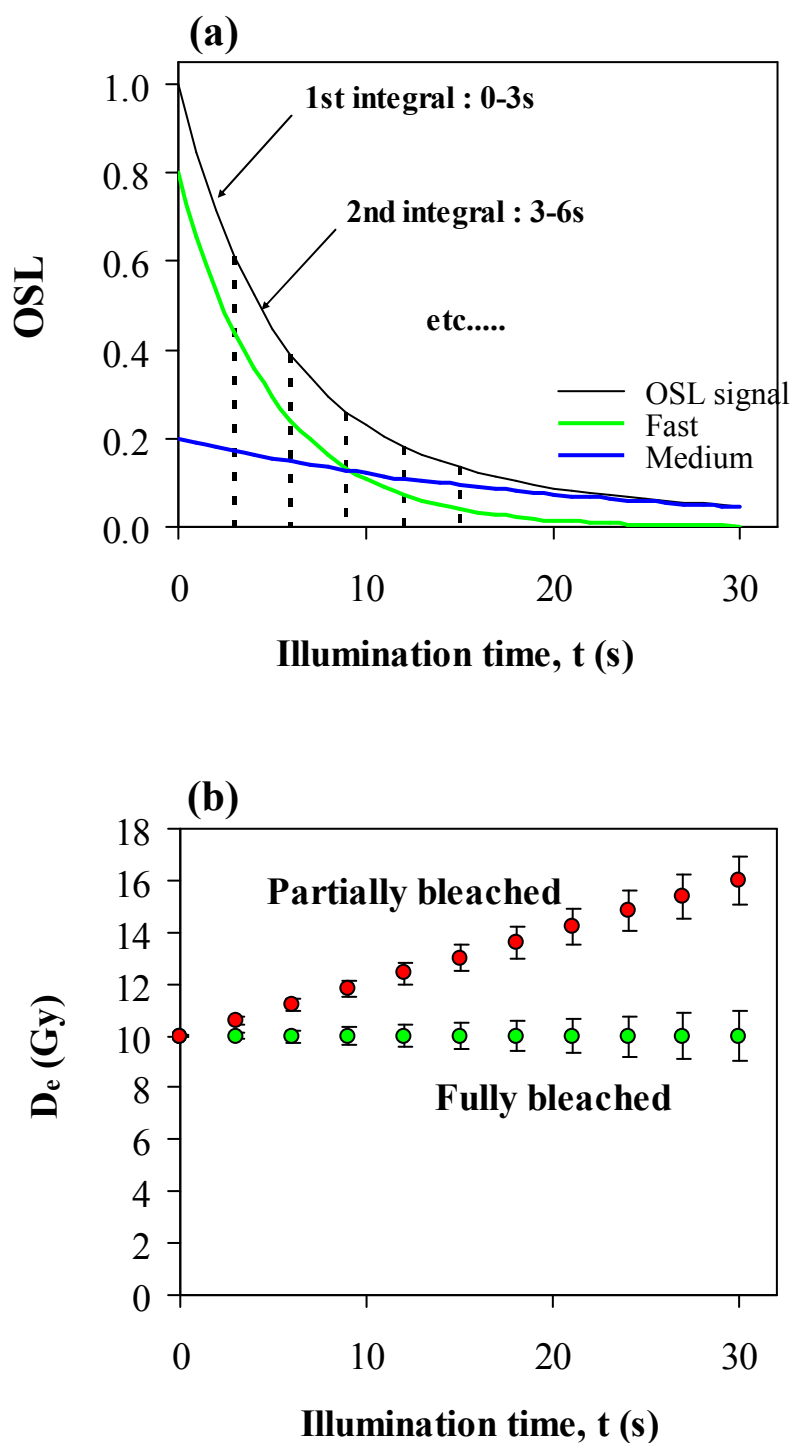
Fig. 7.1 Schematic demonstration of SAR $D_e(t)$ plots (a) OSL decay – fast and medium, take successive integrals to find D_e as a function of measurement time: plotted in (b) for fully bleached flat plot and partially bleached rising plot.

7.2.3 Survey of modern samples: extent of resetting

Testing the completeness of resetting has previously involved: dating of samples with independent chronological control e.g. radiocarbon analysis, (e.g. Murray *et al.*, 1995), direct measurement of the resetting rates/duration (e.g. Gemmell, 1997), or evaluation of the equivalent dose (D_e) from modern (i.e. <500a) samples (Stokes, 1992, Stokes *et al.*, 2001). Using multiple aliquot techniques, Stokes (1992) surveyed young (modern) sediments from a variety of depositional environments, for which observed non-zero D_es were likely to represent residual OSL signals, obtaining promisingly low equivalent doses (typical values ranged from 0.05-0.3Gy). Stokes *et al.* (2001) found similarly encouraging results for fluvial systems applying the single-aliquot regenerative-dose (SAR) technique (Murray and Wintle, 2000). In this section (and results echoed in Singarayer *et al.*, 2002a) a wider range of young/modern samples (less than 700 years) has been investigated. Various procedures were employed to assess the extent of bleaching of samples from different depositional environments. Samples used in Stokes (1994) and Stokes *et al.* (2001) were reanalysed in addition to samples collected specifically for this study (see Appendix A for sample details).

In the initial survey of all the samples a D_e was obtained for each using the standard SAR protocol (Murray and Wintle, 2000). The details of the procedure used are given in Singarayer *et al.* (2002a, see Appendix C). The precision of the SAR D_e estimates was an improvement on previous MAAD results (Stokes, 1992, 1994). The final D_e estimates for all samples are plotted in Fig. 7.2, grouped according to depositional environment to make clearer the general extent of resetting observed from each sample category.

With the exception of three samples (901/4, 901/3 and 838B/1, all taken from sediments layers >1m deep and expected to give non-zero D_e) the aeolian samples gave D_es below 0.2Gy, indicating that full, homogeneous resetting has taken place. This is to be expected given the lengthy transport durations and exposure to the full sunlight spectrum. The coastal sediments displayed similarly low D_e estimates. The fluvial and colluvial samples, however, produced more scattered results including higher D_e estimates. The non-zero D_es are expected to result primarily from heterogeneous, partial bleaching.
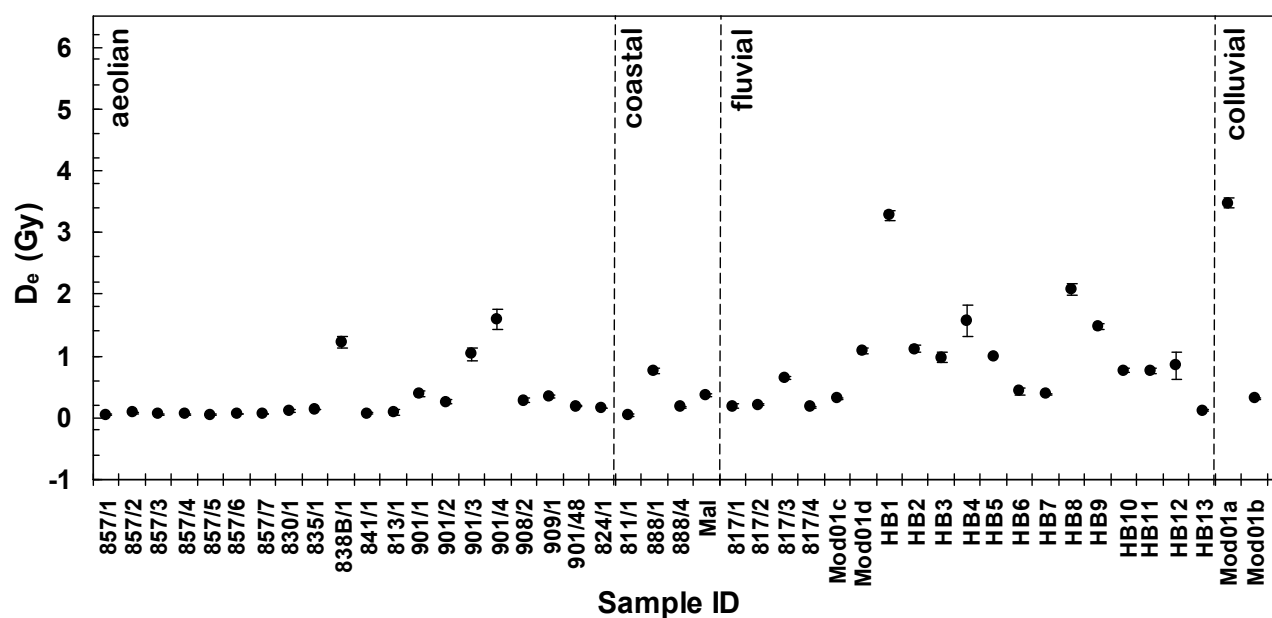
Fig. 7.2 D_e estimates for 45 modern samples obtained using a SAR measurement protocol (Muarray and Wintle, 2000) with a fixed preheat at 240°C. The samples are grouped by depositional type: aeolian, coastal, fluvial and colluvial. Each point is the weighted mean of 6 aliquots (12 aliquots for 'mod01' samples).

Encouragingly, none of the samples from any depositional type displayed a D_e over 5Gy (only four samples D_e > 2Gy). This suggests that even for waterlain sediments, the problem of overestimates due to incomplete resetting is limited to samples ≤20ka. For older samples the magnitude of residual signals is potentially very small compared to the burial dose.

Those samples that displayed significantly non-zero residual doses were subjected to further examination to investigate the use of the signal analysis methods outlined in section 7.2.2 for detection of partial bleaching. These experiments are described in detail in the next section.

7.2.4 Signal analysis investigations

$D_e(t)$ analysis and measurement of LM OSL to obtain D_es from the fast and medium components was undertaken on several of the non-zero De samples. To obtain $D_e(t)$ plots the SAR data was plotted as a function of measurement time. The optical stimulation power had been reduced to 12mWcm^{-2} to reduce the decay rate so that the initial decay of the OSL was spread over a greater number of measurement channels and measured at 130°C, thus allowing D_e calculations up to 10s illumination time.

D_e estimates from the fast and medium components were achieved using a simplified LM OSL SAR approach. Following a preheat of 260°C the natural LM OSL was measured for 200s at 160°C. Regeneration 5Gy and 0Gy doses were given, as well as further preheat and LM OSL measurements. Linear growth was assumed over the dose range used. D_e was found from interpolation.

Two samples have been chosen to illustrate different partial bleaching scenarios. Signal analysis on the first sample, 817/3, is presented in Fig. 7.3. This is a fluvial sediment collected from a point bar sand deposit on the Colorado river, Columbus, Texas (Stokes, 1992, 1994). According to the Stokes (1994) deposition of this sediment took place post 1920. Given an average dose rate of 1Gyka^{-1} the De from this sample should be ~0.1Gy. The mean D_e obtained from 6 aliquots using the SAR method was considerably greater; D_e = 0.64 ± 0.02Gy. D_e (t) plots for the same 6 aliquots (Fig. 7.3) showed systematically rising D_e as a function of measurement time for the first 5 of the aliquots. Such trends should occur only in a sample in which the OSL components have been partially bleached to different degrees, as explained in section 7.2.2. Scatter is observed in the magnitude of the rise in D_e as would perhaps be expected given the heterogeneous nature of bleaching in fluvial environments. Also displayed in the table in Fig. 7.3 are the D_e estimates for the fast and medium components from three aliquots found using LM OSL (an example of which is presented

above the table). Evidence for partial bleaching was observed in aliquots 1 and 2 in that D_e (fast) < D_e (medium), further substantiating the D_e (t) results.

In aliquot 3 D_e (fast) = D_e (medium) was observed, similar to aliquot 6 from the D_e (t) plots, which gave a flat plateau. In these two aliquots the D_e values are larger than the majority showing positive evidence for partial bleaching. It is suggested that the majority of the bright grains comprising these aliquots were hardly bleached at all before the last deposition. This would result in both the most severe overestimate and very little difference in D_e between the components. This is provided that the grains had been fully reset before the previous deposition. Interpretation of all signal analysis methods requires consideration of the last two transport events. Full resetting is assumed to have taken place before the penultimate burial so that the burial doses in the fast and medium prior to the last transport/bleach are equal.

The second sample investigated using signal analysis was 888/1. This sample was collected from Sefton coast, Liverpool, UK. In contrast to the majority of the other samples used in this study independent age control had constrained this sample to the Middle Ages (Pye and Neal, 1993; Stokes, 1994). Therefore a non-zero D_e was expected even in a previously fully reset sediment. The D_e obtained using the SAR protocol on six aliquots was 0.76 ± 0.05Gy. $D_e(t)$ plots from the same six aliquots, presented in Fig. 7.4, showed essentially flat plateaux as a function of measurement time. Due to the low sensitivity of the sample scatter and large errors in the later integrals were observed in all the aliquots, although data obtained from the early integrals are more precise. Using LM OSL on further aliquots equal D_e estimates were obtained from the fast and medium components. The results from both methods of signal analysis suggest that this sample had been fully reset prior to deposition and that the D_e is the result of post-depositional accumulation of signal. The small size of the natural slow OSL components as observed from the LM OSL (Fig. 7.4) when compared to the 5Gy regeneration dose suggests also that even the slowly decaying components had been fully zeroed.

$D_e(t)$ plots

LM OSL
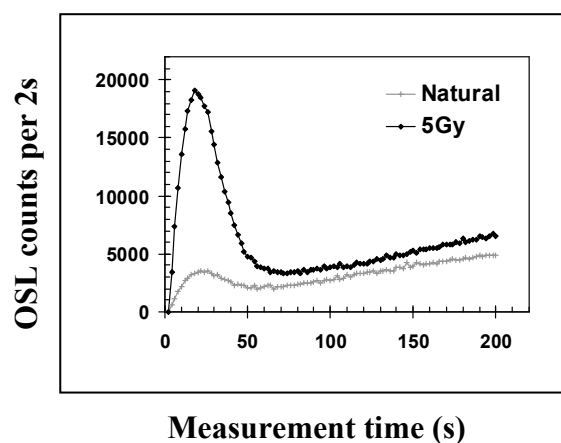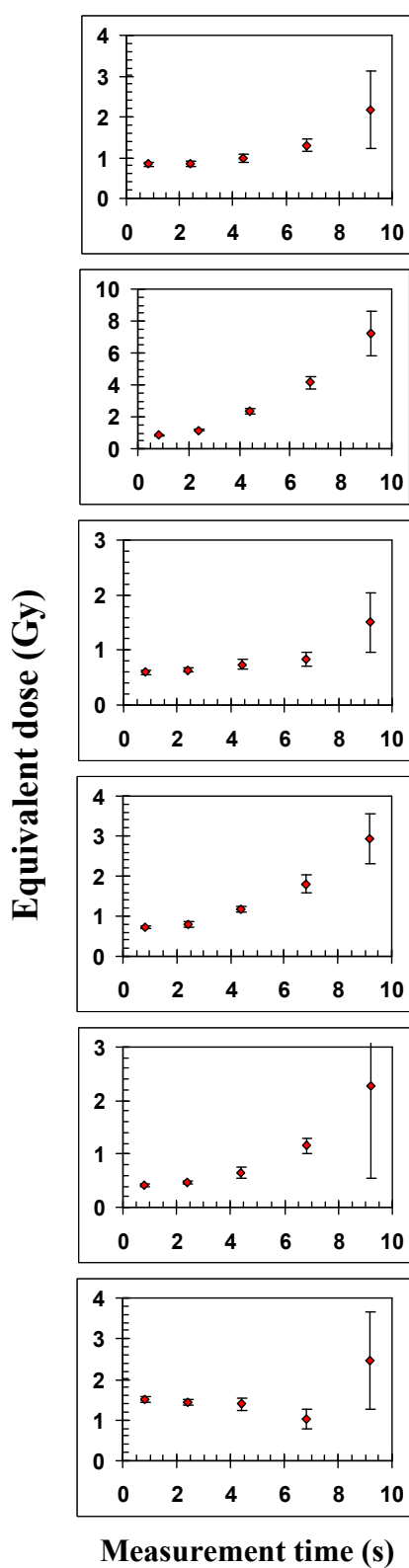
	Fast component De (Gy)	Medium component De (Gy)
Disc 1	0.7 ± 0.02	1.57 ± 0.11
Disc 2	0.49 ± 0.02	0.61 ± 0.06
Disc 3	1.77 ± 0.03	1.79 ± 0.05

Fig. 7.3 D_e(t) plots – D_e as a function of measurement time plotted for 6 aliquots of sample 817/3. Rising plots observed in 5 aliquots suggests partial resetting has occurred. **LM OSL** – D_e estimates from the fast and medium of 3 aliquots was found (example LM OSL are shown above the table). For 2 aliquots D_e (medium) > D_e(fast), also indicative of partial resetting in this sample.

$D_e(t)$ plots

LM OSL
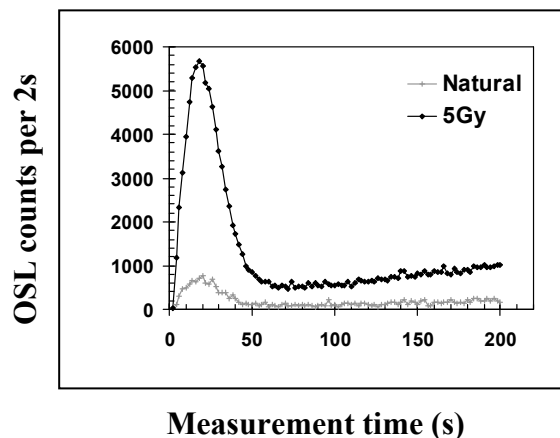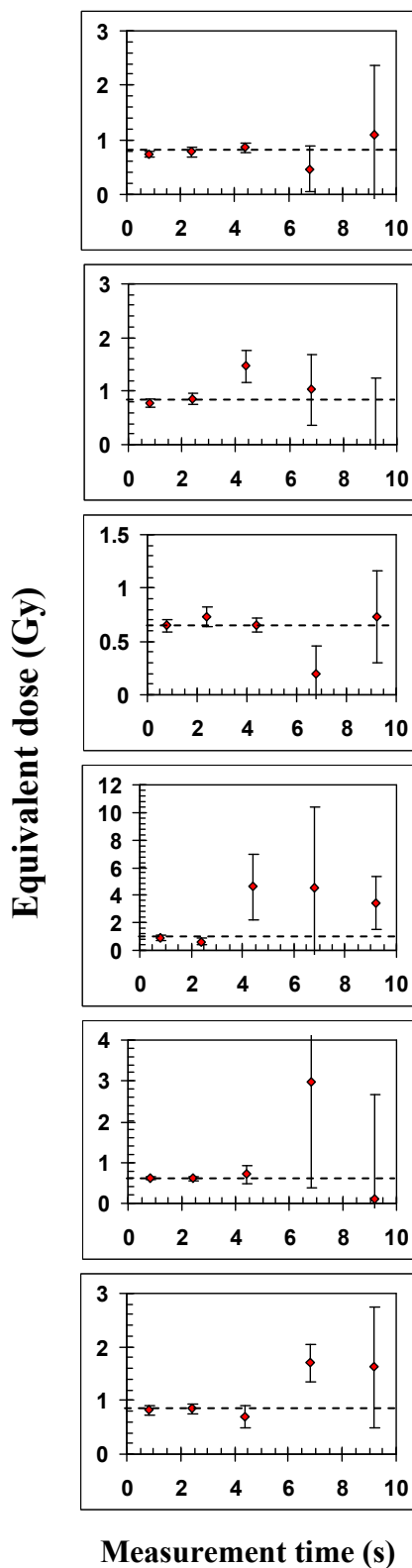
	Fast component De (Gy)	Medium component De (Gy)
Disc 1	0.49 ± 0.02	0.48 ± 0.16
Disc 2	0.51 ± 0.02	0.54 ± 0.1

Fig. 7.4 D_e(t) plots – D_e as a function of measurement time plotted for 6 aliquots of sample 888/1. Flat plateaux are observed in the majority of the aliquots suggesting full resetting had previously taken place. **LM OSL** – D_e estimates from the fast and medium of 2 aliquots was found (example LM OSL are shown above the table). For these aliquots D_e (medium) = D_e(fast).

In the survey of modern (young) samples (Singarayer *et al.*, 2002a) the $D_e(t)$ plots and the LM OSL component-resolved D_es gave corroborating results, as would perhaps be expected given that both techniques have the same basis. Identification of partial bleaching in these sediments was possible using either method. However, in older sediments $D_e(t)$ plots have been observed to decrease with measurement time (S. Armitage, *Pers. Comm.*). Experiments concerning the thermal stability of the quartz OSL components, described in section 4.4, have shown that component S2 is significantly less stable than the fast and medium components (τ = 19ka from isothermal decay analysis). Depending on the relative concentrations of the component trapping states the OSL from S2 may have a significant effect on SAR D_e estimates, especially at later measurements times for $D_e(t)$ plots where the fast and medium are significantly eroded. It is consequently suggested that although the $D_e(t)$ plots work well for younger samples, the observed falling $D_e(t)$ plots in older sediments probably results from the thermal instability of component S2. In the case of a partially bleached sediment it may not be possible to distinguish from the $D_e(t)$ as any rise in D_e may be counteracted by fall from S2. This phenomenon has been further investigated by Bailey *et al.* (2002).

Examples of falling $D_e(t)$ plots from two aliquots of natural sample TQN found using normal SAR techniques are displayed in Fig. 7.5. $D_e(t)$ replacement plots are also shown, as described in Bailey (2002b), where the natural point is replaced with one of the regeneration points (which is removed from the regeneration curve fit) and the $D_e(t)$ relationship recalculated. This plot should yield a flat $D_e(t)$ and was used by Bailey (2002b) to test the analysis method. In Fig. 7.5 the natural $D_e(t)$ fall considerably with measurement time. The replacement plots produce relatively flat $D_e(t)$ indicating that the analysis is appropriate.

One possible advantage of using LM OSL component-resolved measurements is that the contributions from each are separated, and therefore interference from thermally unstable component S2 can be eliminated from the analysis. Described in section 7.3.3 (Fig 7.10) component-resolved D_e estimates for all the OSL components for sample TQN were found using the LM OSL SAR protocol described in section 6.3. The D_e obtained from the fast, medium and S1 components were found to be equal within errors (~210Gy), whereas S2 displayed a very much lower D_e (~57Gy). The $D_e(t)$ from this sample should give a flat plateau given that D_e (fast) = D_e (medium). However, the measured $D_e(t)$ plots (Fig. 7.5) fall due to the contribution from component S2 which has a considerably lower D_e. When the $D_e(t)$ and LM OSL component-resolved results for sample TQN are compared it is clear to see the effect of S2 on the $D_e(t)$ plot.
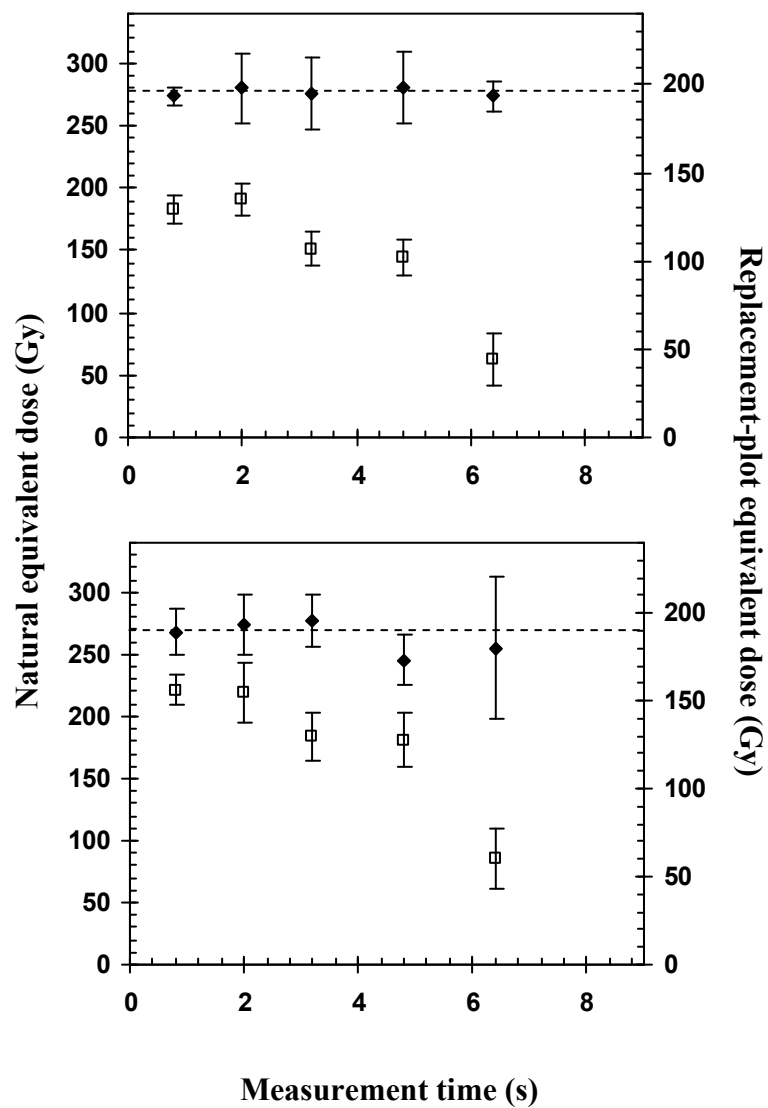
Fig. 7.5 $D_e(t)$ plots for two aliquots of sample TQN. The open symbols represent the natural D_e as a function of measurement time. Filled symbols show the replacement $D_e(t)$ plot, where one of the regenerated doses is used instead of the natural, as suggested by Bailey (2002b); a flat line should be observed.

Potential disadvantages of using the LM OSL SAR procedure to obtain information concerning partial resetting include the relatively complicated fitting routines in comparison with the integrals used in $D_e(t)$ plots and that interpretations are made using only two or at most three D_e values (D_e (fast), D_e (medium) and possibly D_e (S1)), which is only a problem if errors (e.g. introduced by fitting) are large.

In the above experiments partial resetting of magnitudes that may affect standard SAR dating methods (Murray and Wintle, 2000) was investigated, i.e. mainly residuals in the fast and medium components. In consideration of the potential of component-resolved dating, particularly using S3 to extend the upper limit of the datable range, the likelihood of resetting of all the OSL components is an important issue if reliable dates are to be obtained. Therefore, on several of the modern samples LM OSL measurements were made to record all the components. Following a preheat of 240°C for 10s the natural LM OSL was recorded over 7200s at 130°C, 0 – 18Wcm^{-2}. After CW OSL for 5000s at 130°C, 18mWcm^{-2} to bleach further the signal regenerated LM OSL signals were measured after 5Gy and 0Gy doses. Zero LM OSL was observed following the 0Gy dose, indicating that for the doses involved the CW OSL bleach was sufficient to reset the OSL in between measurement cycles.

Data from four samples are presented in Fig. 7.6. The upper two plots of samples 857/2 and 803/1 were collected from aeolian environments (Stokes, 1994). The natural signals in each show no structure and are approximately zero in all components. Measurement of LM OSL compared to CW OSL may not be ideal for observing at such low doses due to the low signal-to-noise ratio obtained that may hide small OSL signals. In any case the natural signal in all components is negligible in comparison to the 5Gy dose. The two lower plots of samples HB8 and 817/3 were taken from fluvial environments, where full resetting of all components is less likely. In the aliquot of HB8 displayed the easy-to-bleach components appear to be reset to a very low level, i.e. there is no measurable first LM peak at ~80s. The slow components were not completely bleached in the natural. Residual D_e estimates were found for component S2 (4.3 ± 0.5Gy) and S3 (5.89 ± 0.9Gy). Using the measurement sequence described above the 0Gy dose produced negligible OSL from any components.

In sample 817/3 the natural appears even less well reset than HB8. Through curve deconvolution equivalent doses for all components were obtained: D_e (fast) = 1.2±0.1Gy; D_e (medium) = 2.4±0.3Gy; D_e (S1) = 7.6±0.7Gy; D_e (S2) = 5.1±0.5Gy; D_e (S3) = 14.3±7.1Gy. None of the components appear to have been completely reset and all have been reset to different degrees. Each component displays a D_e smaller than the next, apart from S2. This

exception is probably due to the thermal instability of this component. A plot of component-resolved D_e versus fitted photoionization cross-section, σ, for this data from sample 817/3 is presented in Fig 7.6 also. This graphical representation is similar to the $D_e(t)$ plots (Fig. 7.1) for which a rising trend (evident in Fig. 7.6) implies partial bleaching.

Although further investigation of a greater number of samples is required these preliminary results suggest that exposure to daylight during aeolian transport is generally of sufficient length to reset all the OSL components. Using the calculated decay constant of component S2 under the simulated solar spectrum at room temperature (section 5.2.2) depletion of S2 to 5% of initial intensity would require 5.5 days. Such prolonged durations of transport are expected for aeolian sediments. The results from fluvial environments are more varied, but suggest that in many cases the slow components will probably retain some residual signal upon deposition.

7.2.5 Discussion

In this section the extent of resetting in samples from various depositional environments was examined. In 45 samples the aeolian examples generally gave D_e estimates close to zero. The maximum D_e obtained from any sample was ~5Gy. From this it was inferred that problems of partial bleaching will in most cases be restricted to relatively young (Holocene-age) sediments. However, this result cannot logically be extended to all samples since all cases are different. Therefore, methods must be developed to assess the degree of resetting prior to deposition. $D_e(t)$ plots and LM OSL component-resolved SAR signal analysis methods were tested in the previous section. When applied to modern/young samples both techniques worked equally well. However, for older samples the results of thermal instability of component S2 dominated any trends in the $D_e(t)$ plots, and so limiting the quality of the information concerning incomplete resetting. In such cases the LM OSL approach could prove invaluable as the contributions from all the components are separated.

Distribution methods of assessing partial, heterogeneous bleaching in single aliquots or single grains were also discussed briefly in section 7.2.1. The difficulty of separating the variation due to various factors including partial bleaching was mentioned as is discussed in detail in Bailey (2002b). In this paper it is suggested that a possible solution might be to take the mean D_e obtained from only the grains/aliquots that show most evidence for full bleaching (as identified using the signal analysis approaches described previously) as this may yield the closest approximation to the true burial age. This approach is recommended by the present author also.

With respect to component-resolved dating, especially given the potential of component S3 as a long-term dating tool, the extent of bleaching of the slow components as found in the last section may limit dating using S3 to aeolian type sediments, or sediments with several 100Gy burial doses (any residual would have negligible effect on final D_e). The fact that no large residual signals (>100Gy) were observed even in fluvial samples is surprising and may suggest that either longer transport times occur than expected or there may be some signal instability.
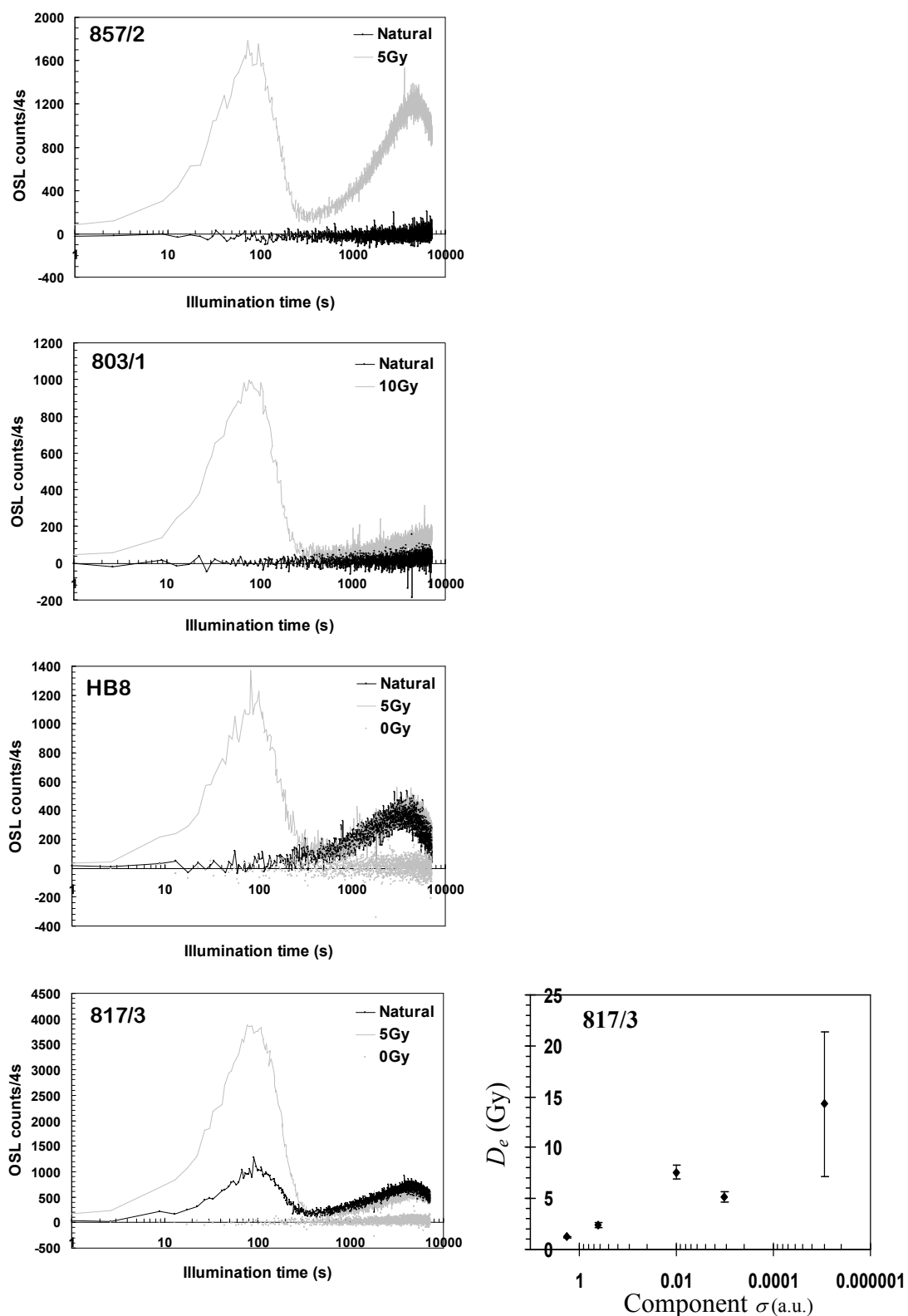
Fig. 7.6 Natural LM OSL from four modern samples (857/2, 803/1, HB8 and 817/3) measured at 130°C up to 18mWcm^{-2}. The LM OSL from a further 5Gy is shown for comparison. For HB8 and 817/3 the LM OSL from a 0Gy dose is shown also. For sample 817/3 a plot of the D_e estimates from all the OSL components vs. fitted photoionization cross-section, σ, is shown.

7.3 Long range dating

The aims of this section were to further investigate the possibility of component-resolved dating techniques developed in Chapter 6 in application to natural samples, and to assess the potential and feasibility of using S3 as a long range dating tool.

The majority of samples used for these purposes were marine and aeolian Quaternary sediments from Casablanca, Morocco. Description of the sampling site, the methodologies used and the results are to be found in the following sections.

7.3.1 Description of the Casablanca sampling sites

The Quaternary deposits at Casablanca have been extensively studied; see Texier *et al.* (1994, 2002) or Raynal *et al.* (2001, 2002) for the most up-to-date summaries. The sediments form a succession of high sea level marine deposits and overlying aeolian sediments spanning the entire Pleistocene. Extensive archaeological materials, including hominid bones have also been found (e.g. Ennouchi, 1972). Thus, the sequence is both of archaeological and geological/climatological significance with an exceptional record of global sea level variations and it is therefore important to obtain a reliable chronology of the area.

The archaeological material lies well beyond the range of radiocarbon, and lies in a time where reliable dating is hard to achieve in many chronometric methods. Two U-series dates on speleothem and AAR measurements have been used on the younger samples (Occhietti *et al.*, 2002). An ESR date on Rhino teeth was obtained by Rhodes *et al.* (1994). Preliminary OSL dates were obtained by Rhodes (1990) and Westerway (1995). Further OSL dates using the SAR protocol (Murray and Wintle, 2000) are described in Rhodes *et al.* (2002).

Samples were collected mainly from the sites of Reddad Ben Ali (RB code), Oulad aj Jmel (OJ sample code), Sidi Abderhamane (SAQ sample code) and Thomas Quarries (TQ sample Code). Fig. 7.7 shows a representation of the sites at Casablanca where samples were taken. The lower samples at Thomas quarries were found to be magnetically reversed (Raynal *et al.*, 1996), providing an additional lower age limit on samples collected below this layer (i.e. TQL and TQK) of 0.778Ma at the Brunhes/Matuyama boundary (Tauxe *et al.*, 1996).

The sediment was well cemented by carbonate deposition (the collection and preparation of cemented samples was explained in section 2.2 and 2.3). For further details see Rhodes *et al.* (2002).
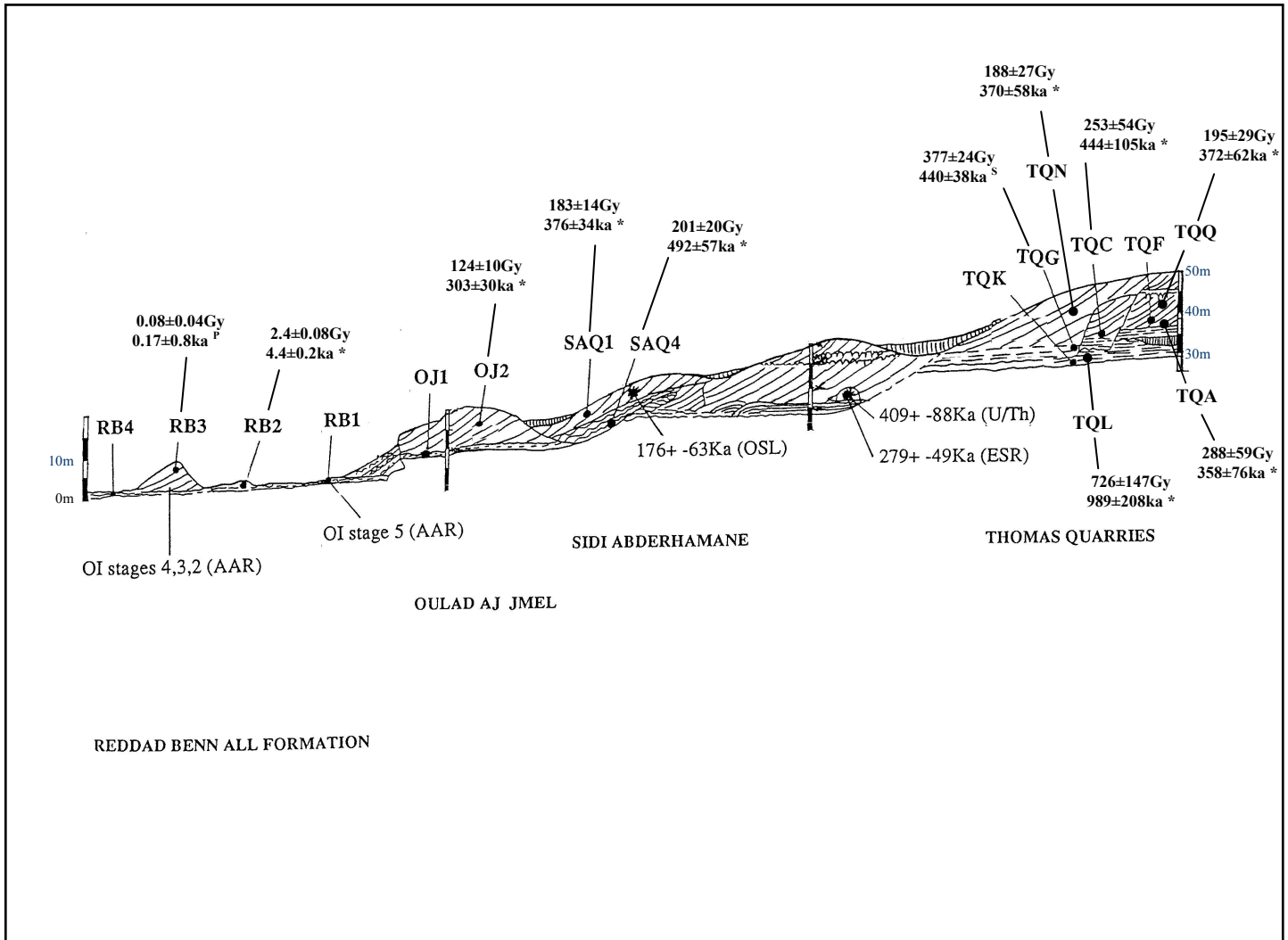
Fig. 7.7 Diagram of the Casablanca site, Morocco. Sampling positions and independent age control are given, including AAR, U/Th, ESR and OSL (all ages shown in **Ka**), modified from Westerway (1995). D_e (in **Gy**) and age (in **ka**) estimates are given for:

* Samples measured by the present author using the SAR protocol (Fig. 7.9) and presented in Rhodes *et al.* (2002).
S Sample TQG dated by using an SAAD slow component method (Singarayer *et al.*, 2000), also published in Rhodes *et al.* (2002).
P Sample RB3 measured by present author using the SAR protocol, not published.

7.3.2 Methods

The first 'slow' component application to the Casablanca site was reported in Singarayer *et al.* (2000) on sample TQG from Thomas Quarries. A single-aliquot additive dose protocol was used that involved a thermal wash of 450°C to deplete the fast and medium components following dosing and CW OSL measurements of 50s at 160°C in order to measure statistically significant counts while minimising the depletion of the slow component. The SAAD growth curve for a single aliquot of TQG is presented in Fig. 7.8. The data fitted well to a single-saturating exponential and from this a D_e of 377 ± 23Gy was calculated. An exceptionally high D_0 value of 2790Gy was also estimated. As stated in Singarayer *et al.* (2000) no in situ dose rate measurements were made for this sample. Therefore the dose rate was approximated using those from adjacent sites. Using this D_e a date of 440 ± 38ka was found by Rhodes *et al.* (2002), which was consistent with the surrounding samples.

In terms of current knowledge of the OSL components it is probable that after a 450°C component S3 was being observed in the CW OSL. Component S3 has been found to display non-first order behaviour (see section 6.3.3) and hence, in taking constant integrals for doses from several hundred to several thousand Gy, different proportions of the OSL signal may be observed at the various doses. Additionally, no sensitivity correction was possible. As a result the measurement sequence used therefore may not be entirely appropriate, if significant sensitivity changes took place or component S3 was significantly non-first order in this sample. Further investigation was not within the scope of this study. The experiments described in this section use the LM OSL SAR procedure outlined in Chapter 6. Due to the lack of reliable dose rate information for sample TQG it was not used in these experiments.

A complete reassessment of all the samples dated in Rhodes *et al.* (2002) on a component-resolved basis was not possible within this study. Instead, one young sample was chosen to investigate the lower limits of the technique, one sample within the range of most of the components was chosen to assess the degree of correspondence between D_e estimates, and one sample of significant age was chosen to investigate the upper datable age limit using component S3.
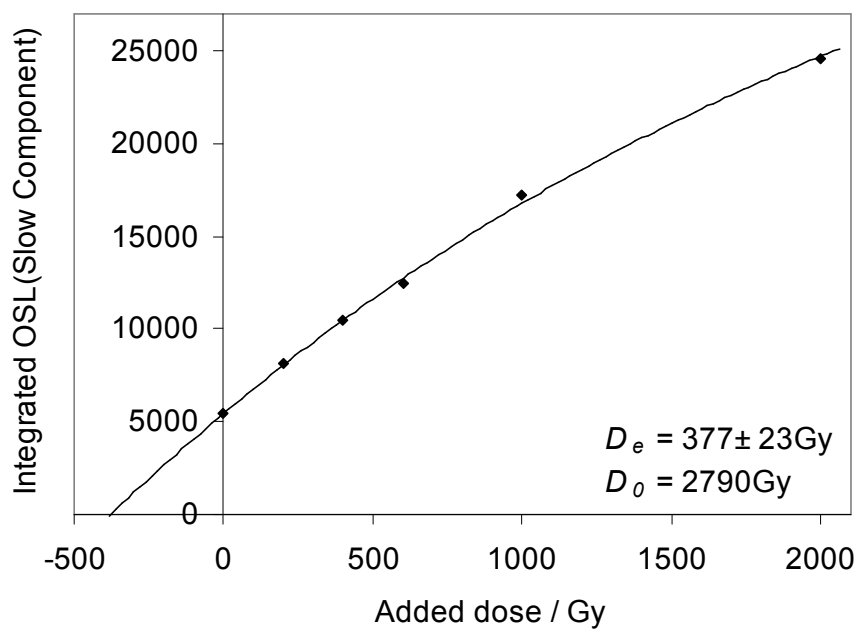
Fig. 7.8 Slow component single-aliquot additive-dose growth curve for sample TQG. The data have been fitted to a single saturating exponential function to estimate De (given in the plot). See text for measurement details, section 7.3.2. [Modified from Singarayer *et al.*, 2000]

To obtain component-resolved D_e measurements the LM OSL SAR protocol (B) developed in Chapter 6 was employed. Regeneration doses were chosen on the basis of equivalent dose estimates found previously and reported in Rhodes *et al.* (2002). The component-resolved regenerated growth curves could all be approximated using the single saturating exponential function given in Equation 6.1. Dose rate data were obtained from either field gamma spectrometry measurements or neutron activation analysis (NAA). The dose rates are explained in detail in Rhodes *et al.* (2002), only the dose rates for the relevant samples will be discussed in the next section.

The ages obtained were firstly compared to the standard SAR results (Rhodes *et al.*, 2002; measured by the preset author) for internal consistency. The SAR procedure used is given in Fig. 7.9. The equivalent dose and age estimates obtained using SAR are given in Fig. 7.7. Comparison to independent age constraints on the sample ages was also made, such as the Brunhes/Matuyama magnetic reversal, to provide further external control.

7.3.3 Results

Equivalent dose results for relatively young sample RB3 are shown in Fig. 7.10. The LM OSL data were fitted to four components only (fast, medium, S1 and S2). It is possible that no component S3 traps were present in this sample. Also it is possible that the detrapping rate of S3 was too slow at such low doses (S3 was found to display dose dependent form, i.e. non-first order behaviour, with larger σ with larger dose) for sufficient charge to be detrapped over the measurement period to be recognised by the deconvolution routine. Dosing the sample to several hundred Gy should allow clear observation of S3, however, no empirical measurements of this kind were made during the experiment. D_e estimates for the other components are given in the Fig. 7.10. Large errors on the D_es result from fitting of the small size of the natural signal. The variation in D_e between the components is considerable.

The ages obtained for this sample are given in Table 7.1. Several of the components are in agreement with the standard SAR date of 0.17 ±0.08ka, and are much younger than the age obtained by Westerway (1995) using MAAD based on gamma dosed samples. Reasons for the discrepancy between the SAR and MAAD ages may be due to the un-normalised data used for the MAAD growth curves. The LM OSL SAR results are in any case in better agreement with the standard SAR data than the previous MAAD age.

The component-resolved SAR growth curve data for sample TQN is shown in Fig. 7.11. The D_e estimates for each of the components are given in the table within Fig. 7.11. All are in

agreement within errors, with the exception of component S2, which has been found from previous experiments to be thermally unstable and therefore in a sample with such a large D_e (from standard SAR results, Fig. 7.9) would be expected to produce an underestimate. The natural OSL is rather close to the saturation dose in the fast and medium components. However, reasonable D_e estimates could be calculated for both. The calculated ages for TQN are shown in Table 7.1. Fairly good agreement with the standard SAR method (where the mean of 10 aliquots was used to obtain D_e) is observed. The average age of TQN from the OSL dates is ~400ka and places the sample at early OI stage 11, consistent with U-series age (done by Schwarz; described in Rhodes *et al.*, 2002) and early uptake ESR ages (Rhodes *et al.,* 2002). For further discussion of interpretation of the OSL ages see Rhodes *et al.* (2002). From the relative ages obtained for the fast and S2 components, and the relative values of A (trapping probabilities) listed in Table 6.1, the lifetime of S2 for TQN was estimated at 1-2ka. This is consistent with the values of lifetime obtained in section 4.4.2 using the method of pulse annealing.

Stratigraphically, the oldest sample collected and prepared from Casablanca was TQL. It was taken from below the magnetic reversal of 0.778Ma (Tauxe *et al.*, 1996). It might be expected that the standard OSL dating signal (i.e. primarily fast component) would be saturated. However, the standard protocol (Fig. 7.9) was still applied to six aliquots. In half of the aliquots the D_e was not measurable as the natural OSL signal size was greater than the regenerated saturation signal size. In an attempt to find some useful results the raw contributions from each aliquot were summed as if having measured one very large aliquot (or 'super-aliquot'). Although almost fully saturated, it was possible to obtain a single D_e, shown in Table 7.1. The final age calculated using this unconventional method, 0.98Ma, is consistent with the stratigraphy, in that it is >0.78Ma.

The component-resolved SAR growth curves for sample TQL are plotted in Fig. 7.12. Regeneration doses up to 900Gy were used with the expectation of a D_e of over 500Gy. It is clear from the figure that the natural signals from the first four components (fast, medium, S1 and S2) are fully saturated. Component S2 seems to display similar behaviour as the standard SAR results whereby the regenerated growth curve doesn't reach the level of the natural signal. Only component S3 continues to grow at doses over 900Gy. Large errors on the data points result from the fact, reiterated from previous sections, that the peak of S3 is not reached in the LM OSL measurement. Nevertheless, a D_e for this component was calculated

of 696 ± 438Gy. The final age estimate of 948 ± 599ka was in agreement with the other SAR result, and also with the B-M boundary lower age limit.
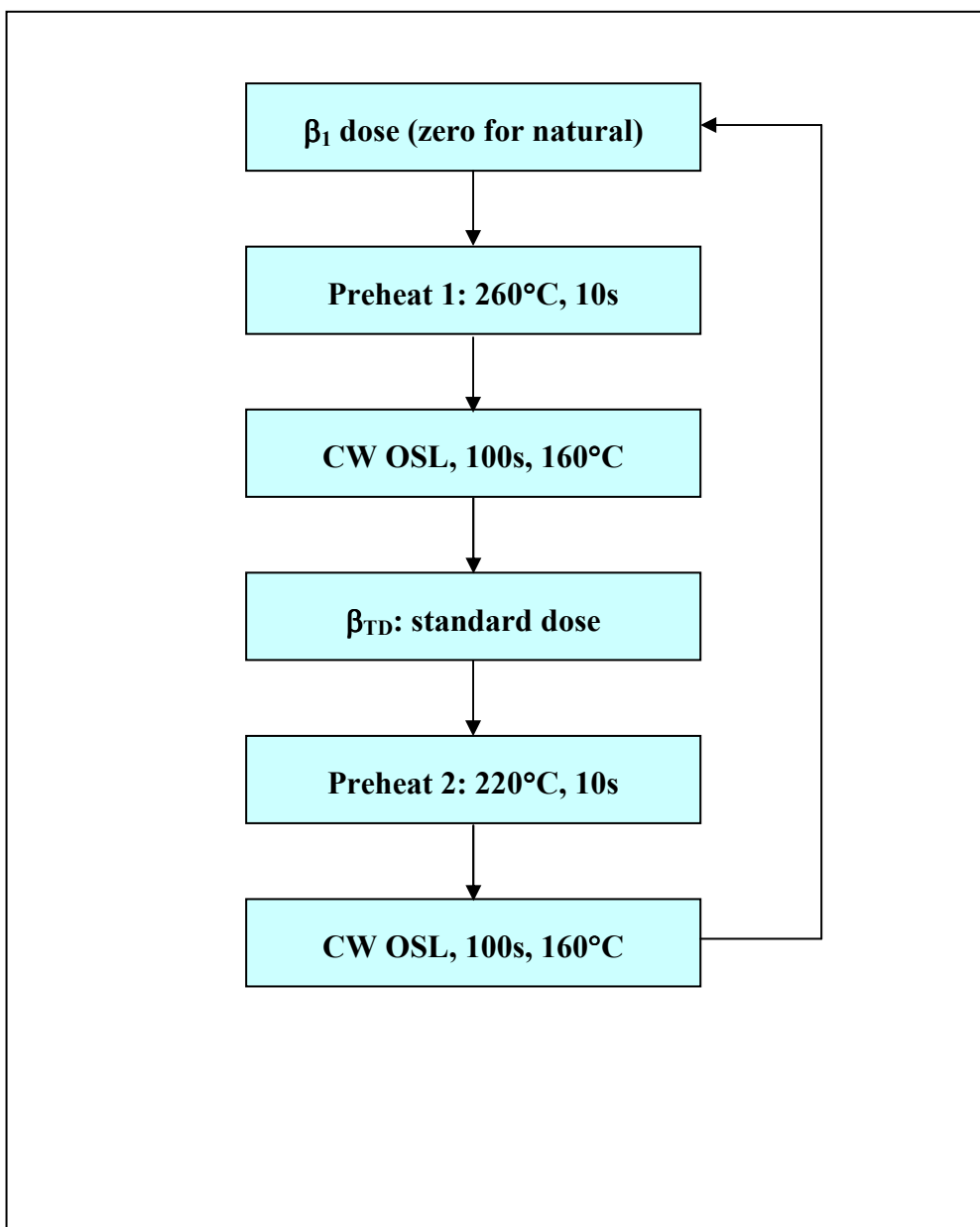
Fig. 7.9 Flowchart outlining the CW OSL single-aliquot regenerative-dose (SAR; Murray and Wintle, 2000) procedure used to obtain standard optical ages presented in Fig. 7.7 for the Casablanca sites.
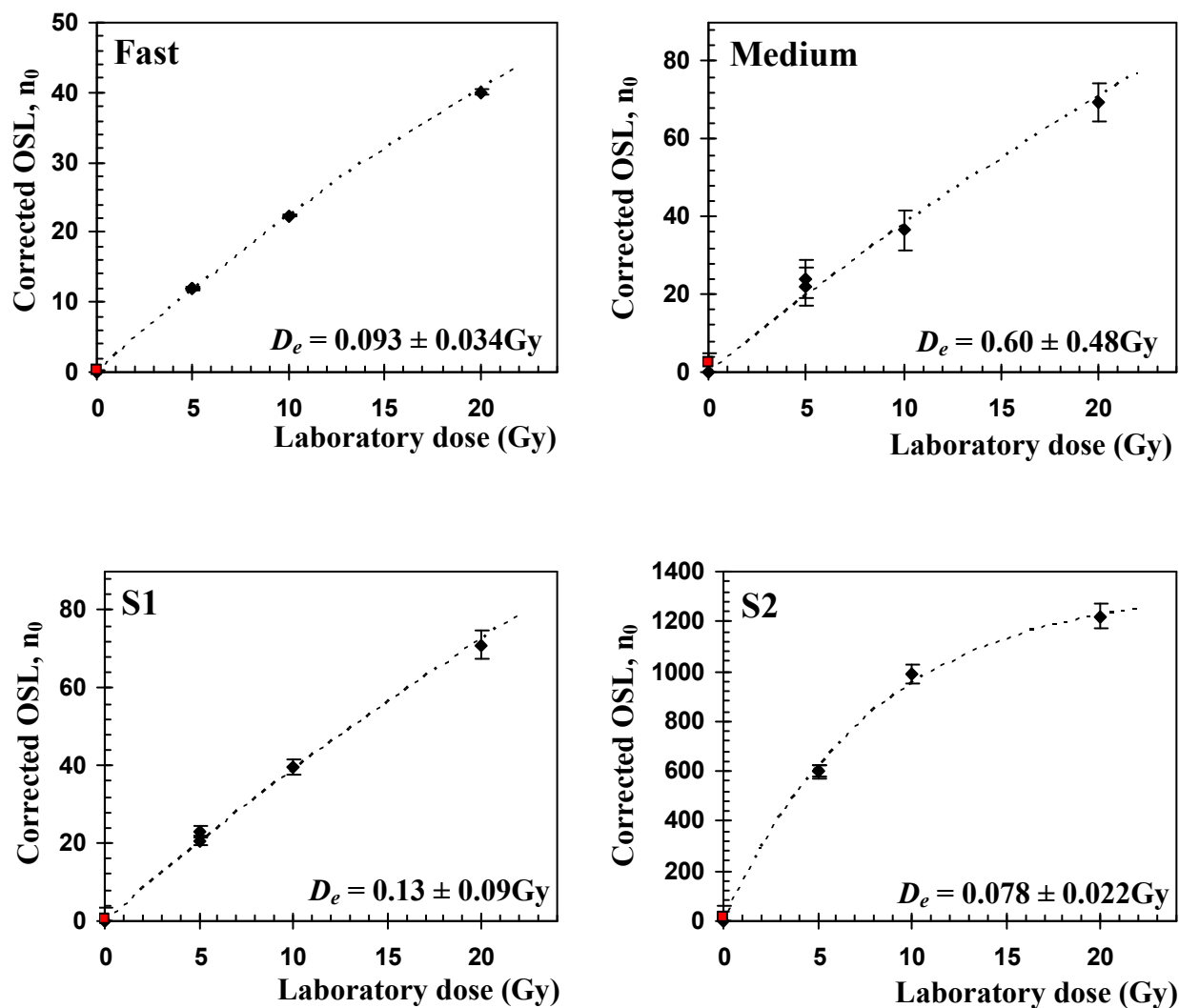
Fig. 7.10 SAR growth curves for fitted OSL components from sample RB3, Casablanca. The growth curve data have been approximated to single saturating exponentials. The equivalent dose estimate for each component is given in the plot.
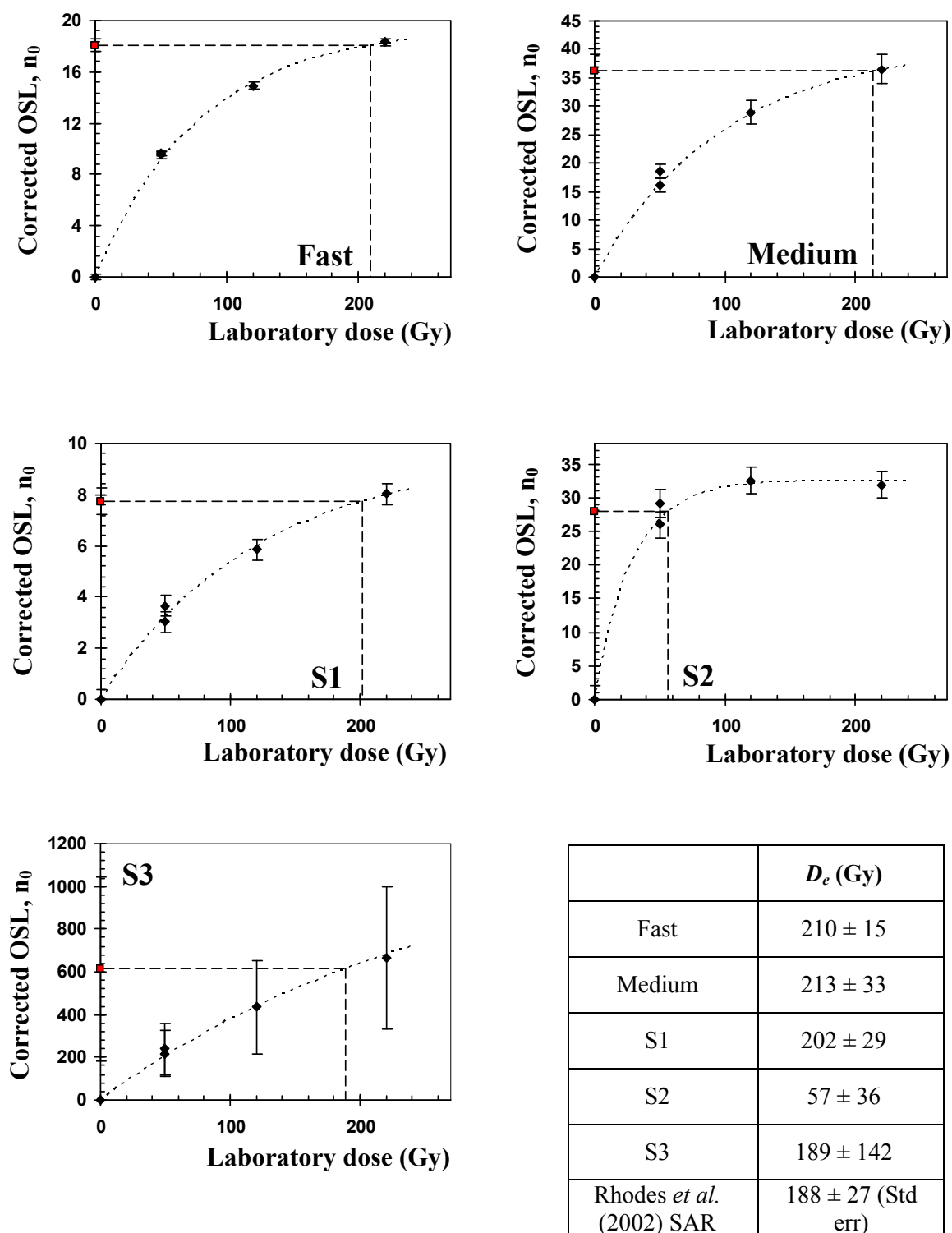
Fig. 7.11 Component-resolved growth curves for natural sample TQN. The regeneration curves have been fitted to single saturating exponential functions to obtain component-resolved D_e estimates (given in the table). The equivalent dose for the same sample, calculated from 10 aliquots using the standard SAR technique (given in Fig. 7.9), is presented for comparison.
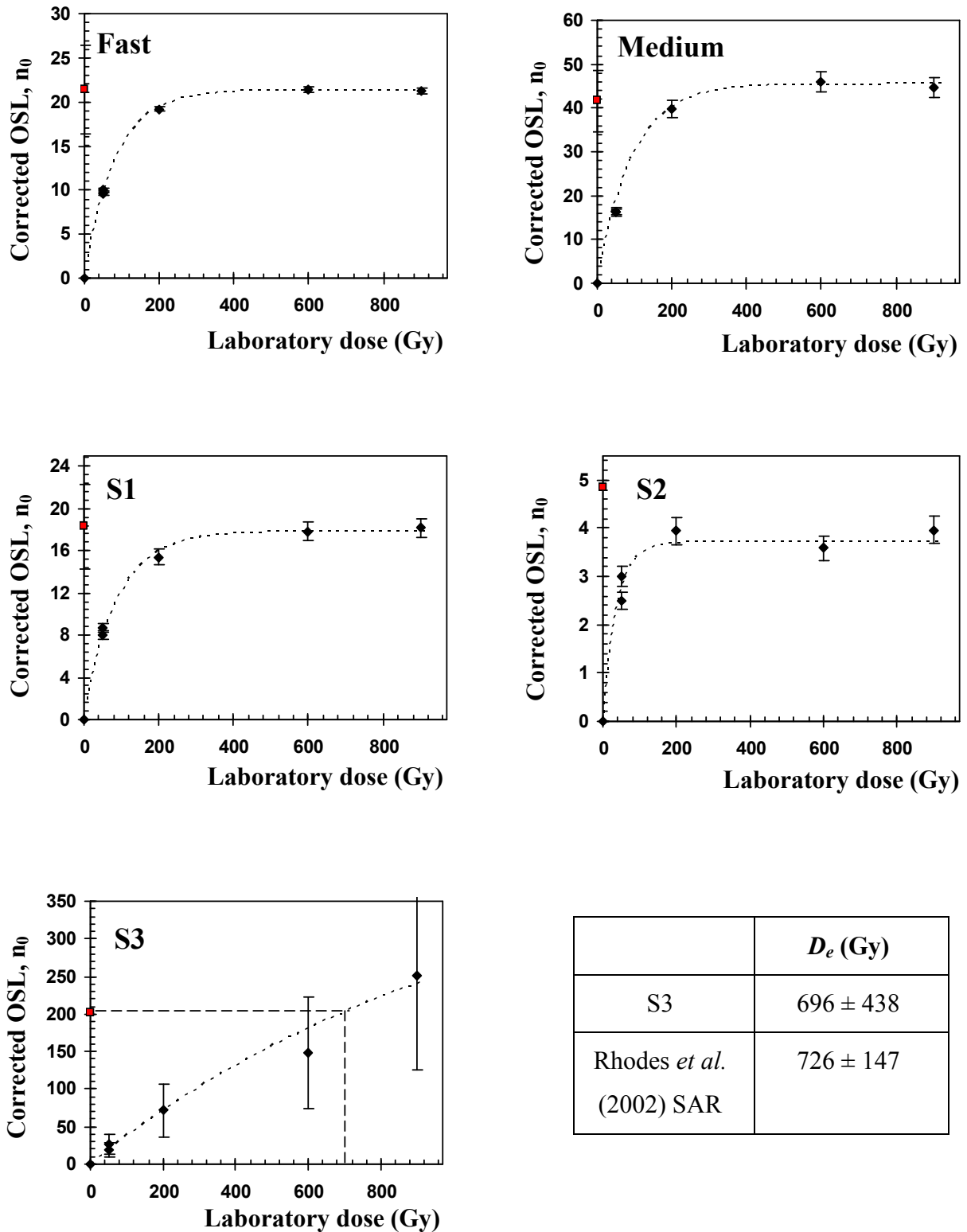
Fig. 7.12 Component-resolved SAR growth curves for a single aliquot of sample TQL. Saturation of the natural signal was observed (within errors) for fast, medium, S1 and S2 components (in S2 the natural is far above saturation level). Component S3 was not saturated, which allowed a D_e to be estimated, given in the table. The single D_e obtained in Rhodes *et al.* (2002) is presented for comparison; see section 7.3.3 for further details.

		Sample		
		RB3	**TQN**	**TQL**
Total Dose rate (Gyka^{-1})		0.48 *	0.51 ± 0.03	0.73 ± 0.04
Standard SAR	D_e (Gy)	0.08 ±0.04	188 ± 27	726 ± 147 [‡]
	Age (ka)	0.17 ± 0.08 [†]	370 ± 58	989 ± 208
Fast	D_e (Gy)	0.093 ± 0.034	210 ± 15	saturated
	Age (ka)	0.19 ± 0.07	414 ± 38	-
Medium	D_e (Gy)	0.6 ± 0.48	213 ± 33	saturated
	Age (ka)	1.25 ± 1.0	419 ± 69	-
S1	D_e (Gy)	0.13 ± 0.09	202 ± 29	saturated
	Age (ka)	0.27 ± 0.19	398 ± 61	-
S2	D_e (Gy)	0.078 ± 0.022	57 ± 36	saturated
	Age (ka)	0.16 ± 0.05	112 ± 71	-
S3	D_e (Gy)	-	189 ± 142	696 ± 438
	Age (ka)	-	372 ± 280	948 ± 599

* Dose rate data taken from Westerway (1995)

[†] The SAR age presented here for RB3 is much smaller than in Rhodes *et al.* (2002), where the calculated age (MAAD) = 2.65 ± 1.06ka, found using MAAD based on gamma dosed samples and partially estimated dose rate (see paper for further details).

[‡] Given the estimated age of sample TQL and the saturation of the fast component it was expected that the standard SAR results would be saturated. In an attempt to get an age, raw data from six aliquots, half displaying natural signals higher than the saturated regeneration OSL, were summed. A single growth curve and single natural point were produced, from which a single D_e could be obtained (albeit the summed natural signal was almost at saturation).

Table 7.1 Summary of equivalent doses and age estimates found for three samples from Casablanca: RB3, TQN and TQL. The dose rates given were obtained using gamma-spectrometry. Ages from the standard SAR method (TQN and TQL also presented in Rhodes *et al.*, 2002) are shown for comparison.

Following the encouraging results on the Moroccan samples the same LM OSL SAR procedure was applied to sample 319 from Chebba, Tunisia. This sample is a high energy marine deposit and was dated as part of a study on catastrophic shoreline activity in the Mediterranean by Wood (1996). Using multiple-aliquot additive-dose procedures he obtained ages of 84±15ka for this sample, and 133±20ka on another sample taken within the same depositional layer at Chebba. These were compared to an ESR age of 113±19ka on *Strombus bubonius* extracted from the same deposit. Wood (1996) concluded from these results, and results from other Tunisian samples collected, that this high energy (Tsunami-type) depositional event took place during either Oxygen Isotope (OI) sub-stage 5e or 5c.

Using LM OSL SAR protocol B (section 6.3.1) component-resolved growth curves and D_e estimates were calculated for sample 319. These are shown in Fig. 7.13. The regeneration curves of all the OSL components were fitted to single saturating exponentials to obtain equivalent dose. The D_e estimates and subsequent ages obtained from each of the component are displayed in the table within Fig. 7.13. The age estimates from the fast, medium, S1 and S3 components agree within errors, although component S1 is higher than the other values. Component S2 produced a significant age underestimate due to the thermal instability discussed in previous chapters.

The difference in the ages obtained for sample 319 in the current study and Wood (1996) may be accounted for in the different equivalent dose estimation measurement techniques used. For example, had sensitivity increases occurred during the MAAD procedure (during dosing and preheating) that were not corrected for this could lead to age underestimation. This sample has not been dated using the standard SAR technique (Fig 7.9), which might have given more reliable internal age control to the LM OSL SAR results. However, the ages obtained agree well with both the second OSL age at Chebba (133 ± 20ka) and the ESR age (113 ± 19ka), which place the depositional event within OI sub-stage 5e.
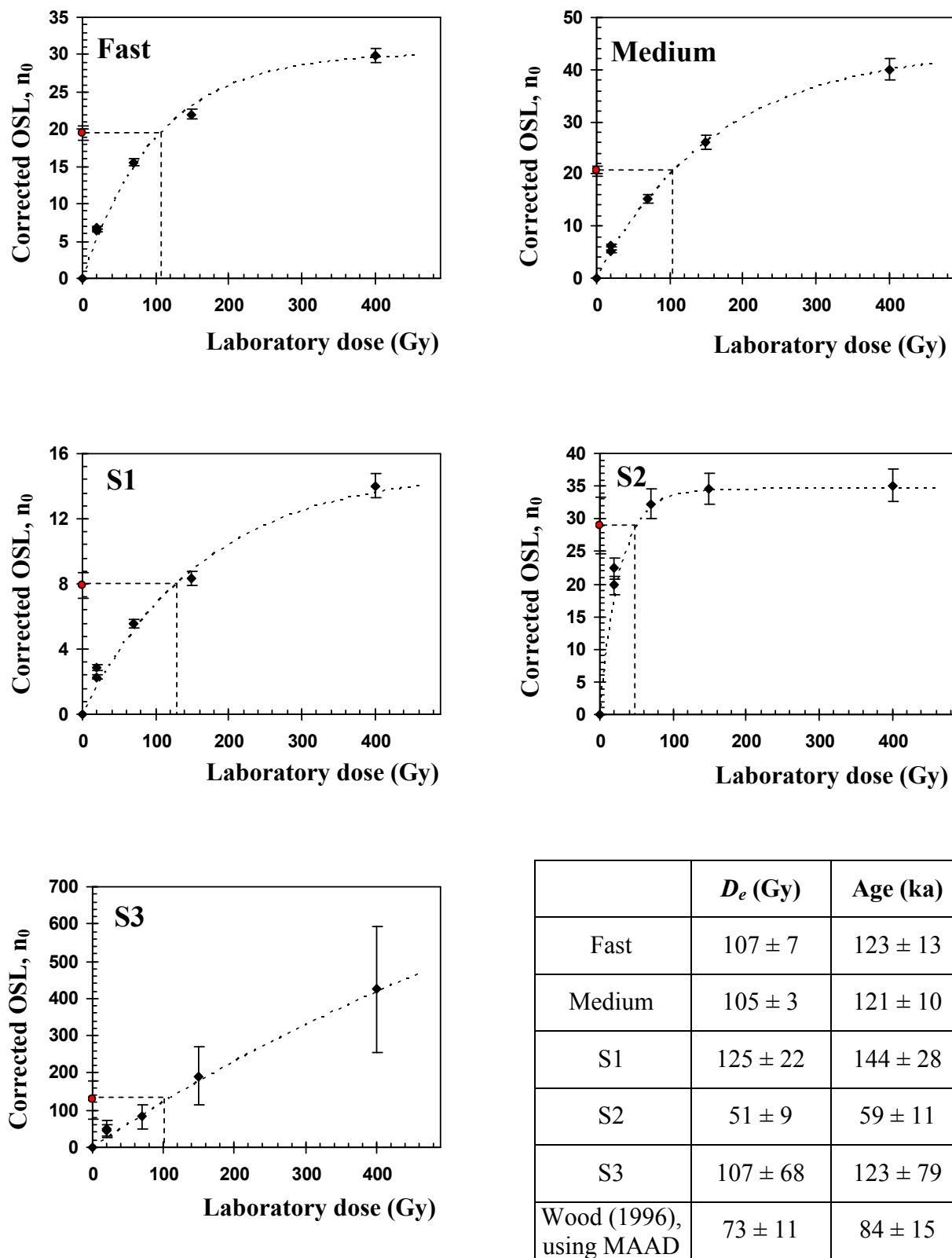
Fig. 7.13 Component-resolved growth curves for natural sample 319. The regeneration curves have been fitted to single saturating exponential functions to obtain component-resolved D_e estimates (given in the table). Age estimates have been calculated using dose rate values given in Wood (1996). The MAAD age found by Wood is given in the table for comparison.

7.3.4 Discussion

Although extensive application of the LM OSL SAR protocol was not reported in this section the examples chosen demonstrate different aspects, advantages and disadvantages of the technique. The results from sample RB3 provide further evidence that all the OSL components can be bleached to very low levels prior to deposition. However, the scatter between the D_e estimates from the different components suggests that the lower age limit possible using the LM OSL SAR is higher than the standard SAR technique (depending also on the brightness of the sample). LM OSL measurements produce lower signal-to-noise ratios than CW OSL measurements. The fitted magnitudes of the small natural signal of RB3 are less reliable than the larger regeneration doses, leading to large errors in the final age.

Encouraging results from sample TQN indicated that if the natural signal is of a reasonable size it is possible to obtain D_e estimates from the OSL components that agree within errors. Only component S2 underestimated the D_e compared to that obtained using the standard SAR technique, due to thermal instability. The regeneration dose response of component S2 fully saturates at doses lower than the expected D_e of this sample in any case. Only component S3 displayed a dose response significantly greater than the fast component, as observed in several samples previously (Chapter 6).

The high dose saturation levels of component S3 were used to obtain a D_e from sample TQL (age > 0.78Ma). Full dose response data up to saturation levels were obtained for the other components. Component S3 was the only component observed to still be growing with dose beyond 900Gy, and the only component in which the natural signal was not saturated. Given the dose rate for this sample this equates to well over 1Ma before the onset of saturation. The age obtained from component S3 was consistent with the minimum age constraint given by the B-M magnetic reversal.

These preliminary applications suggest that component S3 does indeed show some promise for long range dating and a more detailed investigation is required to fully assess this possibility. However, the LM OSL SAR method used above is a relatively lengthy process both in measurement time (because of the slow depletion rate of component S3) and deconvolution analysis (due to the spread in σ and the non-first order behaviour of S3). In section 6.3.2 attempts were made to observe the peak of S3 to enable more reliable fitting by stimulating with full power CW OSL and converting to pseudo-LM OSL. At high doses this method allowed the peak of component S3 to be seen, but the measurement duration was still relatively lengthy (10 000s CW OSL to observe the S3 peak). A more powerful LED system

would be required to shorten the measurement time. Another possibility for shortening the OSL measurement time would be to use higher photon energy stimulation. So that cross-over between the excitation and emission windows is minimised, pulsed stimulation could be used and subsequent light collection after the cessation of the pulse.

7.4 Unexplored possibilities

Measurement with 'stepped' photon energies

In section 5.3.1.4 it was discovered that infrared stimulation (830nm) at 160°C allowed full depletion of the fast component with negligible decay in the medium, or other components. It was hypothesized that this principle could be extended to all the components so that starting with the longest wavelength stimulation and stepping to shorter wavelengths each component could be measured with no contribution from any other. Speculative wavelengths to bleach each component were also suggested in section 5.3.1.4. Provided that sources of sufficient maximum stimulation intensity can be obtained it is believed that such a regime could make component-resolved measurement more accessible and reliable, since the need for complicated fitting routines would be circumvented.

Most useful would perhaps be the successive measurement of the fast and medium components. The identification of partial bleaching by signal analysis, as discussed in section 7.2, works on the basis that the fast and medium component will retain different residual signal sizes, so that D_e(fast) $< D_e$(medium) $< D_e$(S1). Measurement of the equivalent dose from each component separately using the stepped wavelength technique might make the application of this technique easier. Similarly, for samples that display significant recuperation/thermal transfer such a measurement system could prove valuable. Empirical measurements of recuperation using LM OSL were reported in section 4.5 and it was found to exclusively affect the medium component (when initial OSL measurement was made at > 110°C). The adverse effect on equivalent dose has been investigated by, for example, Rhodes (2000), Watanuki (2002). Measurement of OSL/LM OSL at longer wavelengths than 470nm, as in modern Risø readers, should increase the difference in photoionization cross-section between the fast and medium components (e.g. green stimulation) or if long enough wavelengths could allow measurement of the fast component only. Consequently, more reliable equivalent doses could be obtained from the fast component alone, which was found not to suffer from thermal transfer in the same way.

Chapter | 8

8 | CONCLUSIONS

The broad intention of this study was to assess the behaviour of the quartz OSL components. Efforts centred on those properties relevant to optical dating, such as thermal stability and dose response characteristics. Summaries of the investigations undertaken are presented at the end of the respective chapters. In these concluding remarks the general findings are summarized and directions for future study are suggested.

The technique of linearly modulated OSL was used in preference to standard CW OSL for the majority of the experiments. This method of non-constant excitation intensity was found to have several advantages in comparison to CW OSL with respect to the identification of OSL components and their kinetic order. In general five common OSL components were observed in a number of different quartz samples. Similar component detrapping parameters were fitted in the various samples. This indicated that the results from experiments performed on fewer samples would be applicable to sedimentary quartzes in general. However, the relative concentrations of the OSL components did vary significantly from sample to sample, and to a lesser extent, from aliquot to aliquot. [Chapter 4]

The OSL components display markedly different behaviours following heating, irradiation and illumination. The thermal stability of each component was quantified using the two related methods of pulse-annealing and isothermal decay analysis. With the exception of component S2, all of the components were found to be stable over ~10^8 years at 20°C. Component S1 was considerably more stable than both the fast and medium components. [Chapter 4]

Using a single-aliquot regenerative-dose approach, the dose saturation levels of the fast, medium and S1 components were found to be of the same order of magnitude in several different samples. Component S2 was found to saturate at doses far lower than the other components. Only component S3 displayed a significantly higher dose response. Similar dose responses characteristics from the OSL components were obtained in a number of sedimentary samples. The considerable dose response of component S3 suggested that this

component could be used to date samples beyond the typical upper datable age limit of quartz optical dating methods (possibly to >1Ma). [Chapter 6]

The dating protocols developed were applied to several natural sedimentary samples ranging widely in expected age. Reasonably accurate age estimates (based on stratigraphic position) were obtained using component S3 in a sample where the other components were saturated, illustrating its potential as a long range dating tool. Component S2 produced equivalent dose underestimates in older sediments, demonstrating the thermal instability observed in isothermal decay analysis. [Chapter 7]

Another fundamental aspect to consider for reliable dating is zeroing of OSL during sediment transport. This was investigated on a component-resolved basis using two approaches: firstly, the assessment of the bleaching rates of each of the components under the solar spectrum [Chapter 5], and secondly, by investigating the residual doses in modern samples from a variety of depositional environments [Chapter 7]. The calculated bleaching rates suggest that full resetting might be expected in aeolian samples. Modern aeolian samples did indeed give zero signals in general. Full resetting is less likely, especially for the slower components, in water-lain sediments. However, in the modern samples studied the maximum residual dose estimated in a fluvial sample (in component S3) was only ~15Gy (and <5Gy in the fast and medium components). That no substantial residuals were observed is perhaps surprising given the extremely slow bleaching rate of component S3. This may indicate either some instability in the signal or longer transport times occur than expected.

The dependencies of the optical eviction rate of the fast and medium components on photon energy were found, using narrowband stimulation, to be considerably different. Infrared stimulation was used to completely deplete the fast component with negligible loss in the medium component. On this basis a method of 'stepped wavelength' stimulation was suggested to selectively measure single components successively. [Chapter 5]

Using LM OSL to obtain component-resolved D_e estimates an alternative to $D_e(t)$ plots (Bailey, 2002) was investigated to identify incomplete resetting of sediments through comparison of D_e estimates from the fast, medium (and possibly S1) components. This was found to circumvent problems of falling $D_e(t)$ plots in older samples due to thermal instability of component S2. [Chapter 7]

The nature of the quartz OSL has been found to be relatively complex. This study further investigated the properties of the quartz OSL components, following previous studies by Smith and Rhodes (1994), Bailey *et al.* (1997) and Bulur *et al.* (2000). There are still many unanswered questions to be investigated and verification of the current findings to be made on a wider range of samples. Possible starting points for future areas for study may include:

i. Fuller characterization of photoionization cross-section spectra, including temperature dependence, of all the OSL components to investigate the optical and thermal contributions to the detrapping process, and to empirically investigate the possibility of developing a method to separate the components of quartz by finding, experimentally, the optimal wavelengths/temperatures to bleach successive components with negligible reduction of the next.

ii. Further investigation into the properties of component S3. Due to the slow optical depletion rate and non-first order kinetics it was difficult to obtain consistent results at low doses using standard LM OSL on the current equipment. Mathematical conversion of CW OSL after high doses, as in Chapter 6, could be used for further investigation to record a higher proportion of the total signal and obtain more reliable results.

iii. Following (ii), investigation into the potential of component S3 for long range dating. To assess the dose response characteristics of this component on a wider range of samples and application to independently age constrained samples to assess its long term stability and reliability of the dating methods.

iv. Incorporation of OSL trap parameters, estimated empirically in this study, into a general kinetic model for quartz (e.g. Bailey, 2000).

v. Assessment of the potential of component-resolved D_e estimation for the detection of partially bleached sediments. This could be achieved using both laboratory partially-bleached samples and investigation of natural samples from a variety of depositional environments displaying age overestimates and scatter. Comparison to other methods of analysis, $D_e(t)$ and distribution methods would be useful.

Bibliography

Adamiec, G., 2000a. Variations in luminescence properties of single quartz grains and their consequences for equivalent dose estimation. *Radiation Measurements*, **32**, 427-432.

Adamiec, G., 2000b. *Aspects of pre-dose and other luminescence phenomena in quartz absorbed dose estimation.* Unpublished D.Phil. thesis, University of Oxford.

Agersnap Larsen, N., Bulur, E., Bøtter-Jensen, L., McKeever, S. W. S., 2000. Use of the LM OSL technique for the detection of partial bleaching in quartz. *Radiation Measurements*, **32**, 419-425.

Aitken, M. J., 1985. *Thermoluminescence dating*. Academic Press.

Aitken, M. J., 1998. *An introduction to optical dating. The dating of Quaternary sediments by the use of photon-stimulated luminescence*. Oxford University Press.

Aitken, M. J., Smith, B. W., 1988. Optical dating: recuperation after bleaching. *Quaternary Science Reviews*, **7**, 387-393.

Alexander, C. S., Morris, M. F., McKeever, S. W. S., 1997. The time and wavelength response of phototransferred thermoluminescence in natural and synthetic quartz. *Radiation Measurements*, **27**, 153-159.

Bailey, R. M., 1998a. Depletion of the quartz OSL signal using low photon energy stimulation. *Ancient TL*, **16**, 33-36.

Bailey, R. M., 1998b. *The form of the optically stimulated luminescence signal of quartz: implications for dating*. Unpublished Ph.D thesis, University of London.

Bailey, R. M., 2000a. The slow component of quartz optically stimulated luminescence. *Radiation Measurements*, **32**, 233-246.

Bailey, R. M., 2000b. The interpretation of quartz optically stimulated luminescence equivalent dose versus time plots. *Radiation Measurements*, **32**, 129-140.

Bailey, R. M., 2001. Towards a general kinetic model for optically and thermally stimulated luminescence of quartz. *Radiation Measurements*, **33**, 17-45.

Bailey, R. M., 2002a. Simulations of variability in the luminescence characteristics of natural quartz and it's implications for dating. *Radiation Protection Dosimetry*, **100**, 33-38.

Bailey, R. M., 2002b. Identification of partially bleached sedimentary quartz using De-time plots. In press, *Radiation Measurements*.

Bailey, R. M., Smith, B. W., Rhodes, E. J., 1997. Partial bleaching and the decay form characteristics of quartz OSL. *Radiation Measurements*, **27**, 123-136.

Bailey, R. M., Rhodes, E.J., 2001. Research laboratory for archaeology commercial luminescence dating service – standard procedures. Unpublished.

Bailey, R. M., Singarayer, J. S., 2002. Further developments of a general model for quartz optically stimulated luminescence. *Radiation Measurements*, to be submitted.

Bailey, R. M., Singarayer, J. S., Stokes, S., Ward, S., 2002. Identifying partial bleaching in quartz. *Radiation Measurements*, to be submitted.

Berger, G. W., 1990. Effectiveness of natural zeroing of the thermoluminescence in sediments. *Journal of Geophysical Research*, **95**, 12375-12397.

Berger, G. W., 1995. Progress in luminescence dating methods for Quaternary sediments. In *Dating methods for Quaternary deposits*, Geological Association of Canada, GEO text no. 2, (ed N. W. Rutter and N. Catto) pp. 81-104.

Böer, K. W., 1992. *Survey of semiconductor physics*. Chap & H.

Bøtter-Jensen, L. and Duller, G. A. T., 1992. A new system for measuring optically stimulated luminescence from quartz samples. *Nuclear Track and Radiation Measurements*, **20**, 594-553.

Bøtter-Jensen, L., Duller, G. A. T., Murray, A. S., Banerjee, D., 1999. Blue light emitting diodes for optical stimulation of quartz in retrospective dosimetry and dating. *Radiation Protection Dosimetry,* **84**, 335-340.

Bøtter-Jensen, L., Mejdahl, V., Murray, A. S., 1999. New light on OSL. *Quaternary Science Reviews (Quaternary Geochronology)*, **18**, 303-309.

Bøtter-Jensen, L., Bulur, E., Duller, G. A. T., Murray, A. S., 2000. Advances in luminescence instrument systems. *Radiation Measurements*, **32**, 523-528.

Britton, J. C., 1982. A dissection guide, field and laboratory manual for the introduced bivalve *Corbicula fluminea. Malacologia Rev. Supp.*, **3**, 1-82.

Bulur, E., 1996. An alternative technique for optically stimulated luminescence (OSL) experiment. *Radiation Measurements*, **26**, 701-709.

Bulur, E., 2000. A simple transformation for converting CW-OSL curves to LM-OSL curves. *Radiation Measurements*, **32**, 141-145.

Bulur, E., Göksu, H. Y., 1997. IR stimulated luminescence from ZnS and SrS based storage phosphors: a re-examination with linear modulation technique. *Phys. Stat. Sol.* (a), **161**, R9-R10.

Bulur, E., Göksu, H. Y., 1999. Infrared (IR) stimulated luminescence from feldspars with linearly increasing excitation light intensity. *Radiation Measurements*, **30**, 505-512.

Bulur, E., Bøtter-Jensen, L., Murray, A. S., 2000. Optically stimulated luminescence from quartz measured using the linear modulation technique. *Radiation Measurements*, **32**, 407-411.

Bulur, E., Bøtter-Jensen, L., Murray, A. S., 2001a. Frequency modulated pulsed stimulation in optically stimulated luminescence. *Nucl. Instrum. Methods Phys. Res. B*, **179**, 151-159.

Bulur, E., Bøtter-Jensen, L., Murray, A. S., 2001b. LM OSL signals from some insulators: an analysis of the dependency of the detrapping probability on stimulation light intensity. *Radiation Measurements*, **33**, 715-719.

Bulur, E., Duller, G. A. T., Solongo, S., Bøtter-Jensen, L., Murray, A. S., 2002. LM-OSL from single grains of quartz: a preliminary study. *Radiation Measurements*, **35**, 79-85.

Chen, R., Yang, X. H., McKeever, S. W. S., 1998. The strongly superlinear dose dependence of thermo-luminescence in synthetic quartz. *Journal of Physics D – Applied Physics*, **21(9)**, 1452-1457.

Curie, D., 1963. *Luminescence in crystals*. Wiley, New York.

Duller, G. A. T., 1994. A new method for the analysis of infrared stimulated luminescence data from potassium feldspars. *Radiation Measurements*, **23**, 281-285.

Duller, G. A. T., 1995. Luminescence dating using single aliquots: methods and applications. *Radiation Measurements*, **24**, 217-226.

Duller, G.A. T., 1996. Recent developments in luminescence dating of Quaternary sediments. *Progress in Physical Geography*, **20**, 133-151.

Duller, G. A. T., Bøtter-Jensen, L., 1996. Comparison of optically stimulated luminescence signals from quartz using different stimulation wavelengths. *Radiation Measurements*, **26**, 603-609.

Duller, G. A. T., Bøtter-Jensen, L., Murray, A. S., Truscott, A. J., 1999. Single grain laser luminescence (SGLL) measurements using a novel automated reader. *Nucl. Instrum. Methods B* **155**: 506-514.

Duller, G. A. T., Bøtter-Jensen, L., Murray, A. S., 2000. Optical dating of single sand-sized grains of quartz: sources of variability. *Radiation Measurements*, **32**, 453-457.

Embabi, N. S., 1986. Dune movement in the Kharga and Dakhla Oases Depressions, the Western Desert, Egypt. *Bulletin of the Egyptian Geographical society*, **59**, 35-70.

Ennouchi, E., 1972. Nouvelle decouverte d-un Archanthropien au Maroc. C. R. Acad. Sci. Paris.t. 274, serie D, 3088-3090.

Franklin, A. D., Prescott, J. R., Scholefield, R. B., 1995. The mechanism of thermoluminescence in an Australian sedimentary quartz. *Journal of Luminescence*, **63(5-6)**, 317-326.

Garlic, G. F. J., Gibson, A. F., 1948. The electron trap mechanism of luminescence in sulphide and silicate phosphors. *Proceedings of the Royal Society, London*, **A60**, 574-590.

Gemmell, A. M. D., 1997. Fluctuations in the thermoluminescence signal of suspended sediments in an Alpine glacial meltwater stream. *Quaternary Science Reviews (Quaternary Geochronology)*, **16**, 281-290.

Gilmore, G. and Hemingway, J. D., 1995. *Practical gamma-ray spectrometry.* John Wiley and Sons, NY.

Godfrey-Smith, D. I., Huntley, D. J., Chen, W-H., 1988. Optical dating studies of quartz and feldspar sediment extracts. *Quat. Sci. Rev.*, **7**, 373-380.

Green, J. R. and Margerison, D., 1983. *Statistical treatment of experimental data.* Elsevier Science.

Hadamard, J., 1902. Sur les problemes aux derivees parielies et leur signification physique. *Bull. Univ. of Princeton*.

Hofmann, B., 1986. *Regularization for applied inverse and ill-posed problems*. Teubner, Leipzig.

Hornyak, W. F., Chen, R., Franklin, A. D., 1992. Thermoluminescence characteristics of the 375°C electron trap in quartz. *Phys. Rev. B*, **46**, 8036-8049.

Huang, K. and Rhys, A., 1950. Theory of light absorption and non-radiative transitions in F-centres. *Proceedings of the Royal Society, London*, A **204**, 406.

Huntley, D. J., Godfrey-Smith, D. I., Thewalt, M. L. W., 1985. Optical dating of sediments. *Nature*, **313**, 105-107.

Huntley, D. J., Short, M. A., Dunphy, K., 1996. Deep traps in quartz and their use for optical dating. *Can. J. Phys.*, **74**, 81-91.

Hütt, G., Jaek, I., Tchonka, J., 1988. Optical dating: K-feldspars optical response stimulation spectra. *Quaternary Science Reviews*, **7**, 381-386.

Jaros, M., 1977. Wave functions and optical cross-sections associated with deep centers in semiconductors. *Phys. Rev. B.*, **16**, 3694-3706.

Kuhns, C. K., Agersnap Larsen, N., McKeever, S. W. S., 2000. Characteristics of LM-OSL from several different types of quartz. *Radiation Measurements*, **32**, 413-418.

Kurik, M. V., 1971. Urbach rule. *Phys. Stat. Sol.*, (a), **8**, 9-45.

Lanczos, C., 1959. *Applied analysis*. Prentice-Hall, Englewood Cliffs, NJ. p. 272ff.

Lawson, C. L., Hanson, R. J., 1995. *Solving least squares problems*. SIAM, PA.

Lepper, K., Agersnap Larsen, N., McKeever, S. W. S., 2000. Equivalent dose distribution analysis of Holocene eolian and fluvial quartz sands from Central Oklahoma. *Radiation Measurements*, **32**, 603-608.

Lowe, J. J., Walker, M. J. C., 1997. *Reconstructing Quaternary Environments*. Longman, 2nd Ed.

Lucovsky, G., 1965. On the photoionization of deep impurity centres in semiconductors, *Solid State Commun.* **3**, 299-302.

Markey, B. G., Bøtter-Jensen, L., Duller, G. A. T., 1997. A new flexible system for measuring thermally and optically stimulated luminescence. *Radiation Measurements*, **27**, 83-89.

May, C. E., Partridge, J. A., 1964. *J. Chem. Phys.*, **40**, 1401. (cited in McKeever, 1985)

McKeever, S. W. S., 1985. *Thermoluminescence of solids.* Cambridge University Press.

Murray, A. S., Olley, J. M., Caitcheon, G. G., 1995. Measurement of equivalent doses in quartz from contemporary water-lain sediments using optically stimulated luminescence. *Quaternary Science Reviews (Quaternary Geochronology)*, **14**, 365-371.

Murray, A. S., Roberts, R. G., 1997. Determining the burial time of single grains of quartz using optically stimulated luminescence. *Earth and Planetary Science Letters*, **152**, 163-180.

Murray, A. S., Roberts, R. G., 1998. Measurement of the equivalent dose in quartz using a regenerative-dose single-aliquot protocol. *Radiation Measurements*, **29**, 503-515.

Murray, A. S., Wintle, A. G., 1999. Isothermal decay of optically stimulated luminescence in quartz. *Radiation Measurements*, **30**, 119-125.

Murray, A. S., Wintle, A. G., 2000. Luminescence dating of quartz using an improved single-aliquot regenerative-dose protocol. *Radiation Measurements*, **32**, 57-73.

Noras, J .M., 1980. Photoionization and phonon coupling. *J. Phys. C: Solid St. Phys.*, **13**, 4779-4789.

Occhietti, S., Raynal, J. P., Pichet, P., 2002. Aminostratigraphy of Pleistocene and Holocene littoral deposits, Casablanca, Morocco, and correlation with the Mediterranean paleo-shorelines. *Quaternaire*, soumis.

Olley, J. M., Caitcheon, G. G., Murray, A. S., 1998. The distribution of apparent dose as determined by optically stimulated luminescence in small aliquots of fluvial quartz: implications for dating young samples. *Quaternary Science Reviews (Quaternary Geochronology)*, **17**, 1033-1040.

Parry, S. J., 1991. *Activation spectrometry in chemical analysis.* John Wiley and Sons, NY

Poolton, N. R. J., Bøtter-Jensen, L., Ypma, P. J. M., Johnsen, O., 1994. Influence of crystal structure on the optically stimulated luminescence properties of feldspars. *Radiation Measurements*, **23**, 551-554.

Prescott, J. R., Hutton, J. T., (1994). Cosmic ray contributions to dose rates for luminescence and ESR dating: large depths and long-term time variations. *Radiation Measurements*, **23**, 497-500.

Press, W. H., Teukolsky, S. A., Vetterling, W. T., Flanney, B. P., 1992. *Numerical recipes in C: the art of scientific computing.* Cambridge University Press.

Pye, K., Neal, A., 1993. Late Holocene dune formation on the Sefton Coast, Northwest England. In Pye, K. (ed). *The dynamics and environmental context of aeolian sedimentary systems*. Geological Society Special Publication No. 72. pp201-218.

Randall, J. T., Wilkins, M. H. F., 1945. Phosphorescence and electron traps II. The interpretation of long-period phosphorescence. *Proceedings of the Royal Society, London*, **184**, 390-407.

Rasheedy, M. S., 1993. On the general-order kinetics of the thermoluminescence glow peak. *J. Phys.: Condensed Matter*, **5**, 633-636.

Raynal, J. P., Sbihi-Alaoui, F. Z., Amani, F., Bernoussi, R., El Graoui, M., Geraads, D., Hublin, J. J., Lefevre, D., Maogo, L., Mohib, A., Occhietii, S., Rhodes, E. J., Snes, S., Texier, J. P., Zouak, M., 1996. Premiers peuplements du Maroc atlantique: l'exemple de Casablanca. *XII International Congress of Prehistoric and Protohistoric Science*, Forli, Italia, 8-14 Septembre 1996, Abstracts 1, 126.

Raynal, J. P., Sbihi-Alaoui, F. Z., Geraads, D., Mogoga, L., Mohib, A., 2001. The earliest occupation of North Africa: the Moroccan perspective. *Quaternary International*, vol. 75, *Out of Africa in the Pleistocene*, 65-75.

Raynal, J. P., Sbihi-Alaoui, F. Z., Geraads, D., Mogoga, L., Zouak, M., 2002. The acheulean sequence of North Atlantic Morocco after recent excavations at Casablanca. *Quaternaire*, soumis.

Rees-Jones, J., 1995. Dating young sediments using fine-grained quartz. *Ancient TL*, **13**, 9-14.

Rees-Jones, J., Tite, M. S., 1997. Optical dating results from British archaeological sediments. *Archaeometry*, **39**, 177-187.

Rendell, H. M., Wood, R. A, 1994. Quartz sample pre-treatments for TL/OSL dating: studies of TL emission spectra. *Radiation Measurements*, **23**, 575-580.

Rhodes, E. J., 1990. Optical dating of quartz from sediment. Unpublished D.Phil. thesis. Oxford University.

Rhodes, E.J., Bailey, R. M., 1997. The effect of thermal transfer on the zeroing of the luminescence of quartz from recent glaciofluvial sediments. *Quaternary Science Reviews (Quaternary Geochronology)*, **16**, 291-298.

Rhodes, E. J., Pownall, L., 1994. Zeroing of the OSL signal in quartz from young glaciofluvial sediments. *Radiation Measurements*, **23**, 581-585.

Rhodes, E., Raynal, J. P., Geraads, D., Sbihi-Alaoui, F. Z., 1994. Premieres dates RPE pour l'Acheuleen du Maroc atlantique (Grotte des Rhinoceros, Casablanca). C. R. Acad. Sc. Paris, serie II, t.319, 1109-1115.

Rhodes, E. J., Singarayer, J. S., Raynal, J. P., Westerway, K., 2002. New luminescence dating for the Paleolithic assemblages and Pleistocene succession of Casablanca, Morocco. *Quaternaire*, (submitted).

Singarayer, J. S., Bailey, R. M., 2002. Component-resolved bleaching spectra of quartz optically stimulated luminescence: preliminary results and implications for dating. *Radiation Measurements*. (In press)

Singarayer, J. S., Bailey, R. M., Rhodes, E. J., 2000. Potential of the slow component of quartz OSL for age determination of sedimentary samples. *Radiation Measurements*, **32**, 873-880.

Singarayer, J. S., Bailey, R. M., Ward, S., Stokes, S., Bray, H. E., 2002a. Further tests on the completeness of optical bleaching of sand-sized quartz from young sediments. (submitted *Quat. Sci. Rev.*)

Singarayer, J. S., Fattahi, M., Bailey, R. M., Stokes, S., 2002b. LM IRSRL of feldspars. *Radiation Measurements*. (Submitted)

Smith, B. W., Rhodes, E. J., Stokes, S., Spooner, N. A., 1990. The optical dating of sediments using quartz. *Rad. Prot. Dosim.*, **34**, 75-78.

Smith, B. W., Rhodes, E. J., 1994. Charge movements in quartz and their relevance to optical dating. *Radiation Measurements*, **23**, 329-333.

Spooner, N. A., 1994. On the optical dating signal from quartz. *Radiation Measurements*, **23**, 593-600.

Spooner, N. A., Questiaux, D. G., 1989. Optical dating – Achenheim beyond the Eemian using green and infrared stimulation. *Proceedings of a workshop on long and short range limits in luminescence dating*. Oxford. RLAHA Occasional publication No. 9.

Spooner, N. A., Questiaux, D. G., 2000. Kinetics of red, blue and UV thermoluminescence and optically-stimulated luminescence from quartz. *Radiation Measurements*, **32**, 659-666.

Spooner, N. A., Questiaux, D. G. Aitken, M. J., 2000. The use of sodium lamps for low-intensity laboratory safelighting for optical dating. *Ancient TL*, **18**¸45-49.

Stokes, S., 1992. Optical dating of young (modern) sediments using quartz: results from a selection of depositional environments. *Quaternary Science Reviews (Quaternary Geochronology)*, **11**, 153-159.

Stokes, S., 1994. *Optical dating of selected late Quaternary aeolian sediments from the Southwestern United States*. Unpublished D. Phil Thesis. University of Oxford.

Stokes, S., 2002. (Ed.) *Handbook of Luminescence.* Springer-Verlag. (In press)

Stokes, S., Bray, H. E., Blum, M. D., 2001. Optical resetting in large drainage basins: tests of zeroing assumptions using single-aliquot procedures. *Quaternary Science Reviews*, **20**, 879-885.

Stoneham, A. M., 1979. Phonon coupling and photoionization cross-sections in semiconductors. *J. Phys. C: Solid. St. Phys.*, **12**, 1979.

Tauxe, L., Herbert, T., Shackleton, N. J., Kok, Y. S., 1996. Astronomical calibration of the Matuyama-Brunhes boundary: Consequences for magnetic remanence acquisition in marine carbonates and the Asian loess sequences. Earth and Planetary Science Letters, **140**, 133-141.

Texier, J. P., Lefevre, D., Raynal, J. P., 1994. Contribution pour un nouveau cadre stratigraphique des formations littorals quaternaries de la region de Casablanca. C. R. Acad. Sc. Paris., serie II, t. 318, no. 9, 1247-1253.

Texier, J. P., Lefevre, D., Raynal, J. P., El Graoui, M., 2002. Lithostratigraphy of the littoral deposits of the last one million years in the Casablanca region (Morocco). *Quaternaire*, soumis.

Tikhonov, A. N., Arsenin, V. Y., 1977. *Solutions of Ill-posed Problems*. Winston/Wiley, NY.

Urbach, F., 1953. The long-wavelength edge of photographic sensitivity and of the electronic absorption of solids. *Phys. Rev.*, 2nd series, **92**, 1324.

Vermeeersch, P. M., Paulissen, E., Stokes, S., Charlier, C., Van Peer, P., Stringer, C., Lindsay, W., 1998. A middle Palaeolithic burial of a modern human at Taramsa Hill, Egypt. *Antiquity*, **72**, 475-484.

Watanuki, T., 2002. *Chronological study of loess palaeosol by improved method of luminescence dating and application to reconstruct past environmental changes.* Unpublished Ph.D. Thesis. Tokyo Metropolitan University.

Westerway, K., 1995. *An investigation into the reliability and potential age range of optically stimulated luminescence using samples from Casablanca, (Morocco).* Unpublished MSc thesis, University of London.

Whitley, V., 2000. *Optical and thermal studies of deep levels in anion deficient Al_2O_3:C.* Ph.D. Thesis. Oklahoma State University.

Wintle, A. G., 1975. Thermal quenching of thermoluminescence in quartz. *Geophysical Journal of the Royal Astronomical Society*, **41**, 107-113.

Wood, P. B., 1996. *Dating and origin of late Quaternary catastrophic shoreline activity around the Mediterranean Sea.* Unpublished Ph.D. Thesis. University of London.

Zimmerman, J., 1971. Radiation-induced increase of the 110°C thermoluminescence sensitivity of fired quartz. *Journal of Physics C: Solid State Physics*, **4**, 3265-3276.

Appendix A

Table 1. Samples of various age/depositional type:

Sample code	Location/details	De (Gy)
317 [2]	Raised beach, Chebba, Tunisia (Wood, 1996)	Saturated
319 [2]	Raised beach deposit, Tunisia (Wood, 1996)	77 ± 9
338 [2]	Raised beach, Hergla, Tunisia (Wood, 1996)	56.9 ± 9.8
SH1A [2]	Aeolian, Shropham pit, East Anglia	68.8 ± 21.3
SL161 [2]	Sri Lankan dune deposit ca. 18ka	29.2 ± 1.1
SL203 [2]	Sri Lankan dune deposit ca. 36ka	73.3 ± 1.3
TQN [3]	Grey dune deposit, Thomas Quarries, Morocco	188 ± 27
TQL [3]	Aeolian, Thomas Quarries, Morocco. >780ka (stratigraphically below Brunhes-Matuyama boundary)	726 ± 147
TQA [3]	Marine deposit, Thomas Quarries, Morocco	288 ± 59
TQQ [3]	Dune deposit, Thomas Quarries, Morocco	195 ± 29
RB3 [3]	Recent beach, Reddad Ben Ali, Morocco	0.07 ± 0.04
897/3 [1]	Taramsa Hill burial site, Egpyt (Vermeersch *et al.*, 1998)	~52
Van2 [2]	Vanguard Cave site, Gibraltar	?
KG02 [2]	Korea	?
SOT [2]	Stoke-on-Trent	?
MAL [1]	Beach deposit, Malibu	0.36 ± 0.02
EBSan [2]	Eastbourne beach sand, annealed at 580°C, 40min	-
EJR01an [4]	Madagascan vein quartz, annealed 1200°C, 1 hour	-
CdT1	Marine deposit, Campo de Tir, Majorca	78 ± 5
CdT9	Riss dune deposit, Campo de Tir, Majorca	106 ± 5

[1] Supplied by Dr S. Stokes.

[2] Supplied by Dr R. M. Bailey.

[3] Collected by Dr E. J. Rhodes, prepared/measured by the present author.

[4] Supplied by Dr G. Adamiec.

All ages obtained using SAR except 317, 319, 338, MAL and SH1A (MAAD used).

Table 2. Suite of modern samples from a variety of depositional environments:

Sample	Location / Environment	Details / Age control	SAR D$_e$ (Gy)
857/1	New Valley, Egypt (Barchan dune field)	Active Barchan dune turnover estimated to be 50years max. (Embabi, 1986)	0.05 ± 0.02
857/2	New Valley, Egypt (Barchan dune field)		0.08 ± 0.01
857/3	New Valley, Egypt (Barchan dune field)		0.058 ± 0.007
857/4	New Valley, Egypt (Barchan dune field)		0.057 ± 0.007
857/5	New Valley, Egypt (Barchan dune field)		0.052 ± 0007
857/6	New Valley, Egypt (Barchan dune field)		0.067 ± 0.01
857/7	New Valley, Egypt (Barchan dune field)		0.064 ± 0.007
830/1	Utah, US (Active falling self dune)		0.11 ± 0.03
835/1	Wyoming, US (active sand sheet)		0.13 ± 0.003
838B/1			1.23 ± 0.01
841/1	Ward terrace, Arizona, US	Post dust bowlc.1930	0.07 ± 0.007
813/1	S. Texas, US (Fenceline dune)		0.088 ± 0.044
901/1	Fortuna flats, Yuma, Arizona (Aeolian transverse dune)		0.383 ± 0.044
901/2	Fortuna flats, Yuma, Arizona (Aeolian transverse dune)		0.258 ± 0.040
901/3	Fortuna flats, Yuma, Arizona (Active traction load)		1.03 ± 0.11
901/4	Fortuna flats, Yuma, Arizona (Aeolian transverse dune)		1.60 ± 0.16
	Algodunes, California, US (Active sand)		
908/2	Algodunes, California, US (Aeolian)		0.28 ± 0.03

909/1	Gudmunsen ranch, Nebraska (Megabarchanoid)	<270a ^{14}C	0.349 ± 0.02
885/3	Lubbock, Texas, US (Playa margin)	(Stokes, 1994)	0.186 ± 0.007
	Laguna Madras, Texas, US (Coastal Lunette)		
854/1	Sefton coast Liverpool, UK (coastal dune)		0.16 ± 0.01
811/1		Middle ages-later (Pye	0.045 ± 0.015
888/1	Sefton coast Liverpool, UK (coastal dune)	and Neal, 1993)	0.76 ± 0.05
		Post 1900AD (Pye and	
		Neal, 1993)	
888/4	Malibu (beach deposit)		0.174 ± 0.012
Mal	Colorado river, Columbus, Texas (Alluvial bank facies)	Post colonisation (after 1920AD) indicated by	0.36 ± 0.02
817/1	Colorado river, Columbus, Texas (Alluvial bank facies)	introduced mollusc	0.19 ± 0.03
817/2	Colorado river, Columbus, Texas (Alluvial bar facies)	*Corbicula fluminea* (Britton,1982)	0.214 ± 0.008
817/3	Colorado river, Columbus, Texas (Alluvial laminated sand and silt facies)		0.643 ± 0.015
817/4	River Windrush, Oxon, UK (overbank flood deposit		0.174 ± 0.007
MOD01c	River Windrush, Oxon, UK (overbank flood deposit	Soil developed (not modern)	0.31 ± 0.01
	Loire Valley source, Massif Central, France		
MOD01d	Loire valley, 100m downstream		1.09 ± 0.04
	Loire valley, 1km downstream		
HB1	Loire valley, 10km downstream		3.27 ± 0.08
HB2	Retournac, Loire, 100km downstream		1.12 ± 0.06

HB3	Near Degoin, Loire, 300km downstream		0.97 ± 0.09
HB4	Morvan plateau, Loire, 350km downstream		1.6 ± 0.3
HB5	Loire valley, 400km downstream		1.0 ± 0.06
HB6	Near Fourchamboult, Loire, 500km		0.43 ± 0.06
HB7	Gien, Loire valley, 650km downstream		0.39 ± 0.01
HB8	Loire valley, 750km downstream		2.1 ± 0.1
HB9	St. Genouph, Loire 850km downstream		1.48 ± 0.05
HB10	Angers, Loire valley, 950km downstream		0.77 ± 0.04
HB11	Oxon, UK (Roadside colluvium)		0.76 ± 0.04
HB12	Oxon, UK (Roadside colluvium)	Above road tarmac	0.84 ± 0.21
HB13		Above road tarmac	0.122 ± 0.006
MOD01a			3.48 ± 0.08
MOD01b			0.31 ± 0.01

Modern samples kindly supplied by Dr S. Stokes: See Stokes (1992, 1994).

HB – samples from Stokes *et al.* (2001)

Appendix B

Custom written curve-fitting software

The nonnegative least squares (NNLS) fitting routine (described in section 3.5) is one of the methods used for LM OSL curve fitting. Matlab version 5.1 was used as an environment to produce custom written software for this purpose. Matlab is a powerful mathematical tool that incorporates a built-in NNLS algorithm. The Graphical User Interface (GUI) in the Matlab software allowed the creation of a user-friendly curve-fitting program. Below (Fig. B1), is the custom-made user interface of one of the final versions of the fitting program.
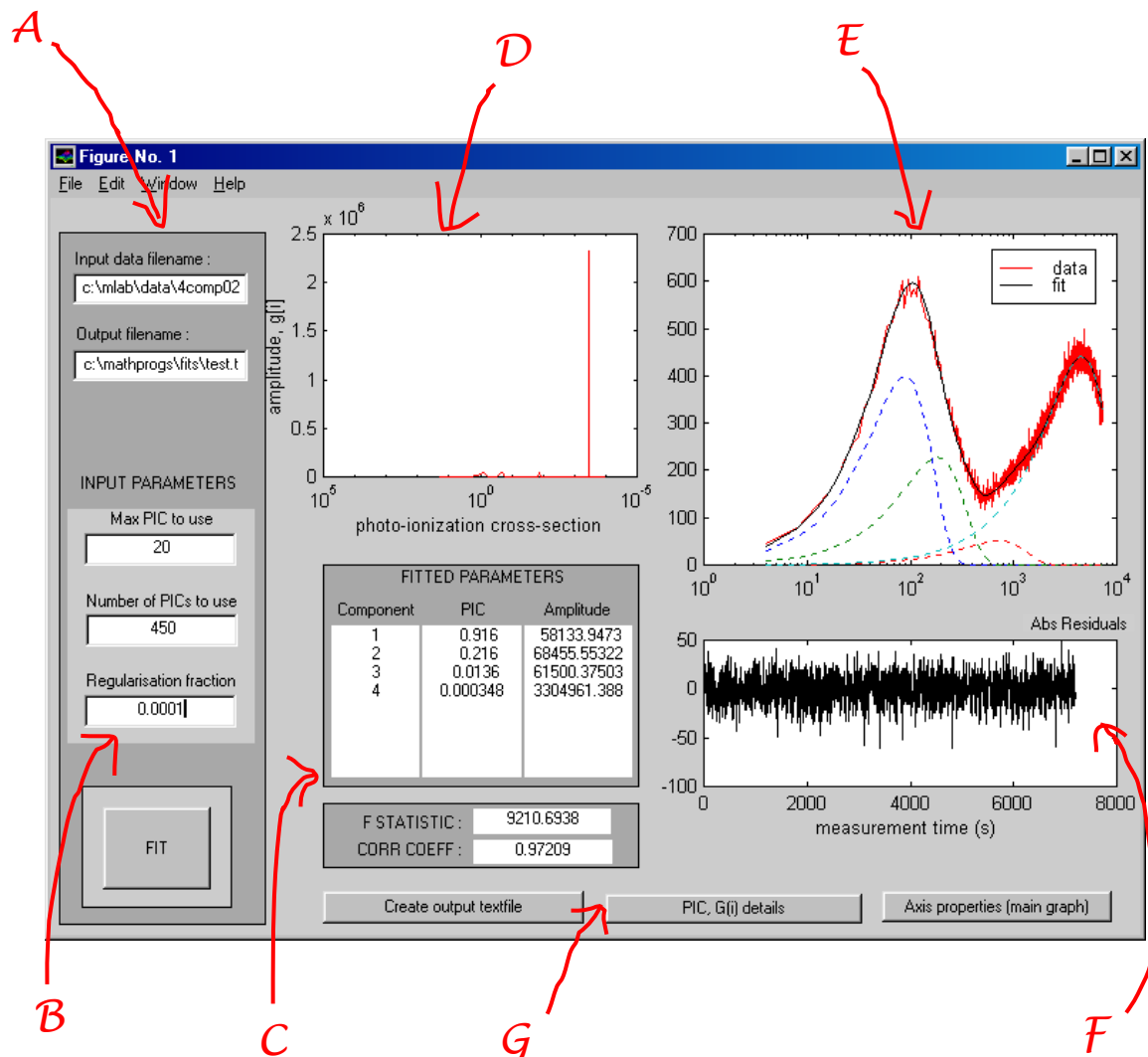
Fig. B1 GUI screen of the NNLS curve fitting used for deconvoluting LM OSL curves. The deconvolution process is described in section 3.5.

To note in Fig. B1:

A. The input/output files, and their file location are input from the screen to allow flexibility.

B. The matrix parameters are input here. 'Max PIC to use' refers to the maximum photo-ionisation cross-section desired. 'Number of PICs to use' refers to the number of cross-sections in matrix K (see equation 3.26), i.e. the width of the matrix. 'Regularisation fraction' is the fraction of the cross-section values to use for the modified Tikhonov regularisation (section 3.5.2).

C. The program calculates the number of components (given a number of criteria), the values of the photo-ionisation, and the magnitudes, n_0. These values are obtained from the spectral function, g. Estimates of the appropriateness of the fit is calculated via the F-statistic and the correlation coefficient ('CORR COEF').

D. A graph of the amplitude, $g(i)$, vs. the photo-ionisation cross-section is illustrated. This graph allows a clear picture of the spectral function, without the assumptions used by the program to calculate the number of components (note C).

E. This graph shows the data (red) and the fit to it (black). The deconvoluted OSL components are shown as the dotted lines.

F. A residual plot is shown (data(t_i) − fit(t_i)) vs. measurement time. Systematic deviations from zero of the residuals are considered as indication of a poor fit.

G. The buttons along the lower edge of the screen allow the user to choose to print the results (i.e. data, fit, spectral function etc.) into a text file (the location and name of which is given in A, top left corner). The user can choose to inspect the spectral function as text ('PIC, G[i] details'), and change the axes properties of the main graph, E.

The following pages show the code initiated by the 'FIT' button using the GUI. This is the basic routine that opens the data and runs the fitting process. The creation of text files of the results, changing axes etc. is achieved through separate buttons with their associated code (not included here, as it is not essential to the understanding of the fitting process).

```matlab
% This is the script that is initiated by the FIT button. It
finds the entire screen and file inputs and rearranges them
for input into the NNLS algorithm. The results are then
processed and graphical output is performed.

clear; %all variable values stored in the memory are cleared

%All relevant screen inputs are found and labelled.
JJ=findobj(gcf,'Tag','reginput');
reg=str2num(get(JJ,'String'));
KK=findobj(gcf,'Tag','maxpic');
picl=str2num(get(KK,'String'));
LL=findobj(gcf,'Tag','numpic');
n=str2num(get(LL,'String'));
FF=findobj(gcf,'Tag','infile');
inputfile=(get(FF,'String'));

% a waitbar is introduced; filled throughout running of
program
G=waitbar(0,'Please wait....');

% The input file is opened, containing 2 columns: time, data.
The number of channels is counted. Separate vectors for
measurement time and data are created.
fid=fopen(inputfile,'rt');
[B,count]=fscanf(fid,'%f',[2,inf]);
m=count/2;
input=B';
for i=1:m,
  trows(i)=input(i,1);
  brows(i)=input(i,2);
end
t=trows';
b=brows';
T=t(m);
waitbar(0.1)

% Formation of matrix K (here called A(i,j).
for j=1:n,
  pic(j)=picl/(j^2);
  for i=1:m,
    A(i,j)=pic(j)*t(i)*(1/T)*exp((-pic(j)*(t(i)^2))/(2*T));
  end
end

% Tikhonov regularisation is added. Matrix becomes Atik=(A'*A)
+ eye1. Data vector is transformed to btik.
for i=1:n,
  for j=1:n,
    if (i==j);
      fracreg=reg*pic(i);
      eye1(i,j)=fracreg;
```

```
      else
         eye1(i,j)=0.0;
      end
   end
end
Atik=(A'*A) + eye1;
btik=A'*b;
waitbar(0.2);

% Atik and bitk are passed into the NNLS routine. The return
vector, X, is the spectral function g[i].
X = NNLS(Atik,btik);
waitbar(0.5);

% Program counts up the number of OSL components found by NNLS
and calculates the cross-section and magnitude of each.
counter = 1;
j=1;
for i=1:n,
  if (X(i) > 0);
    picmat(j,counter) = pic(i);
    gimat(j,counter) = X(i);
    j=j+1;
  else (X(i) == 0);
    if i > 1;
         if (X(i-1) > 0);
            counter=counter+1;
      j=1;
    end
  end
end
end
[p,q]=size(gimat);
multimat=picmat.*gimat;
for i=1:q,
  sum1=0;
  sum2=0;
  for j=1:p,
    sum1=sum1+gimat(j,i);
    sum2=sum2+multimat(j,i);
  end
  mag(i)=sum1;
  multi(i)=sum2;
end
xsection=multi./mag;

% From the OSL cross-sections and magnitudes the components
I(t) are calculated using first order solution. The total fit
I(t) is also calculated.
for j=1:q,
    for i=1:m
```

```matlab
    fitmat(i,j)=mag(j)*xsection(j)*t(i)*(1/T)*exp((-
xsection(j)*(t(i)^2))/(2*T));
end
end
for i=1:m,
  fitsum=0;
  for j=1:q,
    fitsum=fitsum+fitmat(i,j);
  end
  finalfit(i)=fitsum;
end

% Calculation of absolute and percentage residuals.
for i=1:m,
  Abs_residual(i)=finalfit(i)-b(i);
  percent_residual(i)=100*(Abs_residual(i)/b(i));
end
waitbar(0.8);

% formation of screen text output of number of components and
parameter values
component=1:1:q;
out1=component';
out2=xsection';
out3=mag';
textout1=num2str(out1);
textout2=num2str(out2,3);
textout3=num2str(out3,10);
waitbar(0.9);
close(G); %close waitbar

% creation of result plots - spectral function, data and fit,
and residual plots.
hold off;
subplot('position',[0.25 0.62 0.29 0.33])
semilogx(pic,X,'r');
xlabel('photo-ionization cross-section');
ylabel('amplitude, g[i]');
set(gca,'XDir','reverse','YDir','normal');
subplot('position',[0.6 0.2 0.38 0.2])
plot(t,Abs_residual,'k');
xlabel('measurement time (s) ');
subplot('position',[0.6 0.5 0.38 0.45])
plot(t,b,'r');
hold on;
plot(t,finalfit,'k');
legend('data','fit',1);
hold on;
semilogx(t,fitmat,':');
hold off;
```

```matlab
% prints to screen the number of components, cross-section
values and magnitudes.
ZZ=findobj(gcf,'Tag','comp1');
set(ZZ,'String',textout1);
YY=findobj(gcf,'Tag','picout1');
set(YY,'String',textout2);
VV=findobj(gcf,'Tag','giout1');
set(VV,'String',textout3);

% Calculation of F-statistic and Pearson's correlation
coefficient for fit.
alpha = (m-(q*2))/((q*2)-1);
avesumb = 0;
avesumfit = 0;
for i=1:m,
  avesumb = avesumb + b(i);
  avesumfit = avesumfit + finalfit(i);
end
meanb = avesumb/m;
meanfit = avesumfit/m;
beta = 0;
gamma = 0;
for i=1:m,
  beta = beta + (b(i) - meanb).^2;
  gamma=gamma + ((finalfit(i) - b(i)).^2)-1;
end
F = alpha*(beta/gamma);
Fs = num2str(F);
ID=findobj(gcf,'Tag','Fstat');
set(ID,'String',Fs); % print F-statistic to screen text box.
r1=0;
r2=0;
r3=0;
for i=1:m,
  r1 = r1 +((b(i) - meanb)*(finalfit(i) - meanfit));
  r2 = r2 + ((b(i) - meanb).^2);
  r3 = r3 + ((finalfit(i) - meanfit).^2);
end
Pearson = (r1/(sqrt(r2)*sqrt(r3)))^2;
PearsonS = num2str(Pearson);
ID2=findobj(gcf,'Tag','Rcoeff');
set(ID2,'String',PearsonS); %Print correlation coefficient to
screen text box.




%NNLS   Non-negative least-squares.
function [x,w] = nnls(E,f,tol)
```

```
%    X = NNLS(A,b) returns the vector X that minimizes
NORM(A*X - b)
%    subject to X >= 0.    A and b must be real.
%
%    A default tolerance of TOL = MAX(SIZE(A)) * NORM(A,1) *
EPS
%    is used for deciding when elements of X are less than
zero.
%    This can be overridden with X = NNLS(A,b,TOL).
%
%    [X,W] = NNLS(A,b) also returns dual vector W where w(i)
< 0
%    when x(i) = 0 and w(i) is approximately 0 when x(i) > 0.


%    L. Shure 5-8-87
%    Revised, 12-15-88,8-31-89 LS.
%    Copyright (c) 1984-97 by The MathWorks, Inc.
%    $Revision: 5.5 $  $Date: 1997/04/08 06:27:03 $

% Reference:
%  Lawson and Hanson, "Solving Least Squares Problems",
Prentice-Hall, 1974.

if nargin<2, error('Not enough input arguments.'); end
if ~isreal(E) | ~isreal(f), error('A and b must be real.');
end

% initialize variables
if nargin < 3
    tol = 10*eps*norm(E,1)*length(E);
end
[m,n] = size(E);
P = zeros(1,n);
Z = 1:n;
x = P';
ZZ=Z;
w = E'*(f-E*x);

% set up iteration criterion
iter = 0;
itmax = 3*n;

% outer loop to put variables into set to hold positive
coefficients
while any(Z) & any(w(ZZ) > tol)
    [wt,t] = max(w(ZZ));
    t = ZZ(t);
    P(1,t) = t;
    Z(t) = 0;
    PP = find(P); % finds indices of nonzero elements
    ZZ = find(Z);
```

```matlab
    nzz = size(ZZ);
    EP(1:m,PP) = E(:,PP);
    EP(:,ZZ) = zeros(m,nzz(2));
    z = pinv(EP)*f; %pinv produces pseudoinverse matrix
    z(ZZ) = zeros(nzz(2),nzz(1));
% inner loop to remove elements from the positive set which
no longer belong
    while any((z(PP) <= tol))
        iter = iter + 1;
        if iter > itmax
            error(['Iteration count is exceeded.', ...
                '  Try raising the tolerance.'])
        end
        QQ = find((z <= tol) & P');
        alpha = min(x(QQ)./(x(QQ) - z(QQ)));
        x = x + alpha*(z - x);
        ij = find(abs(x) < tol & P' ~= 0);
        Z(ij)=ij';
        P(ij)=zeros(1,length(ij));
        PP = find(P);
        ZZ = find(Z);
        nzz = size(ZZ);
        EP(1:m,PP) = E(:,PP);
        EP(:,ZZ) = zeros(m,nzz(2));
        z = pinv(EP)*f;
        z(ZZ) = zeros(nzz(2),nzz(1));
    end
    x = z;
    w = E'*(f-E*x);
end
```

Appendix | C

PERGAMON

Potential of the slow component of quartz OSL for age determination of sedimentary samples

J.S. Singarayer*, R.M. Bailey, E.J. Rhodes

Research Laboratory for Archaeology and the History of Art, University of Oxford, 6 Keble Road, Oxford OX1 3QJ, UK

Abstract

The slow component of quartz OSL exhibits a high thermal stability, and, in many of the samples studied, a high dose saturation level (several hundreds or, even thousands, of Grays). These properties suggest that the slow component has potential as a long-range dating tool. Initial attempts have been made to obtain equivalent doses for a number of sedimentary samples. Single- and multiple-aliquot techniques were modified for use with the slow component. The results indicate that there is a good potential for sediment dating, particularly for samples of significant age. Experiments concerning the optical resetting of the slow component suggest that, given its slow optical depletion rate, dating may be restricted to aeolian sediments. © 2000 Elsevier Science Ltd. All rights reserved.

1. Introduction

Initial measurements by Huntley et al. (1985) demonstrated that the decrease in OSL emission upon illumination does not follow a simple exponential, as one would expect from a single trap system with first order kinetics. Smith and Rhodes (1994) found the emission to be the sum of three signal components, referred to as the fast, medium and slow, or long-term, components after their relative optical depletion rates. Bailey et al. (1997) show that the most probable explanation is that the OSL signal comes from three different traps with different rates of charge loss, of which the slow component is inferred to be the deepest, based on laboratory measurements of thermal stability.

Direct observation of the slow component at present requires the removal of the other components. This was achieved by Bailey (2000) using either optical washing, 100 s illumination at 160°C (to prevent photo-transfer into thermally unstable TL peaks), or by heating to 450°C or 500°C (thermal washing).

Several observed properties differentiate the slow component from the fast and medium components. It shows remarkable thermal stability and a high dose saturation level, both of which suggest it may be useful for long-range dating. From the observed dependence of the decay form and rate on charge concentration, the recombination mechanism for the slow component was inferred by Bailey (1998, 2000) to involve a proximity-dependent, direct donor-acceptor transition. This mechanism of recombination relies on the overlap of donor and acceptor wave functions. The probability of recombination is exponentially dependent on the distance between the two (McKeever, 1985).

Presented in this paper are attempts at equivalent dose determination on a variety of samples using single- and multiple-aliquot techniques. Results indi-

---

* Corresponding author.
E-mail address: joy.singarayer@linacre.ox.ac.uk (J.S. Singarayer).

cate that there is potential for dating sediments in excess of 1 Ma using this component. Experiments concerning the optical resetting of the slow component suggest that, given its slow depletion rate, its application to dating may be restricted to windblown sediments.

2. Behaviour of the slow component with respect to dating

This section concentrates on the fundamental properties required for successful dating of sedimentary samples. Essentially, the signal must be relatively thermally stable (for the trap(s) to have adequate retention lifetimes for dating), grow with dose, and be reset by exposure to light. Details of samples used, preparation procedures, and measurement conditions are given in Appendix A. OSL measurements were made using a Risø-set (TL-DA-12) unless otherwise stated.

2.1. Thermal stability

One of the most important features of the slow component that distinguishes it from the main part of the OSL signal is its thermal stability. Heating to 400°C is sufficient to remove the fast and medium components; both associated with the 325°C TL region (Smith et al., 1990). However, the slow component remains after heating to > 400°C, as discussed below.

Fig. 1 shows the results of a pulse annealing experiment performed on a number of different samples. Bailey (2000) performed this experiment on a single sample and the work presented here attempts to assess the generality of these findings. For this experiment

the fast and medium components were removed using an optical wash of 100 s OSL at 250°C. This temperature was chosen to minimise photo-transfer whilst being low enough to prevent thermal sensitisation. The OSL of single aliquots was measured for 100 s at 160°C subsequent to ramp heating to progressively higher temperatures (in the range of 300–700°C). A slow linear heating rate of 2°C s^{-1}, with 10 s hold at T_{max}, was used to reduce the effects of thermal lag between sample and heater plate, and with the idea of also shifting any thermally activated responses to lower temperatures.

The decrease in OSL between 300°C and 400°C in Fig. 1 suggests that there has been some recuperation into optically unstable traps during preheating, following the initial optical wash (see Bailey (2000) for further discussion). For all samples tested so far, above a preheat temperature of 500°C there is an increase in OSL with increasing preheating temperature. The maximum level of OSL observed under these conditions was found to vary between 550°C and 600°C. It is unclear, as yet, what mechanisms are responsible for the observed rise in signal. Interpretation of the results is complicated by the opposing effects of thermal sensitisation and thermal erosion, and by possible thermal transfer to the slow component (from centres thermally unstable in the 400–600°C region). Regardless of this, the difference in thermal stability between the fast and medium OSL components and the slow component strongly suggests that different charge populations are responsible.

It was from these results that a temperature of 450–500°C was chosen as an appropriate preheating temperature for thermally washing to remove the fast and medium components without significantly affecting the magnitude of the slow component.

2.2. Dose response: growth curves

As originally observed by Bailey (1998), for a number of samples, the response of the integrated slow component OSL signal to β-dose far exceeds that of both the fast and medium. In many cases, saturation does not occur until several hundreds, or sometimes thousands of Grays.

Bailey (2000) presented growth curves of two samples with remarkable dose responses, produced using a multiple-aliquot additive-dose method that were well described by single saturating exponentials. His initial results provided encouragement for the use of the slow component to date samples of considerable age. Presented in Section 3.2 is a further example of a sample (TQG) with an equally high saturation level.
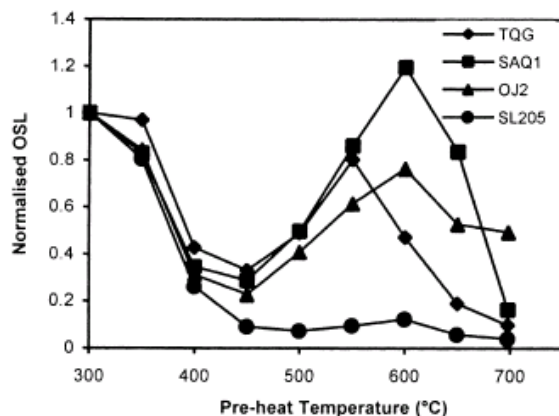

Fig. 1. Pulse annealing of the slow component for various samples show the effect of preheat temperature on the initial signal. See main text for details of the measurement procedure (Section 2.1).

2.3. Signal resetting

One of the main issues surrounding the applicability of the slow component as a dating tool, given its slow optical depletion rate, is signal zeroing. Preliminary investigations into the bleaching response of the slow component have been undertaken using various samples. For each sample, a thermal wash (heating to 400°C in this case) was given to aliquots prior to 50 s OSL (using an Ar-ion laser; see Appendix A) at 15°C (effectively a short shine for the slow component). A series of white light exposures was then administered using an Oriel solar simulator (Model 6114 Universal arc lamp source), each time followed by a 50 s short shine $(OSL_{bleach})_i$. Control aliquots that received no white light exposure were used to account for signal depletion during OSL measurements $(OSL_{control})_i$. Results for sedimentary samples TQG and 897-3 are shown in Fig. 2.

The length of exposure to white light sufficient to bleach the slow component to negligible levels was sample dependent. Between 1000 min (17 h) and 10,000 min (1 week) was required to bleach most samples to "background" levels.

The slow bleaching response may make slow component dating redundant for many types of sediment. Some aeolian deposits may, however, receive adequate light exposure before deposition, enabling the use of this signal. Equivalent doses obtained using the slow component have, in some cases, been in agreement with those obtained by standard methods, using the initial portion of the OSL decay (Section 3.2). These results provide some evidence that sufficient bleaching of the slow component occurs in some sediments.
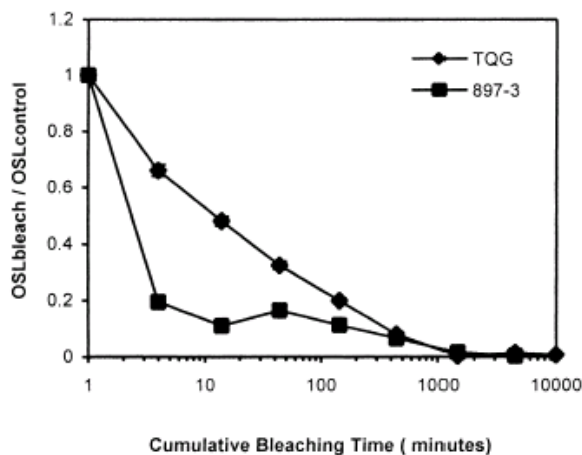

Fig. 2. The white light bleaching response of samples TQG and 897-3. For each point four bleached and four control aliquots were used.

3. Dating applications

The behaviour of the slow component (Section 2) suggests that, in some cases, it may provide a means of dating sediment deposition. Several techniques for obtaining equivalent doses are assessed in the present section.

3.1. Dating procedures

Initial attempts at producing growth curves were made using a multiple-aliquot additive-dose method. Details of the procedure used and examples of multiple-aliquot growth curves are described in Bailey (2000), where signal growth was well described by a single saturating exponential function without the need for inter-aliquot normalisation. However, repetition of this protocol on several other samples has produced a significant amount of scatter between aliquots, necessitating the use of inter-aliquot normalisation. Several existing methods have been tried, including short-shine and zero-glow normalisation. Although all methods reduced scatter, further work is required to determine which of these methods will prove most reliable.

The difficulties of inter-aliquot normalisation are removed with the use of single-aliquot techniques. For this reason recent work has been concentrated on single-aliquot procedures. The methods employed will be examined in the remainder of Section 3.1.

3.1.1. Single-aliquot additive-dose protocol

Application of a modified version of the single-aliquot additive-dose method of Murray et al. (1997) was the focus of initial work. Each aliquot is taken through a measurement cycle of: (i) laboratory added β-dose; (ii) optical/thermal washing; (iii) OSL "short-shine" measurement, following Bailey (2000). Ideally, the OSL measurement must be long enough to record a sufficient number of counts (for statistical precision) without depleting the signal significantly. Generally, a 50 s OSL measurement at 160°C is adequate, but a variety of illumination times and temperatures have been used to respond to sample dependent brightness and decay rate. Section 3.2 contains details of the use of this method on various samples.

Background levels were taken as the counts recorded from a blank disc under the same conditions as for the experiment in progress (following Bailey, 2000). It was thought that, given the thermal stability and slow bleaching characteristics of the slow component, taking measurements from a "dead disc" (that has been bleached or annealed) might not be an appropriate or convenient method to obtain background for subtraction.

3.1.2. Single-aliquot regenerative-dose protocol

A version of the SAR (single-aliquot regenerative-dose) method (Murray and Wintle, 2000) has also been tested on several samples. The depletion rate of the slow component at standard OSL measurement temperatures would make application of the SAR protocol a very lengthy procedure indeed. However, when OSL measurements are made at higher temperatures the rate of depletion increases. The slow component signal has been observed to deplete to ∼5% after 1000 s in many samples when measured at temperatures in excess of 240°C (after optical washing). The decay rate at such temperatures may make the use of a SAR regime a more feasible prospect.

Fig. 3 gives the procedure followed to obtain slow component SAR growth curves. The SAR method has been attempted only applying the optical washing method to remove the fast and medium components as it was found that thermal washing did not produce the same temperature dependence of the slow component decay rate. The reason for this is not understood at present and is under further investigation. The integrated initial portion of the slow component decay was used (0–200 s) with a background subtraction taken from the last 200 s of the decay. Changes in sensitivity are corrected for by the OSL_2 from a test dose in a similar manner as that used by Murray and Wintle (2000).

3.2. Application of dating protocols: examples of equivalent dose determination

Fig. 4(a) shows a growth curve for sample SL161, achieved using the single-aliquot additive-dose method described in Section 3.1.1 (thermal wash at 500°C, 50 s OSL at 120°C). Fig. 4(b) shows results for the same sample using the SAR method on the rapidly bleachable portion of the OSL decay (fast and medium components). Agreement between the equivalent doses

produced using these two methods suggests that the slow component was adequately reset upon deposition. It is also an indication that the procedure used to obtain the slow component D_e was appropriate for this sample. Bailey (2000) also provides an example of agreement between the slow component and the initial OSL signal of sample 897-3, again suggesting that sufficient bleaching of the slow component occurred upon deposition.

The sample represented in Fig. 4 is fairly unusual in that the slow component does not display the high dose saturation levels that have been observed in other samples. Fig. 5(a), in contrast, shows a single-aliquot growth curve for a sample (TQG) with one of the most impressive dose responses observed so far, again produced using the slow component single-aliquot

(a)

$D_e = 28.9 \pm 3.3$ Gy

(b)

$D_e = 29.2 \pm 1.1$ Gy

Fig. 3. Measurement procedure used for initial attempts at a slow component single-aliquot regenerative-dose technique (see Section 3.1).
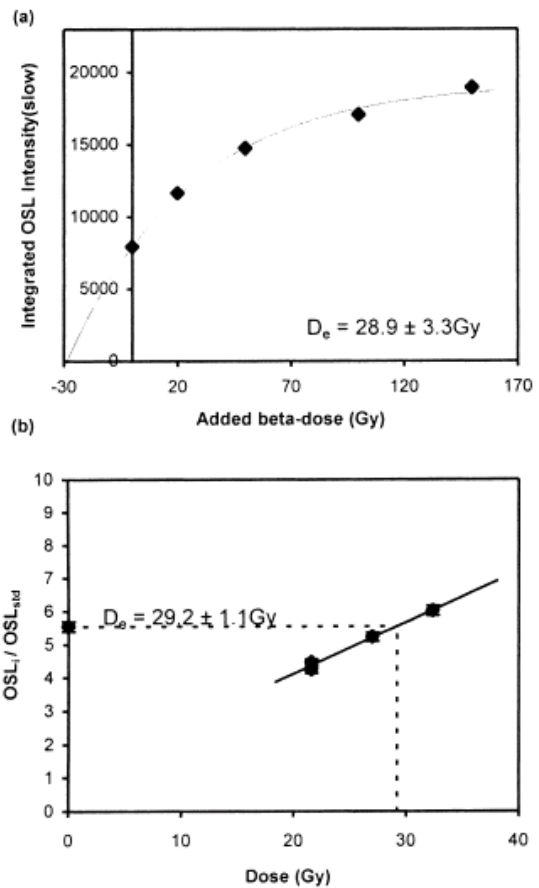
Fig. 4. (a) Slow component growth curve for sample SL161 achieved using a single-aliquot additive-dose procedure (described in Section 3.1). The data were fitted to a single saturating exponential to obtain an estimate of the D_e by extrapolation to zero intensity. (b) SAR growth curve for sample SL161 using the initial rapidly decaying part (fast component) of the OSL decay (measured by RMB for the Oxford Luminescence Dating Facility).

additive-dose protocol (thermal wash of 450°C, 50 s OSL at 160°C). In the SAR growth curve data for the fast component (Fig. 5(b)) the natural signal has reached a state of near saturation. The slow component growth, however, continues beyond 2000 Gy. The in situ dose rate for this sample was approximated from NaI γ-spectrometry results from adjacent samples. A slow component age estimate of 735 ± 71 ka was calculated for this aliquot (TQG was taken from sediment overlying the Brunhes–Matuyama boundary layer; expected age 600–800 ka).

An attempt was made to assess the consistency of the dating techniques through the recovery of known doses given to samples in the laboratory. Successful retrieval of a range of doses gives some indication that the protocols described in Section 3.1 are suitable for use with the slow component. Samples that had been annealed or bleached for a substantial length of time to remove the slow component signal were given

known laboratory doses, β_R. Various dating procedures were carried out on these samples to try to retrieve the artificial doses through equivalent dose determination.

Fig. 6 shows the dose response for annealed sample EBSan when given 0, 5, 30 and 150 Gy β_R-doses, achieved using the single-aliquot additive-dose protocol (thermal wash of 500°C, 50 s OSL at 160°C). Non-uniform, non-monotonically increasing growth was observed in this sample. The size of the observed "dip" was exaggerated with the increasing magnitude of the initial laboratory dose, β_R. This form of growth was also observed when multiple-aliquot methods were employed (using the same sample) and it is therefore not thought to be an artefact of the measurement procedure. The observed growth form, although as yet unaccounted for, is possibly due to dose quenching effects (e.g., Huntley et al., 1996).

In an attempt to characterise the apparent drift per measurement cycle, the integrated OSL measured during repeated pre-heat/stimulation cycles on single aliquots (with no additive doses) was investigated. It is a condition of the single-aliquot additive-dose technique that the integrated OSL signal should either remain at a relatively constant level over a number of measurement cycles, or that it should change in a well-defined manner. The loss of signal should ideally be negligible and no large sensitivity changes should occur throughout the measurement procedure. Repeated pre-heat/stimulation cycles (for EBSan and several other samples) produced a substantial decrease in the integrated signal, particularly between the first and second cycles. The degree of decay (per cycle) was dependent upon the size of the laboratory dose, the rate and amount of loss increasing with larger doses. (Note that the same pre-treatment/stimulation cycles

(a)

$D_e = 377 \pm 23$ Gy
$D_0 = 2790$ Gy

(b)

$D_e = 278 \pm 37$ Gy
$D_0 = 88 \pm 3$ Gy
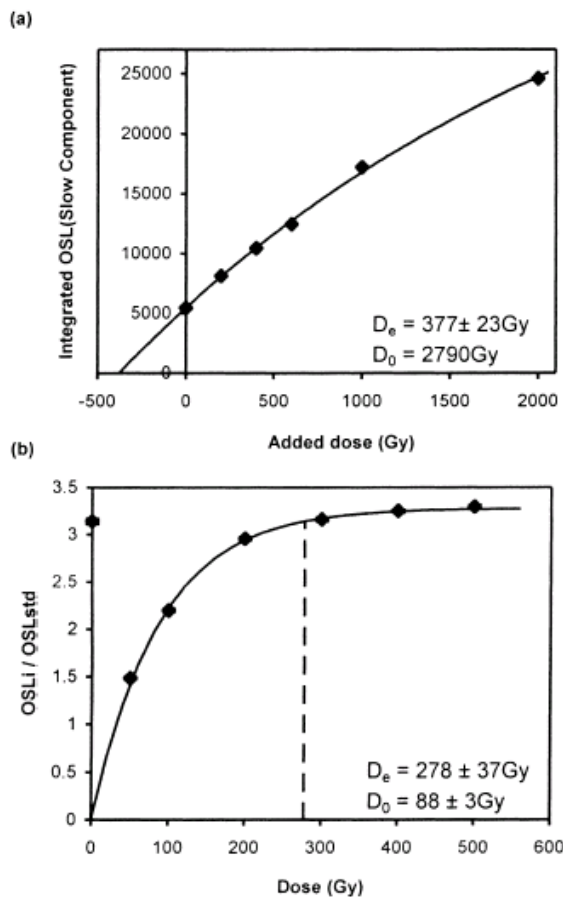
Fig. 5. (a) Single-aliquot growth curve for sample TQG (see Section 3.2 for measurement details). A single saturating exponential fitted to estimate the D_e. (b) SAR growth curve using the fast component of the same sample.
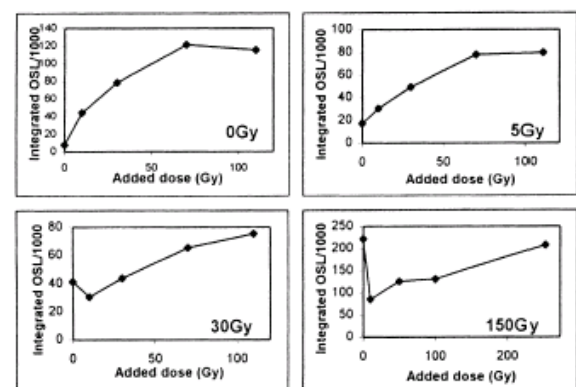
Fig. 6. Application of single-aliquot additive-dose procedure to annealed sample EBSan. Aliquots were given various laboratory β-doses prior to measurement (0, 5, 30 and 150 Gy). The single-aliquot protocol was employed in an attempt to recover the artificial doses.

were performed on samples SL161 and TQG, whose growth curves (Figs. 4 and 5), measured using the single-aliquot additive-dose procedure, showed no sign of complex dose response. For these samples, the integrated OSL was constant over five measurement cycles).

A simple method was devised, using the single-aliquot additive-dose technique, to correct for the dipping growth form of sample EBSan. Fig. 7 shows an example of this method applied to an aliquot of EBSan given a 30 Gy β_R-dose. The additive-dose measurement cycle, described in Section 3.1.1, was performed, with the modification that at each dose point three pre-heat/stimulation cycles were carried out to ascertain the form of the OSL decrease (see Fig. 7(a), solid symbols). The decays at each dose point were separated and fitted individually to a two-exponential function. Interestingly, the decay constants describing the faster exponential decay were the same for all doses. The unfilled symbols in Fig. 7(a) show the extrapolation of the decays at each dose (showing the expected OSL integrals from further measurement cycles had no more additive-doses been given). At each dose the first extrapolated point (fourth cycle) was subtracted from the first measurement in the cycle. The value obtained was added to the next measured dose point to correct for the amount of decay that had occurred. Fig. 7(b) shows the results from the application of this correction procedure. The square symbols represent the first measurement made at each dose. They display a dose response similar in form to that shown Fig. 6 (30 Gy). The solid symbols represent

the same points following the application of the correction procedure. The equivalent dose obtained from these points using a single-saturating exponential fit is 29.9 ± 2.1 Gy.

An attempt to recover a range of known doses using the modified SAR method had not been completed at the time of writing. However, initial results were encouraging. For a single aliquot of EBSan irradiated with 5 Gy (β) the equivalent dose obtained was 4.94 ± 0.59 Gy. Preliminary results suggest that the slow component receives sufficient bleaching during 2000 s OSL at high temperatures to enable the use of this technique.

4. Conclusions

The slow component of quartz OSL displays properties that suggest that it has potential for dating. It has a high thermal stability and saturation level far in excess of existing quartz OSL techniques. Its slow bleaching response may preclude the use of slow component dating for many types of sediment. Certain windblown sediments, however, may receive adequate light exposure to enable the use of these techniques. Inadequate light exposure for full resetting may be less of a problem when dating samples of significant age since any resultant age over-estimates may be negligible in comparison to the burial period.

Existing dating protocols have been modified for use with the slow component and applied to a variety of sedimentary samples. Encouraging results have been
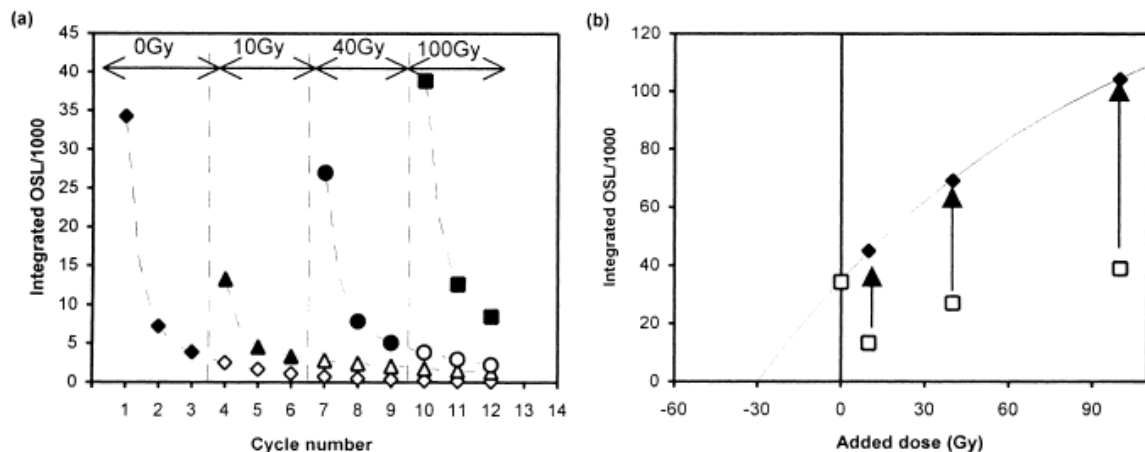
Fig. 7. (a) Repeated pre-heat/stimulation cycles performed on an aliquot of EBSan that had received an initial laboratory dose of 30 Gy. Before every fourth cycle further doses were given (the cumulative added doses are given at the top of the graph). Solid symbols represent actual measurements. Unfilled symbols are extrapolations of OSL decrease for each dose expected had no further doses been administered. (b) Integrated OSL signal vs. additive-dose graph for EBSan (30 Gy initial dose). Unfilled symbols represent the signal recorded from the first preheat/stimulation cycle at each dose point in Fig. 7(a). A correction procedure described in the text was applied to these points to produce the growth curve consisting of the filled points.

obtained that suggest that there is the possibility of extending the datable age range of quartz using this component. There are, however, several potentially problematic issues associated with the application of these techniques. The effects of sensitivity change and thermal transfer (due to the pre-treatments used) on dose response must be investigated in attempting to account (and correct) for some of the unexpected growth forms observed; and to develop appropriate measurement procedures to obtain reliable estimates of equivalent dose.

Acknowledgements

Appendix A

A1. Sample details

EBSan	Eastbourne beach sand, annealed at 580°C for 40 min (modern).
OJ2	Aeolian deposit, Morocco (ca. 330 ka).
RB2	Neolithic beach sand, Morocco (ca. 4 ka).
RB10	Aeolian dune sand, Southern China (ca. 50 ka).
SAQ1	Dune deposit, Morocco (ca. 390 ka).
SL161	Sri Lankan dune deposit (ca. 18 ka).
SL205	Sri Lankan dune deposit (ca. 34 ka).
TQG	Coarse bioclastic aeolian sand dune deposit, Thomas quarries, Morocco (taken from a layer directly overlying the Brunhes–Matuyama boundary, 600–800 ka).
897-3	Taramsa Hill burial site on the Nile valley, Egypt; provided by Dr. S. Stokes (ca. 55 ka, Vermeersch et al., 1998).

A2. Sample preparation

The standard preparation procedure for coarse grain quartz was employed for all samples. Sieved fractions (90–125 μm or 125–180 μm) were treated with 10% HCl to remove carbonate material. Density separation, using sodium polytungstate (2.62 g cm^{-3} to float off feldspars, and 2.68 g cm^{-3} to remove heavy minerals), was subsequently employed. Samples were etched using 40% HF acid for 60 min to remove any traces of feld-

spar and etch the outer (α-irradiated) layer of the quartz grains before sieving again prior to measurement.

A3. Measurement conditions

Measurements were made on a Risø set (TL-DA-12). A 75 W halogen lamp stimulation source was used, filtered with a HA-3 heat absorbing filter, 9 mm of GG420 glass filters and a broadband interference filter (broad-band stimulation between ca. 420–560 nm), at 12 mW cm^{-2} (Bøtter-Jensen and Duller, 1992). Emissions were filtered with two Hoya U340 glass filters (emission window ca. 270–370 nm). Photon detection was achieved using an EMI 9635QA photomultiplier.

Laser measurements were made using an Ar-ion laser, consisting of a focused, collimated 514.5 nm beam sent through a Corning 3-71 pass filter and 514 nm interference filter. Emissions were filtered by 11 mm of Corning 7-51 and 0.85 mm Schott BG39 glass filters. Light emissions were detected using an EMI 9635Q photo-multiplier.

References

Bailey, R.M., Smith, B.W., Rhodes, E.J., 1997. Partial bleaching and the decay form characteristics of quartz OSL. Radiation Measurements 27 (2), 123–136.

Bailey, R.M., 1998. The form of the optically stimulated luminescence signal of quartz: implications for dating. Unpublished Ph.D. thesis, University of London.

Bailey, R.M., 2000. The slow component of quartz optically stimulated luminescence. Radiation Measurements 32, 233–246.

Bøtter-Jensen, L., Duller, G.A.T., 1992. A new system for measuring optically stimulated luminescence from quartz samples. Nuclear Tracks and Radiation Measurements 20, 553–594.

Huntley, D.J., Godfrey-Smith, D.I., Thewalt, M.L.W., Berger, G.W., 1985. Optical dating of sediments. Nature 313, 521–524.

Huntley, D.J., Short, M.A., Dunphy, K., 1996. Deep traps in quartz and their use for optical dating. Can. J. Phys. 74, 81–91.

McKeever, S.W.S., 1985. Thermoluminescence of solids. Cambridge Solid State Science Series.

Murray, A.S., Roberts, R.G., Wintle, A.G., 1997. Equivalent dose measurement using a single aliquot of quartz. Radiation Measurements 27, 171–184.

Murray, A.S., Wintle, A.G., 1000. Luminescence dating of quartz using an improved single-aliquot regenerative-dose protocol. Radiation Measurements 32, 57–73.

Smith, B.W., Rhodes, E.J., Stokes, S., Spooner, N.A., 1990. The optical dating of sediments using quartz. Rad. Prot. Dosim. 34, 75–78.

Smith, B.W., Rhodes, E.J., 1994. Charge movements in quartz

and their relevance to optical dating. Radiation Measurements 23, 329–333.

Vermeersch, P.M., Paulissen E. Stokes, S., Charlier, C., Van, Peer P., Stringer, C., Lindsay, W., 1998. A middle Palaeolithic burial of a modern human at Taramsa Hill, Egypt. Antiquity 72, 475–484.

COMPONENT-RESOLVED BLEACHING SPECTRA OF QUARTZ OPTICALLY STIMULATED LUMINESCENCE: PRELIMINARY RESULTS AND IMPLICATIONS FOR DATING

ABSTRACT

Bleaching spectra of the 'fast' and 'medium' optically stimulated luminescence (OSL) components of quartz are reportred. A significant difference in their responses to stimulation wavelength is observed. Infrared bleaching at raised temperatures allowed the selective removal of the fast component. A method for optically separating the OSL components of quartz is suggested, based on the wavelength dependence of photoionization cross-sections.

1. INTRODUCTION

The form, composition and behaviour of the optically stimulated luminescence (OSL) signal from quartz has been the subject of much study over the last decade. Studies of quartz OSL (e.g. Spooner, 1994; Duller and Bøtter-Jensen, 1996) have found the bleaching rate to increase with incident photon energy (decreasing wavelength) and the de-trapping processes to be thermally assisted (the amount of thermal assistance decreasing with increasing photon energy; Spooner, 1994; Huntley *et al.*, 1996). Smith and Rhodes (1994) observed that the ultra-violet OSL emission from quartz could be described using a sum of three exponential components. Bailey *et al.* (1997) found the most probable explanation of this observation to be that each OSL component originates from a different trap type, each of which has a different rate of charge loss under illumination. Further evidence to support this view was provided by Bulur *et al.* (2000) using the recently developed 'linearly modulated OSL' (LM-OSL) technique, in which the existence of four separate quartz OSL components was demonstrated.

During conventional continuous-wave (CW) OSL measurements, the stimulation power (photon flux) is kept constant, producing a monotonically decaying signal. During LM-OSL measurements the stimulation power is ramped linearly from zero, generating peak-shaped luminescence. Using LM OSL, the structure of the signal, in terms of the number of components present, is recorded with greater clarity. The time dependence of the LM OSL for a single trap obeying first-order kinetics, given by Bulur *et al.* (2000), is

$$L(t) = n_0 \sigma \frac{I_0 t}{T} \exp\left(\frac{-\sigma I_0 t^2}{2T} \right)$$

Eq.1

where n_0 is proportional to the initial trap population, σ is the photoionization cross-section (cm^2), P is the maximum stimulation power (photon flux/cm^2), t is time (s), and T is total illumination time (s). The relative position of the OSL peak depends on σ, and because the OSL components of quartz have different σ (using the usual 470nm stimulation) the LM OSL observed is a series of overlapping peaks. Figure 1 shows an example LM-OSL curve for a natural sedimentary quartz sample, SL203 from Sri Lanka (measurement details given in the figure caption). The LM-OSL from this sample was best fitted using a sum of five first-order components (further evidence for the existence of at least five OSL components in several other samples is presented in Singarayer and Bailey, 2003). Components 1 and 2 are referred to in the literature as the 'fast' and 'medium' components (Bailey *et al.*, 1997); the slower components are referred to here as S_1, S_2, and S_3.

Bleaching spectra of quartz OSL have been published by several authors (e.g. Spooner, 1994; Duller and Bøtter-Jensen, 1996). In all cases the OSL described is the integrated luminescence (the sum of all components) vs. photon energy. No attempts have been made previously to describe the bleaching response of the individual OSL components. This paper reports a first attempt to measure the bleaching spectrum of the fast and medium OSL components. We have aimed specifically at measuring the response of the fast and medium OSL components (i.e. the initial, rapidly decaying, portion of the OSL) in this preliminary study. The fast and medium component responses are likely to be most relevant to the luminescence dating community as this part of the OSL signal is most commonly used in conventional dating techniques. Measurements of components S_{1-3} will be presented elsewhere. Implications for the identification of incompletely bleached sediments from different depositional environments are discussed later in the paper. Also, an alternative method for separating the OSL components of quartz is proposed, based on the different wavelength response of the OSL signal components.

2. EXPERIMENTAL DETAILS

2.1 Apparatus

OSL measurements were performed using either a Risø TLDA-10 or TLDA-15 reader. Both were equipped with excitation units containing blue light-emitting diodes ($\lambda \sim$ 470nm Δ20nm), delivering ~15mWcm^{-2} and ~18mWcm^{-2}, respectively. The luminescence emission was filtered using 6mm Hoya U340, providing an

emission window of $\lambda \sim 340\ \Delta80$nm, and recorded using a bialkali PMT. Irradiations were performed using $^{90}Sr/^{90}Y$ beta sources (dose rates 22 and 50mGy s^{-1}). Only the TLDA-15 reader had the capacity to make ramped power (LM OSL) measurements.

Bleaching of samples with different stimulation wavelengths was achieved using an external unit containing interchangeable LED arrays (λ's $\sim$ 375, 430, 500, 525, 590nm), the blue LEDs in the Risø reader excitation unit, and IR laser diodes ($\lambda \sim 830$nm), also in the Risø reader. An Oriel 300W filtered xenon lamp solar simulator was also used.

2.2 Samples

Quartz was extracted from a Sri Lankan sedimentary sample (SL203) using the procedure described by Stokes (1992). The refined quartz grains (125-180μm) were then mounted on to stainless steel discs (~5mg per aliquot) for measurement. Sample purity (with respect to feldspar contamination) was tested by IR stimulation at 20°C following irradiation and preheating (260°C, 10s). Absence of IRSL was taken as being indicative of sample purity with respect to feldspar.

2.3 OSL measurements

In order to take advantage of reduced measurement time, greater stimulation-power stability and the use of both automated systems (see Section 2.1), a mathematical transformation for converting CW OSL measurements into LM OSL (following Bulur, 2000) was used, i.e. OSL measurements are made in the standard manner (constant stimulation power) and transformed mathematically into the form that would have been observed had the stimulation power been ramped. This alternative is only possible if the detrapping of charge is due to single photon absorption and that this mechanism is independent of stimulation power. Spooner (1994) found a linear response of the OSL from quartz with stimulation power, using a 514nm laser over the range 0 to 238mW cm^{-2}. More recently, Bailey (2000), studying the slow components, and Bulur *et al.* (2001), found a similar linear response for quartz OSL stimulated with 514nm and 470nm stimulation respectively. These results indicate a single-photon absorption mechanism operates for quartz OSL. In the present study, good agreement was found between LM OSL and transformed or 'pseudo-LM OSL' implying that the transformation is a valid approximation for at least the fast and medium components.

Subsequent fitting of pseudo-LM OSL was performed using a non-linear least squares Levenberg-Marquardt algorithm (using the Microcal ORIGIN 4.1 software package). Fitting solutions were found by Chi-squared minimization (the fitted values being the sum of first-order LM-OSL expressions; Equation 1). From each fit n_0 and σ (and their associated uncertainties) were obtained for each component.

3. BLEACHING SPECTRA OF QUARTZ OSL FAST AND MEDIUM COMPONENTS

3.1 Measurement Results

Following bleaching of the natural OSL signal, single aliquots of sample SL203 were given 15Gy beta doses followed by a preheat at 260°C for 10s. The aliquots were then partially bleached at room temperature using the external LED unit described in the previous section. After a subsequent preheat (also 260°C, 10s) the remaining OSL was measured with blue stimulation for 100s at 160°C (a small amount of recuperation may have taken place during the second preheat, but it is not thought to have affected the results significantly). The cycle was repeated for various bleaching lengths and different stimulating wavelengths. In between each cycle of partial bleaching the OSL was measured without the external bleaching treatment in order to monitor sensitivity changes. The recorded OSL was converted into pseudo-LM OSL and fitted to a sum of first order peaks (as described in the previous section) in order to calculate the magnitude of the fast and medium component signals following partial bleaching. [Note: for future studies it would be less complex, in terms of experimental design, to simply record OSL whilst stimulating at the various wavelengths; this was not possible with our current laboratory set-up]

Figure 2 shows representative OSL signal depletion at various stimulation wavelengths, for the fast (upper) and medium (lower) components. Plotted here are the values of n_0 (for each component) found from curve fitting against incident photon flux (at the sample, from the stimulation source during partial bleaching). It can be clearly seen that the OSL signals decay exponentially under illumination (i.e. $OSL=n_0\sigma P\exp(-\sigma Pt)$), the fast component decaying at a greater rate than the medium. Values for photoionization cross-section (σ) at each of the stimulation wavelengths were obtained from the exponential fits, giving σ as a function of λ for both the fast and medium components (Figure 3, upper). The values of σ obtained for the fast and medium components are listed in Table 1.

The form of the σ response to photon energy is similar (through the visible range) to spectra found previously (e.g. Spooner, 1994; Huntley *et al.*, 1996). Not previously observed however is the difference in the responses of the fast and medium OSL components. Figure 3 (lower) shows the ratio $\sigma_{fast}/\sigma_{medium}$ to vary

from 30.6 at 590nm to 1.4 at 375nm. The difference in bleaching rate between the fast and medium components is therefore shown to be wavelength–dependent. This dependence on wavelength can be seen by comparing LM-OSL measured following bleaching with relatively long and short wavelengths. LM OSL curves recorded following partial bleaching with 525nm and 375nm photons are displayed in Figure 4. With increased durations of bleaching with 525nm light, a change in the form (an apparent shift to the right) of the LM peak is clearly observed, suggesting preferential bleaching of the fast component over the medium. However, using 375nm light for partial bleaching, the peak shift is reduced greatly, indicating that the fast and medium components are bleaching at a more similar rate. This observation is discussed further in Section 3.2.

An attempt was made to fit the observed stimulation spectra (σ versus λ) to an appropriate mathematical expression, knowing that the fast and medium are relatively deep trapping levels ($\geq$1eV; Bailey, 1998a). Initially, a fit to the general equation for $\sigma(h\nu)$ by Lucovsky (1965), for the case of a deep centre, was attempted (the Luckovsky function is often quoted in the quartz luminescence literature),

$$\theta(\hbar\omega) = \frac{1}{n}\left(\frac{E_{eff}}{E_0}\right)^2 \frac{16\pi e^2 \hbar}{3m^*c} \sqrt{E_i} \left[\frac{(\hbar\omega - E_i)^{\frac{3}{2}}}{\hbar\omega^3}\right]$$ Eq.2

where n is the index of refraction, E_{eff}/E_0 is the effective field ratio of the incident photon, m^* is the effective mass of the electron and E_i is the threshold energy for excitation.

While this function fitted the data for relatively high photon energies it fails to describe the data at low energy photon stimulation. It is to be noted that the Lucovsky expression is not appropriate for deep levels where coupling to the lattice is strong. In such cases $\sigma(h\nu)$ is temperature dependent, as observed previously for quartz OSL by several authors (see above), and the resulting absorption (bleaching) spectrum is broader due to electron-phonon coupling.

For the case of strong coupling, Huang and Rhys (1950) give the following expression.

$$\sigma_T(h\nu) = \frac{cons\tan t}{h\nu} \sum_{n,\vec{k}} \left|\left\langle \psi \left| \exp(-i\vec{k}_\lambda \cdot \vec{r})\vec{\varepsilon}_\lambda \cdot \vec{p} \right| \phi_{n,\vec{k}} \right\rangle\right|^2 J_{n,k}$$ Eq.3

where $h\nu$ is the incident photon energy, ψ is the localised (impurity) wavefunction, $\phi_{n,k}$ is the band wavefunction associated with reduced wave vector k and band n. The term $J_{n,k}$ describes the temperature dependence (thermal broadening). In the case of a highly

localized (deep) centre (with strong electron-phonon coupling), at high temperatures, $J_{n,k}$ simplifies to

$$J_{n,\bar{k}} = (4\pi k_B TS\hbar\omega)^{-1/2} \exp\left(- \left\{\left[h\nu - (|E_{i0}| + E_{n,\bar{k}})\right]^2 \right\}\middle/ 4k_B TS\hbar\omega\right) \qquad \text{Eq.4}$$

where $S\hbar\omega$ represents the magnitude (energy) of the Franck-Condon effect and E_{io} is the optical ionisation energy of the impurity. As temperature (T) increases, the exponential term in $J_{n,k}$ dominates, giving exponential dependence of σ on T at high temperatures. Empirical evidence for the exponential dependence of photo-eviction rate on temperature can be readily found in the quartz literature.

Jaros (1977) simplified the Huang and Rhys equation to

$$\sigma_T(h\nu) \sim \frac{1}{h\nu} \int_0^\infty dE \rho(E) \left| \frac{(1 \pm \eta)E^{1/2}}{|E_{i0}^T| + E} + \frac{(1 \mp \eta)(E_F)^{1/2}}{|E_{i0}^T| - E - (E_g + E_P)/2} \right|^2 \exp-\left(\frac{\left(h\nu - \left[|E_{i0}^T| + E\right]\right)^2}{4k_B Td_{FC}}\right)$$

Eq. 5

where E_g is the band gap, E_P the optical gap, E_F is the Fermi level energy, d_{FC} is the Frank-Condon effect parameter, E_{i0}^T is the optical ionisation energy, $\rho(E)$ is the density of states, $\eta = \exp(-2E/E_P)$ and $E = h\nu - |Ei|$.

The σ data for each component (Figure 3) were fitted to the simplified Huang and Rhys (1950) expression (Equation 5). However, the results presented must be viewed as preliminary, given that in order to fully evaluate the nature of the photo-eviction mechanism (specifically, the strength of the electron-phonon coupling), measurements at various temperatures and wavelengths are required. We have only been able to vary wavelength under the present experimental setup.

3.2 Implications for optical dating

One of the implications of the data presented in the previous section, for optical dating, is for the identification of sedimentary samples that are incompletely bleached prior to deposition. In order to obtain accurate optical dates, it is essential that the OSL signal be reset to zero at the time of the event being dated. In practice, this resetting is achieved through exposure of the sediment to daylight, in the natural environment (prior to burial). If the duration of light exposure is relatively short then a residual signal component will be present, leading to over-estimation of the absorbed burial dose (and hence age). However, if the residual component can be identified then such problems can be avoided. If various components of the signal decay at different rates during illumination, then a comparison of these signals should correctly identify incomplete resetting (i.e. incomplete resetting should produce greater estimates of the burial dose in the slower-bleaching components; those with smaller σ). Following this rationale, if all components yield the same value for D_e, all must have been fully reset by light, as the only common origin for these signals is zero. That $\sigma_{Fast} > \sigma_{Medium}$ for blue to red stimulation indicates that the identification of incomplete bleaching may indeed be possible in cases where illumination is within this range of wavelengths (this method of identifying incomplete bleaching has been discussed previously in Bailey *et al.*, 1997 and more recently in Bailey 2002a, b; Bailey *et al.*, 2003).

Clearly a key requirement for the application of such a method is that during bleaching, in the natural environment, $\sigma_{Fast} > \sigma_{Medium}$. If $\sigma_{Fast} = \sigma_{Medium}$, then there would be no preferential loss of the fast component and therefore no opportunity to identify partial bleaching. For a typical daylight spectrum, the UV component of the spectrum is significant. Results presented in Figure 3 and 4 suggest that for UV stimulation (375nm), the bleaching rates of the fast and medium components are similar. The implication of this observation is that incomplete resetting could not be identified (by signal form alone) in daylight-bleached sediments. Data consistent with this hypothesis (where no significant changes in OSL decay form were observed following partial bleaching with daylight) have been reported previously in Rhodes, 1990 and Bailey, 1998a. The identification of partial bleaching, using the signal analysis methods described above (and also in detail in Bailey 2002a, b; Bailey *et al.*, 2003) is likely be restricted to environments where the shorter λ's are strongly attenuated (e.g. underwater; see Berger (1990) for details of measured underwater spectra).

With these possibilities in mind, the bleaching measurements reported above were repeated using the solar as a bleaching light source. The results obtained using the solar simulator produced $\sigma_{fast}/\sigma_{medium} \sim 2.7$ (different from a ratio of ~1 expected from earlier observations). Reasons for the difference from earlier findings are unclear but are probably related to differences in the UV component of the stimulating spectra.

Under UV-only stimulation (375nm) the ratio $\sigma_{fast}/\sigma_{medium}$ was calculated to be 1.4. Despite the small discrepancy between the expected and observed bleaching rate ratios, it can be inferred that the potential for the identification of sediments partially bleached by daylight is small.

4. INFRARED STIMULATION OF QUARTZ LUMINESCENCE

4.1 Isolation of the fast and medium OSL components

In many studies (e.g. Stokes, 1992), including this one, the presence of IR stimulated luminescence at ambient temperatures has been attributed to feldspar contamination. However, Spooner (1994) found, during spectral measurements, that IR stimulation produced measurable luminescence in quartz at temperatures greater than 70°C. Bailey (1998b) reported similar results, with stimulation temperatures of at least 200°C when stimulating with relatively low photon energies (880nm). Further, it was shown that the luminescence from IR stimulation corresponded directly to the OSL signal measured using broadband (420-560nm) stimulation, indicating that the IRSL and OSL signals are probably from the same traps (the observed IRSL signal and the (post-IR) residual OSL signal fitted well to single exponentials with indistinguishable decay rates).

Here a similar experiment was performed to look at the component-resolved decay rates of quartz IRSL at raised temperature. A measurement temperature of 160°C was found to be sufficient to observe significant amounts of luminescence while low enough not to sensitise the sample during measurement. The experiment procedure used was the same as that described in the previous section (3), in this instance bleaching with IR photons prior to measurement (using 470nm stimulation). Figure 5 (upper) shows examples of the LM-OSL curves for 470nm-stimulated OSL following IR bleaching.

The n_0 parameters (Equation 1) obtained through curve fitting of all LM OSL (following various durations of IR bleaching) were used to create the (IR-stimulated) OSL depletion curves for the fast and medium OSL components (Figure 5, lower). Interestingly, there appears to be no significant decay from the medium component, while the fast component is depleted to negligible levels by 7000-8000s IR (830nm 1W) at 160°C (this is also demonstrated in figure 5(upper) by the near-complete overlap of the 6000s and 8000s curves, indicating no further decay of the medium component due to increased IR bleaching time). The fast component decay from the post-IR OSL fitted well to a single exponential, and gave a very similar decay rate to the fitted IRSL observed during bleaching (a ratio of ~0.96; note that the IRSL bleaching was performed within the Risø reader and therefore that the resultant IRSL could be directly observed during bleaching). This suggests that the IRSL observed and the depletion curves shown in Figure 5 (lower) are

describing the depletion of the same signal (namely, the fast component), supporting previous findings (Bailey, 1998b).

It is hypothesized that IR stimulation at 160°C is below the stimulation threshold energy for the medium component, thereby allowing total depletion of the fast component signal with no measurable reduction in the medium. The results provide further corroborating evidence for the independent existence of the medium component (visible in figure 5 (upper), after 6000s and 8000s IR bleaching), and aid the determination of its peak position. Additionally, it offers a method of separating the fast and medium components for further research.

4.2 Dose response of the isolated fast and medium components

A crucial part of dating/dosimetry is the accurate measurement of dose response. Previously, the dose responses of the fast and medium components have been obtained using signal deconvolution methods. The separation of the fast and medium OSL components using selective stimulation wavelength (as described above) offers another method for obtaining component-resolved dose response data. In the present study, results from both the deconvolution and selective bleaching methods were compared. The results are presented below.

Bleached aliquots of sample SL203 were used to create regenerated dose response curves using modified single-aliquot regenerative-dose (SAR) protocols (Murray and Wintle, 2000). The measurement procedures used were:

Sequence 1: β-dose1, preheat 260°C 10s (PH1), OSL1 100s at 160°C, β-test dose (10Gy), preheat 260°C 10s (PH2), OSL2 100s at 160°C. Repeat cycle for β-dose1 = 0,10,20,40,80,160 Gy.

Sequence 2: β-dose1, PH1 260°C 10s, IRSL 160°C 7000s, OSL1 100s at 160°C, β-test dose (10Gy), PH2 260°C 10s, IRSL 160°C 7000s, OSL2 100s at 160°C. Repeat cycle for β-dose1 = 0,20,40,80,160,320 Gy.

Using preheats of 260°C for PH1 and PH2 was found to produce constant values for repeated sensitivity corrected SAR points of 10Gy (inset, Figure 6). This is an essential criterion for using the SAR protocol (Murray and Wintle, 2000). The OSL signals from sequence 1 were deconvolved into the fast and medium components. The respective dose response curves obtained are shown in Figure 6 (open symbols). From sequence 2, an integral (0-770s) of the IR stimulated luminescence was used to obtain values for the fast

component. The medium component values were found from the post-IR OSL. The dose response curves for the fast and medium component are shown in Figure 6.

The high level of agreement between the dose response curves produced using the two methods is highly encouraging and suggests that both are adequate ways to produce component-resolved results for the fast and medium components. The dose response curves have been fitted to single saturating exponential functions. D_0, the characteristic dose (where the slope of the dose response is 1/e of the initial slope), was calculated as 69Gy for the fast component, and 127Gy for the medium. As observed previously by Bailey *et al.*, (1997), the medium component commonly has a higher dose saturation level than the fast component and may therefore be useful in extending the dating range of quartz optical dating.

In order that sequences could be conveniently automated (using a Risø reader), IR stimulation (830nm) was used to separate the OSL components in the present case. However, bleaching of single components (the fast component in this case) may be possible using shorter wavelengths, provided that sufficient differences exist in σ. Extrapolation of the fits in Figure 3 gives the ratio $\sigma_{Fast}/\sigma_{Medium}$ ~6000 at 820nm. At 750nm it is ~1400, which will, in all probability, be adequate to bleach the fast component with insignificant loss from the medium. It is postulated that this method could be extended to separate the other components of quartz by finding, experimentally, the optimal wavelengths/temperatures to bleach successive components with negligible reduction of the next. A speculative combination could be 750-850nm (fast), 650-700nm (medium), 570-630nm (S1), and 500-550nm (S2). It is believed that this 'stepped wavelength' approach, where effectively a single component is stimulated during any measurement, could be a potentially useful method of measurement.

5. CONCLUSIONS

Narrow wavelength-band stimulation has been used to obtain bleaching spectra for the fast and medium OSL components of quartz. A significant dependence of σ on wavelength was observed for the fast and medium components. The ratio of fast and medium photoionization cross-sections ($\sigma_{fast}/\sigma_{medium}$) was also found to be wavelength dependent, increasing at longer stimulation wavelengths. At blue/green wavelengths, representative of the spectrum received by waterlain sediments, the ratio is sufficiently large that incomplete bleaching may be identified through signal analysis (using, for example, the $D_e(t)$ plots described in Bailey, 2002a). Using UV stimulation, at ambient temperature, the ratio $\sigma_{fast}/\sigma_{medium}$ obtained was close to unity. This suggests that, under (UV-rich) sunlight exposure, the fast and medium components

will deplete at very similar rates, inhibiting the detection of partial bleaching (using signal analysis) for certain sediment types.

At relatively long (IR) stimulation wavelengths the ratio $\sigma_{fast}/\sigma_{medium}$ was sufficiently large that the fast component could be bleached completely with negligible depletion in the medium component. That is, infrared stimulation allowed the selective removal of the fast component. The application of this method to the remaining OSL components, using progressively shorter wavelengths to optically separate each component, is suggested as a means of simplifying quartz OSL component analysis, removing the need for complicated (and possibly inaccurate) fitting routines.

ACKNOWLEDGEMENTS

REFERENCES

Bailey, R. M. (1998a). *The form of the optically stimulated luminescence signal of quartz: implications for dating*. Unpublished Ph.D. thesis. University of London.

Bailey, R. M. (1998b). Depletion of the quartz OSL signal using low photon energy stimulation. *Ancient TL.*, **16**, 33-36.

Bailey R. M. (2002a) The analysis of measurement-time dependent single aliquot equivalent dose estimates from quartz: implications for the identification of incompletely-bleached sediments. Submitted, *Radiation Measurements*.

Bailey R. M. (2002b) The interpretation of D_e versus measurement-time data using predictions from a simple model. Submitted, *Radiation Measurements*.

Bailey, R. M., Singarayer, J.S., Ward, S., Stokes, S. (2003) Identification of partial resetting using De as a function of illumination time. (in press, Radiation Measurements)

Bailey R. M. (2000) The slow component of quartz optically stimulated luminescence. *Radiation Measurements*, 32, 233-246.

Bailey, R. M., Smith, B. W., Rhodes, E. J. (1997). Partial bleaching and the decay form characteristics of quartz optically stimulated luminescence. *Radiat. Meas,.* **27**, 123-136.

Berger, G. (1990). Effectiveness of natural zeroing of the thermoluminescence in sediments. *Journal of Geophysical Research*, **95**, 12375-12397.

Bulur, E. (2000). A simple transformation for converting CW-OSL curves to LM-OSL curves. *Radiation Measurements*, **32**, 141-145.

Bulur, E., Bøtter-Jensen, L., Murray, A. S. (2000). Optically stimulated luminescence from quartz measured using the linear modulation technique. *Radiat. Meas.*, **32**, 407-411.

Bulur, E., Bøtter-Jensen, L. and Murray, A. S. (2001). LM-OSL signals from some insulators: an analysis of the dependency of the detrapping probability on stimulation light intensity. *Radiat. Meas.,* **33**, 715-719.

Duller, G. A. T., Bøtter-Jensen, L. (1996). Comparison of optically stimulated luminescence signals using different stimulation wavelengths. *Radiat. Meas.*, **26**, 603-609.

Huang, K. and Rhys, A. (1950). Proc. R. Soc. A, **204**, 406.

Huntley, D. J., Short, M. A., Dunphy, K. (1996). Deep traps in quartz and their use for optical dating. *Can. J. Phys.*, **74**, 81-91.

Jaros, M., 1977. Wave functions and optical cross-sections associated with deep centers in semiconductors. *Phys. Rev. B.*, **16**, 3694-3706.

Lucovsky, G. (1965). On the photoionization of deep impurity centres in semiconductors. *Solid State Commun.*, **3**, 299-302.

Murray, A. S. and Wintle, A. G. (2000). Luminescence dating of quartz using an improved single-aliquot regenerative-dose protocol. *Radiat. Meas.*, 32, 57-73.

Rhodes, E. J., 1990. Optical dating of quartz from sediment. Unpublished D.Phil. thesis. Oxford University.

Singarayer J.S. and Bailey R.M. (2003) Further investigations of the quartz OSL components using the linearly modulated technique. (in press, *Radiation Measurements*).

Smith, B. W. and Rhodes, E. J. (1994). Charge movements in quartz and their relevance to optical dating. *Radiat. Meas,.* **23**, 329-333.

Spooner, N. A. (1994). On the optical dating signal from quartz. *Radiat. Meas.*, **23**, 593-600.

Stokes, S. (1992). Optical dating of young sediments using quartz. *Quaternary Science Reviews (Quaternary Geochronology),* **11**, 153-159.

FIGURE CAPTIONS

Figure 1. Quartz LM OSL curve for sample SL203, measured with 0 to 36mW cm^{-2} blue stimulation in 7200s at 160°C, after a 700Gy beta dose and a preheat to 260°C. Five OSL components were found by curve fitting (the photoionization cross-sections, in descending order, being 3.1×10^{-17}, 6.6×10^{-18}, 2.6×10^{-19}, 1.2×10^{-20}, 6.5×10^{-22}). The measurement was made at the Ris∅ National Laboratory, Denmark.

Figure 2. Decays for the fast and medium components of quartz sample SL203 for various stimulation wavelengths (at ~20°C), fitted to exponential functions. For each point, $n_{0,\text{fast}}$ and $n_{0\cdot\text{medium}}$ were found from fitting the blue light pseudo-LM OSL after partial bleaching. See text for details.

Figure 3. Calculated σ vs. stimulation photon energy for the fast and medium components of quartz, at room temperature. The fits shown are to Equation 5 yielding the following values: $E_g = 9.0$eV, $d_{FC} = 1.0$, $E_F = 4.5$eV, $E_0(\text{Fast}) = 2.88$eV, $E_0(\text{Medium}) = 2.99$eV, $E_P(\text{Fast}) = 10$, $E_P(\text{Medium}) = 20$. A plot of the relative sizes of σ vs. photon energy is given (lower).

Figure 4. Pseudo-LM OSL using 470nm stimulation at 160°C, following various durations of partial bleaching at room temperature using 525nm (upper) and 375m (lower) stimulation.

Figure 5. (Upper) Examples of blue-light stimulated pseudo-LM OSL curves following various lengths of IR stimulation at 160°C. These curves were fitted to obtain the fast and medium magnitudes following partial bleaching, and the values used to plot lower figure – the decay curves for the fast and medium components with IR stimulation at 160°C.

Figure 6. Dose response curves for the fast and medium OSL components of quartz using modified SAR techniques. Open symbols – fast and medium separated by curve fitting of blue-light pseudo-LM OSL. Filled symbols – optical pre-treatment (7000s IRSL at 160°C) was used to measure the fast component, the following OSL (blue) was used to measure the medium.

Inset – Sensitivity corrected OSL from repeated SAR cycles of 10Gy (Components found by curve fitting)

Table 1

Wavelength, nm [photon energy, eV]	Photoionization cross-section (cm^2), 20°C	
	Fast component	Medium component
375 [3.31]	6.4×10^{-18}	4.0×10^{-18}
430 [2.88]	3.0×10^{-17}	1.0×10^{-17}
470 [2.64]	1.8×10^{-17}	3.8×10^{-18}
500 [2.48]	1.1×10^{-17}	1.4×10^{-18}
525 [2.36]	3.1×10^{-18}	3.8×10^{-19}
590 [2.10]	1.0×10^{-19}	3.4×10^{-21}

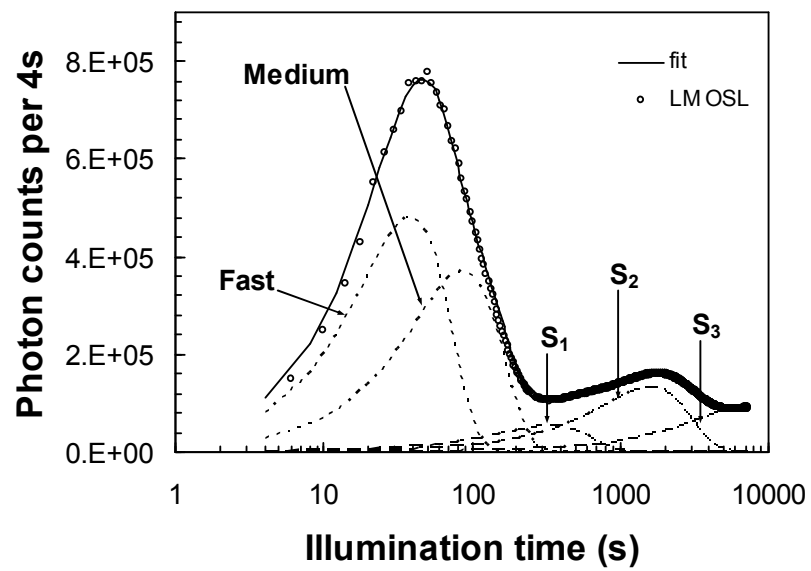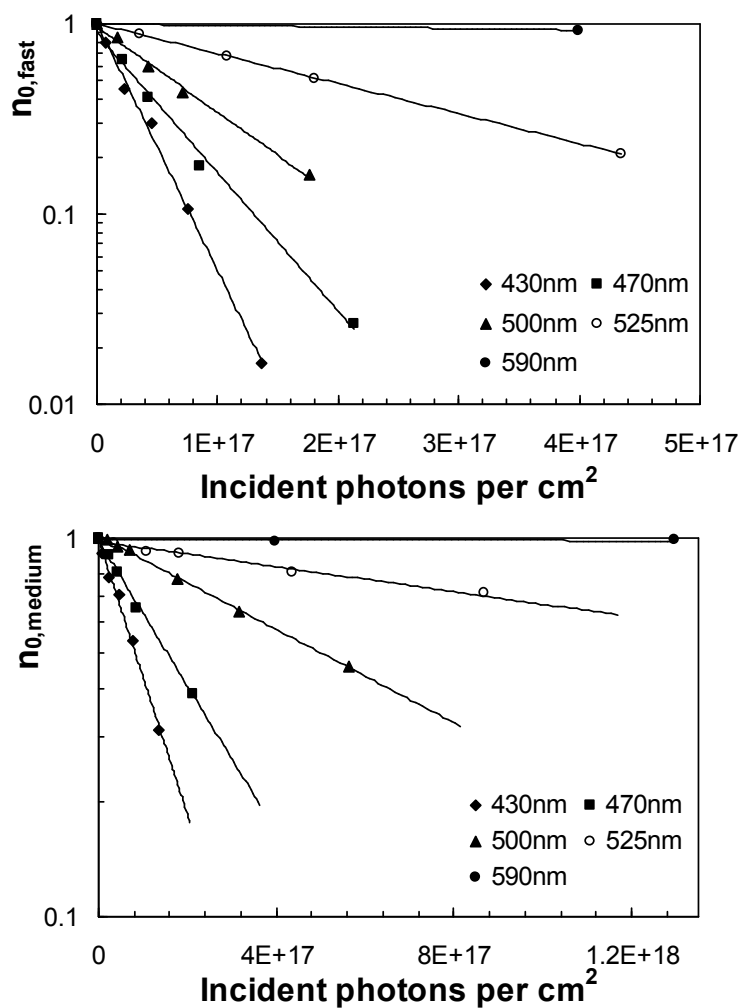Table 1. Values obtained for fast and medium component photoionization cross-sections. Sample temperature during bleaching was 20°C.
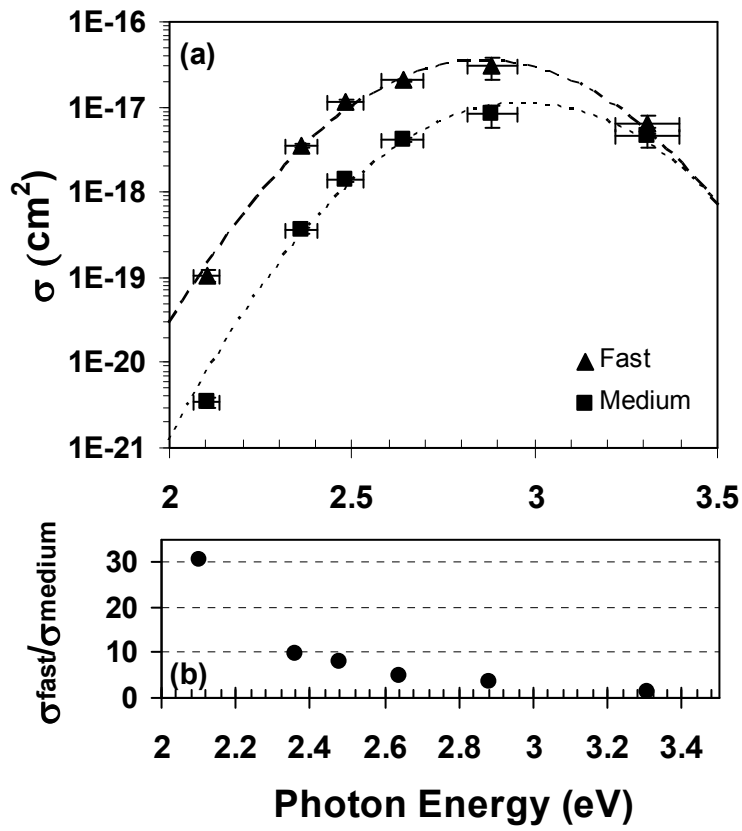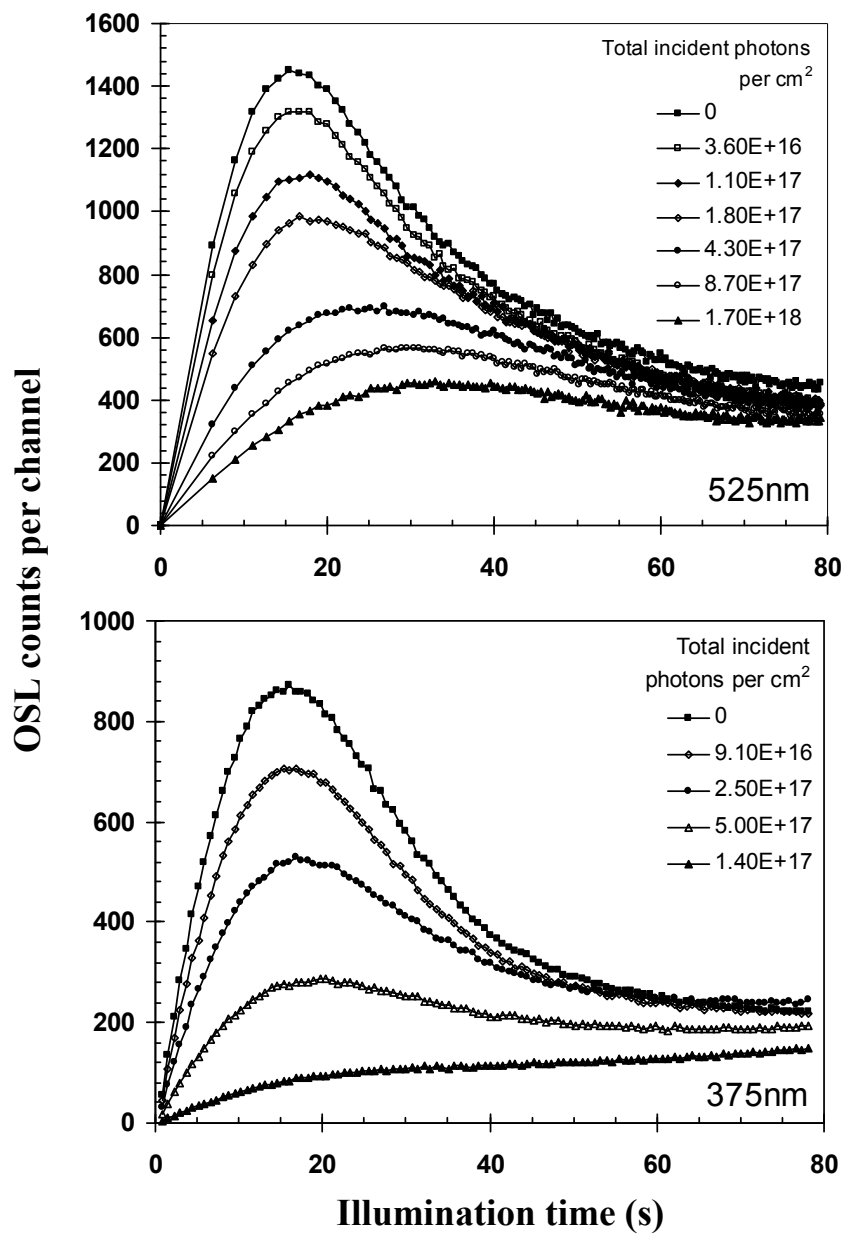
Figure 1

Figure 2

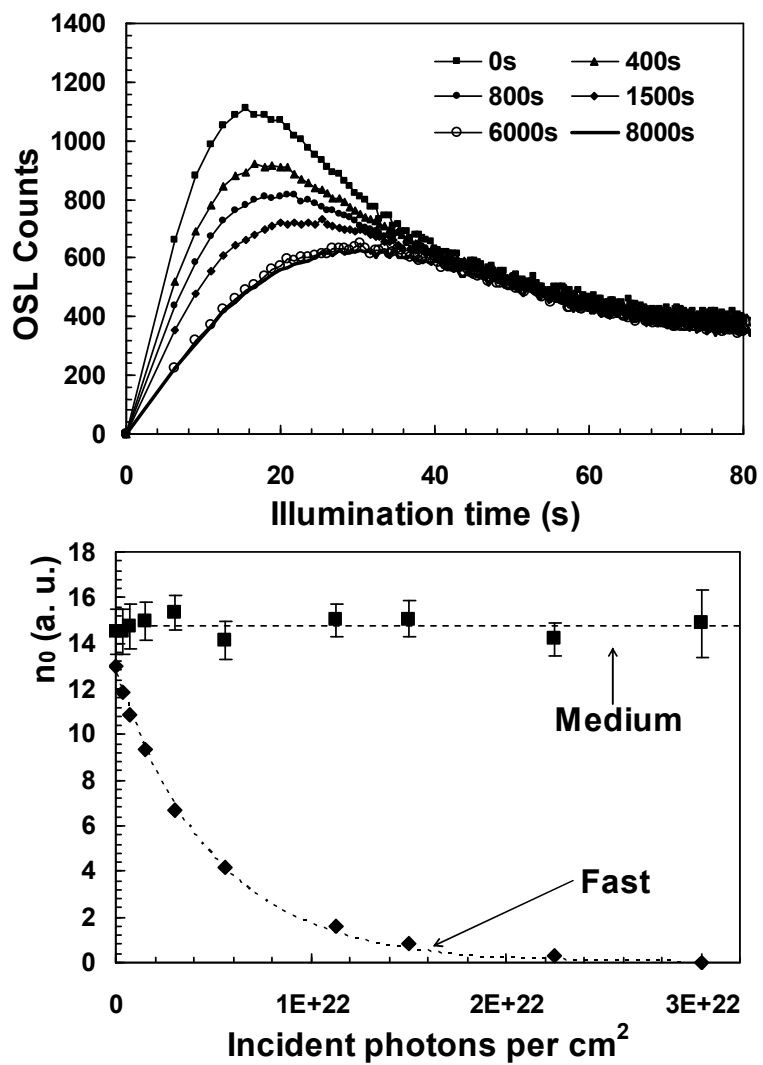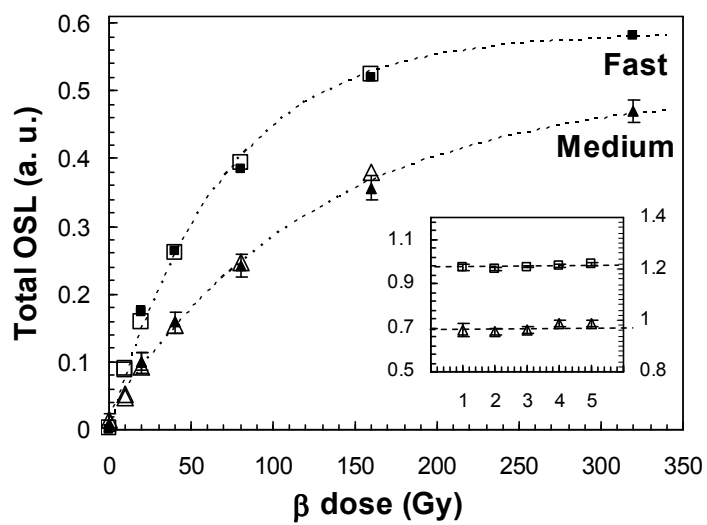Figure 3

Figure 4

Figure 5

Figure 6

FURTHER INVESTIGATIONS OF THE QUARTZ OPTICALLY STIMULATED LUMINESCENCE COMPONENTS USING LINEAR MODULATION

J. S. Singarayer [1*] and R. M. Bailey [2]

[1] *Bristol Glaciology Centre, School of Geographical Sciences, Bristol University, University Road, Bristol, BS8 1SS, U.K.*

[2] *School of Geography and the Environment, Mansfield Road, Oxford, OX1 3TB, U.K.*

Abstract

The optically stimulated luminescence (OSL) from quartz is known to be the sum of several components with different rates of charge loss, originating from different trap types. The OSL components are clearly distinguished using the linear modulation (LM OSL) technique. A variety of pre-treatment and measurement conditions have been used on sedimentary samples in conjunction with linearly modulated optical stimulation to study in detail the behaviour of the OSL components of quartz. Single aliquots of different quartz samples have been found to contain typically five or six common LM OSL components when stimulated at 470nm. The components have been parameterised in terms of thermal stability (i.e. E and s), photoionization cross-section energy dependence and dose response.

The results of studies concerning applications of component-resolved LM OSL measurements on quartz are presented also. These include the detection of partial bleaching in young samples, use of 'stepped wavelength' stimulation to observe OSL from single components and attempts to extend the age range of quartz OSL dating.

1. Introduction

Huntley *et al.* (1985) observed that the decrease in the OSL emission of quartz upon illumination (stimulated with a constant intensity) did not follow a simple exponential, as one would expect from a single trap system with first order kinetics. The same emission was found by Smith and Rhodes (1994) to be well approximated by the sum of three exponential signal components that they called the fast, medium and slow (or long-term) components after their relative optical depletion rates. Bailey *et al.* (1997) demonstrated

---

[*] Corresponding author: Fax +44 (0)117 928 7878
Email address: joy.Singarayer@bristol.ac.uk

that the most probable explanation is that the OSL signal originates from three physically distinct traps with different rates of charge loss. The slow component of quartz appeared to have an exceptionally a high dose saturation level in several samples and high thermal stability, indicating its potential for extending the upper datable limit of optical dating using quartz (Bailey, 2000).

In the studies described above the luminescence emission was stimulated using constant intensity (continuous-wave or CW OSL). A novel method for measuring OSL was proposed by Bulur (1996) which involved linearly ramping the intensity of the stimulation source during measurement of the luminescence, called linearly modulated (or LM) OSL. This technique produces peak-shaped OSL instead of a monotonically decaying CW OSL signal. The LM OSL from a single trap can be described analytically be the following equation:

$$I_{LMOSL} = n_0 \frac{\sigma Pt}{T} \exp\left(\frac{\sigma Pt^2}{2T}\right) \qquad \text{Eq. 1}$$

where n_0 is proportional to initial trapped charge concentration, P is the maximum stimulation intensity, T is the total measurement time and σ is the photoionization cross-section. Parallels can be drawn with the more familiar phenomenon of measuring thermoluminescence (TL) peaks by ramping the temperature during measurement.

Using the LM technique the structure of the signal, in terms of the number of components and their kinetics, may be recorded with greater clarity. LM OSL was applied to a heated quartz sample by Bulur *et al.* (2000) using maximum stimulation power of ~20mWcm[-2]. Through a series of thermal stability and dose response experiments, in conjunction with curve fitting studies, they identified four first-order components with photoionization cross-sections ranging over several orders of magnitude. On a sedimentary, quartz sample an additional fifth slow component was observed by Singarayer and Bailey (2002) using LM OSL measurements.

Linear modulation is increasingly being used in a variety of diagnostic studies and is potentially a very useful tool, for example in the study of partial bleaching (Singarayer *et al.*, 2002) and thermal transfer (Watanuki, 2002 and Jain *et al.*, this volume). However, not many detailed studies have yet been published assessing more completely the behaviour of the quartz LM OSL components. In this study we aimed to investigate and quantify properties of the components of 'typical' sedimentary quartz samples relevant to optical dating using the linear modulation technique. Similar investigations have also been carried out recently by Jain *et al.* (this issue).

2. Experimental details

2.1 Samples

All samples included in the study were sedimentary to be applicable to optical dating. The details of the samples used explicitly in this study are as follows:

SL203: Sri Lankan dune deposit ca. 36ka

TQN: Grey dune deposit, Thomas Quarries, Morocco

TQL: Aeolian, Thomas Quarries, Morocco >790ka

897/3: Taramsa Hill burial site, Egypt (Vermeersch *et al.*, 1998)

317: Raised beach, Chebba, Tunisia (Wood, 1996)

338: Raised beach, Hergla, Tunisia (Wood, 1996)

Van2: Vanguard cave site, Gibraltar

KG02: Korean sample

SH1A: Aeolian, Shropham pit, East Anglia

Quartz was extracted from the samples using standard coarse grain procedures (e.g. Stokes, 1992). Quartz grains (either 90-125μm or 125-180μm) were used to make up ~5mg aliquots of the prepared quartz. IR stimulation at 20°C following beta dose and preheat was used to test for feldspar contamination. Lack of measurable signal was taken as an indication of absence of feldspar.

2.2 Measurement apparatus

OSL measurements were performed using either a Risø TLDA-10 or TLDA-15 reader. Both were equipped with excitation units containing blue light-emitting diodes (λ ~ 470nm Δ20nm), delivering ~15mWcm^{-2} and ~32Wcm^{-2}, respectively. The luminescence emission was filtered using 6mm Hoya U340, providing an emission window of λ ~ 340 Δ80nm, and recorded using a bialkali PMT. Irradiations were done using ^{90}Sr/^{90}Y beta sources (dose rates 22 and 50mGy s^{-1}). Only the TLDA-15 reader had the capacity to make ramped power (LM OSL) measurements.

The majority of the OSL measurements described in the following sections were made by ramping the stimulation intensity during measurement. However, in some situations, for example to take advantage of reduced measurement time, greater stimulation stability and the use of both automated risø readers, a mathematical transformation for converting CW OSL measurements into LM OSL was used (following Bulur, 2000). To achieve this, standard OSL measurements were made using constant stimulation power and

transformed mathematically into the form that would have been observed by linearly modulating the stimulation intensity. The transformation described by Bulur (2000) can be applied to convert first, second and general order OSL decays provided the mechanism of detrapping of charge is independent of stimulation power and is due to single-photon absorption (as found by Spooner, 1994, and Bulur *et al.*, 2001, for quartz).

3. Properties of the quarts OSL components

3.1 Sample variability

Bailey (1998) found that CW OSL from seventeen out of eighteen sedimentary samples could be fitted to three exponential components over a limited range (the slow component decayed non-exponentially). The half-life of the fast and medium components obtained through curve fitting were similar (within errors) in the various samples. The decay of the 'slow' component was much more variable, as might be expected if it consisted of more than one component, as found by e.g. Bulur *et al.* (2000).

Therefore, it was considered important to look at the form of the LM OSL from a number of sedimentary quartzes taken from a variety of locations and depositional environments to re-examine to some degree the variability of the OSL components. The natural LM OSL signal from 12 samples was measured (following preheat to 260°C, 10s) for 3600s at 160°C. Following the bleaching of the natural luminescence a 20Gy beta dose was administered to each of the aliquots used. After a further preheat the LM OSL induced by the 20Gy dose was recorded. Examples from seven of the samples are shown in Fig. 1a.

Large variation in brightness/sensitivity was apparent from the results. The LM OSL peaks, however, occurred in roughly similar positions. The data from the 12 samples were fitted to first order components. In general four or five common components gave good fits to the data, although not all components were present in all samples. One sample could only be fitted to six components. The common components have been called the fast, medium, (as in Bailey *et al.*, 1997) and slow components S1, S2 and S3. An example LM OSL (for 7200s) from sample SL203 is displayed in Fig. 1b with the fitted components. In all the samples except one the fitted photoionization cross-section, σ, parameters of the components overlapped within error. All of the σ values were averaged to give: $\sigma_{fast}=2.5\pm0.3\times10^{-17}cm^2$, $\sigma_{medium}=5.9\pm2\times10^{-18}cm^2$, $\sigma_{S1}=2.1\pm0.5\times10^{-19}cm^2$, $\sigma_{S2}=1.2\pm0.2\times10^{-20}cm^2$, and $\sigma_{S3}=1.9\pm2.8\times10^{-21}cm^2$ (σ of the sixth component in one sample=$7.0\times10^{-16}cm^2$). Only the σ of component S3 was highly variable due to errors in

the fitting induced by the fact that the LM OSL measurements only recorded the initial part of the signal, and it's non-first order behaviour (see section 3.4). Reasonable agreement of the component parameters between all samples was observed. This may indicate that results from experiments described below that examine the behaviour of the OSL components, which have been applied to fewer samples, are more generally applicable to sedimentary quartz.

3.2 Thermal stability

Thermal stability is a crucial consideration for luminescence dating, as the temperature-dependent retention lifetime of a trap type places a fundamental limitation on the age range datable with that component. Trap lifetime, assuming first order kinetics is given by Equation 2:

$$\tau = s^{-1} \exp\left(E \middle/ k_B T \right) \qquad\qquad \text{Eq. 2}$$

where τ is the lifetime (s), s is the frequency factor (s^{-1}), E is trap depth (eV), T is temperature (K) and k is Boltzmann's constant ($\sim 8.615 \times 10^{-5}$ eVK^{-1}).

Attempts to characterise the thermal stability of the quartz OSL components have been attempted by Bailey (1998) and Bulur *et al.* (2000 - on a single heated quartz sample only). In this study a pulse annealing experiment, using a similar procedure to that employed by Bulur *et al.* (2000), of preheating to increasingly high preheating temperatures, was used to look at the thermal stability of various sedimentary samples.

Following a low laboratory dose (20Gy) aliquots were preheated to temperatures between 220 and 450°C. LM OSL was subsequently performed for 7200s at raised temperature (160°C). The long LM measurements were not sufficient to completely zero the slower components. Therefore, an additional CW OSL of 6000s at 170°C was carried out between each measurement to bleach the OSL to negligible levels. A subsequent LM OSL following 20Gy and 220°C preheat was used in an attempt to monitor sensitivity changes throughout the measurement procedure. Negligible sensitivity change was observed during the whole measurement procedure.

Pulse annealing was performed on various samples. The results from sample SL203 are presented here. The LM OSL curves were fitted to the sum of five components. The sensitivity corrected OSL was plotted vs. preheating temperature to obtain the pulse annealing curves for each component. These are displayed in Fig. 2. The fast, medium and S1 components show sharp decays and are all stable up to ~270°C. Component S2,

however, displays some depletion following preheats as low as 220°C and the decay shape is much broader than the other components (as observed by Bulur *et al.*, 2000).

To attempt a more detailed analysis, the data have been fitted to analytical expressions, derived in Singarayer (2002), to describe the pulse annealing curve shape. The remaining OSL following ramping to temperature, T, can be found by assuming that total LM OSL emitted is proportional to the remnant trapped charge, *n*. The following equation for n is derived from Equation 2, assuming 1st order kinetics:

$$n = n_0 \exp\left[\left(\frac{-skT^2}{\beta E} \exp\left(-\frac{E}{kT} \right) \right) + \left(\frac{skT_0^{\;2}}{\beta E} \exp\left(-\frac{E}{kT_0} \right) \right) \right] \qquad \text{Eq. 3}$$

where n_0 is the initial trapped charge concentration, temperature is given in Kelvin, and T_0 is the ambient room temperature (~15°C = 288K), E is trap depth and s is the frequency factor of the trap. Similar equations were also derived for 2nd and general order kinetics.

Equation 3 was used to produce fits to the pulse annealing data, shown in Fig. 2 also (dotted lines). Component S2 was best fitted to a 2nd order curve, the reason for which is unclear at this time given the apparent first order nature of the LM OSL from S2. The fitting allowed estimates of trap parameters, E and s to be made. These are given in Table 1. From this data it can be inferred that the fast, medium and component S1 are of sufficient thermal stability for optical dating whereas component S2 is not adequately stable for dating sediments on Quaternary timescales. Consistent data could not be obtained from component S3 with experimental procedure employed to allow conclusions to be drawn concerning thermal stability. A sufficient proportion of the LM OSL peak could not be measured for this component to allow for consistent fits to be obtained at such low doses (only the initial rising part of the peak was observed). Nevertheless, from the raw LM OSL data for sample SL203 the rising limb of component S3 is visible above background levels after preheating to 500°C suggesting that this component does have significant thermal stability. Bailey et al. (1997) and Bailey (1998b) observed one slow component that appeared to remain intact even after heating to 650°C, using CW OSL measurements. It is tentatively suggested that they were observing the small fraction of component S3 that may remain after such high temperature preheats.

Isothermal decay analysis of the OSL components was also reported in Singarayer (2002) and produced similar findings (except S2 was estimated to be slightly more stable, with a lifetime of 19ka at 20°C).

It is noted, given the pulse annealing results, that using preheats of 260°C or higher results in significant depletion of component S2. Nevertheless such preheat temperatures

have been used in further experiments so that thermal activation occurs mostly during the preheat rather than during the long LM OSL measurements at high temperatures (160°C), which could have a significant effect on the form of the LM OSL (Singarayer, 2002). Additionally, there is a small amount of thermal depletion of S2 during stimulation (<4% in 3600s at 160°C). However, since similar results are observed when experiments were repeated using various OSL stimulation times (e.g. 3600 and 7200s) it is thought that the results are not significantly affected (as long as within each experiment the same measurement conditions are used).

3.3 Optical detrapping

The energy of optical stimulation affects the rapidity of OSL signal depletion under illumination. Previous authors have found an increase in bleaching rate with increasing photon energy for quartz OSL (e.g. Spooner, 1994; Duller and Bøtter-Jensen, 1996) and decrease in thermal assistance energy with increasing photon energy (Spooner, 1994; Huntley et al., 1996). The dependence of the detrapping rate of the OSL components on photon energy was investigated, specifically of the fast and medium components, since it might be argued that these components are more relevant when considering issues related to dating such as partial bleaching.

The experimental details and analysis procedures are explained in more detail in Singarayer and Bailey (2002). Here a summary of those results (Singarayer and Bailey) and additional results are presented. Aliquots of sample SL203 were partially bleached at room temperature using an external unit with interchangeable LED clusters of a variety of wavelengths (photon-energies), ranging from UV to red. The remnant OSL was subsequently measured in the Risø reader using 470nm stimulation at 160°C. The decay rates of the fast and medium components were derived from the remnant OSL following partial bleaching. Given that the observed signal decay was exponential, and that measured recuperation was found to be negligible in this sample, charge recycling through the 110°C TL peak was not considered to have affected the results significantly. The photoionization cross-sections of the fast and medium components at each photon energy were calculated, and the spectra are plotted (σ vs. photon energy) in Fig. 3a.

The data for both components follows a similar form. However, the more important difference in the responses of the fast and medium OSL components can be clearly seen in Fig. 3b where the ratio $\sigma_{fast}/\sigma_{medium}$ is plotted. This varies from 30.6 at 590nm to 3.7 at 430nm, i.e. there is a significant change in the form of the OSL with stimulation

wavelength. At 375nm the ratio of the fast and medium component σ was only 1.4 ± 0.3. The similarity of the detrapping rates of the fast and medium components when stimulated with UV has implications for the identification of incomplete resetting using signal analysis methods. This is discussed further in Singarayer *et al.* (2002).

As the photon energy decreases the separation of the fast and medium components increases, as in Fig. 3a. Using even lower energy IR (830nm) stimulation at 160°C Singarayer and Bailey (2002) reported that there was no depletion in the medium at all, only the fast could be bleached (also found by Jain *et al.*, this volume). This indicates that IR energies are below the optical threshold of the medium component (and S1, S2, S3) but not the fast, allowing the isolation of a single component.

3.4 Dose response characteristics

Bailey *et al.* (1997) published the first component-resolved dose response curves for the fast, medium and slow components. They produced regenerated growth curves using a multiple aliquot technique by fitting CW OSL decays to three components. The slow component was observed to have dose saturation levels far exceeding the other components. Bulur *et al.* (2000) obtained component-resolved growth curves from a heated sample using a single aliquot procedure. This involved no sensitivity monitoring as the sample had been stabilised beforehand by cycles of dosing and annealing. They too observed that the slow components displayed higher saturation levels than the fast and medium.

Bulur *et al.*'s approach was not appropriate for sedimentary samples due to the sensitivity changes that are likely to take place, and multiple aliquot methods were not practical because of the inter-aliquot variation in the proportion of the OSL components. Therefore, a new measurement procedure was developed in order to observe the dose response and estimate equivalent doses (D_es) from sedimentary quartz. Issues such as zeroing between measurement cycles, sensitivity changes during and between OSL were considered.

The sequence used was a modified single-aliquot regenerative-dose procedure (SAR, Murray and Wintle, 2000):

1. Beta dose (0Gy for natural), 2. Preheat to 270°C for 10s (this serves a dual purpose of removing thermally unstable charge and sensitising the aliquot sufficiently so that only limited sensitivity changes would take place during the subsequent lengthy LM OSL measurement at 160°C), 3. LM OSL1 at 160°C for 3600s or 7200s, 4. Small test dose, 5.

Preheat to 220°C for 10s, 6. LM OSL2 for 300s at 160°C, 7. CW OSL at 300°C for 1500s.

Steps 4 – 6 are used to correct sensitivity changes in the initial LM OSL measurements (step 3). It was found that in the samples investigated the sensitivity changes of the components were proportional (Singarayer, 2002), and therefore measurement of the response of the fast component to a test dose could be used to monitor the sensitivity of all the components. Consequently, only a short LM OSL2 measurement was required to measure the fast component sensitivity. This meant that there was no need for stringent zeroing of the OSL between steps 3 and 4 that would result in further (unmonitored) sensitivity changes. A high temperature CW OSL measurement (step 7) was used at the end of each cycle to ensure zeroing of all the components. A 0Gy dose was recorded during the protocol to check this. One of the dose points was repeated at the end of the procedure to check the sensitivity monitoring. The measurement sequence was tested by recovering known 'natural' doses (Singarayer, 2002).

The procedure described above was used to investigate the dose response characteristics of the OSL components. The regenerated LM OSL from an aliquot of sample TQN is displayed in Fig. 4a. No peak shift with dose was observed for the first four components, supporting the choice of 1st order kinetics for fitting. The LM OSL was fitted to separate the components and produce component-resolved growth curves, shown in Fig. 4b. All growth curves could be fitted to a single saturating exponential function (also shown). The fast, medium and S1 components have similar dose saturation levels (characterised by D_0 values of 190, 258 and 250Gy respectively). Component S2 was found to have a relatively low saturation level with $D_0 = 28$Gy and full saturation reached at ~160Gy. The only component to apparently show dose response significantly higher than the fast component was S3. The D_0 of S3 was 850Gy which given a typical dose rate of 1Gyka-1 equates to nearly a million years of growth. Similar patterns were also observed for several other samples (Singarayer, 2002).

One concern is that the LM OSL measurement conditions did not allow the peak of component S3 to be recorded. This may have affects for the appropriateness of the deconvolution. A further experiment was performed to investigate S3 using CW OSL mathematically transformed into LM OSL, in order to maximize total imparted energy at the sample and improve signal-to-noise.

A bleached single aliquot of sample SL203 was given a laboratory dose and preheat to 280°C for 10s. A short LM OSL measurement was performed to deplete the fast and

medium components immediately followed by 10 000s CW OSL at full power at 190°C. The CW OSL decay was transformed to a pseudo-LM OSL curve equivalent to LM empirical measurement of 20 000s. Pseudo-LM OSL following doses of 200, 517 and 1000Gy are shown in Fig. 5. The peak of component S3 was visible at the doses of 500Gy or higher. Significant movement of the S3 peak was observed, indicating non-first order kinetics.

Component S3 was fitted to a general order equation (given in Bulur, 1996) to obtain a regenerated growth curve (components S1, S2 fitted also). The magnitude of component S2 was used to correct for sensitivity change. Since it was known that S2 would be fully saturated at doses higher than 150Gy (as observed for all the samples investigated) any change in magnitude of this component was assumed to be due to sensitivity change only, and therefore it could be used to correct the sensitivity of component S3, assuming that the sensitivity of both components changes proportionally. The growth curve calculated is shown in Fig. 5 (inset). The dose response was approximated by a single-saturating exponential function. The D_0 value obtained for this sample appeared slightly lower than for the other samples, using LM OSL measurements where the peak of S3 was not observed, although still considerably higher than found in general for the other components, and was not saturated at 1000Gy.

With respect to the possible extension of the datable range of quartz, the only component with a dose response significantly larger than the fast component is S3 from the above results.

4. Component-resolved applications in optical dating

The properties of the OSL components of quartz with the greatest potential for direct application to optical dating are arguably the differences in response of the components to stimulating photon energy, dose, and thermal transfer, having possible applications for identification of incomplete resetting, extending the datable upper limit of quartz and correction of samples suffering from recuperation. The different responses of the components to photon energy may also be used to separate the component signals by measurement with the appropriate wavelength. In this section we report an attempt to use component S3 for dating older samples (developing work by Bailey, 2000 and Singarayer et al., 2000). Other possible applications are discussed elsewhere (e.g. for identifying partial bleaching using component-resolved measurements see Singarayer et al., 2002).

Sample TQL from Casablanca, Morocco, taken from below the magnetic reversal of 0.79Ma (Johnson, 1982), was chosen as it was expected that the standard OSL dating signal (i.e. primarily fast component) would be saturated. To obtain component-resolved D_e measurements the LM OSL SAR protocol described in section 3.4 was applied to sample TQL. Regeneration doses up to 900Gy were used with the expectation of a De of over 500Gy. The resultant component-resolved growth curves (plotted in Fig. 6) could all be approximated using a single saturating exponential function.

Only the natural signal of component S3 appears not be in saturation. Large errors on the data points of component S3 result from the fact that the peak of S3 is not reached in the LM OSL measurement. Nevertheless, a D_e for this component was calculated as being 696 ± 438Gy. Dose rate data were obtained from field gamma spectrometry measurements. The final age estimate of 948 ± 599ka, although imprecise, was in agreement with the B-M boundary lower age limit. Greater precision could be gained through measurement of S3 using transformed CW OSL as described in the previous section.

5. Conclusions

In general five common OSL components were observed in a number of different quartz samples. This indicated that the results from experiments performed on fewer samples may be applicable to sedimentary quartzes in general. The OSL components display different thermal stability and dose responses. With the exception of component S2, all of the components were found to be stable over ~10^8 years at 20°C. Using a single-aliquot regenerative-dose approach, the dose saturation levels of the fast, medium and S1 components were found to be of the same order of magnitude in several different samples. Component S2 was found to saturate at doses far lower than the other components. Only component S3 displayed a significantly higher dose response. The considerable dose response of component S3 suggests that this component could be used to date samples beyond the typical upper datable age limit of quartz optical dating methods (possibly to >1Ma). The different responses of the fast and medium detrapping rates to various photon energies were also reported, with implications for partial bleaching identification using signal analysis methods (see Singarayer et al., 2002 and Bailey et al., this issue).

Acknowledgements

References

Bailey, R. M., Smith, B. W., Rhodes, E. J., 1997. Partial bleaching and the decay form characteristics of quartz OSL. *Radiation Measurements*, 27, 123-136.

Bailey, R. M., 1998. *The form of the optically stimulated luminescence signal of quartz: implications for dating*. Unpublished Ph.D thesis, University of London.

Bailey, R. M., 2000. The slow component of quartz optically stimulated luminescence. *Radiation Measurements*, 32, 233-246.

Bailey, R. M., Singarayer, J. S., Ward, S., Stokes, S. Identification of partial resetting using De as a function of illumination time. *Radiation Measurements*, this issue.

Bulur, E., 1996. An alternative technique for optically stimulated luminescence (OSL) experiment. *Radiation Measurements*, 26, 701-709.

Bulur, E., Bøtter-Jensen, L., Murray, A. S., 2000. Optically stimulated luminescence from quartz measured using the linear modulation technique. *Radiation Measurements*, 32, 407-411.

Bulur, E., Bøtter-Jensen, L., Murray, A. S., 2001. LM OSL signals from some insulators: an analysis of the dependency of the detrapping probability on light intensity. *Radiation Measurements*, 33, 715-719.

Duller, G. A. T., Bøtter-Jensen, L., 1996. Comparison of optically stimulated luminescence signals using different stimulation wavelengths, *Radiation Measurements*, 26, 603-609.

Huntley, D. J., Godfrey-Smith, D. I., Thewalt, M. L. W., 1985. Optical dating of sediments. *Nature*, 313, 105-107.

Huntley, D. J., Short, M. A., Dunphy, K., 1996. Optical dating of sediments. *Can. J. Phys.*, 74, 81-91.

Johnson, R. G., 1982. Brunhes-Matuyama reversal dated at 790 000 yr BP by marine-astronomical correlations. *Quat. Res.*, 17, 135-147.

Murray, A. S., Wintle, A. G., 2000. Luminescence dating of quartz using an improved single-aliquot regenerative-dose protocol. *Radiation Measurements*, 32, 57-73.

Singarayer, J. S., Bailey, R. M., Rhodes, E. J., 2000. Age determination using the slow component of quartz optically stimulated luminescence. *Radiation Measurements*, 32, 873-880.

Singarayer, J. S. and Bailey, R. M., 2002. Component-resolved bleaching spectra of quartz optically stimulated luminescence: preliminary results and implications for dating. *Radiation Measurements*. (In press)

Singarayer, J. S., Bailey, R. M., Ward, S., Stokes, S., Bray, H. E., 2002a. Further tests on the completeness of optical bleaching of sand-sized quartz from young sediments. (submitted *Quat. Sci. Rev.*)

Singarayer, J. S., 2002. *Linearly modulated optically stimulated luminescence of sedimentary quartz: physical mechanisms and implications for dating*. Unpublished D.Phil. Thesis, University of Oxford.

Smith, B. W., Rhodes, E. J., 1994. Charge movements in quartz and their relevance to optical dating. *Radiation Measurements*, 23, 329-333.

Spooner, N. A., 1994. On the optical dating signal from quartz. *Radiation Measurements*, 23, 593-600.

Vermeeersch, P. M., Paulissen, E., Stokes, S., Charlier, C., Van Peer, P., Stringer, C., Lindsay, W., 1998. A middle Palaeolithic burial of a modern human at Taramsa Hill, Egypt. *Antiquity*, 72, 475-484.

Watanuki, T., 2002. *Chronological study of loess palaeosol by improved method of luminescence dating and application to reconstruct past environmental changes*. Unpublished Ph.D. Thesis. Tokyo Metropolitan University.

Wood, P. B., 1996. *Dating and origin of late Quaternary catastrophic shoreline activity around the Mediterranean Sea.* Unpublished Ph.D. Thesis. University of London.

Figure Captions

Fig. 1 (a) LM OSL at 470nm from seven sedimentary quartz samples measured at 160°C, following 20Gy and preheat to 260°C. (b) LM OSL from sample SL203. The data were fitted to five components, also plotted.

Fig. 2 Calculated pulse annealing curves (remnant OSL vs. preheat temperature) for the fast, medium, S1 and S2 components of sample TQN. Empirical data (symbols), fits to the data (dotted lines)

Fig. 3 (a) Photoionization cross-section vs. stimulation photon energy at ambient temperature, calculated for the fast and medium components. (b) Ratio of fast to medium photoionization cross-sections vs. photon energy. See text for further details.

Fig. 4 (a) LM OSL curves following various laboratory beta doses (20 − 500Gy). The inset shows the slow components in more detail. (b) Component-resolved growth curves were calculated using the data in (a).

Fig. 5 Regenerated dose response curve for component S3 of sample SL203 shows growth at 1000Gy. Inset shows the raw OSL data used to create the main plot. Measurement details are given in section 3.4.

Fig. 6 Growth curves for the fast, medium, S1, S2 and S3 components of sample TQL. The natural signal is plotted (square symbols). The data were obtained using a modified SAR procedure described in section 3.4.

Table Captions

Table 1. Estimates of component parameters, E and s, derived from pulse annealing data. Trap lifetimes at 20°C, calculated using E and s, are shown also.

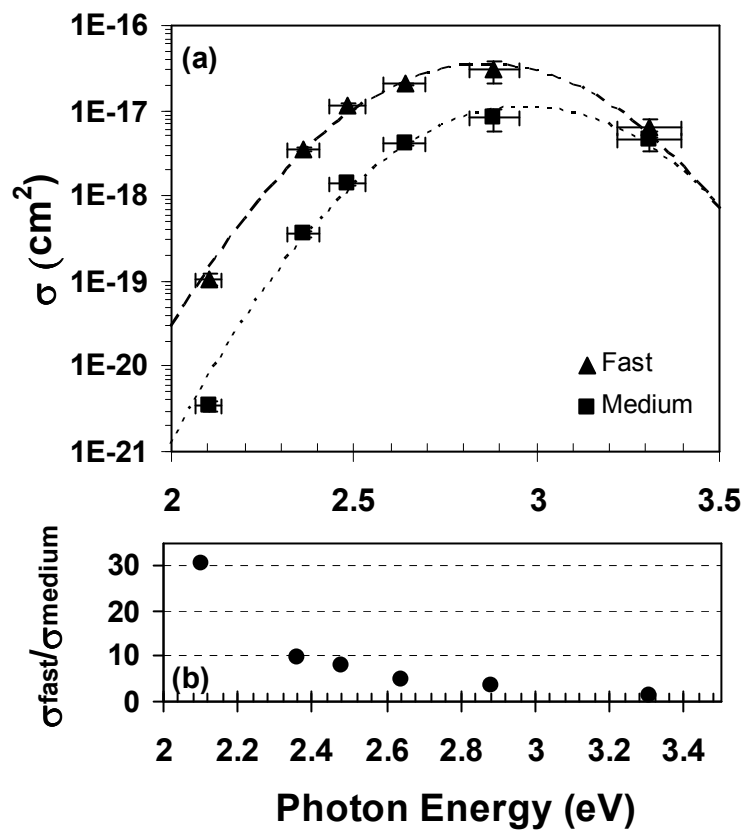| Component	E (eV)	s (s^{-1})	Lifetime at 20°C
Fast	1.74	8.9×10^{13}	310Ma
Medium	1.8	1.5×10^{13}	19000Ma
S1	2.02	6.9×10^{14}	2610000Ma
S2	1.23	4.7×10^{10}	1ka

Table 1.

Fig 1

Fig 2

Fig 3

Fig 3

Fig 4

Fig 5

Fig 6